WASHINGTON UNIVERSITY IN ST. LOUIS

Division of Biology and Biomedical Sciences
Molecular Microbiology and Microbial Pathogenesis

Dissertation Examination Committee:
Sergej Djuranovic, Chair
Daniel Goldberg
Sebla Kutluay
L. David Sibley
Hani Zaher

Protein Synthesis Adaptation to the AU-Rich Transcriptome of *Plasmodium falciparum*

by
Jessey Lee Erath

A dissertation presented to
The Graduate School
of Washington University in
partial fulfillment of the
requirements for the degree
of Doctor of Philosophy

January 2021
St. Louis, Missouri

Table of Contents

List of Figures

List of Tables

Acknowledgements

A scientist's development and contributions, regardless of their station within the scientific community, require the efforts of many. Collaboration, communication, and cooperation within labs and across the globe are vital to this process. I will be forever grateful for the opportunities, experiences, and knowledge gained from the Washington University community. I'm grateful to my lab-mates: Kyle Cottrell, Laura Arthur, Geralle Powell, and Courtney Jungers for their support and making the lab enjoyable even in the most stressful of times. I would like to thank Slavica Pavlovic-Djuranovic, Ph.D., for all her guidance and advice surrounding *Plasmodium*, and in life. I would like to thank my co-mentor and PI, Sergej Djuranovic, Ph.D., for inviting me into the lab. He has been instrumental in my professional development, guiding my work while giving me the freedom to direct it. Thank you to the Goldberg lab for all their input and generosity with reagents. I'm appreciative of the Cell Biology and Physiology department members for their advice, as well as generosity with equipment and reagents. I'd like to thank my committee members for their time, patience, and constructive feedback throughout this process. Lastly, thank you to Professor Jayne Raper for inviting me to join her lab, which first sparked my fascination with parasitology, and Professor Ana Rodriguez for enabling me to further that fascination with work in her lab. Without their help and encouragement, I would not have found my way to Washington University and subsequently the Djuranovic lab.

Jessey Erath

Washington University in St. Louis

January 2021

Dedicated to my family and friends.

ABSTRACT OF THE DISSERTATION

Protein Synthesis Adaptation to the AU-Rich Transcriptome of *Plasmodium falciparum*

Jessey Lee Erath

Doctor of Philosophy in Biology and Biomedical Sciences

Molecular Microbiology and Microbial Pathogenesis

Washington University in St. Louis, 2020

Dr. Sergej Djuranovic, Chair

The process of protein synthesis whereby a messenger RNA is decoded into an amino acid chain is conserved among the domains. Fastidious protein synthesis is necessary for organism survival. However, exceptions negatively affecting the mRNA translation cycle – inadvertently or by design – may occur. Polyadenosine tracts are one such motif causing ribosomal stalling and frameshifting in almost all organisms tested thus far; save *Plasmodium spp.* Thus, with ~60% of their protein-coding genome harboring polyadenosine tracts, the elucidation of such paradigm-breaking adaptations enabling *Plasmodium spp.* to translate this typically problematic motif without issue is salient from both basic science and clinical perspectives. Using biochemical and structural approaches, I report on the parasite ability to express polyA motifs and ribosome alterations enabling polylysine synthesis. The developed PP7-mRIP assay reveals RBP differences among varying mRNA substrates, revealing a previously uncharacterized, parasite-specific AU-rich binding protein bound to polyA tract reporter mRNA. Finally, the parasite exhibits altered binding of the essential ribosomal protein RACK1, vital for translation cap-dependent initiation and quality control activation, that would invariably alter ribosome-associated quality control pathway signaling, ostensibly aiding polyA translation.

Chapter 1: Introduction

1.1 The Central Dogma of Molecular Biology

The faithful maintenance, replication, and conversion of genetic information is necessary for prokaryotic and eukaryotic organism survival. While genetic shift and drift are important for long term evolutionary adaptation, fidelity of these processes is required for meantime population survival. DNA maintenance is characterized by multiple DNA repair mechanisms[1], some of which are active to ensure fidelity during DNA replication via proofreading[2]. RNAs of any type transcribed from DNA also require mechanisms to ensure consistency[3–5]. Although typically associated with viruses, eukaryotic RNA-directed DNA polymerase[6,7] and RNA replication by RNA-dependent RNA polymerases[8–10] have also been studied within eukaryotic systems. Ultimately, the flow of genetic information in a biological system from DNA to RNA to protein is described by the central dogma as: once this information has been synthesized into protein, it cannot be converted backward[11,12]. Therefore, mRNA translation is a critical, unidirectional, RNA-driven process.

1.2 mRNA Translation

The general process of protein synthesis in which a messenger RNA (mRNA) is decoded into a chain of amino acids, *i.e.* a polypeptide chain, that is subsequently folded into a protein, is conserved among the domains and consists of three phases: initiation, elongation, and termination. Each of these phases are, in themselves, regulated stepwise processes. The mRNA

provides the information necessary not only to produce an amino acid sequence, but also to regulation its production. The eukaryotic mRNA is comprised of a 5'-m^7GpppN-cap, a 5' untranslated region (UTR), a start codon (usually AUG), an open reading frame (ORF), a stop codon (UAA, UGA, or UAG), a 3' UTR, and finally a 3'-poly(A) tail. These regions regulate the process of translation in one way or another and will be briefly discussed following the general process of translation.

Initiation is the process whereby the ribosomal machinery is assembled on the mRNA. In eukaryotic systems, canonical mRNA translation initiation requires the 5'-m^7GpppN-cap and the 3'-poly(A) tail[13,14]. These mRNA features are recognized by eukaryotic initiation factors (eIFs) that subsequently recruit the pre-initiation complex (PIC) to the 5' untranslated region (5'UTR) of the mRNA[14]. The 43S PIC – 40S small subunit of the ribosome complexed with the peptidyl (P)-site Met-$tRNA_i$, eIF1, eIF1A, eIF2, eIF3, and eIF5 – then scans the 5' UTR in search of the AUG start codon[14]. Recognition of the AUG start codon halts scanning and results in the irreversible hydrolysis of GTP in the ternary complex (eIF2-GTP-Met-$tRNA_i$) to GDP[14]. This triggers the release of the eIFs, allowing for the 60S large subunit to join forming an initiating 80S complex with empty aminoacyl (A)-site containing the second codon in the open-reading frame (ORF)[14,15].

Elongation commences when the eukaryotic elongation factor (eEF) 1A bound to the cognate aminoacyl (aa)-tRNA in a GTP-dependent manner delivers the tRNA to the ribosome A-site. Correct codon-anticodon interaction, recognized by the decoding region of the 40S subunit,

stimulates GTP hydrolysis by eEF1A resulting in its release[15]. This allows for full accommodation of the aa-tRNA in the A-site and subsequent peptide bond formation. The peptide bond is formed by nucleophilic attack of the A-site aa-tRNA α-amino group on the carbonyl carbon of the P-site peptide-tRNA resulting in peptide elongation[16]. The conformational changes driven by peptide bond formation cause the acceptor ends of the A- and P-site tRNAs to move into the P- and E-site, respectively, resulting in a rotated hybrid tRNA A/P and P/E state[15]. To facilitate complete translocation to the canonical P- and E-sites, eEF2-GTP binds the A-site and is thought to stabilize the hybrid state. Subsequent GTP hydrolysis by the GTPase center of the 60S subunit is then thought to drive a conformational change in eEF2, allowing tRNA and mRNA movement, and translocate the ribosome along the mRNA aligning the anticodon ends of tRNAs into the P- and E-sites[15]. The eEF2-GTD is released and, with the ribosomes in its stable P/E state, the A-site is again available with the next codon in the ORF ready for decoding. This cycle is repeated until the ribosome encounters one of the typical three termination codons. Termination codons are recognized by two eukaryotic release factors: eRF1 and eRF3[15]. The tRNA-shaped eRF1 protein is a class I factor with three domains[15]. The amino-terminal domain recognizes the termination codons with high fidelity similar to the codon-anticodon mechanism[15]. Peptidyl-tRNA hydrolysis is facilitated by the middle (M) domain[15]. The c-terminus interacts with the class II factor eRF3, which is a translational GTPase similar to eEF1A[15]. Ultimately, the eRF1-eRF3-GTP ternary complex interacts with the ribosome. GTP hydrolysis results in a conformational change that places the M domain of eRF1 into the PTC and the amino-terminal domain is able interrogate the stop codon while eRF3 is released[15].

While eRF1 and eRF3 have been shown to have lower rates of ribosome recycling, the ATPase ABCE1 is proposed to promote efficient eRF1-mediated peptide release and subsequent ribosome subunit splitting/recycling[15,17]. Multiple rounds of initiation typically occur on a single mRNA, sequentially. These initiation events often happen prior to the end of previous rounds of translation. This results in an mRNA being translated simultaneously by more than one ribosome, which produce molecular structures known as polysomes[18].

As previously mentioned, the mRNA not only contains protein coding information, but also regulatory information. Already noted are the 5'-m^7GpppN-cap and the 3'-poly(A) tail[13,14] that recruit eIFs to not only promote, but also delay translation initial. The 5' UTR may also contain upstream ORFs (uORFs) can affect the production of desired protein products. Secondary RNA structures in the 5' UTR have also been shown to affect scanning and therefore change the efficiency of translation initiation[19]. Lastly, binding sites for RNA binding proteins (RBPs) and microRNAs (miRNAs), capable of promoting or repressing translation, can be found in the 5' UTR that regulate the stability and translation of the mRNAs[19–26]. The 3' UTR is also host to RNA structures, RBP binding sites, and miRNA binding sites that affect mRNA stability and translation[21,23–28].

The ORF also contains regulatory information in multiple forms. As with 5' and 3' UTRs, miRNAs and RBPs have been shown to bind within ORFs as well and exhibit regulatory function[24,29–32]. Alternative start sites using either cognate start codons, near-cognate start codons, or internal ribosome entry sites (IRESs) are able to impact mRNA products and stability[33–37]. Even codon

usage, *i.e.* codon optimality, within the ORF can affect mRNA stability and protein synthesis[38,39]. Thus, a multitude of translational control mechanisms exist at each step of the process, affecting protein synthesis, all of which are driven by the mRNA and often its translation.

1.3 Ribosome-Associated Quality Control Pathways

Eukaryotes use multiple mechanisms of RNA surveillance and decay for its maintenance, four of which are associated with translation (*i.e.* Nonsense Mediated Decay, NMD; Non-Stop Decay, NSD; No-Go Decay, NGD; Non-functional ribosomal RNA decay, NRD). Although the canonical mRNA substrate(s) identified to activate each is typically different, these pathways require, and are driven by, active translation of mRNAs by the ribosome. Interestingly, one motif is capable of activating all four pathways directly or indirectly: the polyadenosine (polyA) tract. This particular motif is integral to this work and will be briefly associated with the context of each mechanism; particularly NGD and NSD.

1.3.1 Nonsense Mediated Decay (NMD)

NMD results from a ribosome encountering a premature termination codon (PTC). Multiple models of PTC recognition by the NMD machinery have been proposed and are dependent upon whether or not an exon junction complex (EJC) exists[40,41]. Generally speaking, the presence of a PTC increases the length of the 3' UTR and therefore the distance between the translation release factors and polyA-binding protein (PABP); a positive effector of translation termination and inhibitor of NMD factor binding[42]. Upon encountering a PTC in the absence of an EJC, it has been proposed that the release factors are able to directly recruit NMD factors (*e.g.* UPF1-3) while the EJC aids in this recruitment. Ultimately the ribosome subunits are split

and recycled while the mRNA and nascent polypeptide are degraded[40–42]. The polyA tract motif is able to induce NMD via frameshifting events that result ribosomes encountering typically out-of-frame PTCs[43–47].

1.3.2 No-Go Decay (NGD)

NGD occurs in the context of translation elongation of mRNAs containing secondary structures, problematic nucleotide sequences, and inhibitory peptide sequences[40]. This is triggered by ribosome collision, whereby a normally translating ribosome collides with a stalled ribosome[48]. The resulting di-ribosome (disome) results in assembly of the ribosome-associated quality control triggering (RQT) complex. The receptor for activated C kinase 1 (RACK1) is necessary for pathway activation, recruiting the ZNF598 E3 ubiquitin-protein ligase – suggested to recognize the inter-ribosomal interface of interacting RACK1 proteins – resulting in ubiquitination of uS3, uS10, and eS10[48–52]. This ubiquitination recruits other RQT complex factors via ubiquitin-binding CUE domains. The RQT response is dependent on the ATPase hydrolysis-driven helicase activity of activating-signal co-integrator complex (ASC-1) subunit 3 (ASCC3), which is recruited by its CUE domain containing binding partner ASCC2 in complex with the zinc-finger type protein TRIP4; the subunits comprising the RQT complex[51,53].

During NGD the endonuclease N4BP2 is also recruited via its CUE domains where it cleaves the mRNA, which is stimulated by the complexed Pelota and HBS1-like proteins (homologous to eRF1 and eRF3, respectively)[40,54–56]. The Pelota and HBS1-like complex, along with ABCE1, begin the process of ribosome rescue by subunit dissociation[40,57,58]. After subunit dissociation, the cleaved mRNA 5’ fragment is degraded by the Ski complex and exosome in a 3’ to 5’ fashion.

The cleaved mRNA 3’ fragment is degraded by Xrn1, after Rlg1-mediated phosphorylation of the 5’-hydroxy end[59], in a 3’ to 5’ direction[51].

The RQC complex (Ltn1, TCF25, NEMF and p97) rescues the 60S subunit-peptidyl-tRNA complex[51]. The nascent polypeptide is elongated by the C-terminal addition of multiple alanyl and threonyl residues (CAT-tailing) in a template-free, 40S subunit independent manner mediated by NEMF[51]. This is thought to be a fail-safe mechanism ensuring efficient ubiquitination by E3 ubiquitin ligase Ltn1, recruited by NEMF[60], on the extruded lysine residues[61]. Subsequently, p97 with cofactors Ufd1 and Npl4 extricate the nascent polypeptides for proteasomal degradation[51].

Intragenic polyA tracts have been demonstrated to negatively regulate gene expression through stalling and frameshifting; ostensibly an almost universally conserved feature conserved[43,44,47]. The exploitation of this conserved stalling phenotype has been well characterized in other organisms to also generate alternative proteins[44] and has been used regularly to obtain ribosome structural data. However, the details regarding the mechanisms of polyA tract stalling and frameshifting have remained elusive until recently. The data suggests a two-step mechanism for stalling whereby repetitive, cumbersome lysine residues clash in the 60S peptide transferase center, reducing the rate of aminoacyl transfer and subsequently translation. This allows for rearrangement of the 40S decoding center such that the repeating adenosines are able to forma single-stranded mRNA helical structure mediated by 7π-stacking interactions that conserved residues in the decoding center stabilize. This results in a decoding-incompetent nucleotide structure, preventing canonical codon:anticodon

interactions subsequently inhibiting delivery of the tRNA–eEF1A–GTP ternary complex[62,63]. The precise mechanism driving -1 frameshifting is still unknown, but the loss of frame due to more than 3 nucleotides in the decoding region A-site would certainly be influential.

1.3.3 Non-Stop Decay (NSD)

NSD is triggered by the lack of a stop codon; a fault in translation termination. This occurs in the case of a truncated mRNA (stop codon-less mRNA) or the ribosome running into the poly(A) tail (non-stop mRNA), which are identified during translation termination. Truncated mRNA substrates can be produced either endonucleolytic cleavage in the coding region of the ribosome or premature polyadenylation or abortive transcription[64,65]. Non-stop mRNAs are generated by premature polyadenylation[64,65] or frameshifting events[43–46,66]. The stalled ribosome is recognized in the same fashion as NGD[40,41,50,51,64,65,67,68]. The stall results upon the interaction of the positive charge of polybasic lysine stretch and the negatively charged ribosome exit channel cause translational arrest after as few as six lysines[40]. The attempted decoding of polyA tail also plays a role in stalling similar to encountering an internal polyA tract[62,63].

1.3.4 Nonfunctional Ribosome Decay (NRD)

Surveillance of ribosomal RNAs (rRNAs) is also necessary. Ribosome biogenesis is a highly regulated and energetically expensive process[41,69,70]. The NRD pathway is involved in this process to ensure initial proper ribosome synthesis. However, due to the long-lived nature of rRNAs, they are prone to significant damage from genotoxic and proteotoxic stress[70–75]. Therefore, it is also important that once released from the synthesis pathway, monitoring of

mature rRNA function continues. This is also performed by the NRD pathway[70,72–75]. Previous work has shown that this pathway can be separated into two parts, one for each ribosomal subunit[70,72,74]. The 60S subunit NRD is induced by defects in the peptidyl transferase center[70,72] and is associated with factors previously described in DNA repair: CDC34, Hrt1, the ubiquitin E3 ligase Rtt101p, Mms1p, and a yet to be discovered ribosome-specific adaptor protein[73]. This arm of NRD has been thought to rely on ribosomal protein ubiquitination through these proteins. The 40S subunit NRD pathway was initially shown to be dependent on defects in translation elongation and tied into the NGD machinery[70]. However, recent work has demonstrated that ubiquitination of the 40S ribosomal proteins in a site-specific, sequence-dependent manner is also required for 40S NRD, namely uS3 (rps3), by the coordinated efforts of the ubiquitin ligase ZNF598, receptor for activated C-kinase (RACK1), [76,77]. This link between the mRNA surveillance and rRNA surveillance machinery supports the possibility for mRNA-induced rRNA decay. In fact, the polyA motif has been associated with necessary ribosomal protein ubiquitination and NRD activation[78,79].

1.4 Adaptation of Translational Machinery in Malaria Parasites to Accommodate Translation of Poly-Adenosine Stretches Throughout Its Life Cycle

Preface

The following work was completed by myself, Slavica Pavlovic Djuranovic, and Sergej Djuranovic. JE produced all figures and tables. All authors contributed equally to writing and revising of this review. This section is published in its entirety[80] and is available at https://www.frontiersin.org/articles/10.3389/fmicb.2019.02823/full. This article is distributed under the terms of the Creative Commons Attribution License 4.0 (https://creativecommons.org/licenses/by/4.0/), which permits unrestricted use, distribution, and reproduction in any medium, provided the original author and source are credited.

1.4.1 Abstract

Malaria is caused by unicellular apicomplexan parasites of the genus *Plasmodium*, which includes the major human parasite *Plasmodium falciparum*. The complex cycle of the malaria parasite in both mosquito and human hosts has been studied extensively. There is tight control of gene expression in each developmental stage, and at every level of gene synthesis: from RNA transcription, to its subsequent translation, and finally post-translational modifications of the resulting protein. Whole-genome sequencing of *P. falciparum* has laid the foundation for significant biological advances by revealing surprising genomic information. The *P. falciparum*

genome is extremely AT-rich (~80%), with a substantial portion of genes encoding intragenic polyadenosine (polyA) tracks being expressed throughout the entire parasite life cycle. In most eukaryotes, intragenic polyA runs act as negative regulators of gene expression. Recent studies have shown that translation of mRNAs containing 12 or more consecutive adenosines results in ribosomal stalling and frameshifting; activating mRNA surveillance mechanisms. In contrast, *P. falciparum* translational machinery can efficiently and accurately translate polyA tracks without activating mRNA surveillance pathways. This unique feature of *P. falciparum* raises interesting questions: (1) How is *P. falciparum* able to efficiently and correctly translate polyA track transcripts, and (2) What are the specifics of the translational machinery and mRNA surveillance mechanisms that separate *P. falciparum* from other organisms? In this review, we analyze possible evolutionary shifts in *P. falciparum* protein synthesis machinery that allow efficient translation of an AU rich- transcriptome. We focus on physiological and structural differences of *P. falciparum* stage specific ribosomes, ribosome-associated proteins, and changes in mRNA surveillance mechanisms throughout the complete parasite life cycle, with an emphasis on the mosquito and liver stages.

1.4.2 Introduction

Plasmodium spp. has been in existence long before humans were on Earth, with an estimated origin of malaria-causing parasites appearing around 165 million years ago. Consequently, mosquitos and malaria had millions of years to co-evolve before either ever interacted with humans[81]. The infection of humans occurred evolutionarily recently, and probably with multiple *Plasmodium* parasite species. *P. falciparum* and *P. vivax* established themselves as a major

malaria causing species. *P. falciparum* a most virulent agent in human malaria began speciation around 50,000 years ago followed by the population bottleneck around 5000 years ago but higher level of genetic diversity suggests that *P. vivax* is older[82,83]. *P. malariae*, *P. ovale*, and rare cases of *P. knowlesi* were also reported in human hosts. From the mid-19th century onward, malaria reached its global limits and exacted immensely high numbers in sickness and death. While increased malaria prevention and control treatments have reduced the health burden of malaria, there are still 219 million cases of infection per year resulting in 435,000 deaths[84]. The complex cycle of the malaria parasite in both mosquito and human hosts has been studied extensively (**FIGURE 1.1**). In each of these life cycle stages, gene expression is tightly controlled[85–92].

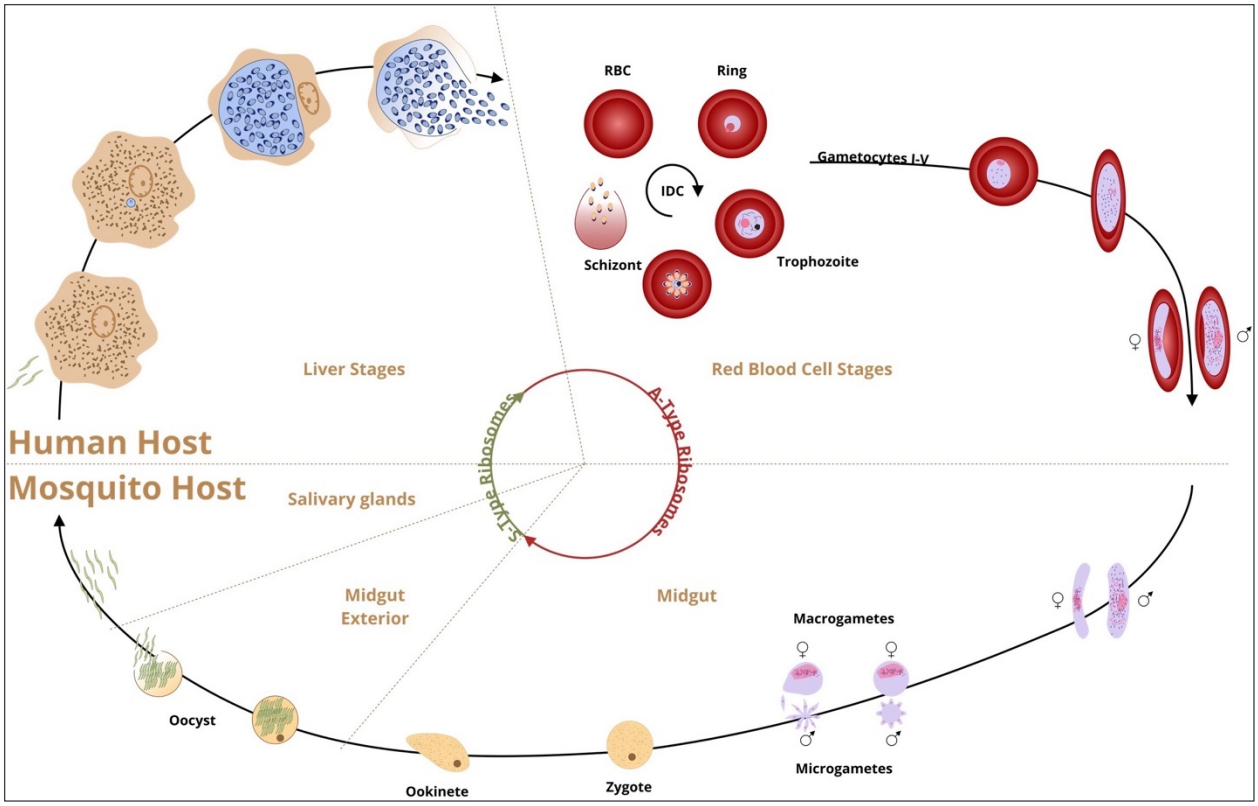

FIGURE 1.1 | Schematic presentation of *P. falciparum* life cycle and stage-specific ribosomal RNAs (A and S type). Human infection by *P. falciparum* begins when an infected female anopheline mosquito inoculates sporozoites into the bloodstream during feeding. The sporozoites invade liver cells and transform into trophozoites. In 6–8 days one mature schizont will release thousands of liver-stage merozoites into the bloodstream (exoerythrocytic schizogony, the first proliferative stage). The second asexual proliferative stage blood stage (erythrocytic schizogony) starts when the liver-stage merozoites invade the erythrocytes About 14–16 erythrocytic merozoites are generated in a 48-h cycle for re-infection and it is the point when the symptoms start. The merozoites may differentiate into single gametocytes, the initial stage of the sexual reproduction (gametogenesis) or continue the asexual cycle. Mosquito infection begins when the gametocytes are taken by mosquito with the blood meal. The male microgametocyte exflagellates into individual microgametes and fertilizes the female macrogamete. The zygote transforms into a motile ookinete, penetrates the mosquito midgut and develops into an oocyst. After 9–14 days, thousands of sporozoites are differentiated in the mature oocyst (sporogony), the only multiplicative stage in the mosquito. Mature sporozoites invade salivary glands and with the next blood meal the cycle continues.

It took years of laborious efforts to sequence *P. falciparum* genome[93]. Sequences of single or multiple chromosomes as well as complete genome were reported over the course of 4 years[94–99]. The high AT-content of the genome made gap closure in sequences extremely difficult. However, long-read, single molecule, real- time sequencing allowed for complete telomere-to-telomere de novo assembly of the *P. falciparum* genome thereby overcoming the problems associated with next generation sequencing of AT- rich genomes[100]. The consequence of AT-richness is the presence of extended tracts of As, Ts, and TAs in introns and intergenic regions[101,102] as well as unusually high number of genes containing coding polyadenosine (polyA) repeats compared to the other species[103,104]. Repetitions of 12 or more adenosine nucleotides in gene coding sequences, so-called polyA tracks, were recently found to act as negative gene regulation motifs at the level of mRNA translation in all tested organisms[43,47]. Consequently, polyA tracks have been evolutionarily preserved in a select set of genes, but are generally selected against in overall gene coding sequences[43].

Recent analysis of 250 eukaryotic genomes found a median of 2% of transcripts with polyA tracks[103]. However, *Plasmodium* species represent an exception to this rule. The percentage of polyA carrying transcripts in the genome exceeds 60% for most *Plasmodium spp.*, including *P. falciparum* (64%)[104]. The pervasive ribosomal stalling and frameshifting found on polyA tracks in other eukaryotes[43,47,105] would make it almost impossible for the majority of *Plasmodium* proteins to be efficiently and correctly synthesized. However, global studies of *Plasmodium* protein composition[106,107] and protein synthesis[85,89,90] do not show any reduction in either the

protein or mRNA abundances of polyA track genes. This suggests that both ribosomal stalling and frameshifting in *Plasmodium* are resolved by adaptations in protein synthesis and mRNA quality control systems. In this review, we will discuss how the extreme AT-rich genome of malaria-causing parasite promoted special features in *P. falciparum* ribosomes to enable translation of polyA tracks throughout the complete life cycle. Additionally, genomic changes and parasitic environment have also influenced variation in mRNA surveillance mechanism within the organism resulting in divergence from other Eukaryotes.

1.4.3 Evolution of AT-Richness in *P. falciparum*

Extremes in genomic base composition toward GC- or AT- richness exist in all domains of life[108–111]. The extent of these extremes in nucleotide composition is limited by the necessity of all 20 amino acids and the subsequent requirement of all four nucleotides to encode them. As such, long homopolymeric amino acid repeats appear to be a characteristic of genomes with either bias[102,112,113]. Harboring either extreme AT- or GC-richness affects genomic structure, stability, transcriptome, and codon bias of organisms[111]. As seen in Table 1.1, the *P. falciparum* mean AT-richness of around 80% appears to be one of the highest in all Eukaryotes[95,114–116]. Surprisingly, the higher AT-content of the *P. falciparum* genome cannot be fully explained by increased AT-richness in intergenic regions, but rather by contributions of AT-richness in both coding 76.22% (**TABLE 1.1**) and non-coding genome 90%[95]. Overall, gene organization patterns in *P. falciparum* are not influenced by the AT-bias[101,102,104]. However, what distinguishes *Plasmodium* species from other AT-rich organisms is distribution of consecutive adenosine nucleotides resulting in unusually high percentage of polyA track genes (**TABLE 1.2**). The genomes of *P. falciparum* and

related *Plasmodium* species have apparently evolved independently to reach extreme AT-bias (**TABLE 1.2**). Interestingly, while the two groups of *Plasmodium* species can be separated based on their AT-genomic content (median of 75% versus a median of 55% AT-richness), both groups accommodate a considerable amount of polyA tracks within the coding regions[104].

TABLE 1.1 | Comparison of AT-richness and polyA track gene ratios over selected Eukaryotic species.

Organism	CDS % AT richness	PolyA track genes
Plasmodium falciparum	76.22%	63.54%
Plasmodium reichenowi	75.93%	62.93%
Dictyostelium discoideum	72.57%	20.96%
Tetrahymena thermophila	72.50%	28.19%
Saccharomyces cerevisiae	60.39%	5.51%
Plasmodium knowlesi	59.77%	41.42%
Caenorhabditis elegans	57.94%	1.93%
Plasmodium vivax	53.51%	38.85%
Drosophila melanogaster	50.66%	1.10%
Pan troglodytes	50.60%	2.17%
Homo sapiens	49.98%	1.40%
Trypanosoma brucei	49.19%	2.89%
Trypanosoma cruzi	46.83%	2.74%
Toxoplasma gondii	42.88%	1.01%
Leishmania donovani	37.63%	0.19%
Leishmania major	37.52%	0.05%
Leishmania infantum jpcm5	37.50%	0.12%
Acanthamoeba castellanii str neff	37.06%	0.11%
Emiliania huxleyi	31.38%	0.10%
Aureococcus anophagefferens	29.37%	0.33%

The coding region AT-richness from a relevant selection of organisms with high, moderate, and low AT-content was compiled from Habich (2016) and Videvall (2018) and sorted in descending order.

Perhaps just as interesting as the consequences of genomic base composition biases are the factors driving it. Previous studies in *P. falciparum* were unable to conclude the primary role of homopolymeric amino acid repeats in the parasite proteome[113,117]. Nutrient availability to intracellular parasites – as well as endosymbionts – appears to be a major factor in driving AT-richness, particularly nitrogen availability[118,119]. De novo synthesis of nucleotides comes at great metabolic expense, especially regarding G+C nucleotides[119]. A+T nucleotides are less metabolically costly to create and tend to be more abundant. Consequently, A+T nucleotides are easier to scavenge, even in intracellular environments where nutrients may not be readily available. In the case of *P. falciparum*, where de novo synthesis of purines does not occur, the parasites must rely upon purine scavenging and salvage pathways[120–122]. Conversely, pyrimidine de novo synthesis occurs using glutamine and aspartic acid precursors. This appears to be the main source for these nucleotides, with the folate pathway being required for thymidine production[123–125]. However, unlike other intracellular organisms referenced above, the intracellular environment for *P. falciparum* is not necessarily nutrient poor, but perhaps nutrient selective; particularly prior to parasite augmentation of the host cell. While *P. falciparum* has multiple means by which amino acids are obtained, much of its initial amino acid supply is from proteolysis of human host red blood cell hemoglobin[126–128].

TABLE 1.2 | Comparison of AT-Richness and polyA track gene ratios over selected *Plasmodium* species.

Organism	CDS % AT richness	PolyA track genes
Plasmodium gallinaceum	78.81%	71.77%
Plasmodium relictum	78.43%	79.18%
Plasmodium berghei	76.26%	68.26%
Plasmodium yoelii 17x	77.03%	64.96%
Plasmodium falciparum	76.22%	63.54%
Plasmodium chabaudi	74.46%	63.37%
Plasmodium reichenowi	75.93%	62.93%
Plasmodium vinckei petteri	74.91%	62.58%
Plasmodium gaboni	77.56%	61.76%
Plasmodium falciparum camp malaysia	76.71%	61.02%
Plasmodium falciparum nf54	76.55%	60.60%
Plasmodium falciparum fch 4	76.67%	60.57%
Plasmodium falciparum ugt5 1	76.49%	60.45%
Plasmodium falciparum santa lucia	76.75%	60.42%
Plasmodium falciparum palo alto uganda	76.56%	60.33%
Plasmodium falciparum nf135 5 c10	76.56%	59.98%
Plasmodium falciparum malips096 e11	76.50%	59.81%
Plasmodium falciparum 7g8	76.65%	59.72%
Plasmodium yoelii yoelii	75.20%	51.06%
Plasmodium knowlesi	59.77%	41.42%
Plasmodium knowlesi strain h	59.76%	41.42%
Plasmodium vivax	53.51%	38.85%
Plasmodium cynomolgi strain b	57.91%	33.83%
Plasmodium inui san antonio 1	56.37%	31.12%

Plasmodium spp. coding region AT-content and the ratio of polyA affected transcripts was collected[103,116]*. The data are organized in the table to demonstrate a separation of two groups with high and low coding region AT-content and subsequently the number of polyA track containing transcripts. The separation notably occurs along the line of geographic region with the high AT-content organisms being predominantly found in Africa and the low AT-content group in Asia, Southeast Asia, and Latin America. However, the low AT-content group still exceeds that of most organisms.*

This brings us to a second major contributor of AT-richness in intracellular organisms: oxidative stress. Reactive nitrogen (RNS) and reactive oxygen species (ROS) generate oxidative stress resulting in 8-oxoguanine production via guanine oxidation. If left unrepaired in DNA, 8-oxoG is able to pair with adenosine; ultimately causing a G:C to T:A conversion. Compounding the process, hemoglobin degradation produces free heme and H2 O2 , which generates further oxidative stress for the parasite[129]. Additionally, NO and other RNS species may be important factors in the soluble heme-hemozoin equilibration[130]. Interestingly, another erythrocytic parasite from *Apicomplexa* phylum*, Babesia microti*, does not degrade hemoglobin and has a considerably less AT-rich genome (61.02%) and polyA tracks (2.17% of genes with polyA tracks) compared to *P. falciparum*[104,131]. Although *Plasmodium spp.* does supply some of its own antioxidants to cope with oxidative assault, the higher than expected G:C to T:A conversion in the organism suggests a lack of full compensation by the biochemical and/or DNA repair safeguards[125]. While 8-oxoG could potentially result in AT-richness imprinted in the DNA sequence, it causes more problems when found in RNA[132]. The oxidative lesion and incorporation of 8- oxoG in mRNAs reduces the rate of peptide-bond formation by more than three orders of magnitude[133]. The effect of 8-oxoG nucleotides in mRNAs is independent of its position within the codon, results in stalling of the translational machinery, and finally activation of No-Go decay mRNA surveillance mechanisms[133]. As such, the presence of oxidative stress may have driven both an increase in genomic AT-richness and changes in mRNA surveillance mechanisms of *P. falciparum*; which are discussed further below.

AT-richness itself appears to provide a feedback loop in the parasite with its increased indel rates, which are thought to be due to DNA replication slippage on AT repeats. These AT tracks provide amplicon breakpoints for copy number variant (CNV) alteration via non-allelic homologous repair-like mechanism that can be advantageous in altering resistance gene CNV numbers[125,134,135]. Altogether, metabolic and biochemical factors continuously drive the parasite genome toward AT richness, which, in turn, drives indels that potentiate genomic plasticity providing an overall platform for relatively rapid adaptive evolution in the parasite. Unarguably, these factors necessitate increased fidelity in DNA replication and RNA transcription. While the exact details specific to *Plasmodium spp.* evolutionary adaptation toward an AT-rich genome, unique codon biases, and polyA encoded lysine stretches remains to be explored, the role ribosomes play as influential factors in this process is certain.

1.4.4 The rRNA and Specialized Ribosomes of *Plasmodium*

The most abundant genes in cells and genomes from bacteria to eukaryotes are those encoding ribosomal RNA. Ribosomal RNA genes in eukaryotic cells form clusters with a highly repetitive structure. *S. cerevisiae*, a single cell organism, has 150 rDNA repeats in one cluster on chromosome XII, while human cells contain five clusters of approximately 70 rDNA repeats on five different chromosomes[136]. The organization of rDNA genes in clusters is conserved among most of the eukaryotic organisms[137]. Transcription of these clusters is highly coordinated to meet the huge demand for ribosomes, which occupy ~50% of the total protein mass in a cell[138]. *Plasmodium* genomes, however, have only 4–8 single copy rDNA units that are encoded on different chromosomes[139–141]. Such a small number of rDNA copies throughout the genome is

seen elsewhere only in bacteria. *E. coli* has seven ribosomal RNA genes spread over its circular genome and well positioned in the regions near an origin of replication. This arrangement in *E. coli* enables maximum ribosomal RNA transcription while preventing possible collisions between replication forks and transcription machinery[142]. Thus, while most of the other organisms have optimized ribosome production, how the malaria-causing parasite produces its significant ribosome numbers is still unknown. It might be possible that massive DNA replication that occurs throughout its lifecycle (during shizogeny) in both hosts may accommodate the rRNA production requirements.

Besides this unusual rDNA arrangement, malaria parasites are pioneers in the new era of specialized ribosomes[140,143–146]. *Plasmodium spp.* has structurally distinct, stage-specific ribosomes and are the most well-known case of rRNA heterogeneity[144]. The difference in sequence and expression profile during the life cycle classified them into A-type (asexual stage specific) and S-type (sporozoite specific) in the majority of *Plasmodium* species, including *P. falciparum*; with *P. vivax* having a third O-type rRNA[141]. The A-type is present in the liver and blood stage and S-type is sporozoite specific rRNA type that emerges during the mosquito stage and ends during the parasite development in hepatocytes[147]. Here, we will focus on the process by which the ribosome types switch and whether ribosomes with distinct rRNA play a selective role in the mRNAs they translate.

Plasmodium spp. have adapted to translation in two different hosts. This requires translation optimization at two distinct temperatures, one of which can be highly variable depending on

the mosquito environment. Even though one would think that changes in temperature and hosts would be the reason for development of different rRNAs, the presence of A-type during the early mosquito stage and S-type during early liver stage does not support that idea[148]. The rRNA sets are not expressed in an exclusive and binary (on/off) fashion, but more as a dynamic, heterogeneous population whereby one subtype, A or S, is the more dominant rRNA type in a particular lifecycle stage. While the idea of a thermoregulatory nature of the rRNA units has been explored earlier in P. berghei, rodent malaria, it has not been followed since[148]. *P. berghei*, contains four distinct copies off the rRNA (A, B, C, D) and they are divided into A-type (A and B) and S-type (C and D). A single copy of the S-type gene, C or D was sufficient for life cycle completion, which only affected the parasite fitness. The group was unable to disrupt both S-type genes simultaneously; nor could they disrupt either of A-type genes[149]. Interestingly, authors noticed growth retardation in oocyst development, which was more pronounced in D-unit disruption rather than in C-unit[149]. Such difference could be explained by difference in ribosomal levels stemming from different transcriptional levels of C- and D-units or functional diversity of C- and D-unit containing ribosomes[146,150]. The disruption of specific S-type rRNA is also associated with oocyst development defects in the second rodent parasite P. yoelii[151]. Finally, van Spaendonk et al. (2001)[149] note a lack in differences between core catalytic components (e.g., GTPase center) of the ribosome large subunit in *P. berghei* that were previously described in *P. falciparum*[145]. These results among species of *Plasmodium* potentiate the question of some aspect of ribosomal specialization[91].

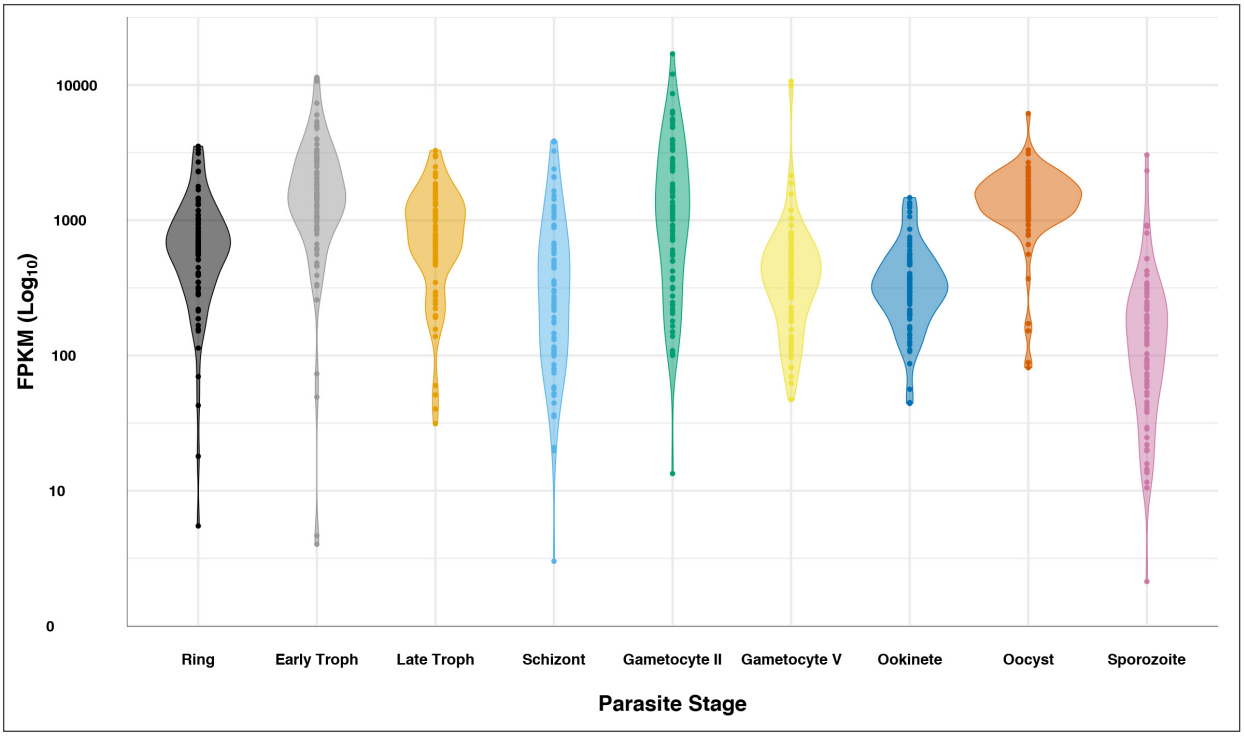

FIGURE 1.2 | *Plasmodium falciparum* ribosomal protein expression over life cycle. RNAseq data[152,153] for the 82 cytosolic ribosomal proteins was queried from PlasmoDB[154] for ring, early trophozoite, late trophozoite, schizont, gametocyte II, gametocyte V, ookinete, oocyst, and sporozoite stages. Data is displayed in log scale as a violin plot, showing the general trend of ribosomal protein transcripts. Data for each ribosomal protein is represented as a dot in the plot.

Previous bacterial work has shown changes in rRNA operon expression in response to stress, resulting in phenotypic changes[155]. The change in *Plasmodium spp.* rRNA population dynamics in response to environmental stress from host transfer is reminiscent of the bacterial changes in rRNA operon expression. However, whether changes in ratios of *Plasmodium spp.* rRNA types drive phenotypic changes is still unknown. Ostensibly, the ribosomes share the same repertoire of ribosomal proteins. RNAseq data shows that while ribosomal protein gene transcription as a whole is fairly persistent throughout the complete life cycle of *P. falciparum*, oscillations in their overall expression pattern match that of stages with increased protein synthesis (**FIGURE 1.2**).

This does not exclude the highly sought-after notion that a specific set of ribosomes may be optimized for specific mRNA substrates or cell populations that may also exist in Plasmodium spp. A recent study in zebrafish showed that embryos have different subtypes of 5.8S, 18S, and 28S rRNAs, creating similar ribosome diversity seen in *Plasmodium* cells[156]. In silico data have shown that the expanded regions of 18S subunit expressed in zebrafish embryos may preferentially bind maternal transcripts when compared to somatic subtypes[156]. Similarly, a shift in the expression of 16S rRNA ribosome variants created populations of *E. coli* cells that accommodated functional differences in tetracycline binding[155]. As was mentioned before, the rRNA heterogeneity that was mostly known in *Plasmodium* parasites[139,140,146,147,157] is now recognized in other organisms[155,156]. However, the role of different *Plasmodium* rRNAs as a response to different environmental conditions is still not defined.

1.4.5 *Plasmodium* Ribosomes, PolyA and Poly-Lysine Sequences

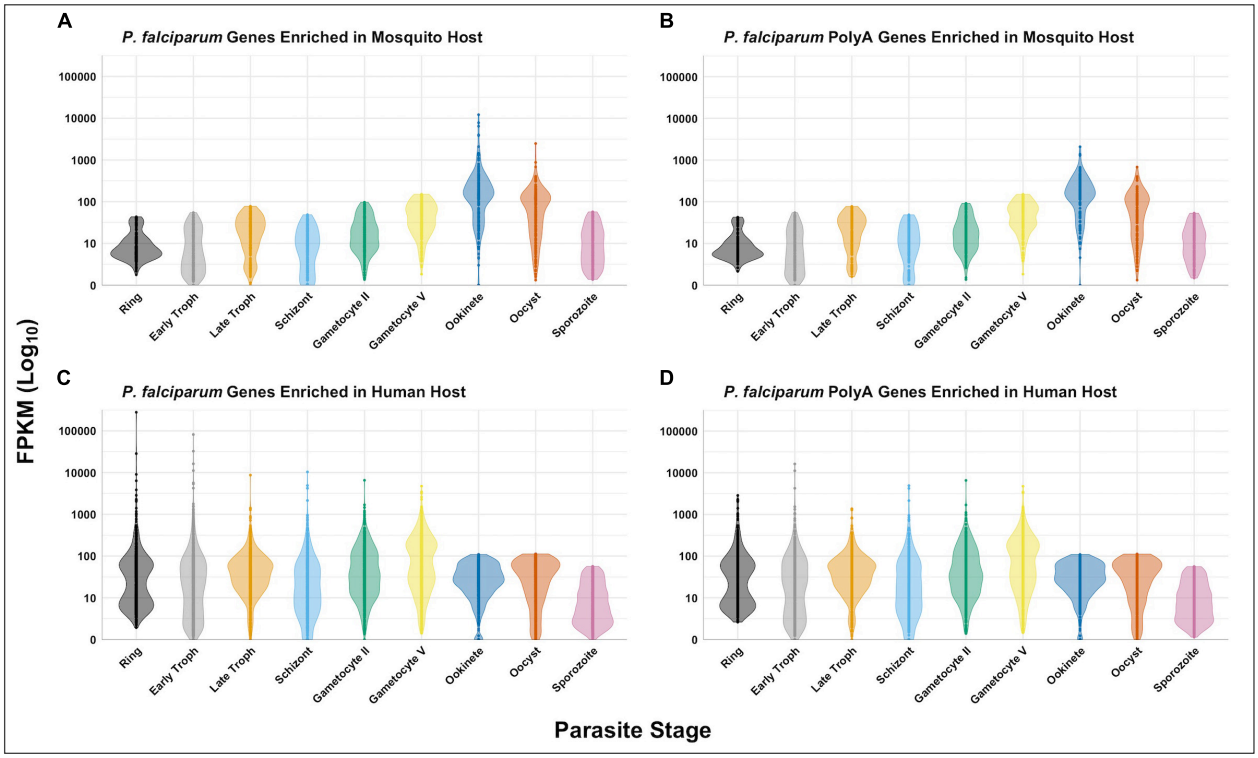

FIGURE 1.3 | Expression of *P. falciparum* genes in different hosts. The data was queried from PlasmoDB[152–154] for protein-coding genes with expression data greater than or equal to the 80th percentile for ring, early trophozoite, late trophozoite, schizont, gametocyte II, gametocyte V, ookinete, oocyst, and sporozoite stages. *P. falciparum* genes enriched in the mosquito host **(A)**, human host **(C)**, and polyA genes for each (**B** and **D**, respectively) are as previously defined. RNAseq data for all stages in both hosts for these gene sets are displayed in log scale as a violin plot with all data points for comparison.

Regardless of the host, all *Plasmodium spp.* rRNA types must contend with the translation of unusually high AU-content and long-coding polyA stretches in mRNAs. RNA-seq data[85,86,89,90,134] indicates that the mRNA levels of genes containing polyA stretches follows the same trend as the general gene expression for all stages in both hosts (**FIGURES 1.3A–D**). We can conclude that both types of ribosomes expressed in both hosts have features allowing efficient translation of transcripts containing long, coding polyA tracks. This indicates that *P. falciparum* ribosomes

have higher fidelity during translation of polyA sequences and are able to accommodate long polybasic peptides coming through their protein-exit channel. Previous ribosome mutagenesis studies in *S. cerevisiae* suggested functional differences in the GTPase centers of *P. falciparum* A- and S-type ribosomes[145]. Despite the differences in yeast viability and growth rates, chimeric yeast ribosomes with either *Plasmodium*'s A- or S-type GTPase centers exhibited increased translational accuracy[145]. Even though there are stage-specific ribosomes, there is a group of genes that is present in human and mosquito that contain polyA tracks (**FIGURE 1.4**). More recently it was also shown that the *P. falciparum* ribosomes have been altered to accommodate the poly-lysine patches that are prolific throughout the proteome[104]. To allow these low-complexity, homopolymeric and polybasic amino acid repeats, the parasite ribosome exit channel has been altered by increasing the channel size at key bottle necks, as well as a reduction in the hydrophobicity patches typically seen in bacterial, yeast, or human ribosomes[104].

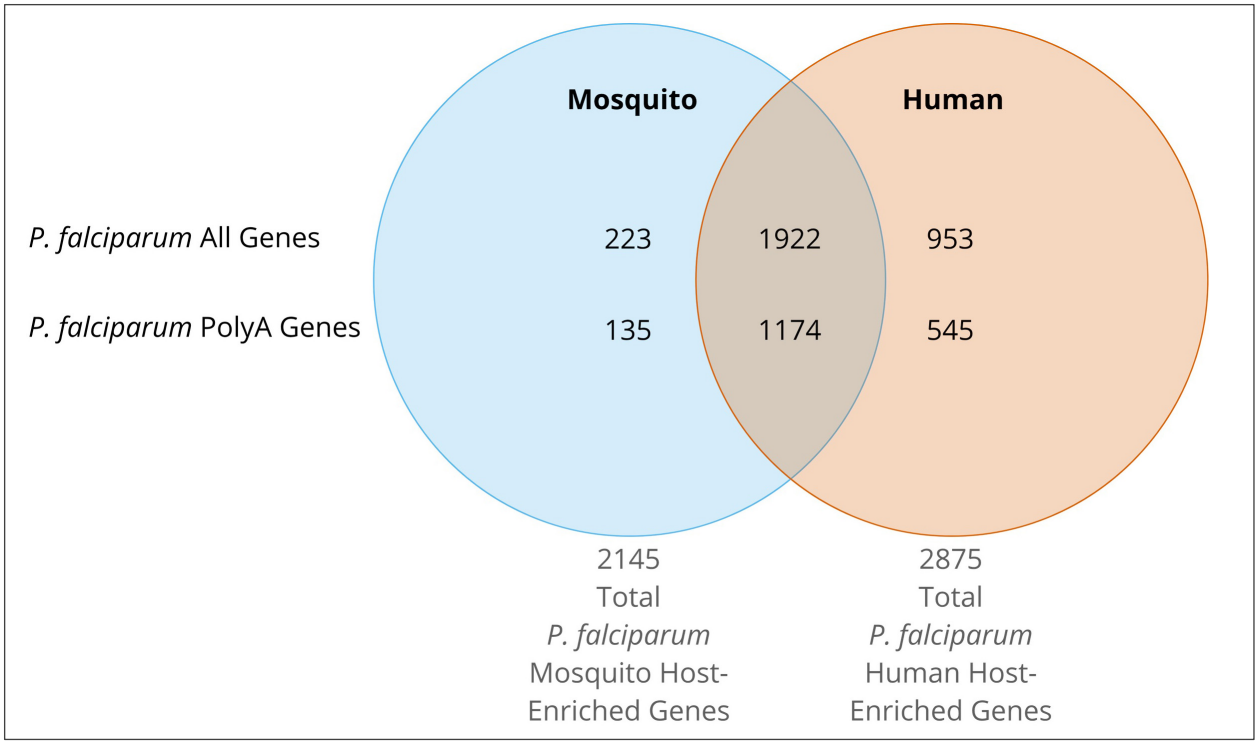

FIGURE 1.4 | Venn Diagram of *P. falciparum* gene expression from RNAseq data. The expression data greater than or equal to the 80th percentile for ring, early trophozoite, late trophozoite, schizont, gametocyte II, gametocyte V, ookinete, oocyst, and sporozoite stages was queried[152,153]. Mosquito stage total genes were defined as those with expression data greater than or equal to the 80th percentile during gametocyte V, ookinete, oocyst, or sporozoite stages. Mosquito host-specific genes are defined as above, but solely in mosquito host stages. Total parasite genes expressed in the human host were defined as those with expression data greater than or equal to the 80th percentile during sporozoite, ring, early trophozoite, late trophozoite, schizont, gametocyte II, or gametocyte V stages. Enriched parasite genes expressed in the human host are defined as above, but solely in human host stages. PolyA genes are those defined as having one or more runs of twelve or more consecutive adenosines in the coding region of the gene.

Ribosome profiling and biochemical assays suggest an increased or modified fidelity such that parasite ribosomes do not stall or frameshift on polyA tracks[104]. The mechanism of this altered fidelity may result from not only modification of the ribosomal RNA sequence, but also via changes to key protein components of ribosomes. Two *P. falciparum* ribosome cryoEM structures suggest a reduced or lost interaction of the receptor for activated C kinase 1 (RACK1)

to *Plasmodium* ribosomes[158,159]. RACK1 has been established as an integral ribosomal scaffold protein[160]. Beside other non-ribosome associated functions, RACK1 was found to be important for cap-dependent translation initiation, IRES-mediated translation, and site-specific translation[161]. RACK1 also contributes to the translation arrest that is induced by translation of polyA sequences[162,163], CGA-CGA codons in yeast[164], or runs of consecutive basic amino-acid[163]. Stalls on polyA tracks can be resolved in mammalian cells by deletion of RACK1 and ZNF598, thus enabling read-through of stall-inducing sequences[50,77,79]. *S. cerevisiae* ribosomes lacking the RACK1 homolog Asc1 are able to translate through the CGA-CGA stalling sequences and increase normally attenuated protein output[164]. The increase in amount of synthesized protein from CGA- CGA sequences is a consequence of overall reduced elongation rates of yeast ribosomes that lack Asc1[165]. Slower elongation rates may also influence cellular responses to ribosome pausing. The position of RACK1/Asc1 near the mRNA exit channel on the ribosome could be important in sensing ribosome collisions that lead to activation of ribosome rescue and mRNA surveillance pathways[132,165,166]. The fact that *Plasmodium* ribosomes lack interaction with PfRACK1 could be beneficial for translation of polyA tracks into poly-lysine runs. However, based on previous conclusions concerning the role of RACK1/Asc1 in correct reading frame maintenance during translation of stalling sequences, the majority of polyA coding sequences in malaria parasites would be predicted to have multiple frameshifted protein products.

Previous studies[163,167,168] proposed that stalling during the translation of polyA tracks is due to synthesis of the poly-lysine rich nascent peptide. Electrostatic interactions of the polybasic peptide and the peptide exit tunnel in the ribosome would elicit ribosomal stalling[167]. Recent

studies revealed that an mRNA-mediated mechanism is directly contributing to stalling[43,47,165]. Consecutive adenosines are engaged by the ribosome decoding center nucleotides, are stabilized on both sides by rRNA base stacking interactions[165], and adopt a helical conformation typical for single stranded polyA stretches[169]. PolyA tracks are highly efficient at causing ribosome stalling, and the inhibitory conformation of polyA mRNA bases can further contribute to a polyA-mediated stalling mechanism. This conclusion is in line with the previous observations that consecutive AAG codons are less efficient at causing stalling than AAA codons[43,47], despite coding for the same amino acid. Altogether, the charge and conformation of the poly-lysine nascent chain in conjunction with the stacked polyA mRNA nucleotides in the decoding center of the ribosome contribute to the overall stalling mechanism[165]. *P. falciparum* ribosomes are again the exception to this rule. The nucleotides that make stacking interactions with polyA repeats are conserved in *P. falciparum* ribosomes. However, both endogenous transcripts and reporter sequences with long runs of polyA tracks are efficiently translated by *Plasmodium*[89,104,170]. Thus, in order to adapt to polyA track translation for production of the polybasic and homopolymeric lysine repeats, the malaria-causing parasite has altered the sequence of its rRNA, its ribosome structure, its ribosomal proteins, and its mRNA translation quality control pathways.

1.4.6 mRNA Surveillance Pathways in AU-Rich Transcriptome of *P. falciparum*

The core elements for mRNA translation are highly conserved in *Plasmodium spp.*[91]. The unique features involving protein synthesis in *Plasmodium*, such as different types of ribosomes in different life cycle stages, were noticed even before genome sequencing of the malaria

parasite[139,147,149,157]. However, the presence of an unusual number of mRNA binding proteins and the absence of some elements of mRNA surveillance mechanism were noticed upon completion of the *P. falciparum* genome sequence[52,85,89,92,139,140,149,157,171]. A recent review elaborated on the translational regulation in blood-stages of malaria parasites[91]. They focused on cytoplasmic mRNA translation and the fate of mRNAs: decoding of the mRNA messages by the 80S ribosomes, degradation of mRNAs by exo- or endonucleases (mRNA decay), and sequestration of mRNAs by protection from mRNA decay or by inhibition of translation. We focus here on the mechanism of activation of mRNA surveillance pathways by aberrant mRNAs in the context of unusual AU-richness and abundance of polyA tracks in *Plasmodium* transcriptome.

Eukaryotic cells have developed mechanisms to protect themselves from the production of the possible toxic proteins due to aberrant mRNA translation events. There are three mRNA quality control systems for translational errors in eukaryotes: Non-sense mediated decay (NMD), No-Go decay (NGD), and Non-Stop decay (NSD). NMD targets transcripts harboring “premature” termination codons (PTC) and nascent polypeptide chains synthesized from such transcripts for efficient degradation[40]. Components of NMD pathway distinguishes PTCs from authentic stop codons in the coding sequence. PTCs are usually the product of point-non-sense mutations, ribosomal frameshifting on slippery sequences, aberrant splicing events, or in some cases, the consequence of targeted gene regulation through alternative splicing[88,172]. In higher eukaryotes, PTCs are generally recognized by their proximity to so-called exon-junction

complexes (EJCs), which are deposited near exon junctions during pre-mRNA splicing in the nucleus[40].

No-Go decay is an "umbrella term" for the mRNA surveillance pathway that deals with either damaged or difficult to translate mRNA sequences that cause the ribosome to stall during the elongation cycle of translation. Besides the previously mentioned mRNA base damages (8-oxoG)[132,133], mRNA translation can be stalled by lack of aminoacylated-tRNAs, strong mRNA secondary structure (i.e., stem-loops or long GC-rich regions), or stable interaction of the nascent polypeptide chain with the translating ribosome. Even though Non-Stop Decay (NSD) was discovered earlier than NGD[58,67,68,75,173,174], it became apparent that in mammals and higher eukaryotes, the NSD and NGD pathways share the same effector protein complexes[67]. The NSD targeted mRNAs that originate from premature 3' adenylation or cryptic polyadenylation signals found in coding sequences indeed represent a similar group of transcripts that would be targeted by NGD pathway[67,173,175]. Ribosomes that translate mRNAs without stop codons would eventually stall while translating long polyA tails into poly-lysine repeats, or because they would simply run out of message. Recognition of these types of transcripts, as well as the aforementioned NGD targets, trigger components of NGD/NSD pathways resulting in targeted mRNA cleavage and degradation.

TABLE 1.3 | Comparison of translation quality control factors in *P. falciparum* and its mosquito and human hosts.

Pathway	*H. sapiens*	*A. gambiae*	*P. falciparum*
NMD	eRF1, eRF3, UPF1, UPF2, UPF3A/UPF3B, eIF4AIII, MLN51, Y14/MAGOH, BTZ, SMG1, SMG5, SMG6, SMG7, PP2, Musashi, PABP1	eRF1 (AGAP010310), eRF3 (AGAP009310), UPF1 (AGAP001133), UPF2 (AGAP000337), UPF3 (AGAP006649), eIF4AIII (AGAP003089), Y14 (AGAP006365)/MAGOH (AGAP010755), SMG1(AGAP000368), SMG5 (AGAP008181), SMG6 (AGAP000894), PP2A (AGAP004096), Musashi (AGAP001930)	UPF1 (PF3D7_1005500), UPF2 (PF3D7_0925800), UPF3B (PF3D7_1327700), eIF4AIII (PF3D7_0422700) PF3D7_1327700), PP2A(PF3D7_0925400 – KEGG, PF3D7_1319700 – Hs homology, or PF3D7_0927700 – name), Musashi (PF3D7_0916700), PABP1 (PF3D7_1224300), eRF1 (PF3D7_0212300), eRF3 (PF3D7_1123400)
NGD/NSD	Pelota/HBS1L, RACK1, ZNF598, N4BP2 (Cue2)	Pelota (AGAP008269), HBS1L (AGAP002603), RACK1 (AGAP010173), ZNF598 homolog (AGAP007725), N4BP2 homolog (AGAP002516)	Pelota (PF3D7_0722100), RACK1 (PF3D7_0826700), ZNF598 (PF3D7_1450400)
RQC	CNOT4, ABCE1, TRIP4, ASCC2, ASCC3, NEMF, Listerin, UBE2D1, XRN1	CNOT4, ABCE1 (AGAP002182), ASCC2 homolog (AGAP000428), ASCC3 (AGAP001234), NEMF homolog (AGAP002680), Ltn1 (AGAP007143), UBE2D1 homolog (AGAP000145), XRN1	ABCE1 (PF3D7_1368200), NEMF homolog (PF3D7_1202600), Listerin homolog (PF3D7_0615600), CNOT4 (PF3D7_1235300), ASCC3 homolog (PF3D7_1439100), UBE2D1 homolog (PF3D7_1203900) XRN1 (PF3D7_0909400)

Factors associated with NMD, NGD/NSD, and RQC pathways from the literature and KEGG pathway database in human cells were collected[176]*. Homologs in A. gambiae, one of the most common and effected vectors of P. falciparum*[177–179]*, were collected using KEGG pathways and performing protein-BLAST searching using VectorBase. Confirmation to FlyBase was also used to confirm vague annotations. P. falciparum factors were similarly documented again using KEGG pathways and PlasmoDB protein-BLAST analysis*[154,176,180]*. Homologous gene database IDs are listed for reference. Notably, NGD/NSD factors Hbs1L and Cue2 endonuclease are missing in P. falciparum genome.*

The majority of mRNA surveillance pathway genes have been annotated in the *P. falciparum* genome (**TABLE 1.3**)[87]. However, there are no mechanistic studies to confirm the activity of these pathways. Most of our knowledge on *Plasmodium*'s mRNA surveillance pathways comes from bioinformatic searches using homologous sequences from other eukaryotes. An indirect proof of the existence of NMD in *Plasmodium* is through the studies of alternative splicing of pre-mRNA[88,172]. Regulated alternative splicing events generating transcripts that do not lead to apparent protein synthesis usually carry PTCs, and thus are committed to NMD. Alternative splicing in *P. falciparum* has been reported for several genes like delta-aminolevulinic acid dehydratase (ALAD), stromal processing peptidase (SPP), and chloroquine resistance transporter (PfCRT); among the others. Additionally, studies on the essentiality of *Plasmodium* genes that use the CRISPR/Cas9 technique[181] or transposon techniques[182] rely partially on silencing targeted genes through the activation of NMD. In this case, activation of NMD is the consequence of either mutations that are generated during CRISPR/Cas9 DNA cleavage, transposon insertion in the coding sequence, or due to aberrant splicing events caused by transposons landing in introns of targeted genes. As noted above, more than 60% of the *P. falciparum* transcripts harbor polyA track motifs that are seen as mRNA "slippery" sequences during translation[103,104]. Translation of runs of poly-adenosine nucleotides results in ribosomal frameshifting in most tested organisms causing activation of NMD pathways[43,47]. However, ribosome profiling[89,170] and reporter assays[104] indicate that *P. falciparum* ribosomes maintain fidelity during translation of rather long polyA stretches (more than 36As in a row). Therefore, while there is indirect evidence that the NMD pathway exists in *Plasmodium*, it seems that this

pathway is not upregulated during *Plasmodium* ribosomes' interactions with its polyA runs and AU- rich coding sequences. The most probable reason for this is the above-mentioned changes in ribosome structure and fidelity.

Genomic sequencing has also revealed several critical components of surveillance pathways that are missing. According to NCBI, KEGG, and plasmoDB databases, *P. falciparum* and the majority of other *Plasmodium spp.* lack the NGD and NSD decay pathways components Hbs1[56] and Cue2-RNA endonuclease[54]. With the exception of *S. cerevisiae*, the Hbs1/Pelo protein complex rescues stalled ribosomes on mRNAs. It was postulated that stalling events cause ribosome collisions[48], generating unique disome units consisting of the stalled ribosome and the following colliding ribosome (Beckman and Inada). The disome, as a minimal ribosome collision unit, is recognized by Ribosome-associated Quality Control (RQC) and NGD pathways[58,68,79,174,183]. Activation of RQC and NGD leads to cleavage of stalled mRNA by Cue2, and possibly other unknown endonucleases, which ultimately leads to ribosome rescue by the activity of the Pelo/Hbs1 complex[58,76,175,183,184]. In most of the above mentioned RQC and NGD studies, a typical substrate for ribosomal stalling is a long polyA run, ranging from 36 to 60 adenosines, coding for a peptide with 12– 20 consecutive lysine residues. However, long polyA stretches in *P. falciparum* cells are efficiently translated into poly-lysine repeats[89,170]. Of note, the longest endogenous polyA runs in different *P. falciparum* species range from 88 to 111 nucleotides and code for *Plasmodium* specific and hypothetical proteins[103], which is longer than the length of the normal 3' polyA tail in either *S. cerevisiae* or human cells[185–187]. As such, many endogenous *Plasmodium* transcripts would be NSD targets in other eukaryotic organisms. It is

also a question as to what the signal for NSD pathway is in *Plasmodium* as recent study on 3' mRNA polyadenylation in apicomplexans did not find any differences in *P. falciparum* polyadenylation complex, polyA binding proteins, or polyA tails when compared to other species[176,188]. Because *Plasmodium* lacks the components to rescue stalled ribosomes, and because *Plasmodium* ribosomes efficiently translate long polyA runs, the function and mechanism of the NGD/NSD pathway in *P. falciparum* remains a mystery.

1.4.7 Conclusion

While it may seem reasonable that *P. falciparum* adapted its ribosomes for higher fidelity on polyA runs and in parallel lost the ability to activate the RQC/NGD/NSD pathways, such a scenario is far from obvious. The absence of mRNA surveillance pathway components or deletion of RQC factors leads to both protein aggregation and proteotoxic stress in yeast cells[189–191]. Protein aggregation is observed in *P. falciparum* in the absence of heat shock protein 110[192] but not due to the absence of mRNA surveillance or RQC pathways or as a consequence of increase in both number or length of polyA tracks[104]. This conflicting result, along with the surprising lack of interaction between the ribosomal scaffold protein RACK1/Asc1 and *Plasmodium* ribosomes[158,159], argue that the mRNA surveillance pathways in *P. falciparum* are inherently different from those in other eukaryotes. The diversity of rRNAs, *Plasmodium*'s ribosome structure, and the activity of yet unknown ribosome associated factors promote the possibility of "specialized ribosomes" in *Plasmodium* that allow for polyA tracks translation into functional proteins. Each of the aforementioned changes in parasites translational machinery and mRNA quality control pathways come at the cost of self-fitness

that would normally be detrimental for survival of *Plasmodium* parasites in both humans and mosquitos. And yet the parasite has persisted in both of these hosts for hundreds of millions of years. Parasitologists and epidemiologists have wondered "How?" for decades; now as translational biologists, we add our voices to the same question.

1.5 Summary

The maintenance, replication, and conversion of genetic information is vital to eukaryotic survival. A significant amount of effort is involved in regulating these processes for not only their faithful execution, but also necessary spatial and temporal aspects. This work examines mechanisms of post-transcriptional regulation, specifically those requiring active translation by the ribosome, in the context of the stall-inducing, intragenic polyA motif.

P. falciparum has over 5,000 genes, with the potential for ≥60% having stall-inducing, intragenic polyA motifs. Previous work has shown that polyA motifs cause stalling and frameshifting, resulting in the recruitment of various quality control factors that subsequently degrade the mRNA, nascent protein, and, in some cases, the rRNA. However, this is not the case in *P. falciparum*. Therefore, how the parasite is able to express most of its genome remains an important question from both basic and clinical biology perspectives. In particular, is this ability RNA-mediated, protein-mediated, RQC-pathway alteration-mediated, or a combination thereof? Here, I report on the likelihood that a combination of these factors is at the root of this genus-associated ability.

The work in Chapter 2 highlights the ability of *P. falciparum* to translate polyA tracks, without stalling or losing frame, in reporter constructs compared to the human host and the AT-rich

organism *Tetrahymena thermophila,* as well as endogenous genes. These motifs are also shown to be conserved throughout the *Plasmodium* genus. Interestingly this increased transcriptome AU-richness does not show any increased propensity for structure in the RNA. The ability to translate lengthy polyA stretches also poses a problem for the ribosome. Increased lengths of polylysine amino acids also cause ribosome stalling through peptide exit channel electrostatic interactions and bulky residue clashing in the peptide transferase center. However, changes to the peptide exit channel of the parasite ribosomes demonstrate translation machinery modifications that would condone polylysine stretches.

In Chapter 3, I adapted RNA immunoprecipitation methods for *P. falciparum.* This method uses the MS2 and PP7 bacteriophage cap proteins to tag rRNAs and mRNAs, respectively. This method allows for the enrichment of the different rRNA types for further examinations. It also enables the isolation of reporter constructs and subsequent analysis of their bound proteome in a context-dependent fashion, which can differ depending on differing RNA motifs.

In Chapter 4, I examine the binding of RACK1 in *P. falciparum*. Previous structural data has suggested that RACK1 does not bind the ribosome. However, given is vital roles in translation and ribosome-associated quality control, how the parasite is able to efficiently translate its mRNA or handle problematic RNAs without any RACK1 interaction suggests a more nuanced modification than the bound/unbound binary. Lastly, in Chapter 5, I discuss the potential future directions of this work, examining vital open questions regarding protein synthesis, ribosome-associated quality control, as well as the still-perplexing topic of ribosome switching in *P. falciparum*.

1.6 References

1. Chatterjee, N. & Walker, G. C. Mechanisms of DNA damage, repair, and mutagenesis. *Environ. Mol. Mutagen.* **58**, 235–263 (2017).
2. Bębenek, A. & Ziuzia-Graczyk, I. Fidelity of DNA replication—a matter of proofreading. *Curr. Genet.* **64**, 985–996 (2018).
3. Sydow, J. F. & Cramer, P. RNA polymerase fidelity and transcriptional proofreading. *Curr. Opin. Struct. Biol.* **19**, 732–739 (2009).
4. Alic, N. *et al.* Selectivity and proofreading both contribute significantly to the fidelity of RNA polymerase III transcription. *Proc. Natl. Acad. Sci.* **104**, 10400–10405 (2007).
5. Gamba, P. & Zenkin, N. Transcription fidelity and its roles in the cell. *Curr. Opin. Microbiol.* **42**, 13–18 (2018).
6. Dey, A. & Chakrabarti, K. Current Perspectives of Telomerase Structure and Function in Eukaryotes with Emerging Views on Telomerase in Human Parasites. *Int. J. Mol. Sci.* **19**, 333 (2018).
7. Su, Y. *et al.* Human DNA polymerase η has reverse transcriptase activity in cellular environments. *J. Biol. Chem.* **294**, 6073–6081 (2019).
8. Lee, H.-C. *et al.* The DNA/RNA-Dependent RNA Polymerase QDE-1 Generates Aberrant RNA and dsRNA for RNAi in a Process Requiring Replication Protein A and a DNA Helicase. *PLoS Biol.* **8**, e1000496 (2010).
9. Cerutti, H. & Casas-Mollano, J. A. On the origin and functions of RNA-mediated silencing: from protists to man. *Curr. Genet.* **50**, 81–99 (2006).

10. Iyer, L. M., Koonin, E. V & Aravind, L. Evolutionary connection between the catalytic subunits of DNA-dependent RNA polymerases and eukaryotic RNA-dependent RNA polymerases and the origin of RNA polymerases. *BMC Struct. Biol.* **3**, 1 (2003).

11. Crick, F. H. On protein synthesis. *Symp Soc Exp Biol.* **12**, 138–63 (1958).

12. Cobb, M. 60 years ago, Francis Crick changed the logic of biology. *PLOS Biol.* **15**, e2003243 (2017).

13. Browning, K. S. & Bailey-Serres, J. Mechanism of Cytoplasmic mRNA Translation. *Arab. B.* **13**, e0176 (2015).

14. Sonenberg, N. & Hinnebusch, A. G. Regulation of Translation Initiation in Eukaryotes: Mechanisms and Biological Targets. *Cell* **136**, 731–745 (2009).

15. Dever, T. E. & Green, R. The Elongation, Termination, and Recycling Phases of Translation in Eukaryotes. *Cold Spring Harb. Perspect. Biol.* **4**, a013706–a013706 (2012).

16. Beringer, M. & Rodnina, M. V. The Ribosomal Peptidyl Transferase. *Mol. Cell* **26**, 311–321 (2007).

17. Shoemaker, C. J. & Green, R. Kinetic analysis reveals the ordered coupling of translation termination and ribosome recycling in yeast. *Proc. Natl. Acad. Sci.* **108**, E1392–E1398 (2011).

18. Warner, J. R., Knopf, P. M. & Rich, A. A multiple ribosomal structure in protein synthesis. *Proc. Natl. Acad. Sci. U. S. A.* **49**, 122–129 (1963).

19. Leppek, K., Das, R. & Barna, M. Functional 5′ UTR mRNA structures in eukaryotic translation regulation and how to find them. *Nat. Rev. Mol. Cell Biol.* **19**, 158–174 (2018).

20. Stripecke, R., Oliveira, C. C., McCarthy, J. E. & Hentze, M. W. Proteins binding to 5' untranslated region sites: a general mechanism for translational regulation of mRNAs in human and yeast cells. *Mol. Cell. Biol.* **14**, 5898–5909 (1994).

21. Wilkie, G. S., Dickson, K. S. & Gray, N. K. Regulation of mRNA translation by 5'- and 3'-UTR-binding factors. *Trends Biochem. Sci.* **28**, 182–188 (2003).

22. Gu, W. *et al.* The role of RNA structure at 5' untranslated region in microRNA-mediated gene regulation. *RNA* **20**, 1369–1375 (2014).

23. O'Brien, J., Hayder, H., Zayed, Y. & Peng, C. Overview of microRNA biogenesis, mechanisms of actions, and circulation. *Front. Endocrinol. (Lausanne).* **9**, 1–12 (2018).

24. Bartel, D. P. MicroRNAs: Genomics, Biogenesis, Mechanism, and Function. *Cell* **116**, 281–297 (2004).

25. Hentze, M. W., Castello, A., Schwarzl, T. & Preiss, T. A brave new world of RNA-binding proteins. *Nat. Rev. Mol. Cell Biol.* **19**, 327–341 (2018).

26. Dassi, E. Handshakes and fights: The regulatory interplay of RNA-binding proteins. *Front. Mol. Biosci.* **4**, 1–8 (2017).

27. Matoulkova, E., Michalova, E., Vojtesek, B. & Hrstka, R. The role of the 3' untranslated region in post-transcriptional regulation of protein expression in mammalian cells. *RNA Biol.* **9**, 563–576 (2012).

28. Mayr, C. Regulation by 3'-Untranslated Regions. *Annu. Rev. Genet.* **51**, 171–194 (2017).

29. Schnall-Levin, M. *et al.* Unusually effective microRNA targeting within repeat-rich coding regions of mammalian mRNAs. *Genome Res.* **21**, 1395–1403 (2011).

30. Zhang, K. *et al.* A novel class of microRNA-recognition elements that function only within open reading frames. *Nat. Struct. Mol. Biol.* **25**, 1019–1027 (2018).

31. Savisaar, R. & Hurst, L. D. Both maintenance and avoidance of RNA-binding protein interactions constrain coding sequence evolution. *Mol. Biol. Evol.* **34**, msx061 (2017).

32. Hafner, M. *et al.* Transcriptome-wide Identification of RNA-Binding Protein and MicroRNA Target Sites by PAR-CLIP. *Cell* **141**, 129–141 (2010).

33. Kochetov, A. V. Alternative translation start sites and hidden coding potential of eukaryotic mRNAs. *BioEssays* **30**, 683–691 (2008).

34. Kochetov, A. V. Alternative translation start sites and their significance for eukaryotic proteomes. *Mol. Biol.* **40**, 705–712 (2006).

35. Rojas-Duran, M. F. & Gilbert, W. V. Alternative transcription start site selection leads to large differences in translation activity in yeast. *RNA* **18**, 2299–2305 (2012).

36. Wang, X., Hou, J., Quedenau, C. & Chen, W. Pervasive isoform-specific translational regulation via alternative transcription start sites in mammals. *Mol. Syst. Biol.* **12**, 875 (2016).

37. Kearse, M. G. & Wilusz, J. E. Non-AUG translation: a new start for protein synthesis in eukaryotes. *Genes Dev.* **31**, 1717–1731 (2017).

38. Wu, Q. *et al.* Translation affects mRNA stability in a codon-dependent manner in human cells. *Elife* **8**, 1–22 (2019).

39. Verma, M. *et al.* A short translational ramp determines the efficiency of protein synthesis. *Nat. Commun.* **10**, 5774 (2019).

40. Shoemaker, C. J. & Green, R. Translation drives mRNA quality control. *Nat. Struct. Mol. Biol.* **19**, 594–601 (2012).

41. Doma, M. K. & Parker, R. RNA Quality Control in Eukaryotes. *Cell* **131**, 660–668 (2007).

42. Brogna, S. & Wen, J. Nonsense-mediated mRNA decay (NMD) mechanisms. *Nat. Struct. Mol. Biol.* **16**, 107–113 (2009).

43. Arthur, L. L. *et al.* Translational control by lysine-encoding A-rich sequences. *Sci. Adv.* **1**, e1500154 (2015).

44. Arthur, L. L. & Djuranovic, S. PolyA tracks, polybasic peptides, poly-translational hurdles. *Wiley Interdiscip. Rev. RNA* **9**, e1486 (2018).

45. Atkins, J. F., Loughran, G., Bhatt, P. R., Firth, A. E. & Baranov, P. V. Ribosomal frameshifting and transcriptional slippage: From genetic steganography and cryptography to adventitious use. *Nucleic Acids Res.* **44**, gkw530 (2016).

46. Advani, V. M. & Dinman, J. D. Reprogramming the genetic code: The emerging role of ribosomal frameshifting in regulating cellular gene expression. *BioEssays* **38**, 21–26 (2016).

47. Koutmou, K. S. *et al.* Ribosomes slide on lysine-encoding homopolymeric A stretches. *Elife* **4**, 1–18 (2015).

48. Simms, C. L., Yan, L. L. & Zaher, H. S. Ribosome Collision Is Critical for Quality Control during No-Go Decay. *Mol. Cell* **68**, 361-373.e5 (2017).

49. Juszkiewicz, S. *et al.* ZNF598 Is a Quality Control Sensor of Collided Ribosomes. *Mol. Cell* **72**, 469-481.e7 (2018).

50. Garzia, A. *et al.* The E3 ubiquitin ligase and RNA-binding protein ZNF598 orchestrates ribosome quality control of premature polyadenylated mRNAs. *Nat. Commun.* **8**, 16056 (2017).

51. Ikeuchi, K., Izawa, T. & Inada, T. Recent Progress on the Molecular Mechanism of Quality Controls Induced by Ribosome Stalling. *Front. Genet.* **9**, 1–7 (2019).

52. Reddy, B. N. *et al.* A bioinformatic survey of RNA-binding proteins in Plasmodium. *BMC Genomics* **16**, 890 (2015).

53. Hashimoto, S., Sugiyama, T., Yamazaki, R., Nobuta, R. & Inada, T. Identification of a novel trigger complex that facilitates ribosome-associated quality control in mammalian cells. *Sci. Rep.* **10**, 3422 (2020).

54. D'Orazio, K. N. *et al.* The endonuclease Cue2 cleaves mRNAs at stalled ribosomes during No Go Decay. *Elife* **8**, 1–27 (2019).

55. Glover, M. L. *et al.* NONU-1 Encodes a Conserved Endonuclease Required for mRNA Translation Surveillance. *Cell Rep.* **30**, 4321-4331.e4 (2020).

56. Doma, M. K. & Parker, R. Endonucleolytic cleavage of eukaryotic mRNAs with stalls in translation elongation. *Nature* **440**, 561–564 (2006).

57. Pisareva, V. P., Skabkin, M. A., Hellen, C. U. T., Pestova, T. V. & Pisarev, A. V. Dissociation by Pelota, Hbs1 and ABCE1 of mammalian vacant 80S ribosomes and stalled elongation complexes. *EMBO J.* **30**, 1804–1817 (2011).

58. Tsuboi, T. *et al.* Dom34:hbs1 plays a general role in quality-control systems by dissociation of a stalled ribosome at the 3' end of aberrant mRNA. *Mol. Cell* **46**, 518–529

(2012).

59. Navickas, A. *et al.* No-Go Decay mRNA cleavage in the ribosome exit tunnel produces 5'-OH ends phosphorylated by Trl1. *Nat. Commun.* **11**, 122 (2020).

60. Shen, P. S. *et al.* Rqc2p and 60 S ribosomal subunits mediate mRNA-independent elongation of nascent chains. *Science (80-.).* **347**, 75–78 (2015).

61. Kostova, K. K. *et al.* CAT-tailing as a fail-safe mechanism for efficient degradation of stalled nascent polypeptides. *Science (80-.).* **357**, 414–417 (2017).

62. Chandrasekaran, V. *et al.* Mechanism of ribosome stalling during translation of a poly(A) tail. *Nat. Struct. Mol. Biol.* **26**, 1132–1140 (2019).

63. Tesina, P. *et al.* Molecular mechanism of translational stalling by inhibitory codon combinations and poly(A) tracts. *EMBO J.* **39**, e103365 (2020).

64. Szádeczky-Kardoss, I. *et al.* The nonstop decay and the RNA silencing systems operate cooperatively in plants. *Nucleic Acids Res.* **46**, 4632–4648 (2018).

65. Klauer, A. A. & van Hoof, A. Degradation of mRNAs that lack a stop codon: a decade of nonstop progress. *Wiley Interdiscip. Rev. RNA* **3**, 649–660 (2012).

66. Ketteler, R. On programmed ribosomal frameshifting: the alternative proteomes. *Front. Genet.* **3**, 1–10 (2012).

67. Saito, S., Hosoda, N. & Hoshino, S. The Hbs1-Dom34 Protein Complex Functions in Non-stop mRNA Decay in Mammalian Cells. *J. Biol. Chem.* **288**, 17832–17843 (2013).

68. Izawa, T. *et al.* Roles of Dom34:Hbs1 in Nonstop Protein Clearance from Translocators for Normal Organelle Protein Influx. *Cell Rep.* **2**, 447–453 (2012).

69. Houseley, J. & Tollervey, D. The Many Pathways of RNA Degradation. *Cell* **136**, 763–776 (2009).

70. Cole, S. E., LaRiviere, F. J., Merrikh, C. N. & Moore, M. J. A Convergence of rRNA and mRNA Quality Control Pathways Revealed by Mechanistic Analysis of Nonfunctional rRNA Decay. *Mol. Cell* **34**, 440–450 (2009).

71. Guerra-Moreno, A. *et al.* Proteomic Analysis Identifies Ribosome Reduction as an Effective Proteotoxic Stress Response. *J. Biol. Chem.* **290**, 29695–29706 (2015).

72. Fujii, K., Kitabatake, M., Sakata, T. & Ohno, M. 40S subunit dissociation and proteasome-dependent RNA degradation in nonfunctional 25S rRNA decay. *EMBO J.* **31**, 2579–2589 (2012).

73. Fujii, K., Kitabatake, M., Sakata, T., Miyata, A. & Ohno, M. A role for ubiquitin in the clearance of nonfunctional rRNAs. *Genes Dev.* **23**, 963–974 (2009).

74. LaRiviere, F. J., Cole, S. E., Ferullo, D. J. & Moore, M. J. A Late-Acting Quality Control Process for Mature Eukaryotic rRNAs. *Mol. Cell* **24**, 619–626 (2006).

75. Doma, M. K. & Parker, R. Revenge of the NRD: Preferential Degradation of Nonfunctional Eukaryotic rRNA. *Dev. Cell* **11**, 757–758 (2006).

76. Sugiyama, T. *et al.* Sequential Ubiquitination of Ribosomal Protein uS3 Triggers the Degradation of Non-functional 18S rRNA. *Cell Rep.* **26**, 3400-3415.e7 (2019).

77. Sundaramoorthy, E. *et al.* ZNF598 and RACK1 Regulate Mammalian Ribosome-Associated Quality Control Function by Mediating Regulatory 40S Ribosomal Ubiquitylation. *Mol Cell* **65**, 751-760.e754 (2017).

78. Limoncelli, K. A., Merrikh, C. N. & Moore, M. J. ASC1 and RPS3 : new actors in 18S nonfunctional rRNA decay. *RNA* **23**, 1946–1960 (2017).

79. Juszkiewicz, S. & Hegde, R. S. Initiation of Quality Control during Poly(A) Translation Requires Site-Specific Ribosome Ubiquitination. *Mol. Cell* **65**, 743-750.e4 (2017).

80. Erath, J., Djuranovic, S. & Djuranovic, S. P. Adaptation of Translational Machinery in Malaria Parasites to Accommodate Translation of Poly-Adenosine Stretches Throughout Its Life Cycle. *Front. Microbiol.* **10**, 2823 (2019).

81. Winegard, T. C. *The Mosquito: A Human History of Our Deadliest Predator*. (Melbourne: Text Publishing Company., 2019).

82. Otto, T. D. *et al.* Genomes of all known members of a Plasmodium subgenus reveal paths to virulent human malaria. *Nat. Microbiol.* **3**, 687–697 (2018).

83. Loy, D. E. *et al.* Evolutionary history of human Plasmodium vivax revealed by genome-wide analyses of related ape parasites. *Proc. Natl. Acad. Sci.* **115**, E8450–E8459 (2018).

84. [who], W. H. O. *World Malaria Report 2018*. (2018).

85. Le Roch, K. G. *et al.* Global analysis of transcript and protein levels across the Plasmodium falciparum life cycle. *Genome Res.* **14**, 2308–18 (2004).

86. Shock, J. L., Fischer, K. F. & DeRisi, J. L. Whole-genome analysis of mRNA decay in Plasmodium falciparum reveals a global lengthening of mRNA half-life during the intra-erythrocytic development cycle. *Genome Biol.* **8**, R134 (2007).

87. Hughes, K. R., Philip, N., Lucas Starnes, G., Taylor, S. & Waters, A. P. From cradle to grave: RNA biology in malaria parasites. *Wiley Interdiscip. Rev. RNA* **1**, 287–303 (2010).

88. Sorber, K., Dimon, M. T. & DeRisi, J. L. RNA-Seq analysis of splicing in Plasmodium falciparum uncovers new splice junctions, alternative splicing and splicing of antisense transcripts. *Nucleic Acids Res.* **39**, 3820–3835 (2011).

89. Bunnik, E. M. *et al.* Polysome profiling reveals translational control of gene expression in the human malaria parasite Plasmodium falciparum. *Genome Biol.* **14**, R128 (2013).

90. Caro, F., Ahyong, V., Betegon, M. & DeRisi, J. L. Genome-wide regulatory dynamics of translation in the Plasmodium falciparum asexual blood stages. *Elife* **3**, 1–24 (2014).

91. Vembar, S. S., Droll, D. & Scherf, A. Translational regulation in blood stages of the malaria parasite Plasmodium spp. : systems-wide studies pave the way. *Wiley Interdiscip. Rev. RNA* **7**, 772–792 (2016).

92. Lu, X. M. *et al.* Nascent RNA sequencing reveals mechanisms of gene regulation in the human malaria parasite Plasmodium falciparum. *Nucleic Acids Res.* **45**, 7825–7840 (2017).

93. Kooij, T. W. A., Janse, C. J. & Waters, A. P. Plasmodium post-genomics: better the bug you know? *Nat. Rev. Microbiol.* **4**, 344–357 (2006).

94. Gardner, M. J. Chromosome 2 Sequence of the Human Malaria Parasite Plasmodium falciparum. *Science (80-.).* **282**, 1126–1132 (1998).

95. Gardner, M. J. *et al.* Genome sequence of the human malaria parasite Plasmodium falciparum. *NatureNature* **419**, (2002).

96. Gardner, M. J. *et al.* Sequence of Plasmodium falciparum chromosomes 2, 10, 11 and 14. *Nature* **419**, 531–534 (2002).

97. Bowman, S. *et al.* The complete nucleotide sequence of chromosome 3 of Plasmodium falciparum. *Nature* **400**, 532–8 (1999).

98. Hall, N. *et al.* Sequence of Plasmodium falciparum chromosomes 1, 3–9 and 13. *Nature* **419**, 527–531 (2002).

99. Hyman, R. W. *et al.* Sequence of Plasmodium falciparum chromosome 12. *Nature* **419**, 534–537 (2002).

100. Vembar, S. S. *et al.* Complete telomere-to-telomere de novo assembly of the Plasmodium falciparum genome through long-read (>11 kb), single molecule, real-time sequencing. *DNA Res.* **23**, 339–351 (2016).

101. Szafranski, K., Lehmann, R., Parra, G., Guigo, R. & Glockner, G. Gene Organization Features in A/T-Rich Organisms. *J. Mol. Evol.* **60**, 90–98 (2005).

102. Glockner, G. Large Scale Sequencing and Analysis of AT Rich Eukaryote Genomes. *Curr. Genomics* **1**, 289–299 (2000).

103. Habich, M., Djuranovic, S., Szczesny, P. & M., H. PATACSDB - The database of polyA translational attenuators in coding sequences. *PeerJ Comput. Sci.* **2**, e45 (2016).

104. Djuranovic, S. P. *et al.* PolyA tracks and poly-lysine repeats are the Achilles heel of Plasmodium falciparum. *bioRxiv* 420109 (2018). doi:10.1101/420109

105. Tournu, H., Butts, A. & Palmer, G. E. Titrating Gene Function in the Human Fungal Pathogen Candida albicans through Poly-Adenosine Tract Insertion. *mSphere* **4**, e192–e119 (2019).

106. Florens, L. *et al.* A proteomic view of the Plasmodium falciparum life cycle. *Nature* **419**,

520–526 (2002).

107. Silvestrini, F. *et al.* Protein Export Marks the Early Phase of Gametocytogenesis of the Human Malaria Parasite Plasmodium falciparum. *Mol. Cell. Proteomics* **9**, 1437–1448 (2010).

108. Sueoka, N. On the Genetic Basis of Variation and Heterogeneity Of DNA Base Composition. *Proc. Natl. Acad. Sci.* **48**, 582–592 (1962).

109. Wernegreen, J. J. & Funk, D. J. Mutation Exposed: A Neutral Explanation for Extreme Base Composition of an Endosymbiont Genome. *J. Mol. Evol.* **59**, 849–858 (2004).

110. Zilversmit, M. M. *et al.* Low-Complexity Regions in Plasmodium falciparum: Missing Links in the Evolution of an Extreme Genome. *Mol. Biol. Evol.* **27**, 2198–2209 (2010).

111. Wu, H., Zhang, Z., Hu, S. & Yu, J. On the molecular mechanism of GC content variation among eubacterial genomes. *Biol. Direct* **7**, 2 (2012).

112. Albà, M. M., Tompa, P. & Veitia, R. A. Amino Acid Repeats and the Structure and Evolution of Proteins. in *Gene and Protein Evolution* 119–130 (KARGER, 2007). doi:10.1159/000107607

113. Muralidharan, V., Oksman, A., Iwamoto, M., Wandless, T. J. & Goldberg, D. E. Asparagine repeat function in a Plasmodium falciparum protein assessed via a regulatable fluorescent affinity tag. *Proc. Natl. Acad. Sci.* **108**, 4411–4416 (2011).

114. Pollack, Y., Katzen, A. L., Spira, D. T. & Golenser, J. The genome of Plasmodium falciparum. I: DNA base composition. *Nucleic Acids Res.* **10**, 539–546 (1982).

115. Musto, H., Romero, H., Zavala, A., Jabbari, K. & Bernardi, G. Synonymous Codon Choices

in the Extremely GC-Poor Genome of Plasmodium falciparum: Compositional Constraints and Translational Selection. *J. Mol. Evol.* **49**, 27–35 (1999).

116. Videvall, E. Plasmodium parasites of birds have the most AT-rich genes of eukaryotes. *Microb. Genomics* **4**, (2018).

117. Muralidharan, V. & Goldberg, D. E. Asparagine Repeats in Plasmodium falciparum Proteins: Good for Nothing? *PLoS Pathog.* **9**, e1003488 (2013).

118. Seward, E. A. & Kelly, S. Dietary nitrogen alters codon bias and genome composition in parasitic microorganisms. *Genome Biol.* **17**, 226 (2016).

119. Dietel, A.-K., Merker, H., Kaltenpoth, M. & Kost, C. Selective advantages favour high genomic AT-contents in intracellular elements. *PLOS Genet.* **15**, e1007778 (2019).

120. Ting, L.-M. *et al.* Targeting a Novel Plasmodium falciparum Purine Recycling Pathway with Specific Immucillins. *J. Biol. Chem.* **280**, 9547–9554 (2005).

121. El Bissati, K. *et al.* The plasma membrane permease PfNT1 is essential for purine salvage in the human malaria parasite Plasmodium falciparum. *Proc. Natl. Acad. Sci.* **103**, 9286–9291 (2006).

122. Quashie, N. B. *et al.* A comprehensive model of purine uptake by the malaria parasite Plasmodium falciparum: identification of four purine transport activities in intraerythrocytic parasites. *Biochem. J.* **411**, 287–295 (2008).

123. Sherman, I. W. Biochemistry of Plasmodium (malarial parasites). *Microbiol. Rev.* **43**, 453–95 (1979).

124. Belen Cassera, M., Zhang, Y., Z. Hazleton, K. & L. Schramm, V. Purine and Pyrimidine

Pathways as Targets in Plasmodium falciparum. *Curr. Top. Med. Chem.* **11**, 2103–2115 (2011).

125. Hamilton, W. L. *et al.* Extreme mutation bias and high AT content in Plasmodium falciparum. *Nucleic Acids Res.* **45**, gkw1259 (2017).

126. Leirião, P., Rodrigues, C. D., Albuquerque, S. S. & Mota, M. M. Survival of protozoan intracellular parasites in host cells. *EMBO Rep.* **5**, 1142–1147 (2004).

127. Liu, J., Istvan, E. S., Gluzman, I. Y., Gross, J. & Goldberg, D. E. Plasmodium falciparum ensures its amino acid supply with multiple acquisition pathways and redundant proteolytic enzyme systems. *Proc. Natl. Acad. Sci.* **103**, 8840–8845 (2006).

128. Babbitt, S. E. *et al.* Plasmodium falciparum responds to amino acid starvation by entering into a hibernatory state. *Proc. Natl. Acad. Sci.* **109**, E3278–E3287 (2012).

129. Becker, K. *et al.* Oxidative stress in malaria parasite-infected erythrocytes: host–parasite interactions. *Int. J. Parasitol.* **34**, 163–189 (2004).

130. Ostera, G. *et al.* Plasmodium falciparum: Nitric oxide modulates heme speciation in isolated food vacuoles. *Exp. Parasitol.* **127**, 1–8 (2011).

131. Cornillot, E. *et al.* Sequencing of the smallest Apicomplexan genome from the human pathogen Babesia microti†. *Nucleic Acids Res.* **40**, 9102–9114 (2012).

132. Simms, C. L. & Zaher, H. S. Quality control of chemically damaged RNA. *Cell. Mol. Life Sci.* **73**, 3639–3653 (2016).

133. Simms, C. L., Hudson, B. H., Mosior, J. W., Rangwala, A. S. & Zaher, H. S. An Active Role for the Ribosome in Determining the Fate of Oxidized mRNA. *Cell Rep.* **9**, 1256–1264

(2014).

134. Guler, J. L. *et al.* Asexual Populations of the Human Malaria Parasite, Plasmodium falciparum, Use a Two-Step Genomic Strategy to Acquire Accurate, Beneficial DNA Amplifications. *PLoS Pathog.* **9**, e1003375 (2013).

135. Huckaby, A. C. *et al.* Complex DNA structures trigger copy number variation across the Plasmodium falciparum genome. *Nucleic Acids Res.* **47**, 1615–1627 (2019).

136. Sakai, K. *et al.* Human ribosomal RNA gene cluster: identification of the proximal end containing a novel tandem repeat sequence. *Genomics* **26**, 521–526 (1995).

137. KOBAYASHI, T. Ribosomal RNA gene repeats, their stability and cellular senescence. *Proc. Japan Acad. Ser. B* **90**, 119–129 (2014).

138. Warner, J. R. The economics of ribosome biosynthesis in yeast. *Trends Biochem. Sci.* **24**, 437–440 (1999).

139. Gunderson, J. *et al.* Structurally distinct, stage-specific ribosomes occur in Plasmodium. *Science (80-.).* **238**, 933–937 (1987).

140. Waters, A. P., Syin, C. & McCutchan, T. F. Developmental regulation of stage-specific ribosome populations in Plasmodium. *Nature* **342**, 438–440 (1989).

141. Li, J. *et al.* Regulation and trafficking of three distinct 18 S ribosomal RNAs during development of the malaria parasite. *J. Mol. Biol.* **269**, 203–213 (1997).

142. Ellwood, M. & Nomura, M. Chromosomal locations of the genes for rRNA in Escherichia coli K-12. *J. Bacteriol.* **149**, 458–68 (1982).

143. Walliker, D. *et al.* Genetic analysis of the human malaria parasite Plasmodium falciparum.

Science (80-.). **236**, 1661–1666 (1987).

144. McCutchan, T. F. *et al.* Primary sequences of two small subunit ribosomal RNA genes from Plasmodium falciparum. *Mol. Biochem. Parasitol.* **28**, 63–68 (1988).

145. VELICHUTINA, I. V., ROGERS, M. J., McCUTCHAN, T. F. & LIEBMAN, S. W. Chimeric rRNAs containing the GTPase centers of the developmentally regulated ribosomal rRNAs of Plasmodium falciparum are functionally distinct. *RNA* **4**, S1355838298980049 (1998).

146. Xue, S. & Barna, M. Specialized ribosomes: a new frontier in gene regulation and organismal biology. *Nat. Rev. Mol. Cell Biol.* **13**, 355–369 (2012).

147. Zhu, J. D. *et al.* Stage-specific ribosomal RNA expression switches during sporozoite invasion of hepatocytes. *J. Biol. Chem.* **265**, 12740–4 (1990).

148. Fang, J. & McCutchan, T. F. Thermoregulation in a parasite's life cycle. *Nature* **418**, 742–742 (2002).

149. van Spaendonk, R. M. L. *et al.* Functional Equivalence of Structurally Distinct Ribosomes in the Malaria Parasite, Plasmodium berghei. *J. Biol. Chem.* **276**, 22638–22647 (2001).

150. Mills, E. W. & Green, R. Ribosomopathies: There's strength in numbers. *Science (80-.).* **358**, eaan2755 (2017).

151. Qi, Y. *et al.* Regulation of Plasmodium yoelii Oocyst Development by Strain- and Stage-Specific Small-Subunit rRNA. *MBio* **6**, (2015).

152. López-Barragán, M. J. *et al.* Directional gene expression and antisense transcripts in sexual and asexual stages of Plasmodium falciparum. *BMC Genomics* **12**, 587 (2011).

153. Zanghì, G. *et al.* A Specific PfEMP1 Is Expressed in P. falciparum Sporozoites and Plays a

Role in Hepatocyte Infection. *Cell Rep.* **22**, 2951–2963 (2018).

154. Aurrecoechea, C. *et al.* PlasmoDB: a functional genomic database for malaria parasites. *Nucleic Acids Res.* **37**, D539–D543 (2009).

155. Kurylo, C. M. *et al.* Endogenous rRNA Sequence Variation Can Regulate Stress Response Gene Expression and Phenotype. *Cell Rep.* **25**, 236-248.e6 (2018).

156. Locati, M. D. *et al.* Expression of distinct maternal and somatic 5.8S, 18S, and 28S rRNA types during zebrafish development. *RNA* **23**, 1188–1199 (2017).

157. Rogers, M. J. *et al.* Structural features of the large subunit rRNA expressed in Plasmodium falciparum sporozoites that distinguish it from the asexually expressed subunit rRNA. *RNA* **2**, 134–45 (1996).

158. Wong, W. *et al.* Cryo-EM structure of the Plasmodium falciparum 80S ribosome bound to the anti-protozoan drug emetine. *Elife* **3**, (2014).

159. Sun, M. *et al.* Dynamical features of the Plasmodium falciparum ribosome during translation. *Nucleic Acids Res.* **43**, gkv991 (2015).

160. Sengupta, J. *et al.* Identification of the versatile scaffold protein RACK1 on the eukaryotic ribosome by cryo-EM. *Nat. Struct. Mol. Biol.* **11**, 957–962 (2004).

161. Majzoub, K. *et al.* RACK1 Controls IRES-Mediated Translation of Viruses. *Cell* **159**, 1086–1095 (2014).

162. Dimitrova, L. N., Kuroha, K., Tatematsu, T. & Inada, T. Nascent Peptide-dependent Translation Arrest Leads to Not4p-mediated Protein Degradation by the Proteasome. *J. Biol. Chem.* **284**, 10343–10352 (2009).

163. Kuroha, K. *et al.* Receptor for activated C kinase 1 stimulates nascent polypeptide-dependent translation arrest. *EMBO Rep.* **11**, 956–961 (2010).

164. Wolf, A. S. & Grayhack, E. J. Asc1, homolog of human RACK1, prevents frameshifting in yeast by ribosomes stalled at CGA codon repeats. *RNA* **21**, 935–945 (2015).

165. Tesina, P. *et al.* Molecular mechanism of translational stalling by inhibitory codon combinations and poly(A) tracts. *bioRxiv [Preprint]* (2019). doi:10.1101/755652

166. Kim, H.-K. *et al.* A frameshifting stimulatory stem loop destabilizes the hybrid state and impedes ribosomal translocation. *Proc. Natl. Acad. Sci.* **111**, 5538–5543 (2014).

167. Lu, J. & Deutsch, C. Electrostatics in the Ribosomal Tunnel Modulate Chain Elongation Rates. *J. Mol. Biol.* **384**, 73–86 (2008).

168. Brandman, O. *et al.* A Ribosome-Bound Quality Control Complex Triggers Degradation of Nascent Peptides and Signals Translation Stress. *Cell* **151**, 1042–1054 (2012).

169. Tang, T. T. L., Stowell, J. A. W., Hill, C. H. & Passmore, L. A. The intrinsic structure of poly(A) RNA determines the specificity of Pan2 and Caf1 deadenylases. *Nat. Struct. Mol. Biol.* **26**, 433–442 (2019).

170. Lacsina, J. R., LaMonte, G., Nicchitta, C. V & Chi, J.-T. Polysome profiling of the malaria parasite Plasmodium falciparum. *Mol. Biochem. Parasitol.* **179**, 42–6 (2011).

171. Cui, L., Lindner, S. & Miao, J. Translational regulation during stage transitions in malaria parasites. *Ann. N. Y. Acad. Sci.* **1342**, 1–9 (2015).

172. Yeoh, L. M. *et al.* Alternative splicing is required for stage differentiation in malaria parasites. *Genome Biol.* **20**, 151 (2019).

173. Martin, L. *et al.* Identification and Characterization of Small Molecules That Inhibit Nonsense-Mediated RNA Decay and Suppress Nonsense p53 Mutations. *Cancer Res.* **74**, 3104–3113 (2014).

174. Guydosh, N. R. & Green, R. Translation of poly(A) tails leads to precise mRNA cleavage. *RNA* **23**, 749–761 (2017).

175. Kashima, I. *et al.* A functional involvement of ABCE1, eukaryotic ribosome recycling factor, in nonstop mRNA decay in Drosophila melanogaster cells. *Biochimie* **106**, 10–16 (2014).

176. Kanehisa, M., Sato, Y., Furumichi, M., Morishima, K. & Tanabe, M. New approach for understanding genome variations in KEGG. *Nucleic Acids Res.* **47**, D590–D595 (2019).

177. Cohuet, A. *et al.* Anopheles and Plasmodium : from laboratory models to natural systems in the field. *EMBO Rep.* **7**, 1285–1289 (2006).

178. Annan, Z. *et al.* Population genetic structure of Plasmodium falciparum in the two main African vectors, Anopheles gambiae and Anopheles funestus. *Proc. Natl. Acad. Sci.* **104**, 7987–7992 (2007).

179. Giraldo-Calderón, G. I. *et al.* VectorBase: an updated bioinformatics resource for invertebrate vectors and other organisms related with human diseases. *Nucleic Acids Res.* **43**, D707–D713 (2015).

180. Thurmond, J. *et al.* FlyBase 2.0: the next generation. *Nucleic Acids Res.* **47**, D759–D765 (2019).

181. Ghorbal, M. *et al.* Genome editing in the human malaria parasite Plasmodium falciparum

using the CRISPR-Cas9 system. *Nat. Biotechnol.* **32**, 819–821 (2014).

182. Zhang, M. *et al.* Uncovering the essential genes of the human malaria parasite Plasmodium falciparum by saturation mutagenesis. *Science (80-.).* **360**, eaap7847 (2018).

183. Ito-Harashima, S., Kuroha, K., Tatematsu, T. & Inada, T. Translation of the poly(A) tail plays crucial roles in nonstop mRNA surveillance via translation repression and protein destabilization by proteasome in yeast. *Genes Dev.* **21**, 519–524 (2007).

184. Matsuda, R., Ikeuchi, K., Nomura, S. & Inada, T. Protein quality control systems associated with no-go and nonstop mRNA surveillance in yeast. *Genes to Cells* **19**, 1–12 (2014).

185. Brown, C. E. & Sachs, A. B. Poly(A) Tail Length Control in Saccharomyces cerevisiae Occurs by Message-Specific Deadenylation. *Mol. Cell. Biol.* **18**, 6548–6559 (1998).

186. Chang, H., Lim, J., Ha, M. & Kim, V. N. TAIL-seq: Genome-wide Determination of Poly(A) Tail Length and 3′ End Modifications. *Mol. Cell* **53**, 1044–1052 (2014).

187. Subtelny, A. O., Eichhorn, S. W., Chen, G. R., Sive, H. & Bartel, D. P. Poly(A)-tail profiling reveals an embryonic switch in translational control. *Nature* **508**, 66–71 (2014).

188. Stevens, A. T., Howe, D. K. & Hunt, A. G. Characterization of mRNA polyadenylation in the apicomplexa. *PLoS One* **13**, e0203317 (2018).

189. Choe, Y.-J. *et al.* Failure of RQC machinery causes protein aggregation and proteotoxic stress. *Nature* **531**, 191–195 (2016).

190. Yonashiro, R. *et al.* The Rqc2/Tae2 subunit of the ribosome-associated quality control (RQC) complex marks ribosome-stalled nascent polypeptide chains for aggregation. *Elife*

5, (2016).

191. Jamar, N. H., Kritsiligkou, P. & Grant, C. M. Loss of mRNA surveillance pathways results in widespread protein aggregation. *Sci. Rep.* **8**, 3894 (2018).

192. Muralidharan, V., Oksman, A., Pal, P., Lindquist, S. & Goldberg, D. E. Plasmodium falciparum heat shock protein 110 stabilizes the asparagine repeat-rich parasite proteome during malarial fevers. *Nat. Commun.* **3**, 1310 (2012).

Chapter 2: *Plasmodium falciparum* Translational Machinery Condones Polyadenosine Repeats

Preface

The following work was completed by myself, Slavica Pavlovic Djuranovic, Ryan J Andrews, Peter O Bayguinov, Joyce J Chung, Douglas L Chalker, James AJ Fitzpatrick, Walter N. Moss, Pawel Szczesny, and Sergej Djuranovic. SPD and JE designed and conducted experiments, analyzed and interpreted biochemical data and drafted the article; RJA, WM, JE, SD and PS conducted, analyzed and interpreted bioinformatics data; SPD, POB, and JAJF conducted, analyzed and interpreted microscopy data; JJC and DLC, conducted experiments, analyzed and interpreted biochemical data from *T. thermophila*; SD, SPD, PS, and JE are responsible for conception and design of the study. All the authors contributed to the revision of the article.

This chapter is published in its entirety[1]. and is available at https://elifesciences.org/articles/57799.

2.1 Abstract

Plasmodium falciparum is a causative agent of human malaria. Sixty percent of mRNAs from its extremely AT-rich (81%) genome harbor long polyadenosine (polyA) runs within their ORFs, distinguishing the parasite from its hosts and other sequenced organisms. Recent studies indicate polyA runs cause ribosome stalling and frameshifting, triggering mRNA surveillance pathways and attenuating protein synthesis. Here, we show that *P. falciparum* is an exception to this rule. We demonstrate that both endogenous genes and reporter sequences containing long polyA runs are efficiently and accurately translated in *P. falciparum* cells. We show that polyA runs do not elicit any response from No Go Decay (NGD) or result in the production of frameshifted proteins. This is in stark contrast to what we observe in human cells or *T. thermophila*, an organism with similar AT- content. Finally, using stalling reporters we show that *Plasmodium* cells evolved not to have a fully functional NGD pathway

2.2 Introduction

The complex life cycle of *Plasmodium falciparum*, responsible for 90% of all malaria-associated deaths, involves multiple stages in both the human and mosquito hosts. Asexual replication during the intraerythrocytic development cycle (IDC) is tightly regulated over a 48 hr period, involving the expression of the majority of its genes[2–4]. Progression through asexual stages (ring, trophozoite, schizont) of the IDC requires a strictly controlled panel of gene expression profiles for each stage. A range of 16–32 daughter cells results from the IDC. Thus, a single, originating merozoite must undergo several rounds of DNA synthesis, mitosis, and nuclear

division in a relatively short period[2–4]. The apparent necessity for rapid and accurate DNA replication needs to be accompanied by large-scale RNA transcription and protein synthesis. These processes occur during the 24 hr of the trophozoite stage before erythrocytic schizogeny and cytokinesis. Recent saturation-level mutagenesis of the *P. falciparum* genome further emphasized and demonstrated that genes associated with cell cycle control, translation, RNA metabolism, protein folding, and drug resistance are more likely to be essential for parasites fitness and survival[5]. However, a faithful execution of these fundamental processes is challenged by the extremely AT-rich *P. falciparum* genome: averaging ~81% in overall AT content. With a relatively small difference in AT-richness between the non-coding and coding regions; *P. falciparum* represents a unique case from other AT-rich organisms[6–9]. While the underlying reasons for such disproportionate representation of the four nucleotides in any given genome may be different, it is of vital importance that shifts towards extreme AT- or GC-richness must be accommodated by adaptation of the transcription and translation apparatuses; enabling the cell to transcribe and translate each gene appropriately.

Recently, it was demonstrated that the translation of genes with polyadenosine runs (polyA tracts), primarily coding for lysine residues, is attenuated in the majority of tested organisms presumably due to ribosomal stalling and frameshifting on such RNA motifs by action of ribosome-quality control complex (RQC) and mRNA surveillance mechanisms[10–22]. In human tissue cultures, the presence of just 12 adenosines in an mRNA-coding region was found to reduce the yield of protein synthesis by more than 40%, and runs of 30–60 adenosine nucleotides reduce protein synthesis by more than 90%[11,15,20]. This effect on translation was

observed in all tested organisms that include fruit flies (*Drosophila melanogaster*), yeasts (*Saccharomyces cerevisiae* and *Candida albicans*), plants (*Arabidopsis thaliana* and *Nicotiana benthamiana*) and *E. coli*[8,11,13,17,21,22]; arguing for a universal response to coding polyA repeats. The consequence of translational arrest or slippage on polyA runs is the activation of RQC and one or more mRNA surveillance mechanisms, mainly No-Go (NGD) and Non-sense Mediated Decay (NMD)[16]. High AU-content within transcript coding regions and an extreme AAA and AAU codon bias increase the propensity for polyA tracts in the *P. falciparum* transcriptome[23]. Additionally, a 'just-in-time' transcriptional and translational model of gene expression during the relatively short trophozoite stage of the *P. falciparum* IDC[3,24] make a rapid protein synthesis in an AU-rich transcriptome an appealing problem. While both, DNA and RNA polymerases must contend with high DNA AT-content, it is also puzzling what adaptations P. falciparum have made to its translational machinery to overcome the unusual AU-richness of mRNAs, which would affect the fidelity and efficacy of protein synthesis. With 'just-in-time' translation of numerous A-rich coding sequences[7,9] and poly-lysine proteins harboring an AAA codon bias, expressed at all stages in the parasite life cycle[3,4,25], the *Plasmodium* translation machinery would represent an exception in protein synthesis compared to other organisms.

Here we present data that indicate that the *P. falciparum* translational machinery and its NGD pathway have adapted to translate long runs of polyadenosine nucleotides into poly-lysine repeats. Using comparative bioinformatic analyses, we show that malaria parasites contain an unusually high numbers of polyA-tract-containing genes compared to other eukaryotic organisms. We find this to be a common feature of all analyzed *Plasmodium* species regardless

of their AT-content, arguing for evolutionary conservation of such sequences in *Plasmodium* genomes. Expression of endogenous genes and reporters with polyA tract motifs in *P. falciparum* cells results in efficient and accurate protein synthesis in direct contrast to what we observe for human-tissue cultures and *T. thermophila* cells. We find no evidence for either ribosomal stalling or frameshifting during the translation of long polyadenosine runs in P. falciparum cells. Interestingly, induction of the NGD pathway by either reporter with stable RNA structure or isoleucine starvation results in reduced reporter protein levels but without any detectable changes in mRNA levels, arguing for alterations in the NGD pathway. Finally, our analysis of *P. falciparum* ribosome structure suggests a model whereby multiple changes may have evolved to accommodate the unusual AU-richness and high percentage of poly-lysine runs of the *P. falciparum* transcriptome and proteome, respectively.

2.3 Results

2.3.1 *Plasmodium* species: A paradigm-breaking genus.

Previous studies indicated that polyA runs in the coding sequences serve as hurdles to translation[10,11,15,16,18–22,26] that efficiently reduce protein yield and initiate NGD to degrade the mRNA. Given the very high AT-content in certain eukaryotic species[6] we sought to explore the association between coding region AT-content and transcript polyA-tract-motif abundance. In doing so, we analyzed 152 eukaryotic genomes (**FIGURE 2.1A**). We focused on stretches of polyadenosine nucleotides, or as defined previously 12A-1 motifs; sequences with a minimal length of 12 A's allowing for one mismatched base[11]. We settled on 12A-1 sequence pattern since the presence of this motif reduces protein production by 40–60% in multiple human

genes[11,13,15]. Subsequent analyses indicated that the reduction in protein amounts for genes with 12A-1 motif could be attributed to ribosome stalling and frameshifting[15,17]. Analyses of the selected set of eukaryotic genomes indicate that *P. falciparum* and other members of the *Plasmodium* genus have a much higher ratio of polyA tract genes when normalized to genomic AT-content (**FIGURE 2.1A**).

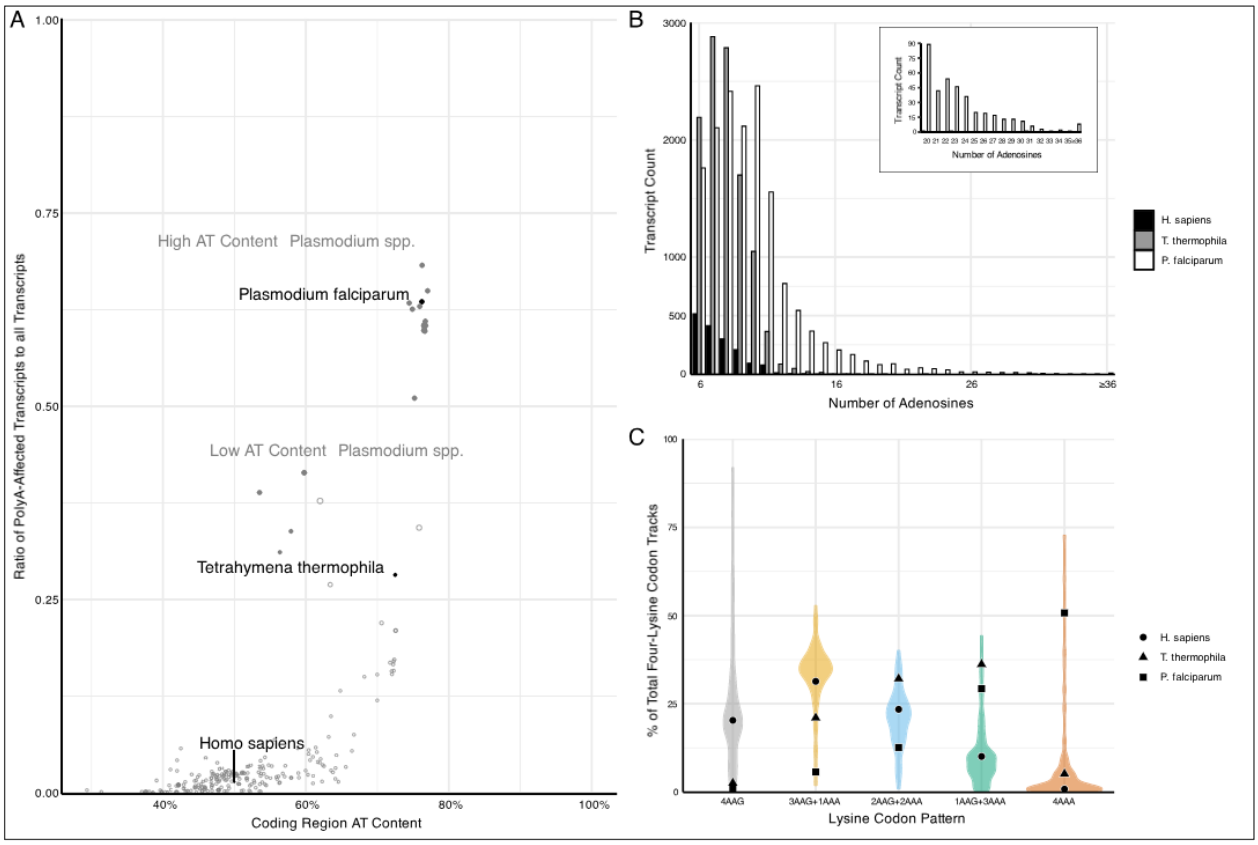

FIGURE 2.1 | Bioinformatic analysis of transcriptome polyA motifs. (A) The plot of 152 species representing a comparison of the ratio of polyA-affected transcripts (over a total number of transcripts) to the AT content of the coding region for each organism. *H. sapiens*, *T. thermophila*, and *P. falciparum*, as organisms pertinent to this paper are in black. For reference, other model organisms of interest are displayed in gray, including a position of high (65% average) and low (35%) AT-content *Plasmodium spp*. **(B)** Transcript counts for genes with 6 to 36 consecutive adenosines for *H. sapiens*, *T. thermophila*, and *P. falciparum*. *H. sapiens* and *T. thermophila* are limited to a single transcript at length of ≤17 As. The longest P. falciparum 3D7 transcript reaches maximal 65As, with multiple transcripts of ≤36 As. **(C)** Violin plot of lysine codon usage distribution in tracts of four lysine residues for 152 organisms. 3AAG+1AAA, 2AAG+2AAA and 1AAG+3AAA indicate different ratios of AAG and AAA codons in runs of four consecutive lysine codons. 4AAG and 4AAA indicate poly-lysine runs with only AAG or AAA codons, respectively. *H. sapiens* (circle), *T. thermophila* (triangle), and *P. falciparum* (square) are specifically noted.

Interestingly, this feature of *Plasmodium* species is conserved regardless of their genomic AT-content, resulting in two groups (LOW AND HIGH AT-CONTENT *PLASMODIUM SPP.*) with unusually large portions of polyA tract genes ranging from 35 to over 65% of the total transcriptome (**FIGURE 2.1A**)[9]. These two groups, which also appear to be separated geographically, demonstrate that even with a reduction in genomic AT-content, selective pressure exists for *Plasmodium spp.* to maintain polyA tract motifs. However, regardless of a selective reduction of AT-content in some *Plasmodium* species, or an almost complete lack thereof in the case of avian *Plasmodium* counterparts[27], the trend of harboring a high ratio of polyA-affected transcripts given a particular AT-richness, as well as their conservation within a significant number of genes across species, remains a paradigm-breaking hallmark of the genus.

To further emphasize the differences between *P. falciparum* and other organisms, we analyzed the number of genes that harbor polyA runs as well as the total length of consecutive adenosine nucleotides in transcripts (**SUPPLEMENTAL FIGURE 2.1** AND **FIGURE 2.1B**, RESPECTIVELY). *P. falciparum* showed a significantly higher amount of genes with polyA runs of ≥12 A's in a row when compared with its human and mosquito (*Anopheles gambiae*) hosts (**SUPPLEMENTAL FIGURE 2.1**). Over 63% of genes in *P. falciparum* have polyA tract motifs, while only 0.7–2% of total genes in humans and mosquito genomes, respectively, contain these motifs. We used the most recently updated Ensembl database to look into coding sequences of lab strain of malaria *P. falciparum* 3D7, H. sapiens, and *T. thermophila*[28]. While there is already a significant difference in the number of genes with eleven consecutive adenosines (*P. falciparum* 3D7 - 1555, *T. thermophila* - 364 and *H. sapiens* - 77 genes), the most striking sequence difference is

associated with 16 consecutive adenosines (16As). The *P. falciparum* 3D7 genome contains 188 genes with 16As, while the human host and AT-rich *T. thermophila* together have only three genes (*T. thermophila* two and *H. sapiens* 1) (**FIGURE 2.1B**). Additionally, *T. thermophila* a protozoan with an overall 73% AT-rich genome and 24,000 predicted genes, had almost nine times less genes with twelve consecutive adenosines than *P. falciparum*, 172 and 1526, respectively. Ensembl database reports 105 *P. falciparum* 3D7 genes with exactly 18As and more than 150 genes with more than 20 consecutive adenosines (20-65As, **FIGURE 2.1B**). Analyses of *P. falciparum* genomes in the PlasmoDB database[29], curated explicitly for malaria parasite species, report more than double that number with 329 genes having runs of ≥20 consecutive adenosines. Most of these genes appear to be annotated as *Plasmodium* specific. However, PlasmoDB also shows genes with up to 59 consecutive adenosines in conserved pathways, such as the phosphatidylinositol-4-phosphate 5-kinase gene (PfML01_010014200), which is involved in the inositol metabolism and signaling pathways[30]. Finally, the maximum length of consecutive adenosine runs in coding sequences of *Plasmodium* genomes indicated 111 As in *P. falciparum* fch four strain with the human host or 132 As in *P. reichenowi*, strain causing chimpanzee malaria[9,31]. As such, the length of polyA runs in coding sequences of malaria parasites exceeds the length of the average size of 3'UTR polyA tails found on the majority of transcripts in eukaryotic species[32–34]. Translation of 3'UTR located polyA tail in eukaryotic organism activates yet another mRNA surveillance pathway - non-stop decay (NSD)[12,14,35].

The disparity in the number of genes with polyA tracts could be due to previously observed codon biases in *P. falciparum*[23]. However, it was already shown that codon bias and tRNA abundance do not correlate with codon selection in genes coding for lysine repeats[11,17]. The poly-lysine repeats in proteins of the analyzed model organisms are usually encoded by AAG codons. To investigate the distribution of AAA and AAG codons in poly-lysine tracts in more detail, we analyzed transcripts from *P. falciparum* and 152 other eukaryotic genomes (**FIGURE 2.1C**). We observed a complete reversal of the trend exhibited in other organisms, including humans and the AT-rich *T. thermophila*. *P. falciparum* had the highest abundance of transcripts hosting four consecutive AAA codons in runs of four lysine residues (**FIGURE 2.1C**). This divergence from other analyzed transcriptomes is preserved in other members of *Plasmodium spp.*, with *P. berghei* being an extreme example using only AAA codons in 68% of transcripts coding for poly-lysine runs. Finally, we analyzed the biological function and essentiality of the polyA tract and poly-lysine containing genes in *P. falciparum* genome. Previous analysis indicated that 70–85% of orthologs of polyA tract carrying genes from *P. falciparum* have the same polyA motifs in genes from other *Plasmodium* species, regardless of their genomic AT content[31]. The high degree of the conservation of polyA tracts has also been noted for other eukaryotic organisms[11]. A majority of *Plasmodium* polyA tracts genes and poly-lysine proteins fall into the group of essential genes based on the recent mutagenesis studies[5]. This outcome is expected given that gene ontology results indicate enrichment in gene products involved in crucial cellular processes such as protein synthesis, RNA biogenesis, and chromosome segregation. The same gene ontology groups were previously observed in poly-lysine repeats

and polyA tract genes of the other organisms[11]. In addition to these groups, *Plasmodium* species also had enrichment of polyA tract motifs in a group of genes defined as the cellular and pathological cell adhesion ontology group (**SUPPLEMENTAL TABLE 2.1**). As such, our overall bioinformatic analyses demonstrate that *Plasmodium* genomes represent a unique set of organisms that have an enrichment of polyA tracts in the coding sequences. The overall conservation of both polyA tracts in the transcriptome and poly-lysine repeats in the proteome of *P. falciparum* has been evolutionary selected and conserved due to possible benefits for the parasite.

2.3.2 Reporters with polyA track are not a problem for *P. falciparum*

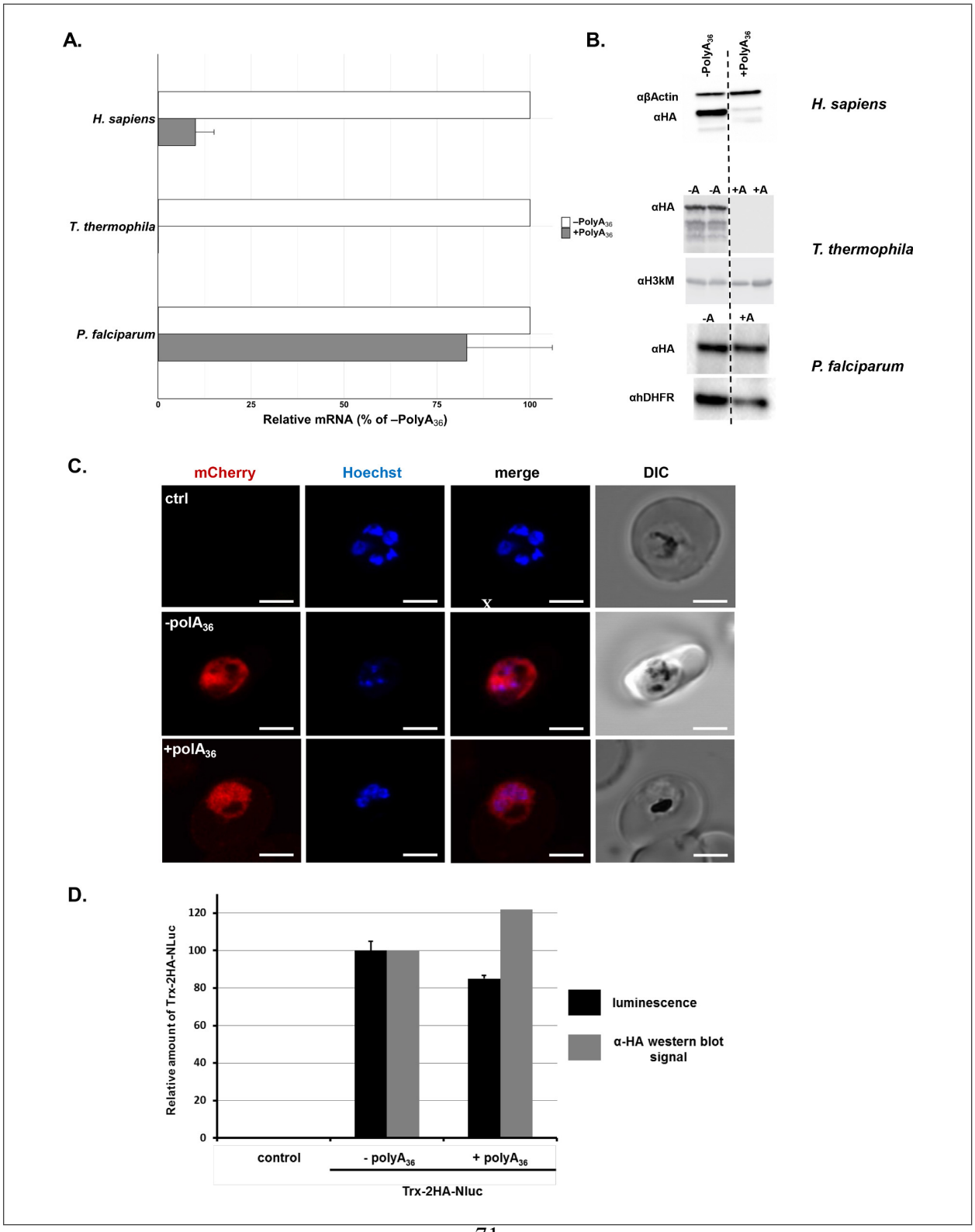

FIGURE 2.2 | Expression analysis of ±polyA reporter constructs in *H. sapiens*, *T. thermophila*, and *P. falciparum*. (A) mRNA abundance of reporter constructs (+polyA36) by qRT-PCR relative to their counterpart lacking polyA stretches (-polyA36) in *H. sapiens*, *T. thermophila*, and *P. falciparum* cells. Data represent three biological replicates with a standard deviation. **(B)** Expression of reporter constructs in *H. sapiens*, *T. thermophila*, and *P. falciparum* followed by western blot analysis with aHA or aGFP antisera. Samples from two integrated clones for the -polyA36 control (-A) and the +polyA36 reporter (+A) are shown for *T. thermophila*. αβ-actin, α-Histone H3 trimethyl-lysine (H3kM) and α-hDHFR are used as loading controls for western blot analysis from *H. sapiens*, *T. thermophila* and *P. falciparum* cells, respectively. **(C)** Images from live fluorescence microscopy of *P. falciparum* expression of reporter constructs with (+polyA36) and without (-polyA36) polyA tracts as well as parent (non- transfected) line, 2.5 mm scale bar. **(D)** Quantification of protein amounts for Thioredoxin-2HA-NanoLuciferase (Trx-2HA-NLuc) reporter without (-polyA36) and with 36 adenosine stretch (+polyA36) expressed in *P. falciparum* cells. Western blot analysis of Trx-2HA-NLuc reporter (**SUPPLEMENTAL FIGURE 2.3**) and luminescence measurements were normalized to hDHFR or cell number, respectively. Luminescence data represent the mean value of three biological replicates with standard deviation.

As mentioned earlier, polyA tracts and poly-lysine repeats cause a reduction in mRNA stability and protein amounts, respectively, due to the ribosomal stalling and frameshifting on such motifs[10,11,14–22]. To investigate further how the AU-rich *P. falciparum* transcriptome with multiple polyA tracts gets effectively translated, we used double HA-tagged reporter constructs. The 36 adenosine nucleotide (36 As) insertion, coding for 12 lysine residues, was inserted between the sequence of double HA-tag and a fluorescent protein (+POLYA36, **SUPPLEMENTAL FIGURE 2.2**). As a control, we used a reporter that had only double HA-tag in front of the fluorescent-protein sequence (-POLYA36, **SUPPLEMENTAL FIGURE 2.2**). We expressed our reporter constructs from plasmid vectors in the *P. falciparum* Dd2 lab strain. In parallel, we expressed the same constructs in human dermal fibroblasts (HDFs) and *T. thermophila* cells (**FIGURE 2.2A–B**). We followed mRNA abundance of each construct by qRT-PCR (**FIGURE 2.2A**), and expression of the reporter protein was followed by western blot detection of the double HA-tag in all three organisms (**FIGURE 2.2B**). We observed robust changes in normalized mRNA levels (**FIGURE 2.2A**)

and substantial losses in protein expression (**FIGURE 2.2B**) for reporters with polyA tracts (+POLYA36) in both HDFs and AT-rich *T. thermophila*[15,16]. In comparison to HDFs and *T. thermophila*, we observed minimal, if any, effects from polyA tract insertion on reporter mRNA and protein expression in *P. falciparum* cells (**FIGURE 2.2A–B**). Further analysis of *P. falciparum* cells by live-fluorescence microscopy confirms the equivalent expression of mCherry reporter, judging by the intensity of fluorescence between constructs with and without polyA tract (+POLYA36 AND -POLYA36, **FIGURE 2.2C**).

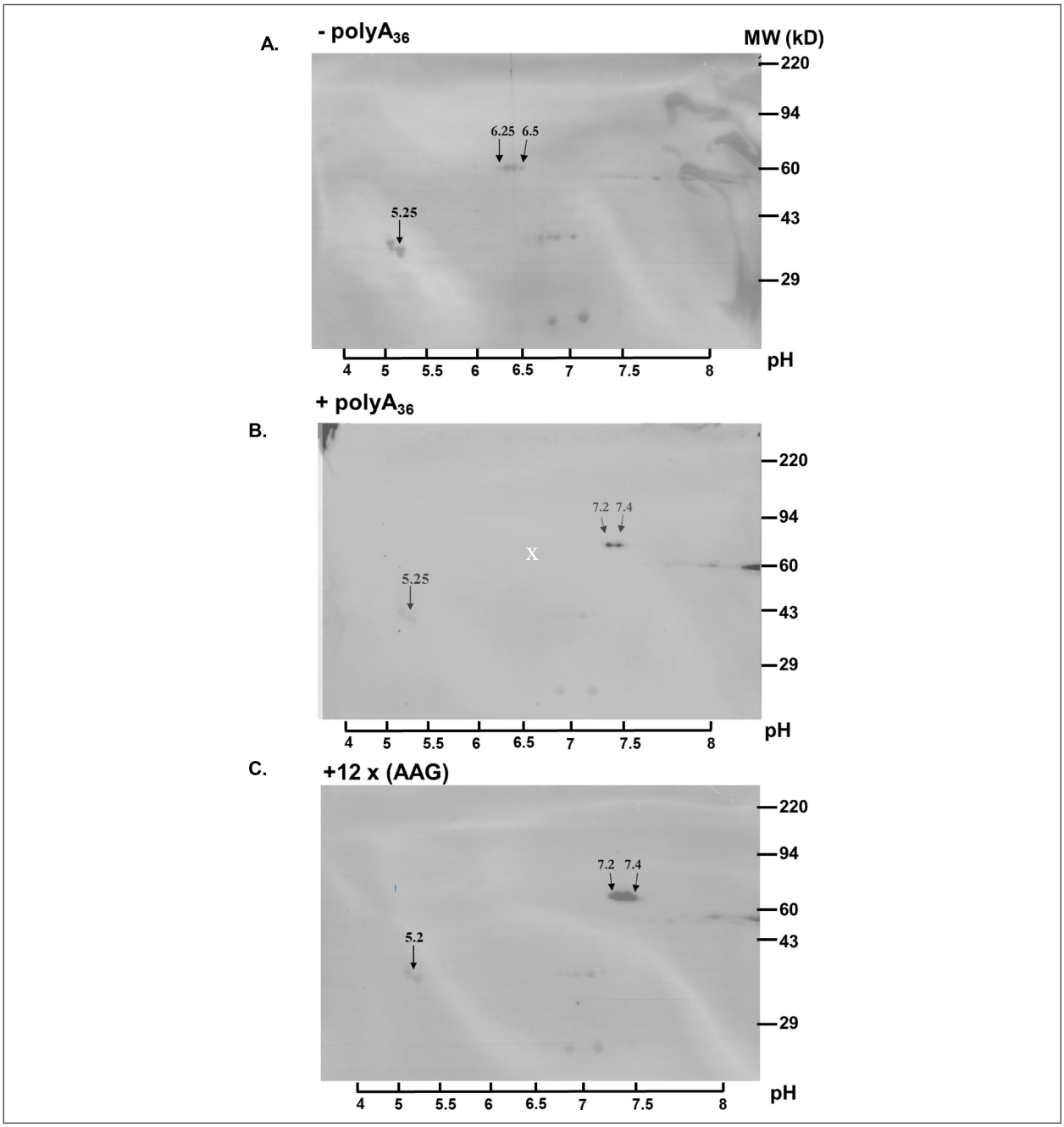

FIGURE 2.3 | Analysis of ±polyA protein expression in *P. falciparum* by 2D gel electrophoresis. (A) 2D gel analysis of HA-IP samples of wild type reporter (-polyA36). The western blots show isoelectric point (pI) at 6.25 and 6.5 (arrows). **(B)** 2D gel of reporter with polyA tract (+polyA36) sample indicates pI 7.25 and 7.4 (arrows). **(C)** 2D gel analyses of reporter with twelve lysines coded by AAG codons (12 x AAG) indicates the same effect on pI value, pI is 7.25 and 7.4 (arrows). Overlay of images of PVDF membranes stained with Coomassie Brilliant Blue, and images of western blots probed with HA-antibody. The scale with pH is on the bottom. Coomassie-stained membranes show markers (right side) and tropomyosin (33 kDa) and pI at 5.2 (arrow) as an internal standard for Isoelectric focusing (IEF).

To assess whether the efficiency of protein synthesis is altered when the polyA tract is located further downstream of the start codon, we designed a construct with thioredoxin (Trx) and nano-luciferase (nanoluc) proteins separated with a double HA-tag and 36As coding for a poly-lysine run (**SUPPLEMENTAL FIGURE 2.3**). Measurement of nanoluc luminescence from the same number of drug-selected parasites indicates similar expression of a reporter with a polyA tract (+POLYA36) compared with the control reporter (-POLYA36, **FIGURE 2.2D**). We observed the same ratio when we analyzed the expression of reporters using western blot analysis (**FIGURE 2.2D** and **SUPPLEMENTAL FIGURE 2.3**), arguing that the position of polyA tracts in coding sequence does not influence the efficiency of protein synthesis in *P. falciparum* cells.

Since polyA tracts cause ribosomal frameshifting[11,17,20] we analyzed the expression of our nanoluc and fluorescent reporters for the possible presence of frameshifted protein products. Western blot analyses of nanoluc reporters did not indicate the HA-tagged protein band at 14kD that would represent frameshifted nanoluc (**SUPPLEMENTAL FIGURE 2.3**). Moreover, the immunoprecipitation of mCherry reporters showed only equivalent amounts of the full-length product (**SUPPLEMENTAL FIGURE 2.4**). There is a still possibility that ribosomal frameshifting occurred in polyA tract reporters, but the protein product was unstable in *P. falciparum* cells, and we failed to detect it. However, if such frameshifting events did happen, they did not reduce overall levels of the full-length protein. Finally, to check whether polyA tract constructs resulted in the synthesis of poly-lysine peptides, we analyzed all constructs using 2D PAGE

electrophoresis (**FIGURE 2.3**). This analysis indicated a shift in isoelectric point (pI) of approximately one pH unit for the (+POLYA36) construct compared to the wild-type one (-POLYA36), 7.2–7.4 and 6.25–6.5, respectively. This shift on the 2D PAGE gels was the same for construct with 12xAAG lysine codons and is expected based on the calculated isoelectric points if all 12xAAA or 12xAAG codons were translated into lysine residues. Taken together, our analyses of different reporter expression data (**FIGURES 2.2–2.3**, **SUPPLEMENTAL FIGURES 2.3–2.4**) indicates that polyA tracts are tolerated by the parasite translational machinery, without apparent effects on either stability of mRNA or quality of synthesized protein.

2.3.3 Endogenous polyA tract genes are efficiently expressed in *P. falciparum*

Due to the potential for negative selection against polyA tracts[36], particularly in laboratory conditions, we also wanted to investigate how *P. falciparum* translates endogenous genes with polyA tracts. With as much as 60% of the parasite transcriptome harboring polyA tract motifs, we performed a comparative analysis of ribosome profiling data from *P. falciparum*[4] and aggregated data for human tissues conveniently harmonized at GWIPS database[37]. We analyzed whether endogenous polyA tracts and poly-lysine sequences induce translational pausing in both sets of data. Ribosome stalling can be observed in the ribosome profiling data as an increase in the abundance of ribosome footprints on sequences that cause ribosomes to pause during translation[38]. Cumulative data for all transcripts with polyA tracts from human cells indicates substantial translational pausing on these sequences (**FIGURE 2.4A**). The same effect was noted on poly-lysine sequences that contained more than four consecutive lysine residues in multiple other studies using *S. cerevisiae* ribosome profiling datasets with- out cycloheximide

treatment or datasets from human tissue cultures regardless of cycloheximide treatment[11,39–41]. However, analyses of previously published *P. falciparum* ribosome profiling dataset[4] indicated no evidence for ribosome stalling in *P. falciparum* transcripts containing polyA tracts. Normalized ribosome occupancy for *P. falciparum* transcripts with a length of less than or equal to 22 consecutive adenosine nucleotides (≤22 As), that code for more than seven consecutive lysines, indicated more or less equal ribosome occupancy over polyA tract (**FIGURE 2.4B**). We limited our ribosome profiling analyses of *P. falciparum* transcripts to polyA tracts of ≤22 As, since the cumulative transcript analyses become hindered by the low sequence complexity of the region, or reduced number of reads, for the long polyA tracts (**SUPPLEMENTAL FIGURE 2.5**). As such, the dip in *P. falciparum* occupancy plot is a result of a reads mapping artifacts. The longer the polyA segment, the harder it is to uniquely map a read – typically such reads are discarded. This artifact is clearly seen in the **SUPPLEMENTAL FIGURE 2.5**, where the occupancy is shown per length of polyA segment – the larger polyA track, the larger symmetrical gap around position 0. The correlation holds true to about 30 nt, which is the read length in the original experiment by Caro et al., 2014.

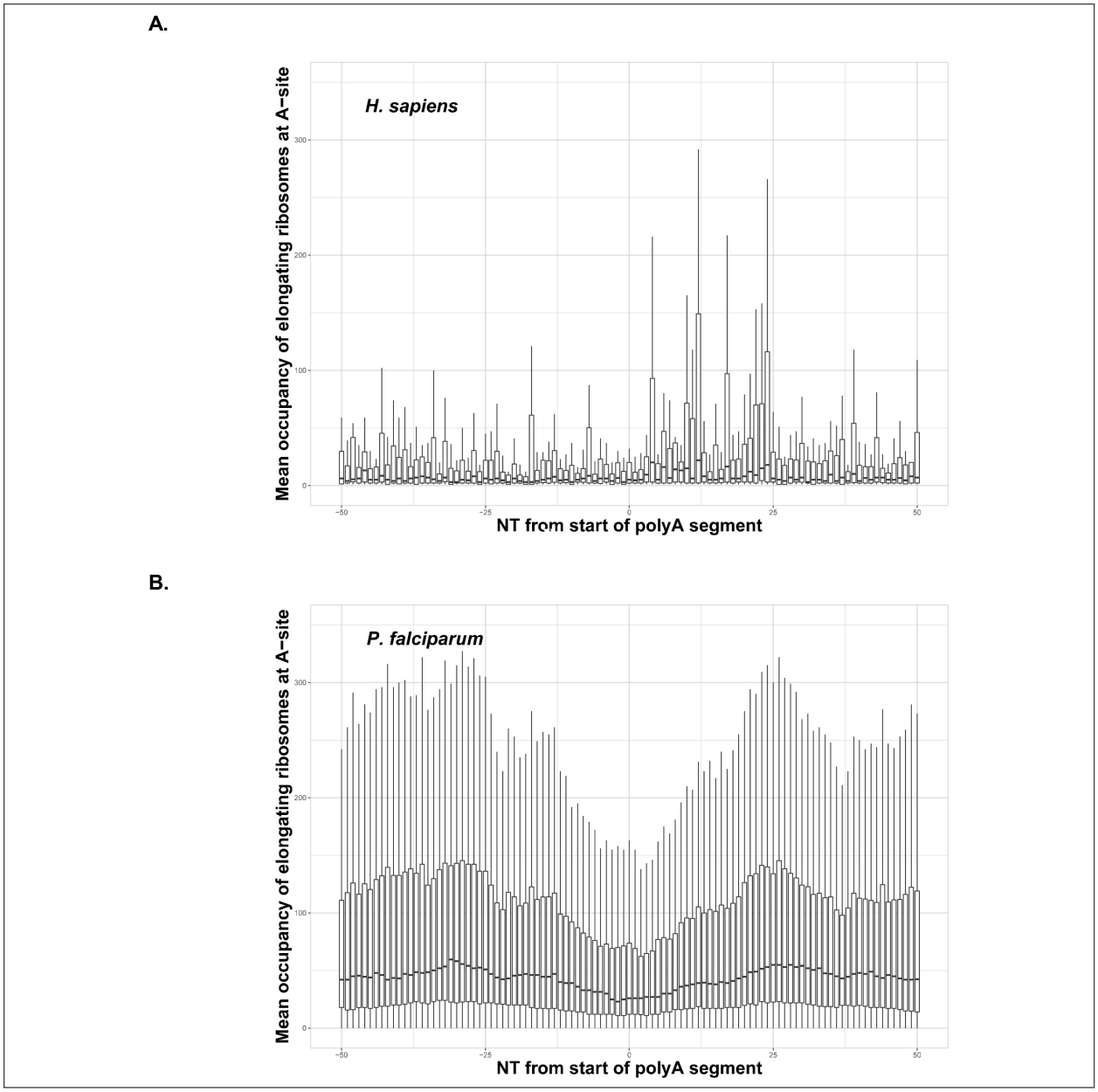

FIGURE 2.4 | Cumulative ribosome profiling analysis of polyA segments in *H. sapiens* and *P. falciparum*. Occupancy of elongating ribosomes (mapped to A-site) around the start of polyA segments in human **(A)** and *P. falciparum* **(B)**. Occupancy is shown on the same scale. In both cases, to avoid the inclusion of sparsely mapped segments, regions with average occupancy below the mean for the whole dataset were excluded. In the case of *P. falciparum* gene segments with polyA tracts shorter than 22 adenosine nucleotides were taken into account. Centerlines show the medians; box limits indicate the 25th and 75th percentiles; whiskers extend 1.5 times the interquartile range from the 25th and 75th percentiles. Dip in around position 0 in the *P. falciparum* plot is an artifact of the reads mapping procedure shown in **SUPPLEMENTAL FIGURE 2.5**. It is not observed in human data, because of shorter polyA segments and lower occupancy overall around these segments.

Since there is a massive increase in protein synthesis in *P. falciparum* cells during the trophozoite and schizont stage of IDC[4,25] we analyzed whether there is a different distribution of ribosome profiling reads surrounding polyA tracts at different stages of *P. falciparum* development. We found that the translation of endogenous polyA tracts is independent of different stages of *P. falciparum* IDC, as we did not notice any significant difference in the distribution of ribosome protected fragments (**SUPPLEMENTAL FIGURE 2.6**) and ostensibly irrespective of the length of polyA tracts or poly-lysine runs. While we observe a relatively small increase in the number of elongating ribosomes on polyA segments in the late trophozoite and schizont stages of IDC (**SUPPLEMENTAL FIGURE 2.6**), it is unclear if these indicate higher protein expression or are just an artifact of a general increase in protein synthesis at this IDC stages.

In parallel with analyses of ribosome profiling data, we also selected a small subset of polyA tract-containing genes for independent expression analysis. We followed PfGAPDH (PF3D7_1462800) as a control gene without polyA tract, and PfZFP (PF3D7_1464200 (three polyA tracts and run of 20 consecutive adenosines), PfCRK5 - PF3D7_0615500 (four polyA tracts and run of 20As) and PfIWS1L - PF3D7_1108000 (three polyA tracts and run of 31As), to represent genes with polyA tracts (**SUPPLEMENTAL FIGURE 2.7**). PfZFP is a zinc-binding protein with homology to the human ZC3H6 gene (Zinc Finger CCCH Domain-Containing Protein 6), PfCRK5 is cdc2-related protein kinase five and PfIWS1L is transcription elongation factor associated with RNA Polymerase II. We used a sorbitol-based method to synchronize *P. falciparum* Dd2 strain at

the ring stage of IDC and followed transcript profiles over the next 48 hr of the parasite life cycle. The mRNA profiles of three polyA tract genes were analyzed using qRT-PCR and normalized to the expression of PfGAPDH in *P. falciparum* Dd2 lab strain. A time-course study of synchronized parasite culture indicated that the selected polyA tract transcripts are efficiently transcribed at all-time points when compared to the control gene (**SUPPLEMENTAL FIGURE 2.8**). Moreover, the increase in transcription of all three polyA tract genes followed previously described just-in-time transcription profile in trophozoite and schizont IDC stage of *P. falciparum*.

Finally, mRNA translation could also be affected by the ability of RNA to fold into unique functional structures; for example RNA secondary structures have been shown to coordinate ribosomal frameshifting[42,43], slow ribosomal progression to allow protein folding[44] and to affect ribosomal density[45,46]. To determine the RNA structural characteristics of the *P. falciparum* transcriptome, we analyzed the ability of all coding sequences to form thermodynamically stable RNA secondary structures using an *in silico* approach to characterize RNA folding landscapes[46,47]. We compared the relative structural stability of the *P. falciparum* transcriptome to that of humans and the AU-rich *T. thermophila*. On average, the coding sequences from *T. thermophila* and *P. falciparum* yielded structures with higher predicted minimum free energy (MFE; **SUPPLEMENTAL FIGURE 2.9**), than those from the coding sequences of human genes; a result which mostly correlates with the higher overall AU-content of *P. falciparum* and *T. thermophila* transcripts. In this analysis, each MFE is also characterized by a thermodynamic z-score (SEE MATERIALS AND METHODS). The thermodynamic z-score normalizes for nucleotide content and

suggests whether sequences may form potentially functional structures[48]. Specifically, the thermodynamic z-score indicates whether a nucleotide sequence has been ordered to adopt a more stable secondary structure than its nucleotide content would typically produce[48] (which is the case for many ncRNAs[49] as well as RNA regulatory structures embedded in mRNAs[50,51]).

Interestingly, transcriptome z-scores revealed no significant differences between *P. falciparum* and *T. thermophila* (**SUPPLEMENTAL FIGURE 2.9**). This result indicates that while RNA folding stability varies between species, following from skews in nucleotide content, the potential occurrence of ordered, structured motifs does not. This suggests that globally, *P. falciparum* coding sequences do not appear ordered to adopt structures any more stable than would be expected for random sequences or with the same nucleotide content found in *T. thermophila*. However, expression of reporters with polyA-tracts in *T. thermophila* is strongly attenuated (**FIGURE 2.2**). This computational effort does not take into account the most recent work describing the m6A mRNA methylation dynamics within *P. falciparum* coding sequences[52]. The m6A modification may impact RNA structure and association of *P. falciparum* mRNAs with certain RNA binding proteins[53]. However, previous work has demonstrated that m6A methylation does not affect the ability of the ribosome to decode mRNAs but instead has a modest impact on the rate of translation[54,55], which could in-turn reduce the rate of protein synthesis in *P. falciparum*. Taken together, our analyses of the *P. falciparum* transcriptome and translation of genes with endogenous polyA tracts, as well as in silico assessment of overall structure and stability of AU-rich transcripts indicates that the *P. falciparum* translation

machinery adapted to long and numerous polyA tracts in coding sequences of the majority of genes.

2.3.4 NGD pathway is not connected to mRNA degradation in *Plasmodium*

PolyA tracts and poly-lysine repeats are highly efficient at causing ribosome stalling and frameshifting in bacteria and most eukaryotes[10–22]. However, our analyses of endogenous *P. falciparum* genes and reporters with long polyA runs, as well as immunoprecipitations did not indicate any changes in either mRNA stability, protein amounts, or protein quality (**FIGURES 2.2–2.3**) that was previously observed in *E. coli*, yeast, and human cells[11,13,15,17]. So, we turned towards analyses of mRNA surveillance pathways in *P. falciparum* cells and their contribution to the synthesis of poly-lysine peptides from long polyA tracts. The NMD pathway seems to be intact in *Plasmodium* cells[56], while the existence of the NGD pathway has not been previously tested. We initially focused our analysis on two proteins that have been documented to be crucial for NGD pathways in eukaryotes, Hbs1 and Pelota[35]. The Pelota protein in complex with Hbs1 recognizes and rescues stalled ribosomes with empty A site on long polyA stretches, absence of tRNAs during starvation, damaged mRNAs, or stable RNA structures[35,39,57–59]. Our bioinformatics search of the *P. falciparum* genome did not identify an apparent homolog of Hbs1 nor the recently reported *S. cerevisiae* endonuclease Cue2 (NONU-1 in *C. elegans*)[60–62] in *P. falciparum* (**SUPPLEMENTAL TABLE 2.2**). To explore whether changes in the NGD pathway are potential adaptations of *P. falciparum* to polyA tracts and poly-lysine repeats, we first used CRISPR/Cas9 technology[63,64] to HA-tag the endogenous Pelota homolog (PFPELO, PF3D7_0722100, **SUPPLEMENTAL FIGURE 2.10**) in *P. falciparum* Dd2 cells.

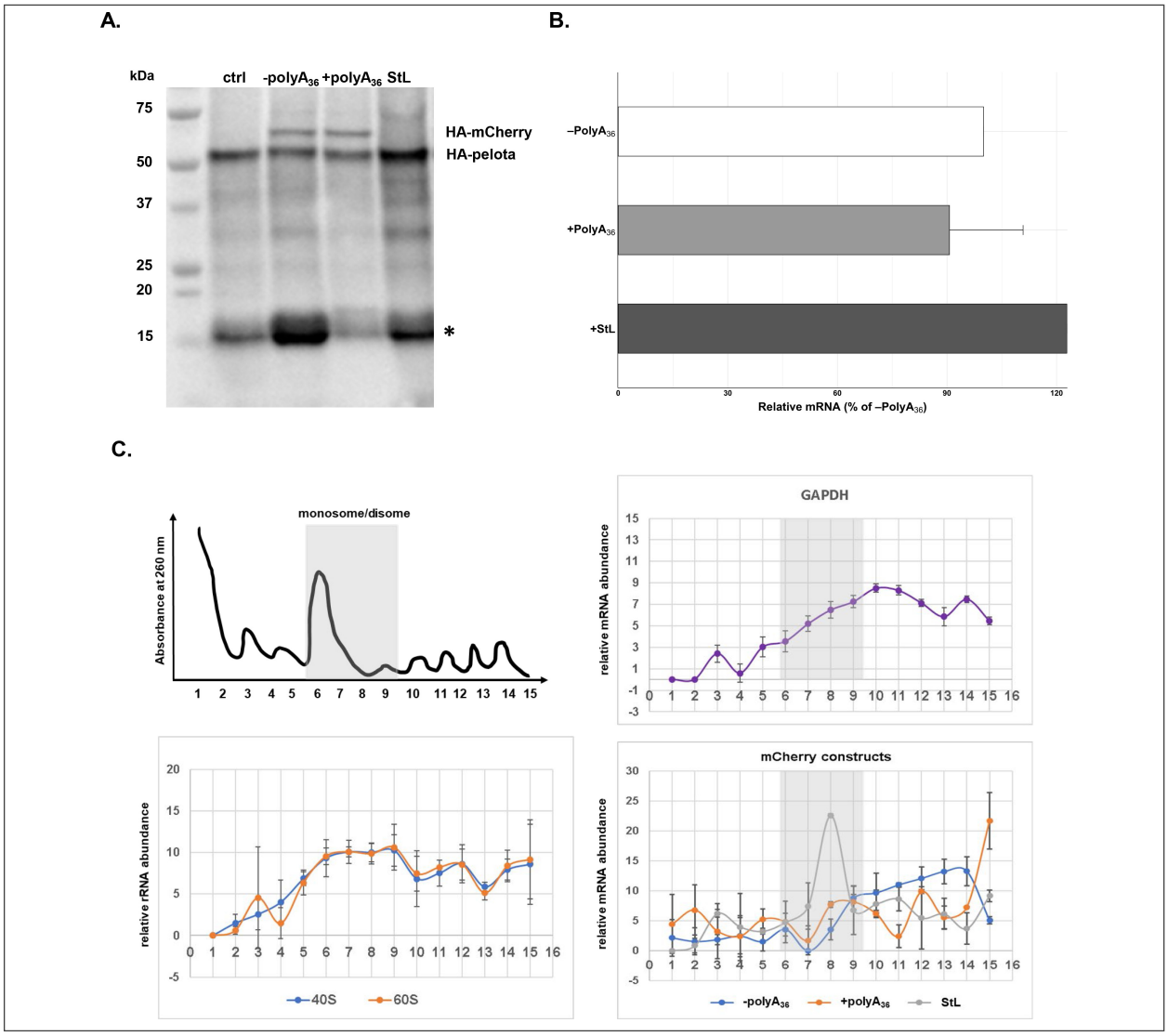

FIGURE 2.5 | Expression and polysome profiling analysis of ±polyA and StL constructs in *P. falciparum*. (A) The western blot of -polyA36, +polyA36, and stem-loop (StL) tagged reporter gene. The blot was probed with anti-HA antibody HRP labeled (sc-7392HRP). The HA-tagged proteins were episomally expressed in HA-tagged pelota *P. falciparum* Dd2 strain. HA-tagged Pelota protein serves as normalization control. (*) denotes human hemoglobin as 15kD contaminant band appearing and causing cross-reactivity in western blot analyses. **(B)** qRT-PCR measured mRNA levels of of reporter constructs with polyA tract and stem-loop insertions (polyA36, +polyA36, Stl). In each case, data represent the mean value of three biological replicates with standard deviation. **(C)** Distributions of mRNA (GAPDH, -polyA36, +polyA36, Stl) and rRNA, in polysome gradients as determined by RT-qPCR. Error bars represent measurement variability as determined by two qPCR replicates. The position of monosome and disome peaks is indicated in each analyzed sample (gray shade).

Since polyA-containing reporters, as well as endogenous genes, were efficiently and correctly translated in *P. falciparum* cells, we decided to test the *P. falciparum* NGD pathway with a common NGD substrate[35,65]. We inserted a 78 bp long RNA stem-loop into the fluorescent reporter sequence (StL, **Supplemental Figure 2.11**). The same stem-loop was previously described to stall ribosomes and induce NGD response with subsequent endonucleolytic cleavage in various reporters and multiple organisms[11,65–68]. We followed both protein synthesis and mRNA abundance from the StL construct in *P. falciparum* cells (**Figure 2.5A–B**). Insertion of the RNA stem-loop resulted in a severe reduction of reporter protein levels (**Figure 2.5A**, **Supplemental Figure 2.11**), but moderate increase in mRNA levels (**Figure 2.5B**). While we could not detect any HA-tagged StL reporter using western blot analyses (**Figure 2.5A**), we did notice the small but detectable amount of fluorescent reporter in the *P. falciparum* cells during live imaging (**Supplemental Figure 2.11**). To test whether stem-loop structure caused ribosomes to stall, we analyzed the distribution of StL transcript in polysome profile (**Figure 2.5C**). We used constructs with and without polyA tracts as controls. Polysome profile analyses indicated that mRNA of StL construct was associated mostly with polysome fractions 7–9 that correspond to the disome peak. Such mRNA distribution was in sharp contrast with the distribution of mRNAs for constructs with and without polyA tracts (±polyA36) and argues for the potential translational stall (**Figure 2.5A**). mRNAs for constructs with and without polyA tracts (±polyA36) and for PfGAPDH were distributed more evenly along the polysome fractions (fractions 9–16). These experiments argue that stable RNA structures in mRNAs stall *P. falciparum* ribosomes,

reducing protein synthesis from such transcript, however without significant impact on mRNA stability.

To further test whether global arrest of translation leads to the activation of RQC and NGD mechanisms, we used isoleucine (Ile) starvation (**FIGURE 2.6A**) to induce widespread ribosome pausing on Ile-codons[69,70]. Parasites rely on extensive proteolysis of human serum proteins to supplement Ile, which is found in 99% of all *P. falciparum* proteins[70]. As such, the majority of ribosomes will have either a reduced rate of protein synthesis or will be stalled on runs of Ile-residues encoded in endogenous *P. falciparum* transcripts. Ile starvation in *P. falciparum* was previously reported to induce a state of hibernation through the arrest of protein synthesis with phosphorylation of eIF2a, but in a GCN2-independent fashion, and without existing TOR-nutrient sensing pathway nor activation of ATF4 homologue[69]. Surprisingly, during the metabolically induced hibernation, parasites maintain their morphology while slowing down protein synthesis, and importantly more than 50% of parasites recover even after 4 days of starvation[69]. By analyzing *P. falciparum* cells 72 hr into Ile-starvation, we found that expression of PfPelo and PfHsp70 chaperone were upregulated in starved cells (**FIGURE 2.6B–C**). The mRNA and protein levels of PfPelo were moderately increased (approximately two-fold), while levels of PfHsp70 were strongly induced (five-fold increase) in response to the Ile-starvation. This increase in PfPelo levels is reminiscent of the recently reported increased human Pelo expression during elevated ribosome stalling and the absence of recycling during the developmental transition from reticulocyte to erythrocyte[71]. The substantial increase in Hsp70

levels upon starvation in human cells was associated with cell protective mechanisms against global protein misfolding[72,73].

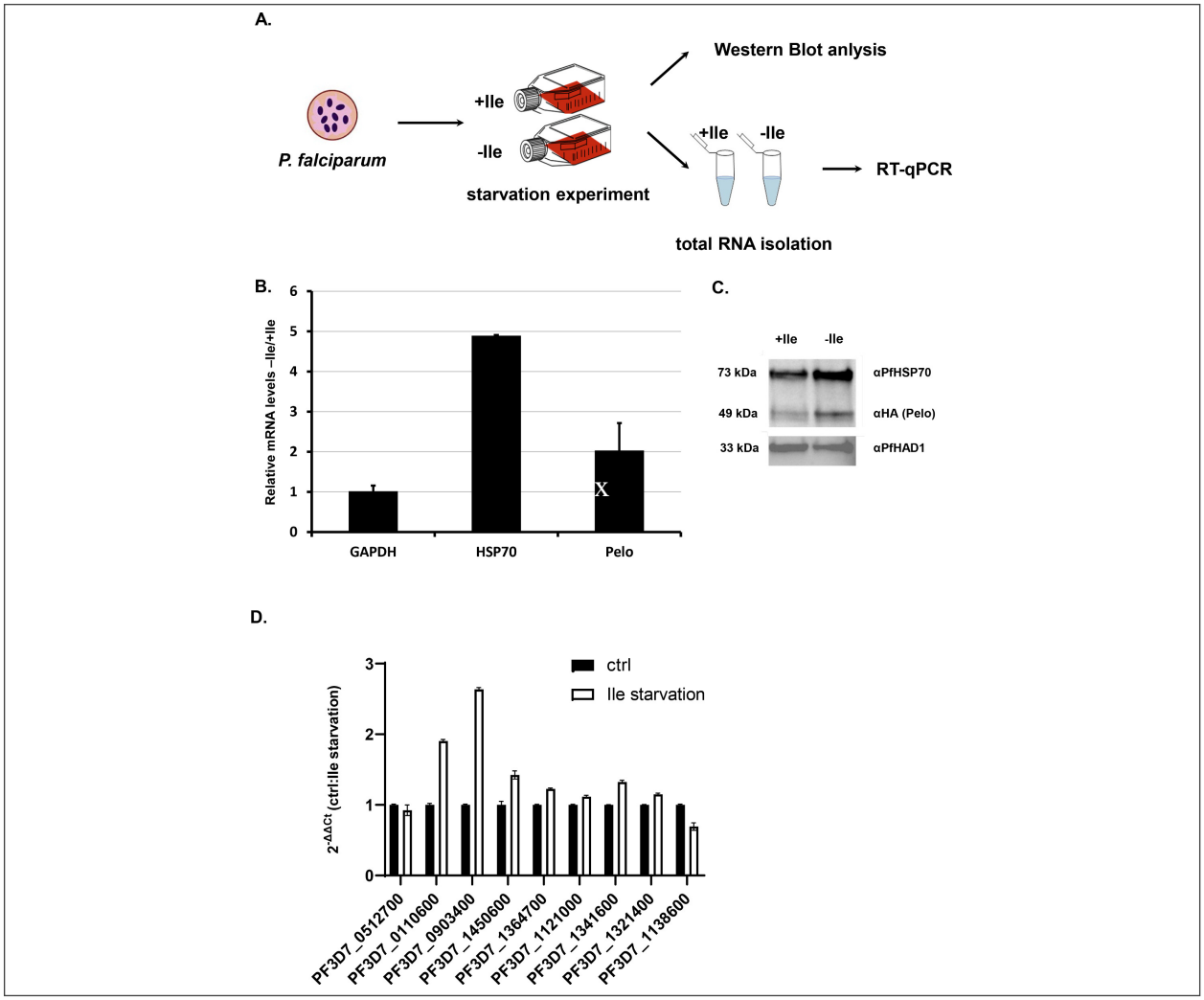

FIGURE 2.6 | Isoleucine starvation assay in *P. falciparum*. (A) The schematic presentation of the starvation experiment design. The cells were incubated for 48 hr in medium with and without Ile (+ / - Ile). After 48 hr samples were collected and protein and total RNA was isolated. **(B)** Relative mRNA of *P. falciparum* GAPDH (PF3D7_1462800), HSP70 (PF3D7_0818900), Pelo (PF3D7_0722100) transcripts after 48 hr isoleucine (Ile) starvation of the *P. falciparum* cells. Levels of each transcript are normalized to total GAPDH levels and represented as a ratio of transcript levels under Ile starvation (-Ile) over the control conditions (+Ile). In each case, data represent the mean value of three biological replicates with standard deviation. **(C)** Levels of *P. falciparum* HSP70 and Pelo proteins after 48 hr of Ile starvation. Western blot analysis of Ile starved (-Ile), and control (+Ile) sample are normalized to PfHAD1 (PF3D7_1033400) levels. HA-tagged *P. falciparum* Pelo protein was CRISPR/Cas9 engineered and detected using mouse HA-antibody. The molecular weight of each protein is indicated. **(D)** qRT-PCR measured mRNA levels of genes containing 3–7 Ile. PF3D7_0322300, PF3D7_0512700, PF3D7_0110600, PF3D7_0903400, PF3D7_1450600, PF3D7_1364700, PF3D7_1121000, PF3D7_1341600, PF3D7_1321400, PF3D7_1138600. Levels of each transcript are normalized to total GAPDH level and represented as a ratio of transcript levels under Ile starvation (-Ile) over the control conditions (+Ile). In each case, data represent the mean value of three biological replicates with standard deviation.

To test whether Ile-rich transcripts were targeted specifically by the RQC and NGD pathway during Ile-starvation, we examined transcripts that encode Ile-rich proteins in the *P. falciparum* genome. Previous studies indicated that while protein levels did not drastically change throughout starvation, protein synthesis was significantly reduced[69]. The microarray analyses of mRNAs in Ile-starvation samples also showed similar overall levels for the majority of mRNA transcripts when compared to non-starved controls. To specifically test transcripts with three and more consecutive Ile-codons, we analyzed mRNA abundance for nine *P. falciparum* genes during Ile-starvation (**SUPPLEMENTAL FIGURE 2.12**). We did not observe the general reduction in mRNA levels for Ile-*rich P. falciparum* genes when we compared starved to non-starved control samples. We instead found a slight increase in mRNA abundance for several Ile-rich transcripts during starvation (**FIGURE 2.6C**). This result is rather similar to Leu- and Arg-starvation in mammalian cells, where no overall change in mRNA stability is observed during amino acid starvation[74]. However, our result indicated that both increase in expression of NGD-associated factor, Pelota, and protein chaperone HSP70 may contribute to cell survival, ribosome recycling and mRNA stabilization during amino acid starvation in *P. falciparum*. This result is opposite to the recently reported role of human Pelo protein in the regulation of global mRNA decay on stalled mRNAs in platelets[75]. Transgenic overexpression of human Pelo protein potentially releases unrecycled ribosomes and stimulates mRNA degradation during translational arrest in platelet differentiation. This is not the case in P. falciparum, where the production of the PfPelo protein is increased during the *P. falciparum* Ile-starvation; however, there was a lack of

targeted mRNA degradation (**FIGURE 2.6C**). We observed, rather, stabilization of mRNAs that should cause ribosomal stalling, like in the case of StL construct (**FIGURE 2.5B**). These results may indicate that RQC and NGD pathway in *P. falciparum* cells are not connected, at least directly, to targeted mRNA degradation.

2.3.5 *Plasmodium* ribosome structure accommodates poly-lysine repeats

In the light of our data with different reporters and analyses of endogenous *P. falciparum* genes (**FIGURES 2.2–2.6**), we were still interested as to how the *P. falciparum* translation machinery deals with polyA tracts and poly-lysine sequences. Ribosomal stalling on long poly-lysine runs[11,19,20,68,76–78] was classically explained by electrostatic interactions of the polybasic peptide and the exit tunnel of the ribosome[78]. More recent studies revealed that polyA tracts and mRNA directly contribute to ribosomal stalling and frameshifting[11,12,14,17]. Consecutive adenosines are engaged by the ribosome decoding center nucleotides and are stabilized on both sides by rRNA base stacking interactions[12,14], and adopt a helical conformation typical for single-stranded polyA stretches[79]. Based on these reports, we analyzed *P. falciparum* ribosomes as the principal components that could accommodate translation of long polyA stretches.

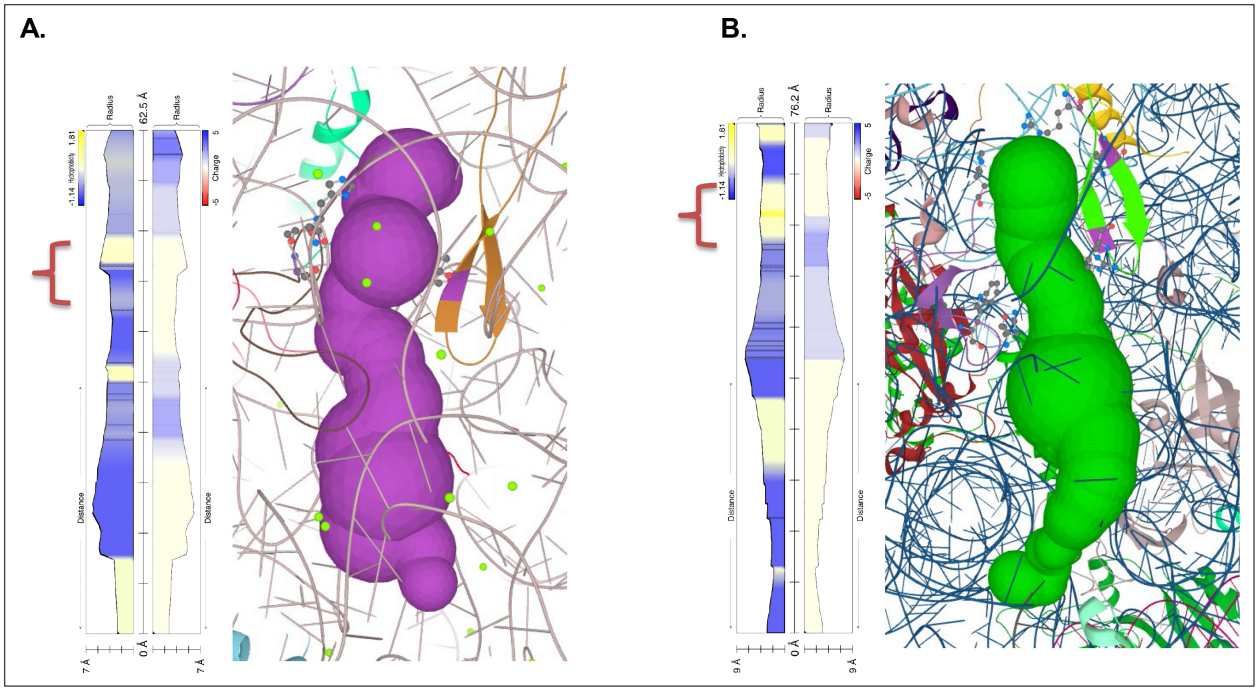

FIGURE 2.7 | Characterization of polypeptide exit tunnel in *H. sapiens* and *P. falciparum*. Polypeptide exit tunnel as predicted by MOLE service from *Plasmodium* ribosome (PDB:3j79) **(A)** and human ribosome (PDB: 6d90) **(B)**. The constriction site flanked by L22 and L4 is marked in the orange clamp, and lining residues in both cases are marked with ball-and-stick visualization. Vertical plot outline hydrophobicity (left) and charge (right) profiles across the tunnel (Pravda et al., 2018). The width of the tunnel is indicated on the scale at the bottom of the plot. The total lengths of the tunnel are indicated at the top of the plots.

The retention and conservation of polyA tracts, as well as the stage-independent expression of polyA genes (**FIGURE 2.1**), reveals that all rRNAs within Plasmodium spp. must deal with them. The structural data on *Plasmodium* ribosomes are limited to two recent cryo-EM studies of *P. falciparum* ribosomes isolated during the schizont stage of the IDC[80,81]. Both studies reported that *P. falciparum* ribosomes have different structural and dynamic features that distinguish them from other organisms. While the majority of *P. falciparum* 28S associated rRNA expansion segments (ESs) are shorter than in human rRNA, 18S ESs are generally larger (**SUPPLEMENTAL**

FIGURE 2.13). The ES6S/7S is located next to the binding pocket of eIF3 and might be necessary for translation initiation or termination[30,80,82]. ES9S/10S are positioned at the head of the 40S subunit and are probably important for the recruitment of additional translation factors as well as for mobility of the head region of 40S subunit[80,81]. Previous studies had shown that the absence of ZNF598 and RACK1 would help in the resolution of putative stalling and subsequent read through of polyA sequences[18–20]. However, the P. falciparum homolog of ZNF598 (PF3D7_1450400), appears to be abundantly expressed according to PaxDB database[83].

On the other hand, while being essential and one of the most well-expressed proteins in *P. falciparum* cells[83,84], the absence of RACK1 protein on *Plasmodium* ribosomes could be the most prominent features regarding the translation of polyA tracts and poly-lysine repeats (**SUPPLEMENTAL FIGURE 2.13**)[80,81]. Asc1 (yeast RACK1 homolog) is required for endonucleolytic cleavage of stalled mRNAs in yeast cells[85,86]. The deletion of RACK1/Asc1 in human or yeast cells was also shown to increase the production of proteins with polybasic peptides, however, at the cost of increased frameshifting[20,76,87]. The recent report has shown that the absence of Asc1 in yeast generally slows down elongation, promoting frameshifting on problematic CGA-CGA pairs[14]. However, the mechanisms proposed for the polyA-induced ribosome stalling involves the inhibitory conformation of polyA tract mRNA in the A site of the ribosome[12,14]. This proposed mechanism for polyA stalling induction should not depend on species, because ribosome nucleotides interacting with π-stacked polyA sequences are universally conserved (A1756 AND C1634, **SUPPLEMENTAL FIGURE 2.14**). No significant differences in the mRNA tunnel have been observed in *P. falciparum* ribosome structures[80,81]. However, differences in the

resolution and absence of mRNA in *P. falciparum* ribosome cryo-EM structures do not allow for precise comparison of the conformation of rRNA between *Plasmodium* and either yeast or mammalian ribosomes[80,81]. Altogether these observations do not explain why the mRNA tunnel and interactors of the *P. falciparum* ribosome could influence the efficient translation of polyA tracts.

Recently it was postulated that the stalling on the polyA tracts is an effect of a synergy between polyA-induced suboptimal geometry at PTC and poly-lysine interactions with ribosome exit tunnel[12].To further investigate whether additional differences in the ribosome structure contributed to *P. falciparum* adaptation to long polyA tracts and poly-lysine repeats, we analyzed the ribosome peptide exit tunnel of *P. falciparum* as predicted by the MOLE 2.5 toolkit[88] (**FIGURE 2.7**). While a recent study found no differences in charge pattern along the peptide tunnel in eukaryotes, notably between *P. falciparum* and human[89], we observed changes in hydrophobicity across the tunnel (**FIGURE 2.7** AND **SUPPLEMENTAL FIGURE 2.15**). Interactions between clusters of positive charges and hydrophobic environments are generally unfavorable even during protein translocation[90]. Along this line, the ribosome exit tunnel of *P. falciparum* seems to be generally more hydrophilic, including the constriction site. Given a substantial length of poly-lysine peptide required to induce stalling on downstream polyA tracts (6 to 11, depending on the experimental system)[12] it is plausible that the upper and the central tunnel are contributing to the observed effects. This is what is observed in other organisms. The free energy profile of lysine across the *H. marismortui* ribosome exit tunnel, which also has a hydrophobic region between the PTC and constriction site (**SUPPLEMENTAL FIGURE 2.15**), indicates

the presence of a significant energy barrier after the constriction site, not before[91]. Indeed, *in vitro* translation of poly-lysine and poly-phenylalanine using *E. coli* ribosomes resulted in rather different paths and rates of the extension of nascent peptide due to postulated hydrophobic entry to the ribosome exit tunnel[92]. Moreover, in a recent structure of the polyA stalled yeast ribosome, the unresolved density was also indicated in this part of the exit tunnel next to the PTC and above the constriction site[14]. Taken together, it seems that the ribosome peptide exit tunnel of parasites adapted to accommodate synthesis of long runs of poly-lysine residues by reducing electrostatic barriers below the PTC and at the constriction site. The resulting dynamics of translation of poly-lysine might be high enough to reduce the chances for unfavorable interactions between mRNA and ribosome.

2.4 Discussion

Runs of lysine and arginine residues are underrepresented in the proteome of multiple organisms compared to the runs of other amino acids, suggesting a selective pressure against polybasic amino acid sequences[93]. One potential explanation for this evolutionary selection is electrostatic interactions of the polybasic peptide and the exit tunnel of the ribosome that would impact the rate of protein synthesis[77,78]. However, multiple biochemical analyses of poly-lysine stalling sequences, in both prokaryotic and eukaryotic systems, revealed that runs of lysine AAA codons exhibit a more significant delay in ribosome movement than an equivalent number of AAG lysine codons[6–8,11–14,17,21,22]. More recent study in mouse embryonic stem cells indicates that besides 12A-1 sequences endogenous sites with 8–9 As are sufficient to cause recruitment of mRNA surveillance pathways[13]. So as is the case of polybasic residues, analyses

of codon usage within poly-lysine peptides revealed that the expected frequency of AAA codons compared to AAG codons in runs of four consecutive lysine residues is lower in the coding regions of genes for multiple organisms (**FIGURE 2.1**)[11,17,31]. However, ribosome stalling and frameshifting induced by polyA runs depend on the sequence and conformation of the mRNA in the ribosome, with a questionable contribution by the nascent polypeptide chain[11,14,16,17]. As such, both polyA tracts and poly-lysine sequences are unfavorable in mRNAs or proteins, respectively, of most tested organisms.

Data presented here indicate *P. falciparum*, the most studied malaria-causing human pathogen, is an exception to this rule. With an 80% AT-rich genome and more than 63% of transcripts containing polyA tracts, *P. falciparum* represents a paradigm breaking species for polyA tracts (**FIGURE 2.1**). The atypical enrichment in polyA tracts in the coding sequence of mRNAs, translated into long poly-lysine runs in proteins, is a feature that is conserved in most *Plasmodium* species (**FIGURE 2.1**)[4,29,31,83]. Such species-specific evolutionary conservations usually result in traits that are beneficial for survival. The increased AT-richness and number of polyA tracts in *P. falciparum*, as such, could be a result of selective pressure on biosynthetic pathways (AT vs. GC biosynthesis)[94,95] and the oxidative intraerythrocytic environment[96]. An increase in poly-lysine runs might have been of different etiology. Gene ontology analyses of polyA tract and poly-lysine genes in *P. falciparum* suggested cellular and pathological adhesion proteins as one of the enriched gene groups (**SUPPLEMENTAL TABLE 2.1**). It is attractive to speculate that advantages for the parasites to synthesize proteins with poly-lysine repeats

could be solely driven by benefits in the adhesion and invasion of host cells[97,98] or export of numerous parasite proteins to the surface of infected erythrocytes[99–101].

Our data further indicate that the *P. falciparum* translational machinery permits the translation of polyA tracts and poly-lysine repeats without mRNA degradation, protein synthesis attenuation, nor obvious activation of translational surveillance pathways (**FIGURES 2.2–2.5**). The biochemical assays with reporter sequences (**FIGURES 2.2, 2.3,** AND **2.5**) as well as analyses of ribosome profiling data[4] (**FIGURE 2.4**) suggest that parasite ribosomes do not stall or frameshift on long polyA tracts and poly-lysine runs. Even though RNA folding propensity in *P. falciparum* has been skewed due to the nucleotide content, the predicted stability of native *P. falciparum* transcripts did not show differences compared to human cells. However, the change in nucleotide composition and a number of long polyA tracts of *P. falciparum* (**FIGURE 2.1**) probably shaped NGD/NSD mRNA surveillance responses in parasites (SEEN IN **FIGURES 2.5–2.6**). Insertion of the stable stem-loop structure (StL) in the reporter construct resulted in reduced protein synthesis and ribosome stalling but without noticeable mRNA degradation (**FIGURE 2.5** AND **SUPPLEMENTAL FIGURE 2.11**). Our results with stem-loop construct and Ile-starvation are rather disparate to experiments in other eukaryotes, including the human host[11,65–68], and argues for significant differences between human and *Plasmodium* NGD mRNA surveillance pathways.

Similarly, while following the general cellular response to induced metabolic stress with Ile-starvation we noticed the upregulation of Pelo and Hsp70 levels[71–73], however again with the lack of targeted mRNA degradation of Ile-rich transcripts or reduction in global mRNA stability

(**FIGURE 2.6**)[69]. It seems plausible that amino acid starvation could allow uncharged Ile-tRNAs to fill the A-site and block Pelo binding thus preventing NGD and RQC activation in this case. Similarly, Leu- or Arg-starvation experiments in HEK293 cells do not result in global change in mRNA stability but rather increase in translation termination and ribosome recycling[74]. While authors in Hek293 amino acid starvation studies did not follow changes in Pelota protein levels, it was shown recently that transgenic overexpression of Pelo protein in human platelets led to rapid degradation of most cytoplasmic platelet transcripts[75]. Our studies indicate that increased *P. falciparum* Pelo levels, at least during the amino acid starvation, do not cause targeted mRNA degradation. However, future studies on the role PfPelo levels during amino acid starvation, its role in ribosome recycling as well as identification of missing *P. falciparum* Hbs1 protein will give more insight in NGD and RQC process in *Plasmodium*. Nonetheless the results with StL construct and amino acid starvation suggest a difference between human and *Plasmodium* NGD mRNA surveillance and mRNA degradation pathways in both signaling and resolution of ribosome stalling events[102]. One of these differences could be potentially attributed to the loss of recently reported NGD endonucleases[60–62] in *P. falciparum* cells. The bioinformatics analyses of the *P. falciparum* genome did not indicate a homolog of either Cue2 or Nonu-1 endonuclease (**SUPPLEMENTAL TABLE 2.2**)[60–62]. However, the loss of Cue2/Nonu-1 in *Plasmodium* cells can not completely explain the lack of mRNA degradation on the stem-loop construct (**FIGURE 2.5**) or in Ile-starvation experiments (**FIGURE 2.6**). Given that the majority of observed NGD-induced mRNA decay is processed by canonical exonucleolytic decay by Xrn1[60,62], stabilization of NGD substrates in *P. falciparum* remains puzzling.

It is apparent that the accommodation of polyA tracts and poly-lysine repeats in translation required multiple adaptations to be vital and typically highly conserved components of the translation and mRNA surveillance pathways. Unambiguously, *P. falciparum* ribosomes had to change to accommodate correct and efficient protein synthesis from the runs of coding polyA tracts that are longer than the average size of 3'-UTR polyA tails in other organisms[32–34]. The fact that recent cryo-EM structures indicated that the *Plasmodium* ribosome lacks interaction with PfRACK1 protein (**FIGURE 2.7**) could be beneficial for the translation of polyA tracts into poly-lysine runs[80,81]. Albeit, it is not clear what would substitute the role of RACK1/Asc1 in the correct reading frame maintenance during translation of long polyA tract or other stalling sequences[14,20,76,87]. The lack of Asc1/RACK1 association with *P. falciparum* ribosomes could affect its association with other RQC protein homologs, such as ZNF598, which can influence the activation of RQC pathway and endonucleolytic cleavage[86]. It is possible to speculate that *P. falciparum* specific ribosome extension segments in the 40S subunit may have the role in recruiting other *Plasmodium* proteins that may help with translation of polyA tracts and poly-lysine repeats[80,81]. However, it was recently indicated that an inhibitory conformation of mRNA in the A-site of the ribosome, as well as the polybasic character of the nascent polypeptide chain in the ribosome, peptide exit tunnel, are crucial for the poly(A)-mediated stalling mechanism[12,14]. It is not clear from the conservation of the 18S rRNA sequence (**SUPPLEMENTAL FIGURE 2.14**) and structure of the ribosome A-site in *P. falciparum* ribosomes[80,81] how parasite ribosomes would circumvent an inhibitory conformation of the polyA mRNA in the A site seen in yeast and mammalian ribosomes[12,14]. It might be that changes in the peptide exit tunnel of *P.*

falciparum ribosomes (**FIGURE 2.7**) have partially contributed to the adaptation to the synthesis of long poly-lysine runs by reducing the potential stalling effects associated with translocation of polybasic peptides through hydrophobic environment[90]. However, contributions of *Plasmodium*'s ribosome exit tunnel in overcoming poly-lysine induced ribosome stalling still need to be tested experimentally. It is also plausible that translation rate is also a factor here. Chandrasekaran and coworkers[12] in their polyA stalling study had observed a significantly different in number of lysines required for stalling between in vitro system and cells. They have explained the observation by 5-fold differences in translation rate.

In conclusion, to adapt to polyA tract translation for the production of the polybasic and homopolymeric lysine repeats, the malaria-causing parasite has altered its mRNA translation quality control pathways as well as its ribosomal proteins and ribosome structure. The additional diversity of *Plasmodium spp.* rRNAs[103–105] and possible activity of yet unknown ribosome-associated factors promote the possibility of *Plasmodium* 'specialized ribosomes,' which allow for polyA tract translation into poly-lysine sequences of functional proteins. Further insights into differences between components of translational machinery and mRNA surveillance pathways present in *P. falciparum* and host organisms, as well as the physiological role(s) of conserved poly-lysine repeats, will provide answers to these questions and enable identification of new drug targets against malaria.

2.5 Materials and Methods

KEY RESOURCES TABLE

Reagent type (species) or resource	Designation	Source or reference	Identifiers	Additional information
Gene (*Plasmodium falciparum*)	Pelota gene	This paper	PF3D7_0722100	CRISPR/Cas9 engineered with C-terminal 3xHA tag
Cell line (*Plasmodium falciparum*)	Dd2 strain	Goldberg lab	http://neurolex.com/wiki/NCBITaxon:57267	*P. falciparum* strain used for all experiments
Cell line (*Homo sapiens*)	Dermal fibroblast (normal, Adult)	ATCC	PCS-201–012	
Cell line (*Homo sapiens*)	Adult erythrocytes (primary cell line)	Goldberg lab and BJCIH Children Hospital		Deidentified human blood. 50% haematocrit, washed in complete medium (MCM)
Cell line (*Tetrahymena thermophila*)	strain B2086 (II)	Chalker Lab	http://neurolex.com/wiki/NCBITaxon:5911	
Recombinant DNA reagent	pBSICY-gtw (plasmid)	Chalker Lab		·PMCID: ·PMC3232721 ·*T. thermophila* transfection plasmid
Recombinant DNA reagent	pc-DNA-DEST40 (plasmid)	Thermo Fisher Scientific	RRID: Addgene_45597	HDF transfection plasmid
Recombinant DNA reagent	pHHT-TK (plasmid)	Goldberg lab		Plasmid for standard CRISPR/Cas9 knock out approach in *P. falciparum* cells.
Recombinant DNA reagent	pyDHOD-2A-Cas9 (plasmid)	Goldberg lab		All-in-one Cas9+gRNA cassette vector DSM-1 resistance
Antibody	anti-HA antibody (mouse monoclonal antibody)	Santa Cruz Biotechnology	Cat# sc-7392, RRID: AB_627809	WB (1:5000), used also as HRP conjugated
Antibody	anti-mouse (horse unknown clonality)	Cell Signaling Technology	Cat# 7076, RRID: AB_330924	WB (1:5000)
Antibody	anti-rabbit (goat polyclonal antibody)	Cell Signaling Technology		WB (1:5000)
Antibody	Anti-HSP70 (rabbit polyclonal antibody)	AgriSera		WB (1:1000)
Antibody	anti-PfHAD1 rabbit	Odom lab		WB (1:10000) PMID:25058848
Chemical compound, drug	Cycloheximide	Sigma Aldrich	Cat# C1988	200 µM
Chemical compound, drug	WR99210	Sigma Aldrich	Cat# W1770	10 nM
Chemical compound, drug	DSM1	Sigma Aldrich	Cat#533304	DHODH Inhibitor 1.5 µM
Commercial assay or kit	llustra triplePrep Kit	GE Healthcare	Cat# 28942544	DNA, RNA and protein isolation kit

2.5.1 Parasite culturing

P. falciparum line Dd2 was cultured at 2-5% hematocrit in O^+ erythrocytes in RPMI 1640 supplemented with 5 g/L Albumax II (Gibco), 0.12 mM hypoxanthine (1.2 mL 0.1M hypoxanthine in 1 M NaOH), 10 µg/mL gentamicin[106]. Cultures were grown statically in a candle jar atmosphere. As required, cultures were synchronized with 5% (w/v) sorbitol. Medium for Isoleucine starvation: 16.1g RPMI medium 1640 per l (ME011232P1 Gibco), 2 g of sodium bicarbonate, 0.12 mM hypoxanthine, 10 µg/mL gentamicin, and with and w/o 100 µM Isoleucine.

2.5.2 Generation of mCherry-GFP–Expressing plasmids with and without 12 lysines coded with 36 As in a row (polyA- and polyA+)

mCherry with and without polyA was amplified from plasmids previously created[11] pBttlysforXhoI 5'- gcgcctcgagatgggctacccatacga-3' (XhoI site underlined) and mCherryrevAvrII 5'- gcgccctaggcttgtacagctcgtccatgccg3' (AvrII site highlighted) digested with XhoI and AvrII, and ligated into the same sites of the episomal over-expression (EOE) a containing the promoter region for PfHsp86, a C-terminal GFP tag, and a human dihydrofolate reductase (hDHFR) drug-selection cassette[107]. mCherry reporter in pc-DNA-DEST40 previously published[11,15] used to transfect HDF cells.

2.5.3 HDF cells culturing and transfection

HDF cells were cultured in Dulbecco's modified Eagle's medium (DMEM) (Gibco) and supplemented with 10% fetal bovine serum, 5% minimum essential medium nonessential amino acids (100×, Gibco), 5% penicillin and streptomycin (Gibco), and L-glutamine (Gibco). mCherry reporter in pc-DNA-DEST40 plasmid (1 µg) was introduced to the cells by the Neon Transfection System (Invitrogen) with 100 µL tips according to cell-specific protocols (**www.lifetechnologies.com/us/en/home/life-science/cell-culture/transfection/transfection---selection-misc/neon-transfection-system/neon-protocols-cell-line-data.html**). Cells electroporated with DNA plasmids were harvested after 48 hours if not indicated differently[11].

2.5.4 Parasite transfection

Asynchronous Dd2 parasites were incubated with 100 µg of maxi-prep DNA of each of the EOE constructs described above encoding mCherry-GFP (with and w/o polyA), transfected in Bio-Rad Gene Pulser cuvette (0.2 cm), 0.31 kV, 950 up, infinity resistance. 10 nM WR99210 was added to parasite 48 h after transfection and used to select resistant parasites[108].

2.5.5 Saponin lysis of infected red blood cells (iRBCs)

The cell iRBCs were resuspended in two volumes of PBS containing 0.15% saponin, and incubated on ice for 10 min, with vigorous mixing every 3 min. Afterward, the samples were centrifuged 7000g, 5 min, 4°C, and the pellets were washed three times more with the same buffer.

2.5.6 Genomic DNA isolation

The extraction of gDNA was done from samples pretreated with a saponin lysis buffer, and we followed the protocol of the DNeasy Qiagen kit.

2.5.7 RNA extraction and qRT-PCR

Total RNA was extracted from iRBCs using the RiboZol RNA extraction reagent (Amresco) with some changes (protocol from Jabos-Lorrrena Laboratory at Johns Hopkins School of Public Health), or we used Illustra triplePrep Kit GE Health Care. In 1 mL of pelleted iRBCs (500g, 5min, room temperature), parasitemia 5-7%, 5 mL of RiboZol was added. It was mixed thoroughly that all cells lysed. At this step, the sample can be snap-frozen and stored at -80°C or proceed further. Add 1 mL of chloroform and mix for 20 sec. Transfer the aqueous phase to a new tube and add 1/10^{th} of the volume of 3 M sodium acetate, mix well and add 10 µL GlycoBlue. Add 2.5 mL of cold iso-propanol and leave overnight at -80°C. After overnight precipitation, the samples were centrifuged at 16000xg, 1h, 4°C. The supernatant was discarded and washed twice with 5 and 1 mL of cold ethanol. The pellets were dried and resuspended in pure water. RNA concentration was measured by NanoDrop (OD260/280). For total RNA extraction using Illustra TriplePrep Kit (item# 28942544 GE Health Care), we used 200 µL of iRBCs, parasitemia 5-7%. The cell pellet was resuspended in 600 µL PBS buffer containing 0.15% saponin (item# 47036-50G-F Sigma), cOmplete™ Protease Inhibitor Cocktail without EDTA (item# 11873580001 Roche), RNase OUT 1ul/mL (item# 10777019 Invitrogen), and incubated at RT for 10 min on ice. Afterward, it was centrifuged 7000xg, 5 min, 4°C, and the pellets were washed three times

more with the same buffer. After this pretreatment to get rid of hemoglobin pellets were used for total RNA isolation following Illustra TriplePrep Kit protocol.

iScript Adv cDNAkit for RT-qPCR (item# 172-5037, Bio-Rad) or SuperScript *IV VILO* Master Mix (item# 11756050 Life Technologies Corporation), was used with 100-200 ng of total RNA following the manufacturer's protocol. iQ SYBR Green Supermix (item# 1708886, Bio-Rad) protocol was used for qRT-PCR on the CFX96 Real-Time system with Bio-Rad CFX Manager 3.0 software[11]. Cycle threshold (C_t) values were normalized to the hDHFR resistance gene expressed from the same plasmid or HSP86, GAPDH genes.

2.5.8 qPCR Primers

PF3D7_1462800

2GAPDHqf 5'-ACCAAAGGATGACACCCCAA

2GAPDHqf 5'-ACCACCCTTTGATGGACCAT

PF3D7_1464200

610gf 5'-CGACAAGGCCATTTTAGAGAA-3'

610gR 5'TTTCGTTTTATCTCCGCTTACA-3'

PF3D7_0615500

0615500for 5'-CCACAATTGGAGTCGTCGTA-3'

0615500rev 5'-TCAAATCGAATTCTGTGACTCCT-3'

UniProtKB - P00374

qPCR_ hDHFR_F_5′-TCCTCCTGGACATCAGAGAGA-3′

qPCR_ hDHFR_R_5′-CTCAAGGAACCTCCACAAGG-3′

PF3D7_0818900

Hsp70qf 5′-GAATCGGTTTGTGCTCCAAT-3′

Hsp70qr 5′-CAACTGTTGGTCCACTTCCA-3′

PF3D7_1108000

qPCRrevIWS1w 5′-TGGTTGAAGAGGATGAGGAGA-3′

qPCRrevIWS1w 5′-ACCTTGTGCATATCATCATTTTCC-3′

mCherryqF 5′-TGACGTACCGGATTATGCAA-3′

mCherryqR 5′-ATATGAACTGAGGGGACAGG-3′

Ile rich genes

PF3D7_0322300_F 5′-TGGATGATCTGAGCAACAAAA-3′

PF3D7_0322300_R 5′-GGGTGGATCTTTATGCAAGC-3′

PF3D7_0512700_F 5′-TGGAACAGCATTAACGGAAA-3′

PF3D7_0512700_R 5′-GAGGTATTCCTACCCTTTTCTCAA-3′

PF3D7_0110600_F 5′-AGCATCACGACCTTTCCATC-3′

PF3D7_0110600_R 5′-TTGCATAAGCATTGGGATGA-3′

PF3D7_0903400_F 5′-TTCCATTATTGCATGCTCTCC-3′

PF3D7_0903400_R 5′-TCACACATGGATGTTGCTCA-3′

PF3D7_1450600_F 5′-ACGGATTACATGCAGCACAA-3′

PF3D7_1450600_R 5′-GATGACGTGTCGTCAAAAA-3′

PF3D7_1364700_F 5′-AAGGAAGCTCGGTTTTATTTGA-3′

PF3D7_1364700_R 5′-AAACCCTTCTTTTGTTTTGACA-3′

PF3D7_1121000_F 5′-CAAAAACAAATCCCGTAGATCC-3′

PF3D7_1121000_R 5′-CGATACAATTGTTGACCCACAT-3′

PF3D7_1341600_F 5′-GGGAATGGGAACCTTGTGTA-3′

PF3D7_1341600_R 5′-TCTTCATTTATCCATGCGTCA-3′

PF3D7_1321400_F 5′-TCCTTTCCATCCTCCCTTTT-3′

PF3D7_1321400_R 5′-TGGATTTTATCCACGGGTGT-3′

PF3D7_1138600_F 5′-ACAAGCGGAAAATATCGAATG-3′

PF3D7_1138600_R 5′-TCGTCTAAGTCCACTTCACTGC-3′

2.5.9 Immunoblotting and Antibodies

Samples pretreated with lysis buffer supplemented with cOmplete™ Protease Inhibitor Cocktail without EDTA were prepared with passive lysis buffer (Promega), BioRad sample buffer and BioRad reducing buffer. For immunoblotting, the PVDF membranes were blocked in 5% milk in PBS. The membranes were probed with anti-HA, or Anti-HA HRP (sc-7392, sc-7392HRP, Santa

Cruz) or anti-HA mouse or rabbit antibody (7076s, 7074s respectively, Cell Signaling) diluted in 2.5% milk in PBS-Tween20 0.1% PBST) 1: 5000, an anti-hDHFR mouse antibody (sc-377091, Santa Cruz) diluted 1:5000 in 2.5% milk in PBST, anti- HSP70 mouse (AS08 371, Agrisera, generous gift of Goldberg lab) 1:1000 in 2.5% milk in PBST, anti- PfHAD1 rabbit antibody (generous gift of Odom lab) 1:10000 in 2.5% milk PBST. Secondary HRP-labeled anti-mouse or anti-rabbit antibodies are diluted 1:5000 in 2.5% milk in PBST and incubated for an hour. After incubation with the primary antibody, the PVDF membranes were washed three times for 5 min in PBST, Prepare Working Solution by mixing equal parts of the Stable Peroxide Solution and the Luminol/Enhancer Solution (34577 SUPERSIGNAL WEST PICO PLUS, 34096 SUPERSIGNAL WEST FEMTO MAXIMUM SENSITIVITY SUBSTRATE respectively). We incubate the blot in Working Solution for 5 minutes. Remove the blot from Working Solution and drain excess reagent. Afterward we took images were generated by BioRad Molecular Imager CHemiDoc XRS System with Image Lab software.

2.5.10 Starvation assay

Asynchronous *P. falciparum* Dd2 parasites clones, with HA-tagged Pelota gene cultured in complete RPMI at 5% hematocrit and grown to ~3–5% parasitemia. The parasites were washed twice in PBS, equally partitioned, and washed in complete, isoleucine-free, and then were replated in their respective medium. Parasite cultures were incubated at 37 °C, in a candle jar atmosphere for 48h. After incubation, parasites were harvested. After harvesting, infected RBCs were lysed for total RNA/protein isolation or polysome profiling[69].

2.5.11 Polysome-associated RNA isolation

For polysome/RNA isolation we did according to published protocols[25,109]. Shortly, cycloheximide (100 mM) was added to parasite-infected red blood cell cultures to a final concentration of 200 µM. The culture was incubated for 10 minutes at 37°C following with pelleting erythrocytes (5 minutes at 500 x g at room temperature) and washed twice in PBS containing 200 µM cycloheximide. After the last wash, pellets were kept on ice and were subsequently lysed by adding 2.2 volumes of lysis buffer (1% (v/v) Nonident P-40 and 0.5% (w/v) sodium deoxycholate in polysome buffer (400 mM potassium acetate, 25 mM potassium HEPES pH 7.2, 15 mM magnesium acetate, 200 µM cycloheximide, 1 mM dithiothreitol (DTT), and 1mM 4-(2-aminoethyl) benzenesulfonyl fluoride HCl (AEBSF))) or cOmplete™ Protease Inhibitor Cocktail without EDTA (Roche), RNase OUT 1 µL/mL (Invitrogen) . After a 10 minute incubation on ice, lysates were centrifuged for 15 minutes at 20,000xg at 4°C, at this point, the pellets were flash-freeze and stored at -80°C. The clarified lysates were then loaded on top of a sucrose cushion (35% sucrose in polysome buffer) to concentrate the ribosomes (4 mL polycarbonate ultracentrifuge tubes and then centrifuged for two h at 150000xg at 4°C in a Type 100.3 Ti rotor (Beckman Coulter, Brea, CA, USA). Ribosome pellets were resuspended in polysome buffer. Afterward, the ribosome suspension was layered on top of a 15 mL continuous linear 15 to 60% sucrose (w/v) 2h 40 min 260343xg (Beckman Optima XPN-90 and the swinging bucket rotor SW41 Ti). Fractions of 500 µl were collected using a UA-5 UV detector and model 185 gradient fractionator (ISCO, Lincoln, NE, USA). RNA was extracted with acid-

phenol: chloroform pH 4.5 (Life Technologies), extracted twice with chloroform, and then precipitated using isopropanol.

Plasmodium falciparum Sucrose Cushion for Polysome Profiling: This prep is used to isolate crude ribosome pellet, removing hemoglobin, which can then be later used for polysome profiling. We used 2 mL 100% hematocrit erythrocytes 8% parasitemia. The pellets were washed with 10 mL PBS and flash freeze in liquid nitrogen. Samples were stored at -80C before further use. **Reagents**: To make 10 mL ***Plasmodium falciparum*** **Polysome Lysis Buffer (2.2 V/sample)**, we used 25 mM K-HEPES (1 M stock) 250 µL, 400 mM K-OAc (4 M stock) 1000 µL, 15 mM Mg-OAc (1 M stock) 150 µL, 1% Igepal CA-360 (100% stock), 100 µL 0.5% Na Deoxycholate (10% stock) 500 µL, 200 µM cycloheximide (100 mM stock) 20 µL, 1 mM AEBSF (200 mM stock) 50 µL, 1 mM DTT (1 M stock) 10 µL, RNase Inhibitory (40 U/µL stock) 10 µL, Molecular Grade Water 7 mL, 910 µL. ***Plasmodium falciparum*** **Sucrose Cushion for Polysome Profiling (15 mL)**, 25 mM K-HEPES (1 M stock) 375 µL, 400 mM K-OAc (4 M stock) 1500 µL, 15 mM Mg-OAc (1 M stock) 225 µL, 200 µM cycloheximide (100 mM stock) 30 µL, 1 mM AEBSF (200 mM stock) 75 µL, 1 mM DTT (1 M stock) 15 µL, 40 U/mL RNase Inhibitory (40 U/µL stock) 15 µL, Ultrapure sucrose 5.135 g, Molecular Grade Water (to start, complete to 15 mL after dissolved and all components added) 7.5 mL. ***Plasmodium falciparum*** **Polysome Wash Buffer** (1.5 mL/sample) 25 mL. 25 mM K-HEPES (1 M stock) 625 µL, 400 mM K-OAc (4 M stock) 2500 µL, 15 mM Mg-OAc (1 M stock) 375 µL, 200 µM cycloheximide (100 mM stock) 50 µL, 0.1 mM AEBSF (200 mM stock) 12.5 µL, 1 mM DTT (1 M stock) 25 µL, 10 U/mL RNase Inhibitory (40 U/µL stock) 6.25 µL, Molecular Grade Water 21 mL. 406.25 µL *Plasmodium falciparum* Polysome Lysis Buffer (500

µL/sample) 2.5 mL 25 mM K-HEPES (1 M stock) 62.5 µL 400 mM K-OAc (4 M stock) 250 µL, *Plasmodium falciparum* Sucrose Cushion for Polysome Profiling - 15 mM Mg- OAc (1 M stock) 37.5 µL, 1% Igepal CA-360 (100% stock) 25 µL, 200 µM cycloheximide (100 mM stock) 5 µL, 1 mM AEBSF (200 mM stock) 12.5 µL, 1 mM DTT (1 M stock) 2.5 µL, 40 U/mL RNase Inhibitory (40 2 mL, were lysed with 2.2 V of lysis buffer, vortex to mix well. Incubate at 4°C for 10 mins while rocking or rotating. Centrifuge 11,800xg, move lysate to the fresh tube (~ 6.2 mL) For Sucrose Cushion Setup, we needed 3 cushions per sample. We were using 1 mL cushion per ~2 mL lysate. Add 1 mL sucrose to each tube. Layer sample lysates over sucrose cushion. Add 2 mL to each, then split the remainder (usually a few hundred microliters) over the 3 tubes. We used TLA 100.3 rotor (kept cold in the refrigerator) for ultracentrifugation. Speed: 100,000 x g, Time: 1 hour 30 mins. Temp: 4°C. When the centrifugation is finished, carefully aspirate off supernatant without touching sides so as not to disrupt pellets. Wash pellet 3X with 500 µL wash buffer, gently pipetting on the side opposite the pellet near the bottom of the tube. Resuspend and combine pellets for each sample in a total of 500 µL ribosome resuspension buffer. Pipet to disperse pellet. Use 200 µL tips to further disperse. Move to 1.5 mL microcentrifuge tube Incubate at 4°C, rotating end-over-end, for at least 10 min. To remove remaining hemoglobin, set up another 1 mL sucrose cushion for each sample as previously[23]. A quick spin to collect samples to the bottom of the tube. Layer ribosome suspension over sucrose cushion, balance using ribosome resuspension buffer. Centrifuge as previously. Wash 3X with 500 µL wash buffer as previously. Resuspend in 500 µL ribosome resuspension buffer as

previously. If not, proceed to the next steps immediately, flash-freeze in liquid nitrogen and store at -80°C.

2.5.12 Parasite live imaging

To image *P. falciparum* Dd2 strain episomally expressing polyA- and polyA+ constructs, we used 50 µL of infected erythrocytes, washed two times in PBS. The nucleus was stained with 1:1000 dilution of Hoechst® 33342 for 10 min at room temperature. The cells were washed two times with PBS (500xg, 5 min, room temperature). After the washing step, the cells were resuspended in PBS (500 µL), 5µL of cell resuspension was put on positively charged slides and put Zeiss cover glasses (item number: 474030- 9000-000). The cover glasses were sealed with nail polish, and subsequently, microscopy was performed.

Samples were visualized using an upright Zeiss Examiner.Z1-based 880 LSM with a 100x/1.46 oil- immersion objective. DAPI was excited using a 405 nm diode laser, mCherry was excited with a 561 nm DPSS laser, and GFP was excited with an Argon laser tuned to 488 nm. Optical sections (0.3 µm) were acquired with an Airyscan super-resolution detector and were processed using ZEN Blue v. 2.3.

2.5.13 Generating Tetrahymena thermophila expressing YFP plasmids without (polyA-) and with (polyA+) coding for 12 lysines

Tetrahymena thermophila strain B2086 (II) was used for all experiments reported. Similar results were obtained with strain CU428 [(VII) mpr1-1/mpr1-1]. To assess the effect of LysAAA codons on protein accumulation, we modified a fluorescent protein tagging vector, pBSICY-

gtw[110] so as to fuse YFP to the carboxyl-terminus of a macronucleus-localized protein of unknown function (TTHERM_00384860), separated by a Gateway recombination cassette (Invitrogen/Life Technologies, Inc), and expressed from the cadmium inducible *MTT1* promoter[111]. The TTHERM_00384860 coding region was amplified with oligonucleotides 5' ALM Bsi' 5' - CAC CCG TAC GAA TAA AAT GAG CAT TAA TAA AGA AGA AGT-3' and 3' ALM RV 5'- GAT ATC TTC AAT TTT AAT TTT TCT TCG AAG TTG C 3' and cloned into pENTR-D in a topoisomerase mediated reaction prior to digesting with BsiWI and EcoRV and inserting into BsiWI/PmeI digested pBSICY-gtw. Subsequently, LR Clonase II was used to insert a linker containing the sequence coding for an HA epitope tag alone (N) or the tag plus 36 adenosines (K12) in place of the Gateway cassette. The expression cassette is located within the 5' flanking region of a cycloheximide resistant allele of the rpL29 gene to direct its integration into this genomic locus. These constructs were linearized with PvuI and SacI in the region flanking the Tetrahymena rpl29 sequences and introduced into starved *Tetrahymena* cells by biolistic transformation[112,113]. Transformants were selected in 1X SPP medium containing 12.5 µg/mL cycloheximide. To control for copy number, PCR assays with primers MTT2386 5'- TC TTA GCT ACG TGA TTC ACG -3'and Chx-117, 5'- ATG TGT TAT TAA TCG ATT GAT -3' and Chx85r, 5'- TCT CTT TCA TGC ATG CTA GC – 3' verified that all rpL29 loci contained the integrated expression construct. Transgene expression was induced by addition of 0.4 µg/mL $CdCl_2$ and cells were grown 12-16 hours before monitoring protein accumulation. YFP accumulation was visualized by epifluorescence microscopy as previously described[114]. Whole cells extracts were generated by boiling concentrated cell pellets in 1x Laemmli sample buffer, followed by were fractionation

on 10% SDS polyacrylamide gels and transferred to nitrocellulose. YFP accumulation was a monitored with mouse anti-GFP antisera (G28R anti-GFP (OAEA00007) antibody, Aviva Systems Biology) and normalized to acetylated Rabbit anti- Histone H3 trimethyl-lysine (Upstate Biotechnologies/Millipore, NY, 07-473). Accumulation of transcripts was assessed on Northern blots as previously described using a ^{32}P-random-primer-labeled YFP probe[115].

2.5.14 2 D-electrophoresis

2 mL (100% hct) of P. falciparum infected erytrocyes (HA-pelo Dd2 strain, parasitemia 7-9%) were treated with PBS saponin 0.15%, and protease inhibitor w/o EDTA. The pellets were washed in PBS- saponin buffer 3 times. Afterwards, the samples were used to do immunoprecipitation (IP). We used Pierce HA-magnetic beads 25 µL and further proceeded with cell lysis: Lysis Buffer: 150 mM NaCl, 50 mM Tris pH 7.5, 1% IGPAL-CA-630 (Sigma, #I8896), 5% Glycerol, Protease (1mM PMSF) and phosphatase inhibitors. Sample wash: Wash Buffer: 150 mM NaCl, 50 mM Tris pH 7.5, 5% Glycerol. After the washing step the samples were snap frozen in liquid nitrogen for 2D gel analysis.

Two-dimensional electrophoresis was performed according to the carrier ampholine method of isoelectric focusing[116,117] by Kendrick Labs, Inc. (Madison, WI) as follows: Isoelectric focusing was carried out in a glass tube of inner diameter 2.0 mm using 2% pH 3-10 isodalt servalytes (Serva, Heidelberg, Germany) for 9600 volt-hrs. One µg of an IEF internal standard, tropomyosin, was added to the sample. This protein migrates as a doublet with lower polypeptide spot of MW 33,000 and pI 5.2. The enclosed tube gel pH gradient plot for this set of ampholines was determined with a surface pH electrode.

After equilibration for 10 min in Buffer 'O' (10% glycerol, 50 mM dithiothreitol, 2.3% SDS and 0.0625 M tris, pH 6.8), each tube gel was sealed to the top of a stacking gel that overlaid a 10% acrylamide slab gel (0.75 mm thick). SDS slab gel electrophoresis was carried out for about 4 hrs at 15 mA/gel. After slab gel electrophoresis, the duplicate gel for blotting was placed in transfer buffer (10mMCaps, pH 11.0, 10% MeOH) and transblotted onto a PVDF membrane overnight at 200 mA and approximately 100 volts/ two gels. The following proteins (Millipore Sigma) were used as molecular weight standards: myosin (220,000), phosphorylase A (94,000), catalase (60,000), actin (43,000) carbonic anhydrase (29,000) and lysozyme (14,000). These standards appear as bands at the basic edge of the Coomassie Brilliant Blue R- 250-stained membrane.

2.5.15 Coding Sequence Metrics

Coding sequences for each organism (*Plasmodium falciparum* 3D7 - EPr 1, *Tetrahymena thermophila* – JCVI-TTA1-2.2, and human - GRCh38.p7) were downloaded from their respective Ensembl BioMart pages (accessed on March 19th 2018). Each set of genes was filtered to include only the longest coding sequence variant. The resulting sequences were each analyzed using a folding window approach; a window of 120 nt was scanned across each sequence with a single nucleotide step size. Each window sequence was folded (using RNAfold) to determine its minimum free energy structure/value (MFE_{native})[118]. At the same time, MFE values were calculated for 30 randomized versions of the native window sequence (MFE_{random}). The mean of MFE_{random} values were compared to that of the native in a method adapted from Clote et al., 2005 and illustrated in the following equation:

$$z - score = \frac{MFE_{native} - \overline{MFE_{random}}}{Std\ Dev_{MFE}}$$

The mean window MFE and z-score values of each gene were calculated and compiled in separate spreadsheets. Box and whisker plots (generated using BoxPlotR[119] are shown, depicting the distribution of these means for each organism.

2.5.16 Bioinformatics analyses

2.5.16.1 Ribosome profiling

GWIPS database was used as the source of ribosome profiling data. We downloaded Caro et al., 2010 dataset for *Plasmodium falciparum* (the only dataset available for that species), while for humans, we used aggregate for all deposited studies. In both cases, we took a dataset for elongating ribosomes mapped to A-site.

The definition of polyA-tracts was taken from Arthur et al., 2015, which is twelve consecutive adenines allowing for one mismatch. Genomic coordinates of such segments were downloaded from PATACSDB[31]. We took 50 residues upstream and downstream from the beginning of the polyA segment, preserving the proper strand orientation. Occupancy plot was generated with two conditions:

1. discarding fragments that had less than five occupancy values in the given window of 101 nucleotides

2. taking into account fragments that had the average occupancy equal or higher than the mean for the dataset (this was to remove the influence of poorly mapped segments from the plots)

To make occupancy plots between different life stages comparable (**SUPPLEMENTAL FIGURE 2.5**), we have introduced a normalization mechanism, where occupancy of polyA region was divided by a mean from similarly sized distribution of random fragments of the same length that had the 0 position within the coding region. Randomization was preserving chromosome distribution of the original polyA-carrying genes dataset. All the analyses were done using R language.

2.5.16.2 Gene ontology analysis

Gene Ontology analysis was done using the Gene Ontology Enrichment tool at PlasmoDB website[29], using default options. For **SUPPLEMENTAL TABLE 2.1** we took only those terms that had Bonferroni-adjusted p-value better than 0.05.

2.5.16.3 Structural analyses

Structural analyses were done using MOLEonline service version 2.5[120] using default parameters, with manual selection of the proper tunnel among all predicted by this service. Due to limits of the method, it was not possible to enforce the same length of the channel in all structures, yet the hydrophobic patches formed by interaction with rRNA and L4/L22 proteins were easy to observe in all structures.

2.6 References

1. Pavlovic Djuranovic, S., Erath, J., Andrews, R. J., Bayguinov, P. O. & Joyce, J. Plasmodium falciparum translational machinery condones polyadenosine repeats. *Elife* **9**, e57799 (2020).

2. Gerald, N., Mahajan, B. & Kumar, S. Mitosis in the Human Malaria Parasite Plasmodium falciparum. *Eukaryot. Cell* **10**, 474–482 (2011).

3. Lu, X. M. *et al.* Nascent RNA sequencing reveals mechanisms of gene regulation in the human malaria parasite Plasmodium falciparum. *Nucleic Acids Res.* **45**, 7825–7840 (2017).

4. Caro, F., Ahyong, V., Betegon, M. & DeRisi, J. L. Genome-wide regulatory dynamics of translation in the Plasmodium falciparum asexual blood stages. *Elife* **3**, 1–24 (2014).

5. Zhang, M. *et al.* Uncovering the essential genes of the human malaria parasite Plasmodium falciparum by saturation mutagenesis. *Science (80-.).* **360**, eaap7847 (2018).

6. Glockner, G. Large Scale Sequencing and Analysis of AT Rich Eukaryote Genomes. *Curr. Genomics* **1**, 289–299 (2000).

7. Szafranski, K., Lehmann, R., Parra, G., Guigo, R. & Glockner, G. Gene Organization Features in A/T-Rich Organisms. *J. Mol. Evol.* **60**, 90–98 (2005).

8. Zilversmit, M. M. *et al.* Low-Complexity Regions in Plasmodium falciparum: Missing Links in the Evolution of an Extreme Genome. *Mol. Biol. Evol.* **27**, 2198–2209 (2010).

9. Erath, J., Djuranovic, S. & Djuranovic, S. P. Adaptation of Translational Machinery in Malaria Parasites to Accommodate Translation of Poly-Adenosine Stretches Throughout Its Life Cycle.

Front. Microbiol. **10**, 2823 (2019).

10. Ito-Harashima, S., Kuroha, K., Tatematsu, T. & Inada, T. Translation of the poly(A) tail plays crucial roles in nonstop mRNA surveillance via translation repression and protein destabilization by proteasome in yeast. *Genes Dev.* **21**, 519–524 (2007).

11. Arthur, L. L. *et al.* Translational control by lysine-encoding A-rich sequences. *Sci. Adv.* **1**, e1500154 (2015).

12. Chandrasekaran, V. *et al.* Mechanism of ribosome stalling during translation of a poly(A) tail. *Nat. Struct. Mol. Biol.* **26**, 1132–1140 (2019).

13. Tuck, A. C. *et al.* Mammalian RNA Decay Pathways Are Highly Specialized and Widely Linked to Translation. *Mol. Cell* **77**, 1222-1236.e13 (2020).

14. Tesina, P. *et al.* Molecular mechanism of translational stalling by inhibitory codon combinations and poly(A) tracts. *EMBO J.* **39**, e103365 (2020).

15. Arthur, L. L. *et al.* Rapid generation of hypomorphic mutations. *Nat. Commun.* **8**, 14112 (2017).

16. Arthur, L. L. & Djuranovic, S. PolyA tracks, polybasic peptides, poly-translational hurdles. *Wiley Interdiscip. Rev. RNA* **9**, e1486 (2018).

17. Koutmou, K. S. *et al.* Ribosomes slide on lysine-encoding homopolymeric A stretches. *Elife* **4**, 1–18 (2015).

18. Garzia, A. *et al.* The E3 ubiquitin ligase and RNA-binding protein ZNF598 orchestrates ribosome quality control of premature polyadenylated mRNAs. *Nat. Commun.* **8**, 16056 (2017).

19. Juszkiewicz, S. & Hegde, R. S. Initiation of Quality Control during Poly(A) Translation Requires Site-Specific Ribosome Ubiquitination. *Mol. Cell* **65**, 743-750.e4 (2017).

20. Sundaramoorthy, E. *et al.* ZNF598 and RACK1 Regulate Mammalian Ribosome-Associated Quality Control Function by Mediating Regulatory 40S Ribosomal Ubiquitylation. *Mol Cell* **65**, 751-760.e754 (2017).

21. Tournu, H., Butts, A. & Palmer, G. E. Titrating Gene Function in the Human Fungal Pathogen Candida albicans through Poly-Adenosine Tract Insertion. *mSphere* **4**, e192–e119 (2019).

22. Szádeczky-Kardoss, I., Gál, L., Auber, A., Taller, J. & Silhavy, D. The No-go decay system degrades plant mRNAs that contain a long A-stretch in the coding region. *Plant Sci.* **275**, 19–27 (2018).

23. Saul, A. & Battistutta, D. Codon usage in Plasmodium falciparum. *Mol. Biochem. Parasitol.* **27**, 35–42 (1988).

24. Coulson, R. M. R. Comparative Genomics of Transcriptional Control in the Human Malaria Parasite Plasmodium falciparum. *Genome Res.* **14**, 1548–1554 (2004).

25. Bunnik, E. M. *et al.* Polysome profiling reveals translational control of gene expression in the human malaria parasite Plasmodium falciparum. *Genome Biol.* **14**, R128 (2013).

26. Koutmou, K. S. & others. Ribosomes slide on lysine-encoding homopolymeric A stretches. *Elife* **4**, 1–18 (2015).

27. Videvall, E. Plasmodium parasites of birds have the most AT-rich genes of eukaryotes. *Microb. Genomics* **4**, (2018).

28. Hunt, S. E. *et al.* Ensembl variation resources. *Database* **2018**, (2018).

29. Aurrecoechea, C. *et al.* PlasmoDB: a functional genomic database for malaria parasites. *Nucleic Acids Res.* **37**, D539–D543 (2009).

30. Beznosková, P. *et al.* Translation Initiation Factors eIF3 and HCR1 Control Translation Termination and Stop Codon Read-Through in Yeast Cells. *PLoS Genet.* **9**, e1003962 (2013).

31. Habich, M., Djuranovic, S., Szczesny, P. & M., H. PATACSDB - The database of polyA translational attenuators in coding sequences. *PeerJ Comput. Sci.* **2**, e45 (2016).

32. Subtelny, A. O., Eichhorn, S. W., Chen, G. R., Sive, H. & Bartel, D. P. Poly(A)-tail profiling reveals an embryonic switch in translational control. *Nature* **508**, 66–71 (2014).

33. Brown, C. E. & Sachs, A. B. Poly(A) Tail Length Control in Saccharomyces cerevisiae Occurs by Message-Specific Deadenylation. *Mol. Cell. Biol.* **18**, 6548–6559 (1998).

34. Chang, H., Lim, J., Ha, M. & Kim, V. N. TAIL-seq: Genome-wide Determination of Poly(A) Tail Length and 3' End Modifications. *Mol. Cell* **53**, 1044–1052 (2014).

35. Shoemaker, C. J. & Green, R. Translation drives mRNA quality control. *Nat. Struct. Mol. Biol.* **19**, 594–601 (2012).

36. Guler, J. L. *et al.* Asexual Populations of the Human Malaria Parasite, Plasmodium falciparum, Use a Two-Step Genomic Strategy to Acquire Accurate, Beneficial DNA Amplifications. *PLoS Pathog.* **9**, e1003375 (2013).

37. Michel, A. M. *et al.* GWIPS-viz: development of a ribo-seq genome browser. *Nucleic Acids Res.* **42**, D859–D864 (2014).

38. Ingolia, N. T. *et al.* Ribosome Profiling Reveals Pervasive Translation Outside of Annotated

Protein-Coding Genes. *Cell Rep.* **8**, 1365–1379 (2014).

39. Guydosh, N. R. & Green, R. Translation of poly(A) tails leads to precise mRNA cleavage. *RNA* **23**, 749–761 (2017).

40. Requião, R. D., de Souza, H. J. A., Rossetto, S., Domitrovic, T. & Palhano, F. L. Increased ribosome density associated to positively charged residues is evident in ribosome profiling experiments performed in the absence of translation inhibitors. *RNA Biol.* **13**, 561–568 (2016).

41. Charneski, C. A. & Hurst, L. D. Positively Charged Residues Are the Major Determinants of Ribosomal Velocity. *PLoS Biol.* **11**, e1001508 (2013).

42. Kim, H.-K. *et al.* A frameshifting stimulatory stem loop destabilizes the hybrid state and impedes ribosomal translocation. *Proc. Natl. Acad. Sci.* **111**, 5538–5543 (2014).

43. Mouzakis, K. D., Lang, A. L., Vander Meulen, K. A., Easterday, P. D. & Butcher, S. E. HIV-1 frameshift efficiency is primarily determined by the stability of base pairs positioned at the mRNA entrance channel of the ribosome. *Nucleic Acids Res.* **41**, 1901–1913 (2013).

44. Faure, G., Ogurtsov, A. Y., Shabalina, S. A. & Koonin, E. V. Role of mRNA structure in the control of protein folding. *Nucleic Acids Res.* **44**, 10898–10911 (2016).

45. Zur, H. & Tuller, T. Strong association between mRNA folding strength and protein abundance in S. cerevisiae. *EMBO Rep.* **13**, 272–277 (2012).

46. Andrews, R. J., Baber, L. & Moss, W. N. RNAStructuromeDB: A genome-wide database for RNA structural inference. *Sci. Rep.* **7**, 17269 (2017).

47. Andrews, R. J., Baber, L. & Moss, W. N. Mapping the RNA structural landscape of viral genomes.

Methods (2019). doi:10.1016/j.ymeth.2019.11.001

48. Clote, P. Structural RNA has lower folding energy than random RNA of the same dinucleotide frequency. *RNA* **11**, 578–591 (2005).

49. Freyhult, E., Gardner, P. P. & Moulton, V. A comparison of RNA folding measures. *BMC Bioinformatics* **6**, 241 (2005).

50. O'Leary, C. A. *et al.* RNA structural analysis of the MYC mRNA reveals conserved motifs that affect gene expression. *PLoS One* **14**, e0213758 (2019).

51. Andrews, R. J., Roche, J. & Moss, W. N. ScanFold: an approach for genome-wide discovery of local RNA structural elements—applications to Zika virus and HIV. *PeerJ* **6**, e6136 (2018).

52. Baumgarten, S. *et al.* Transcriptome-wide dynamics of extensive m6A mRNA methylation during Plasmodium falciparum blood-stage development. *Nat. Microbiol.* **4**, 2246–2259 (2019).

53. Liu, N. *et al.* N6-methyladenosine-dependent RNA structural switches regulate RNA–protein interactions. *Nature* **518**, 560–564 (2015).

54. Hudson, B. H. & Zaher, H. S. O 6-Methylguanosine leads to position-dependent effects on ribosome speed and fidelity. *RNA* **21**, 1648–1659 (2015).

55. Choi, J. *et al.* N6-methyladenosine in mRNA disrupts tRNA selection and translation-elongation dynamics. *Nat. Struct. Mol. Biol.* **23**, 110–115 (2016).

56. Sorber, K., Dimon, M. T. & DeRisi, J. L. RNA-Seq analysis of splicing in Plasmodium falciparum uncovers new splice junctions, alternative splicing and splicing of antisense transcripts. *Nucleic Acids Res.* **39**, 3820–3835 (2011).

57. Tsuboi, T. *et al.* Dom34:hbs1 plays a general role in quality-control systems by dissociation of a stalled ribosome at the 3' end of aberrant mRNA. *Mol. Cell* **46**, 518–529 (2012).

58. Hilal, T. *et al.* Structural insights into ribosomal rescue by Dom34 and Hbs1 at near-atomic resolution. *Nat. Commun.* **7**, 13521 (2016).

59. Becker, T. *et al.* Structure of the no-go mRNA decay complex Dom34–Hbs1 bound to a stalled 80S ribosome. *Nat. Struct. Mol. Biol.* **18**, 715–720 (2011).

60. D'Orazio, K. N. *et al.* The endonuclease Cue2 cleaves mRNAs at stalled ribosomes during No Go Decay. *Elife* **8**, 1–27 (2019).

61. Glover, M. L. *et al.* NONU-1 encodes a conserved endonuclease required for mRNA translation surveillance. *bioRxiv* **674358**, (2019).

62. Navickas, A. *et al.* A unique No-Go Decay cleavage in mRNA exit-tunnel of ribosome produces 5'-OH ends phosphorylated by Rlg1. *bioRxiv* **465633**, (2019).

63. Ghorbal, M. *et al.* Genome editing in the human malaria parasite Plasmodium falciparum using the CRISPR-Cas9 system. *Nat. Biotechnol.* **32**, 819–821 (2014).

64. Nasamu, A. S. *et al.* Plasmepsins IX and X are essential and druggable mediators of malaria parasite egress and invasion. *Science (80-.).* **358**, 518–522 (2017).

65. Doma, M. K. & Parker, R. Endonucleolytic cleavage of eukaryotic mRNAs with stalls in translation elongation. *Nature* **440**, 561–564 (2006).

66. Simms, C. L., Yan, L. L. & Zaher, H. S. Ribosome Collision Is Critical for Quality Control during No-Go Decay. *Mol. Cell* **68**, 361-373.e5 (2017).

67. Passos, D. O. *et al.* Analysis of Dom34 and Its Function in No-Go Decay. *Mol. Biol. Cell* **20**, 3025–3032 (2009).

68. Dimitrova, L. N., Kuroha, K., Tatematsu, T. & Inada, T. Nascent Peptide-dependent Translation Arrest Leads to Not4p-mediated Protein Degradation by the Proteasome. *J. Biol. Chem.* **284**, 10343–10352 (2009).

69. Babbitt, S. E. *et al.* Plasmodium falciparum responds to amino acid starvation by entering into a hibernatory state. *Proc. Natl. Acad. Sci.* **109**, E3278–E3287 (2012).

70. Liu, J., Istvan, E. S., Gluzman, I. Y., Gross, J. & Goldberg, D. E. Plasmodium falciparum ensures its amino acid supply with multiple acquisition pathways and redundant proteolytic enzyme systems. *Proc. Natl. Acad. Sci.* **103**, 8840–8845 (2006).

71. Mills, E. W., Wangen, J., Green, R. & Ingolia, N. T. Dynamic Regulation of a Ribosome Rescue Pathway in Erythroid Cells and Platelets. *Cell Rep.* **17**, 1–10 (2016).

72. Wu, B., Hunt, C. & Morimoto, R. Structure and expression of the human gene encoding major heat shock protein HSP70. *Mol. Cell. Biol.* **5**, 330–341 (1985).

73. Rosenzweig, R., Nillegoda, N. B., Mayer, M. P. & Bukau, B. The Hsp70 chaperone network. *Nat. Rev. Mol. Cell Biol.* **20**, 665–680 (2019).

74. Darnell, A. M., Subramaniam, A. R. & O'Shea, E. K. Translational Control through Differential Ribosome Pausing during Amino Acid Limitation in Mammalian Cells. *Mol. Cell* **71**, 229-243.e11 (2018).

75. Mills, E. W., Green, R. & Ingolia, N. T. Slowed decay of mRNAs enhances platelet specific

translation. *Blood* **129**, e38–e48 (2017).

76. Kuroha, K. *et al.* Receptor for activated C kinase 1 stimulates nascent polypeptide-dependent translation arrest. *EMBO Rep.* **11**, 956–961 (2010).

77. Brandman, O. *et al.* A Ribosome-Bound Quality Control Complex Triggers Degradation of Nascent Peptides and Signals Translation Stress. *Cell* **151**, 1042–1054 (2012).

78. Lu, J. & Deutsch, C. Electrostatics in the Ribosomal Tunnel Modulate Chain Elongation Rates. *J. Mol. Biol.* **384**, 73–86 (2008).

79. Tang, T. T. L., Stowell, J. A. W., Hill, C. H. & Passmore, L. A. The intrinsic structure of poly(A) RNA determines the specificity of Pan2 and Caf1 deadenylases. *Nat. Struct. Mol. Biol.* **26**, 433–442 (2019).

80. Wong, W. *et al.* Cryo-EM structure of the Plasmodium falciparum 80S ribosome bound to the anti-protozoan drug emetine. *Elife* **3**, (2014).

81. Sun, M. *et al.* Dynamical features of the Plasmodium falciparum ribosome during translation. *Nucleic Acids Res.* **43**, gkv991 (2015).

82. Hashem, Y. *et al.* Structure of the Mammalian Ribosomal 43S Preinitiation Complex Bound to the Scanning Factor DHX29. *Cell* **153**, 1108–1119 (2013).

83. Wang, M., Herrmann, C. J., Simonovic, M., Szklarczyk, D. & von Mering, C. Version 4.0 of PaxDb: Protein abundance data, integrated across model organisms, tissues, and cell-lines. *Proteomics* **15**, 3163–3168 (2015).

84. Blomqvist, K., DiPetrillo, C., Streva, V. A., Pine, S. & Dvorin, J. D. Receptor for Activated C-Kinase 1

(PfRACK1) is required for Plasmodium falciparum intra-erythrocytic proliferation. *Mol. Biochem. Parasitol.* **211**, 62–66 (2017).

85. Matsuo, Y. *et al.* Ubiquitination of stalled ribosome triggers ribosome-associated quality control. *Nat. Commun.* **8**, 159 (2017).

86. Ikeuchi, K. & Inada, T. Ribosome-associated Asc1/RACK1 is required for endonucleolytic cleavage induced by stalled ribosome at the 3' end of nonstop mRNA. *Sci. Rep.* **6**, 28234 (2016).

87. Wolf, A. S. & Grayhack, E. J. Asc1, homolog of human RACK1, prevents frameshifting in yeast by ribosomes stalled at CGA codon repeats. *RNA* **21**, 935–945 (2015).

88. Sehnal, D. *et al.* MOLE 2.0: advanced approach for analysis of biomacromolecular channels. *J. Cheminform.* **5**, 39 (2013).

89. Dao Duc, K., Batra, S. S., Bhattacharya, N., Cate, J. H. D. & Song, Y. S. Differences in the path to exit the ribosome across the three domains of life. *Nucleic Acids Res.* **47**, 4198–4210 (2019).

90. Fujita, H., Yamagishi, M., Kida, Y. & Sakaguchi, M. Positive charges on the translocating polypeptide chain arrest movement through the translocon. *J. Cell Sci.* **124**, 4184–4193 (2011).

91. Petrone, P. M., Snow, C. D., Lucent, D. & Pande, V. S. Side-chain recognition and gating in the ribosome exit tunnel. *Proc. Natl. Acad. Sci.* **105**, 16549–16554 (2008).

92. Picking, W. D., Odom, O. W., Tsalkova, T., Serdyuk, I. & Hardesty, B. The conformation of nascent polylysine and polyphenylalanine peptides on ribosomes. *J. Biol. Chem.* **266**, 1534–42 (1991).

93. Karlin, S., Brocchieri, L., Bergman, A., Mrazek, J. & Gentles, A. J. Amino acid runs in eukaryotic proteomes and disease associations. *Proc. Natl. Acad. Sci.* **99**, 333–338 (2002).

94. Seward, E. A. & Kelly, S. Dietary nitrogen alters codon bias and genome composition in parasitic microorganisms. *Genome Biol.* **17**, 226 (2016).

95. Dietel, A.-K., Merker, H., Kaltenpoth, M. & Kost, C. Selective advantages favour high genomic AT-contents in intracellular elements. *PLOS Genet.* **15**, e1007778 (2019).

96. Becker, K. *et al.* Oxidative stress in malaria parasite-infected erythrocytes: host–parasite interactions. *Int. J. Parasitol.* **34**, 163–189 (2004).

97. Kobayashi, K. *et al.* Analyses of Interactions Between Heparin and the Apical Surface Proteins of Plasmodium falciparum. *Sci. Rep.* **3**, 3178 (2013).

98. Leitgeb, A. M. *et al.* Low Anticoagulant Heparin Disrupts Plasmodium falciparum Rosettes in Fresh Clinical Isolates. *Am. J. Trop. Med. Hyg.* **84**, 390–396 (2011).

99. Davies, H. M., Thalassinos, K. & Osborne, A. R. Expansion of Lysine-rich Repeats in Plasmodium Proteins Generates Novel Localization Sequences That Target the Periphery of the Host Erythrocyte. *J. Biol. Chem.* **291**, 26188–26207 (2016).

100. Romero, L. C., Nguyen, T. V, Deville, B., Ogunjumo, O. & James, A. A. The MB2 gene family of Plasmodium species has a unique combination of S1 and GTP-binding domains. *BMC Bioinformatics* **5**, 83 (2004).

101. Hancock, J. F., Paterson, H. & Marshall, C. J. A polybasic domain or palmitoylation is required in addition to the CAAX motif to localize p21ras to the plasma membrane. *Cell* **63**, 133–139 (1990).

102. Joazeiro, C. A. P. Ribosomal Stalling During Translation: Providing Substrates for Ribosome-Associated Protein Quality Control. *Annu. Rev. Cell Dev. Biol.* **33**, 343–368 (2017).

103. Walliker, D. *et al.* Genetic analysis of the human malaria parasite Plasmodium falciparum. *Science (80-.).* **236**, 1661–1666 (1987).

104. McCutchan, T. F. *et al.* Primary sequences of two small subunit ribosomal RNA genes from Plasmodium falciparum. *Mol. Biochem. Parasitol.* **28**, 63–68 (1988).

105. Waters, A. P., Syin, C. & McCutchan, T. F. Developmental regulation of stage-specific ribosome populations in Plasmodium. *Nature* **342**, 438–440 (1989).

106. Trager, W. & Jensen, J. B. Human malaria parasites in continuous culture. 1976. *J. Parasitol.* **91**, 484–6 (2005).

107. Russo, I., Oksman, A. & Goldberg, D. E. Fatty acid acylation regulates trafficking of the unusual Plasmodium falciparum calpain to the nucleolus. *Mol. Microbiol.* **72**, 229–245 (2009).

108. Fidock, D. A. & Wellems, T. E. Transformation with human dihydrofolate reductase renders malaria parasites insensitive to WR99210 but does not affect the intrinsic activity of proguanil. *Proc. Natl. Acad. Sci.* **94**, 10931–10936 (1997).

109. Lacsina, J. R., LaMonte, G., Nicchitta, C. V & Chi, J.-T. Polysome profiling of the malaria parasite Plasmodium falciparum. *Mol. Biochem. Parasitol.* **179**, 42–6 (2011).

110. Motl, J. A. & Chalker, D. L. Zygotic Expression of the Double-Stranded RNA Binding Motif Protein Drb2p Is Required for DNA Elimination in the Ciliate Tetrahymena thermophila. *Eukaryot. Cell* **10**, 1648–1659 (2011).

111. Shang, Y. *et al.* A robust inducible-repressible promoter greatly facilitates gene knockouts, conditional expression, and overexpression of homologous and heterologous genes in

Tetrahymena thermophila. *Proc. Natl. Acad. Sci.* **99**, 3734–3739 (2002).

112. Bruns, P. J. & Cassidy-Hanley, D. Chapter 27 Biolistic Transformation of Macro- and Micronuclei. in 501–512 (1999). doi:10.1016/S0091-679X(08)61553-8

113. Cassidy-Hanley, D. *et al.* Germline and somatic transformation of mating Tetrahymena thermophila by particle bombardment. *Genetics* **146**, 135–147 (1997).

114. Matsuda, A., Shieh, A. W.-Y., Chalker, D. L. & Forney, J. D. The Conjugation-Specific Die5 Protein Is Required for Development of the Somatic Nucleus in both Paramecium and Tetrahymena. *Eukaryot. Cell* **9**, 1087–1099 (2010).

115. Chalker, D. L. Nongenic, bidirectional transcription precedes and may promote developmental DNA deletion in Tetrahymena thermophila. *Genes Dev.* **15**, 1287–1298 (2001).

116. O'Farrell, P. H. High Resolution Two-Dimensional Electrophoresis of Proteins. *J. Biol. Chem.* **250**, 4007–4021 (1975).

117. Burgess-Cassler, A., Johansen, J. J., Santek, D. A., Ide, J. R. & Kendrick, N. C. Computerized quantitative analysis of coomassie-blue-stained serum proteins separated by two-dimensional electrophoresis. *Clin. Chem.* **35**, 2297–2304 (1989).

118. Lorenz, R. *et al.* ViennaRNA Package 2.0. *Algorithms Mol. Biol.* **6**, 26 (2011).

119. Spitzer, M., Wildenhain, J., Rappsilber, J. & Tyers, M. BoxPlotR: a web tool for generation of box plots. *Nat. Methods* **11**, 121–122 (2014).

120. Pravda, L. *et al.* MOLEonline: a web-based tool for analyzing channels, tunnels and pores (2018 update). *Nucleic Acids Res.* **46**, W368–W373 (2018).

2.7 Supplemental Material

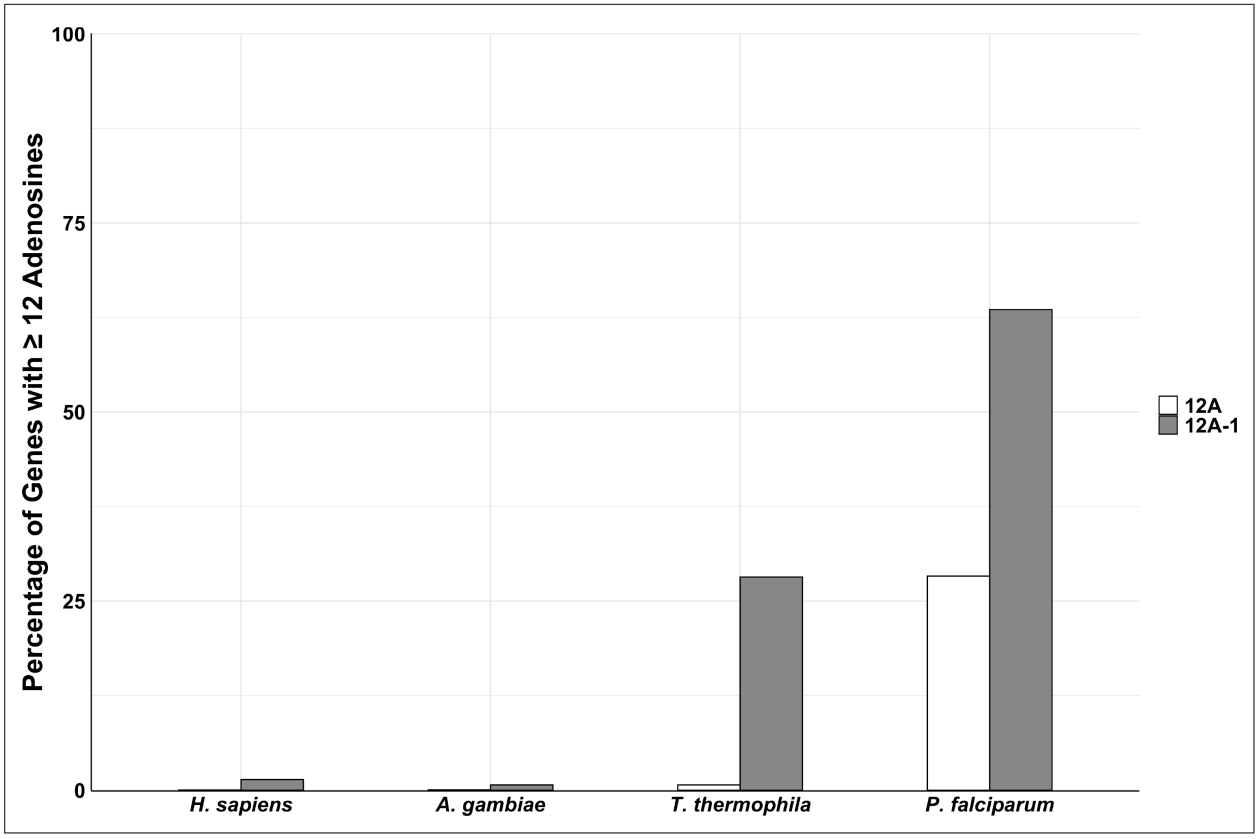

SUPPLEMENTAL FIGURE 2.1 | Percentage of genes with ≥12A (white) and ≥12A-1 (gray) consecutive adenosine nucleotides for each organism.

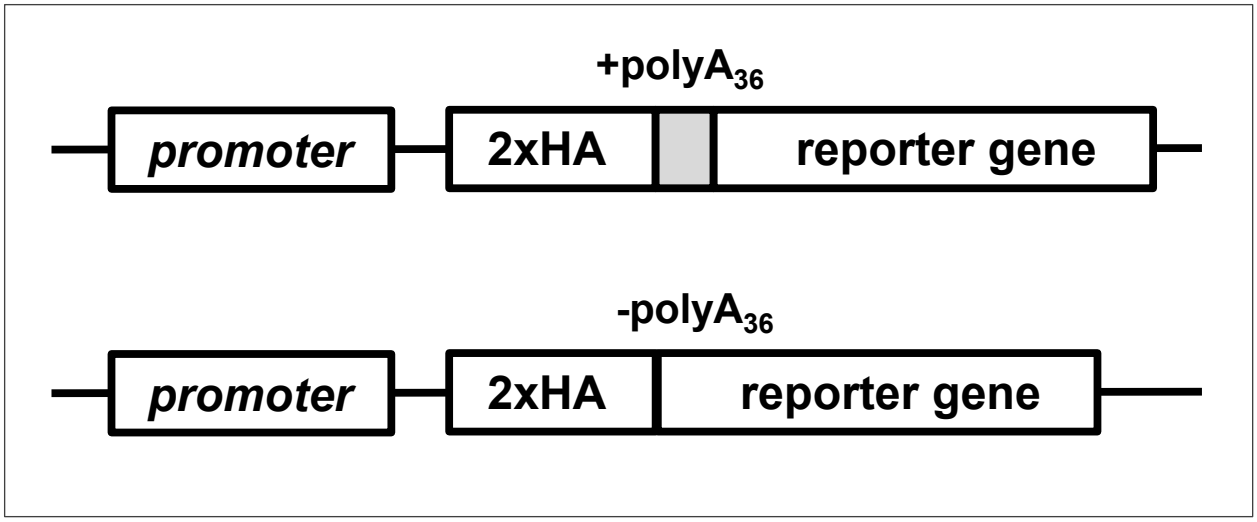

SUPPLEMENTAL FIGURE 2.2 | Generalized scheme of reporter constructs used for expression in *H. sapiens*, *T. thermophila*, and *P. falciparum*.

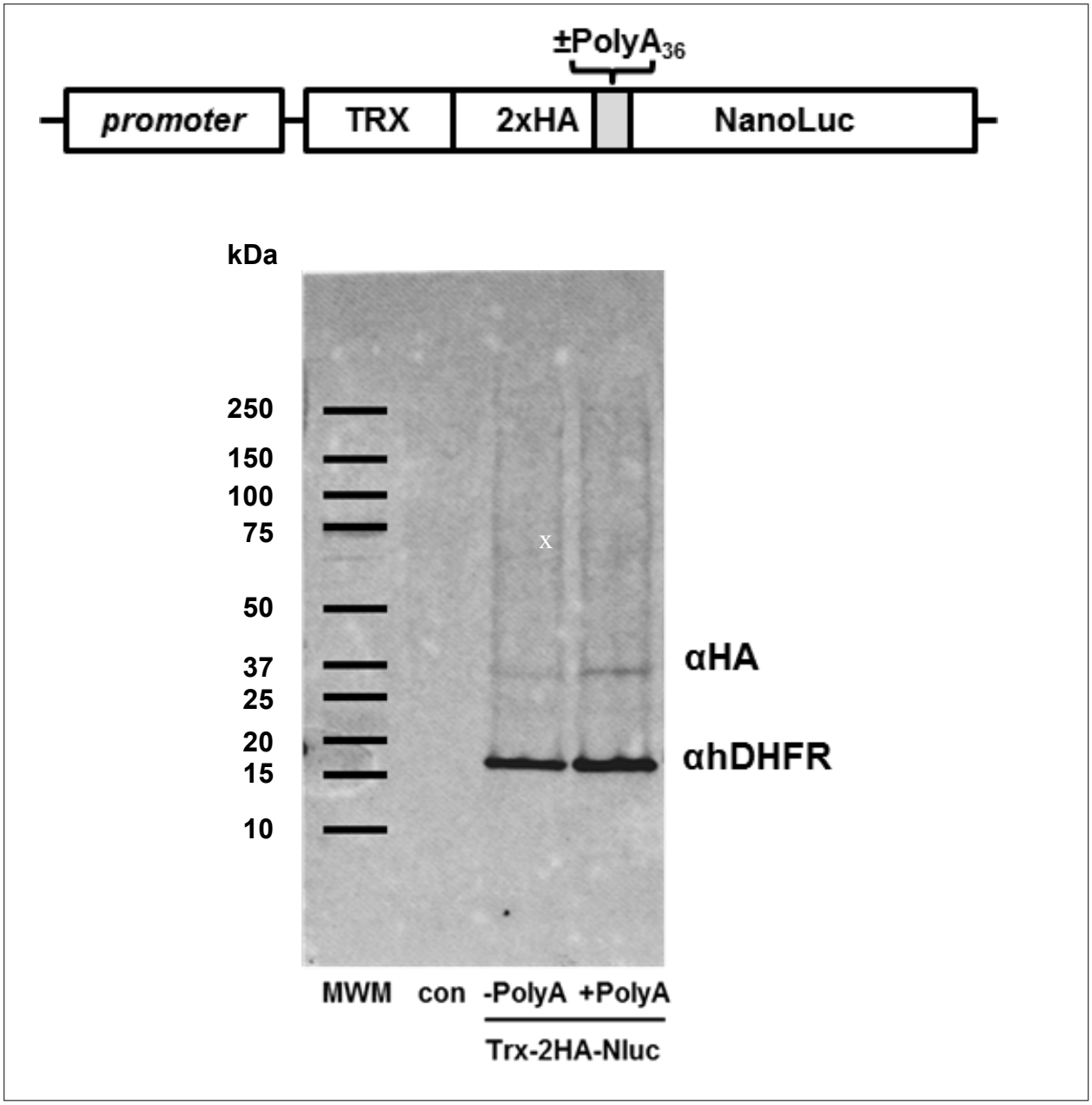

SUPPLEMENTAL FIGURE 2.3 | Generalized schematic of Thioredoxin fusion NanoLuc reporter construct used for episomal expression in *P. falciparum* cells (Trx-2HA-Nluc) .

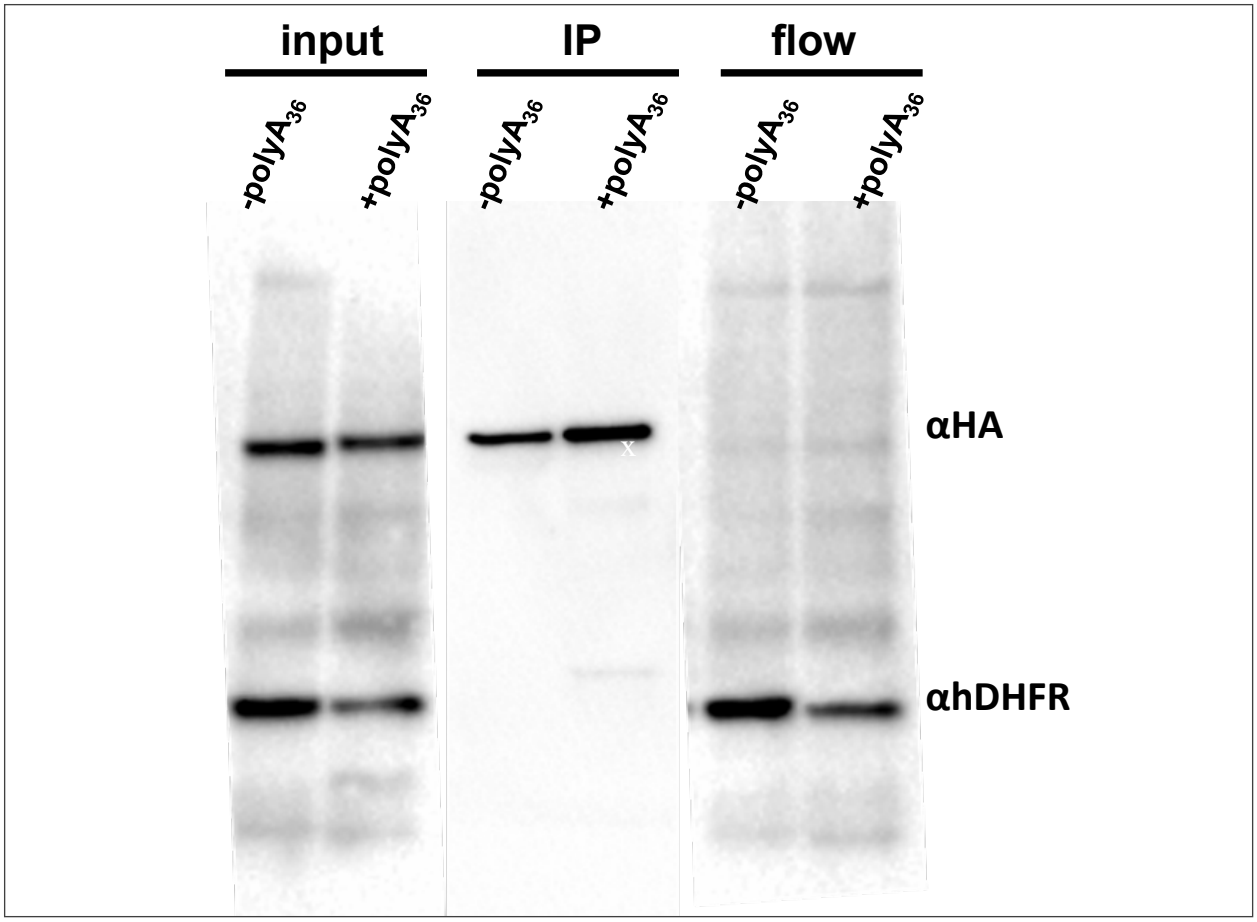

SUPPLEMENTAL FIGURE 2.4 | HA-pull-down assay of -polyA36, +polyA36 reporters.

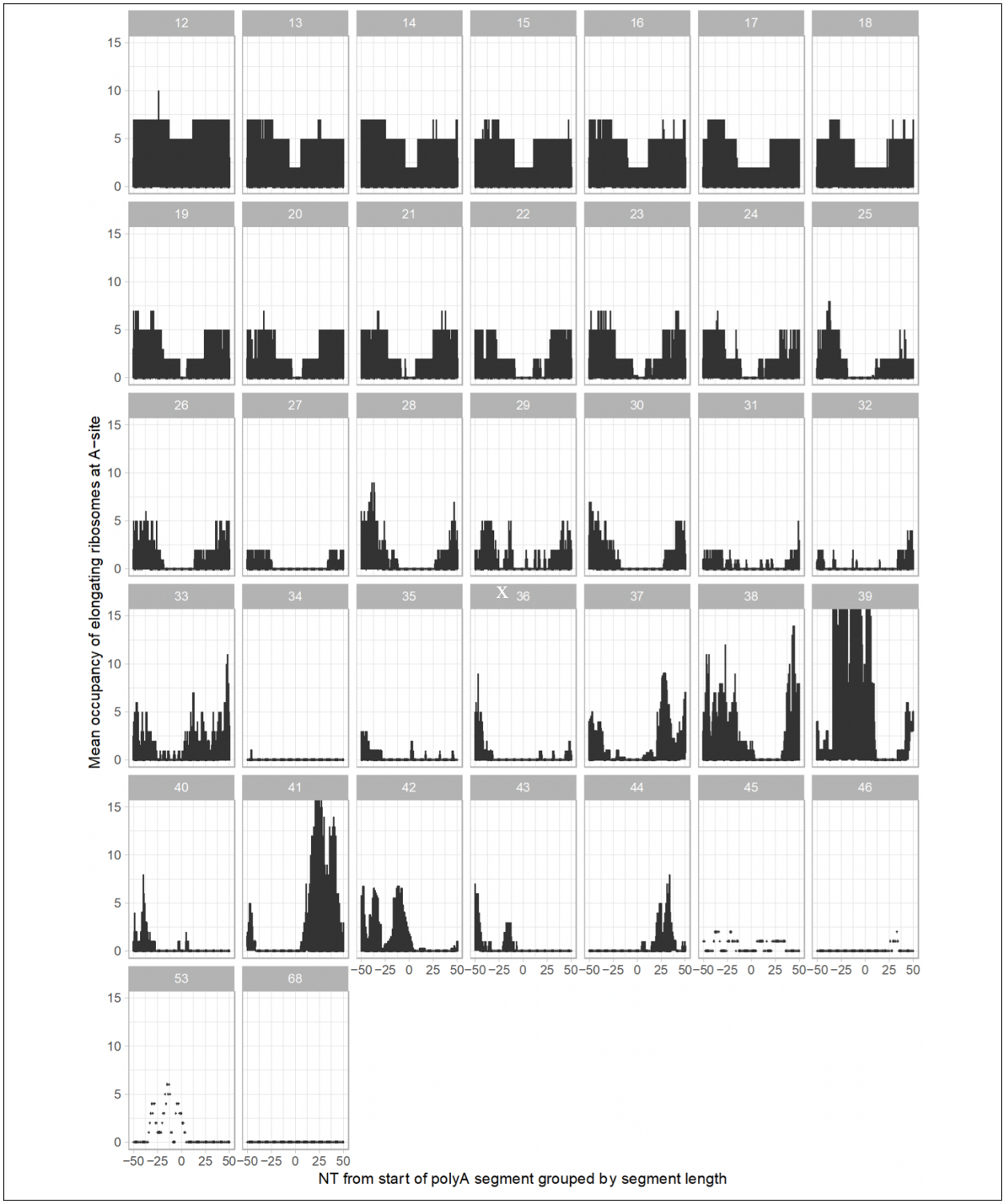

SUPPLEMENTAL FIGURE 2.5 | Ribosome occupancy around polyA segment of *P. falciparum* transcripts (summarized across all life stages) and grouped by polyA segment length (12–68 adenosine nucleotides in a row transcripts are shown).

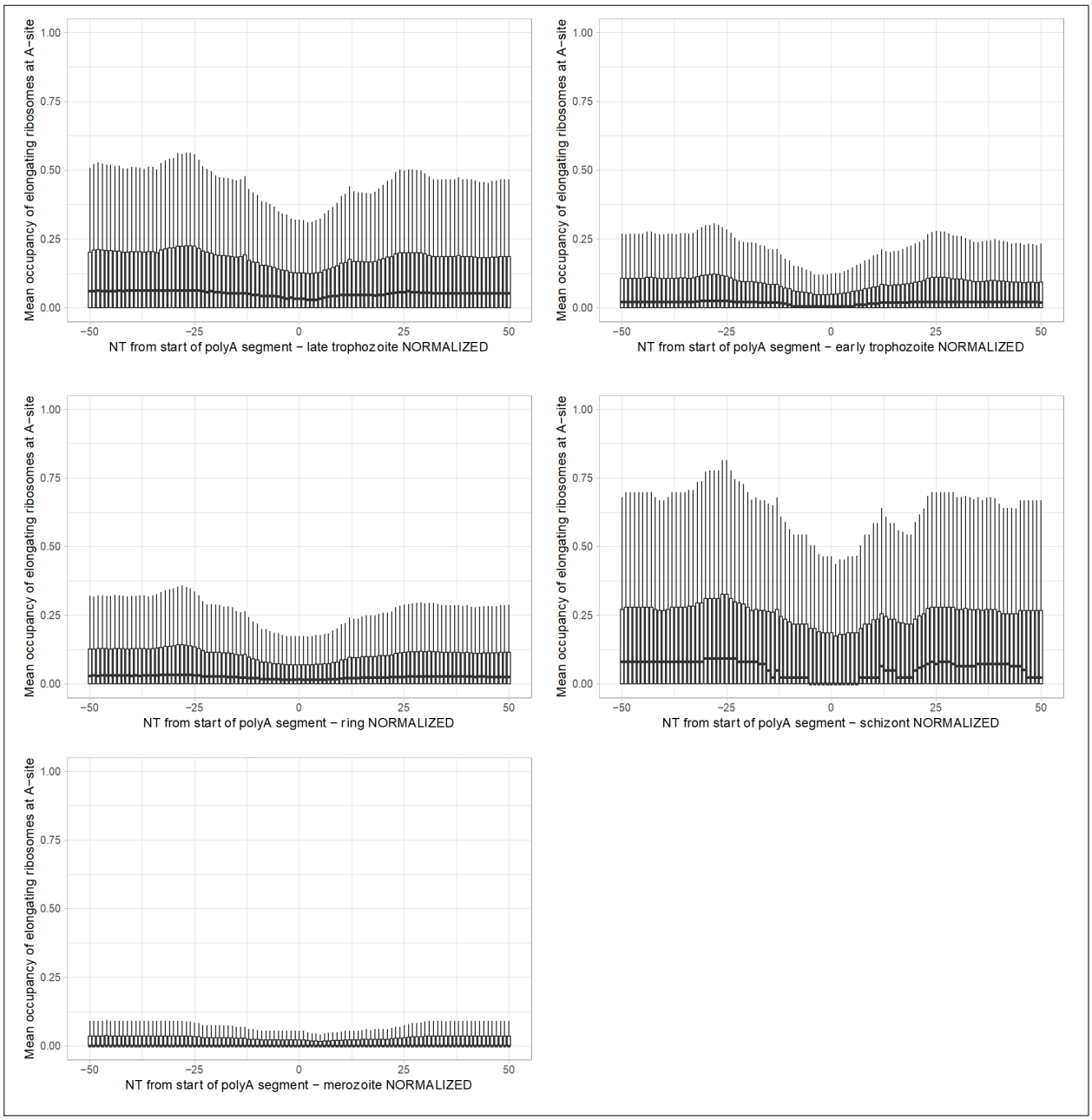

SUPPLEMENTAL FIGURE 2.6 | Occupancy of elongating ribosomes (mapped to A-site) around start of polyA segment in *Plasmodium* at different life stages.

PF3D7_1464200zincfingerprotein

ATGGAAAAAATAAACGACAAGGCCATTTTAGAGAAAATATCTGACATAACAGGAAATACAACCAAGAATACTCTTCTTAGCTTTAAAAAAAAGAAGAAAAAAAAAAAAAAAAAA
ATGTAGATGTAAGCGGAGATAAAACGAAAAAGATAAAAAATAAAAAAATTAACAAGACAGAAAACACTTTTGATAATTTTAAATATGAACCAAAAAAAGAAACATGTAAATTTTT
TTTTAAAAAAGGGAAATGTATACATAATGATAAATGTACTTATTCACATGATGTTATTCCAATATATAAAATATCAAAGTTATGTAAATTTTTAGTTAAAGGTACATGTCATAAA
CAAAATTGTATCTTTTCTCATGATTATCAACTTTTTTTATTGTCGTAATAATGTTATATATAATTCATGTCATAATCCTGCATGTAAATTTAAACATGTAAAAATAGATAATAGTA
TTAATAATGCAGATGAATATAATAAAGAAGTAGATAATGTTCTAACAAAAGATGATAAAATTAGATTTCTTTATAATAATAAAAATTATATAATGGAGTTATTAATTCATAAATA
TCATACTTTTGATAATACGGATCATAAAATAAATATAGATAATTTAATAAAAAAAAAATAATTATCCATGGTTTATTAATGGAATTATAGATATTATTAAGTTAGACTTTAAATAT
AATAAAGCAGATAGTTTTTTTAAATTAATAAATATAGCCAAAAATAATCAAAATAATAATTTAAAATCATACATGGATAATTCTGCTAATCAAAATGATCAAAATAATGATCTTA
CAAATAACACAAATGTCAATAATCAAGATATTAAATCATCACAGCCGTCAATAAAAGATGGGGAATTCAAAAATAATAATGATAATCAAAATGGGGATAACAAATTAGAAAATAA
TGTGGAACAAAATTTCGATGACTATAATTTCTATTCAAGTGAAGAAGAAGATTATACGCAGTACTTGAATAAGTACTTTGACATGGACACATAA

PF3D7_0615500cdc2-relatedproteinkinase5

ATGTTTGGAATTACATTAACAAAGTGCAAAATATACTTCAATAATATATATTCGACCGTATCTCTCGAAGAAAAATTAGGGGGGGGCACCTATGGTGACGTGTACAAAGGGAAAG
TAATAAAATATAATAATAATAATAATAATAATGATTTATATCAAAATACAAATTATTTACCTTATGATTATTATACTGATGAATTTGTTTTTTTTCGTAAAAATGTTTATGCCAT
AAAATTTTTTCGAGACGATTTAAGGACCATAAATGAAGAAGGTATAAGTTGTACAACATTAAGAGAATTAAGCTGTTTAAAAAATATTGGGAGGCATCCTAATATCCTTCGTTTA
ATAGATGTTACTATAGATAGACAAAAGCTTATAAGTGAATATATAAATAGACAGATATTACAACATTATACATCAAATTATCATCATCATCATCATAGTAAATTAGATATCACAC
CCTTGGCAGCTGATCAGAAATTTATTTTTGCTGCTTATGAATATTGTGATGGTGGAGATCTAAAAAAGCTTATACAAAAAACAAAAATTAGTGATGATCAAGCGGGACTTAATTT
GAAAGAAGCCAAATGGCTATCCTTCCAACTATTAAATGGATTAGCTTATTTACATAATAATAAATAAATGTGTCATAGAGATTTGAAACCTGAGAATGTTATGTTACAAGAGACATCT
AATCATAAGTATCTTTTAAAAATTGGAGATTTAGGTTTATGCAGAGAATTAAAAAACGATGGTGACATGACACCTACTGTTTGTACAATATATTACCGACCTTTGGAAGTGCTGC
TTTCGAAATTTGAATTATCTAATAAGCATCATCATAAAAGTCATGCAACAAATCATAGAAGGGATGACAATGATGATGATGAAGATGAAGATGATGATGATGAAGATGAAGA
TGATGATGATGAAGAAGAAGAAGATGACGATGTAGATGAAAATGTAGAAGTAAAATTACATGGTCGTAATAAAACTAGTAGTAATAATAAAAATAATAATAACAAAAACCATAAT
AGTAACATTAATTATAATAACCACAATTGGAGTCGTCGTAAAAATAAAATGAAAAAAAAAAAAAAAAAAAAAGAAAAAAAAAAAAGAGCAAGATGATGATTATTATAATAAAGATT
TTCAATATGGTTTAAATGTTGATATATGGTCAGCTGCATGCATTATATGTGAACTTATTATTGGAAGACCTCTTTTTAAAGGAGTCACAGAATTCGATTTGATTATTAGGATCGT
TAATTCTTTAGGTAAACCTAATAAAGATGAACTAGAATTTTTTAGTAATTCCCGTTTTTATCCTTTAAAGGAGGATTTTTTTAATGTTCATATAAAAAATAAAAAGGATGCTTTA
AACGTTATTACGAATGGACGAATAGACGAGTTAGGTATTGATTTGCTTGTTAAGATGTTGAAATATAATCCGAATGATCGTATTACGGCAGCTGATGCTTTATCGCATCCTTGGT
TTTCAGATATAAGATTTGATAACTTGGATGGTATAGGTGTTTATAATTGGTATGTACATTGTTTAAAATATTATATTGGTATTAAAACTTTTAGAGAAATTGAACAAAAAAAAAA
AAATTTACTTACGACAACTATGATTTCTCATTTTTTATGTAAATCAAATGATAAGTATGCTAAGGTTATTTTTAAGTTAATTAATGATACCTTTAAAAATTTAGGAGGATATAAA
AAAAGTGGACGAAGATCTTTTGCTATTTTTTCAGATAAATATGCTCATGATGAAAAGAATACAAATGGATTTATTAAAAGAGCAAGTATTAAAGTATTAAATGATATGAAAGAAA
AAAATGTGAAAGAAACAAAAGAAGAGTTTTCTTTTTATGATGAAAGTACAACTTATATGACACCACCAACATCTGTTAAAAGAAGAAAATTCAATAGATCAAGTTATCATGTTAT
GAACCCAGAACATTCATATGAATTTACAAATAAAATCAGAATGAAAAGAAATCTATCCATTCCAGATTTTTCAACACCTGATAAAAGTATACAAAAACAAAAAAAAATAAAAGCT
GCTACGACAAAGAATAAAGCAAGTCATCTAGAATTTTCTCATTTTTAA

PF3D7_1108000IWS1-likeprotein

ATGGATAGCGATTCAAATAAGAATGACCACGAGTCGTTAGAAAACTCAGGTTTATTCAACGACGAAAATGCATCTGATGGAAATAATGTTGAGAACTTTAAGAAAAAAATGAAAA
TGATAAAAGTATTAAATGTAAAGAAAAATAAAGAAATAAAGAAAGATAGAAAGGATAAGAAGAAAAGAAAACTTCAAAGGATTATCGATGATGATAATGAAGATGAAGATGATGT
TATTGAGAAAGAAAATGATCAAGGAAAAGATCAAGGAAAAGATCAAGGAAAAGATCAAGGAAAAGATCAAGAGGATGTGTTTCTTTTTGGTAATGATGATTTGGTTGAAGAGGAT
GAGGAGAGACATAAGAAGAAAAGGAAAAAAGAAAAGGAAGAAAGAGGTAAACACAAAAAAAAAAAAAGTATAAAGCGAATAATGGAAAATGATGATATGCACAAGGTTCATAGTG
ATGATAGTAATTATAATAATAATAACAATAATATTAGTGATGATAATAATAATAATAATTATTAGCGATGATTATAATAATAATAATTATTAGCGATGATGATGATAGTAATAATAG
TGATAGCAGCTATGATAATACTATGAGTGATCATAGTGATATGAAGAAGAAGAAAAAAAAAAAAAAAAAAAAAAAAAAAAAAAAAAAGCGAATTTATCGATACCATTGCAGAAGAAGGT
GATGAAGATGAAAAAGAAGAAGATGACGATTATGATGATGAAAATAATATAAATATAGATAAAATGACCAACGAAAATAAAAAATCGAAGAAAATAGATTTTGATAAATTAGGCT
TAGGTGATGATGATGAAGACGAGGATAATTATATGAACGATTTTGGAAATCATTCTAATATATCTGAAAAAAAAAAAAAATCTCATTTTGACGAAATATTAGAAAATTTTAAATC
GAAAAGAAAAAGAGTTCATAAAATTTCAGAAGATGATGGATTAGAATATTGTGAAAATATTTTGAATCAGATGATATTAATGCATGAACAAGATTTAAAAAGTATGAAAGAAAAA
AAACCAGCAACAGCTAAATTACAAATTATAGATAATGTTTGTAAAATATTGACAAAACCGAAATGGAAACCATTCTTTATGAAACTAAATATATATCATGTATTAGCCTTATGGT
TGATGCCGACATCCAAAAATACATTACCCAATTTTACTATAAGAACGAATTTATTAAAAGTAATTCAACAATTACCAATTACTATTAAATCATTAAGAGGAAGCCAGCTAGGAAA
AATATTGACTTACCTACATTCACATAAACATGAAACAGAAGAAAATAAAAAACTCATAAAAAATATTATGCAAAATTGGATGGGCCCAATTATAGGAATTAATACGAACTATAAA
CAATATTTAAAAGAAAGACAAAAAAGGATATCTGAAAATCCTGAATATCACAAAAAAGTTCTTGAAAAGGCAAAAACATTAATACCTGATTCAATATGTATAGAAAGGAAGAAG
AACAAAATGAAATGAAAAGACATGCAAGTATTCCTTATAATAGTGAATGCTCATTTCTAATTAATGTCCCCTCTTCTATACCTAGTATTAGTAAAAAAATCATTCCCAAAAGTAA
AATTAAGAGGTTAACAGATAATATGAAATTGTTAAAAAGATGTAAAAAAATGCAAAAGGTTTCAATTGAAGGAAAGGGTGTAGCTGTTGCACCATAA

PF3D7_1462800glyceraldehyde-3-phosphatedehydrogenase(GAPDH)

ATGGCAGTAACAAAACTTGGAATTAATGGATTTGGTCGTATCGGACGTTTAGTATTTAGAGCAGCCTTTGGAAGGAAAGATATCGAAGTAGTTGCTATTAACGACCCATTTATGG
ACCTTAACCACTTATGCTATCTCTTGAAATACGATTCAGTACATGGTCAATTTCCATGTGAGGTAACCCACGCTGATGGATTTTTATTAATCGGAGAAAAGAAAGTCAGTGTTTT
TGCTGAAAAGGATCCATCTCAAATTCCTTGGGGAAAATGCCAAGTAGATGTTGTATGTGAATCAACTGGTGTATTTTTAACCAAAGAATTAGCTAGCAGTCACCTTAAGGGAGGA
GCCAAGAAGGTTATTATGTCCGCCCCACCAAAGGATGACACCCCAATTTATGTTATGGGTATTAACCACCACCAATATGATACCAAACAACTTATTGTTTCCAATGCATCATGTA
CCACAAACTGCTTAGCTCCATTAGCTAAAGTTATTAATGATCGTTTTGGAATTGTTGAAGGTTTAATGACCACCGTTCATGCATCCACTGCTAACCAATTAGTTGTTGATGGTCC
ATCAAAGGGTGGTAAGGACTGGAGAGCAGGTAGATGTGCATTATCCAACATTATTCCAGCTTCCACTGGTGCAGCTAAAGCTGTAGGTAAAGTTTTACCTGAACTTAATGGAAAA
TTAACAGGTGTAGCTTTCAGAGTACCAATTGGAACTGTATCAGTTGTTGATTTAGTTTGCAGATTACAAAAACCAGCAAAATATGAAGAAGTTGCTTTAGAAATTAAAAAAGCTG
CTGAAGGTCCACTTAAAGGAATCTTAGGATACACTGAAGATGAAGTTGTTTCTCAAGATTTCGTTCATGATAACAGATCATCAATCTTTGACATGAAAGCTGGTTTAGCCTTAAA
CGACAATTTCTTCAAATTAGTTTCATGGTACGATAATGAATGGGGATACTCAAACCGTGTTCTTGATTTAGCCGTACACATTACTAACAACTAA

SUPPLEMENTAL FIGURE 2.7 | Sequences of three *P. falciparum* polyA tract genes (PF3D7_1464200, PF3D7_0615500, PF3D7_1108000).

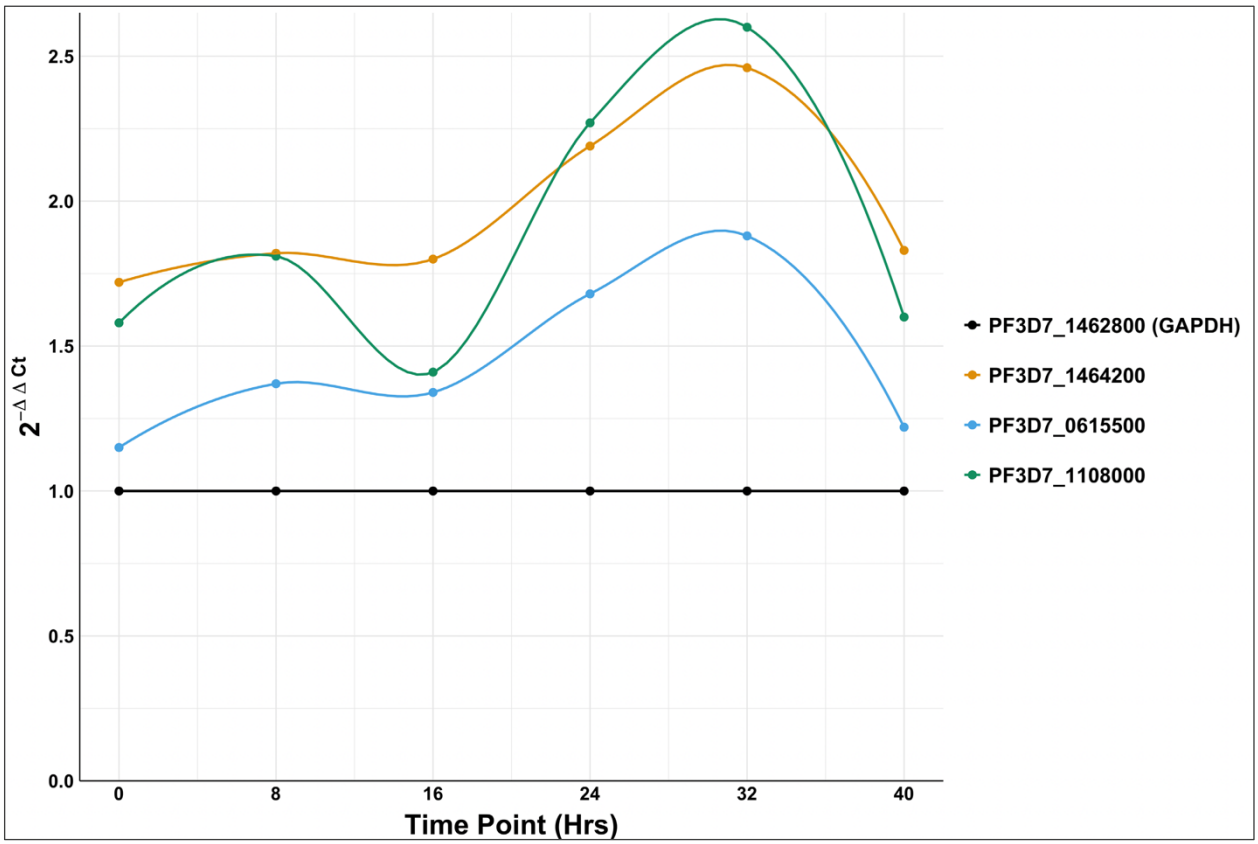

SUPPLEMENTAL FIGURE 2.8 | Endogenous polyA genes are expressed in *P. falciparum*. Time course mRNA expression analysis of three genes (PF3D7_1464200, PF3D7_0615500, PF3D7_1108000) containing polyA stretches of varying lengths (largest: 20, 20, and 31 adenosines respectively) normalized to GAPDH (PF3D7_1462800) starting with highly synchronized rings at time zero.

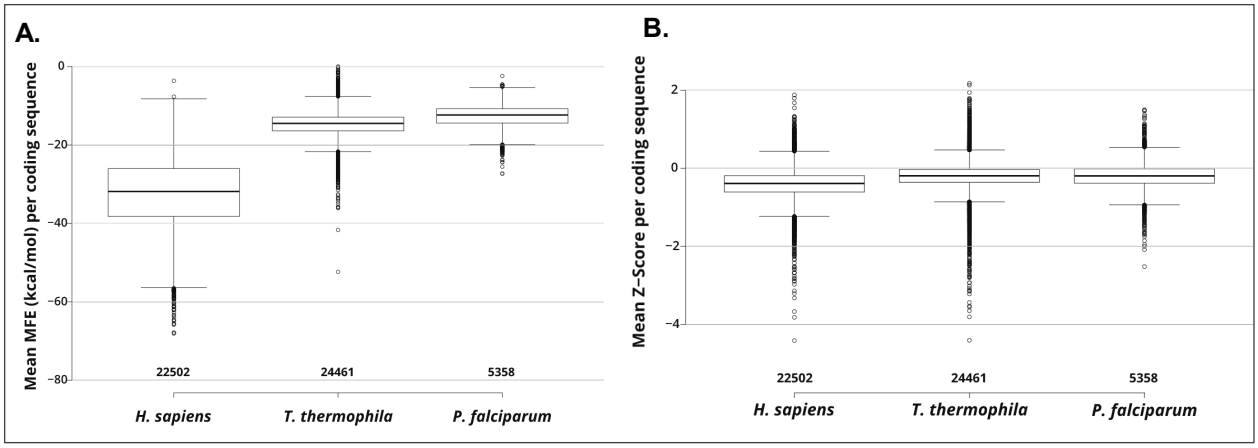

SUPPLEMENTAL FIGURE 2.9 | MFE from scanning window analysis in *H. sapiens*, *T. thermophila*, and *P. falciparum*. Box and whisker plots showing the distribution of mean folding energy values (kcal/mol; measures the stability of RNA structure) calculated for each coding sequence from *H. sapiens*, *T. thermophila*, and *P. falciparum*, resulting from a scanning window analysis (SEE MATERIALS AND METHODS).

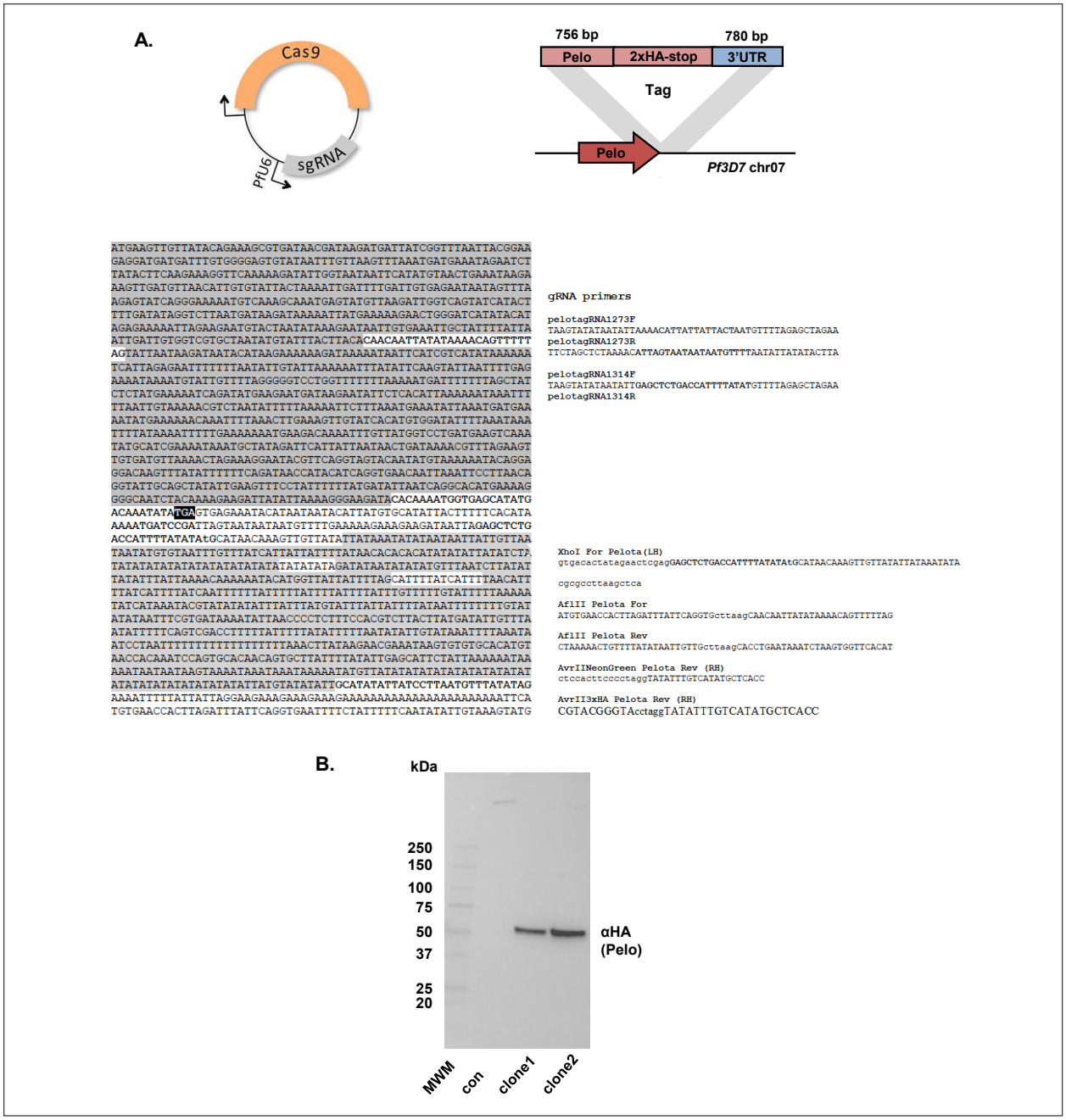

SUPPLEMENTAL FIGURE 2.10 | Alteration of endogenous PfPelo gene by CRISPR/Cas9. (A) Schematic of CRISPR/Cas9 engineering of *P. falciparum* Pelo (PF3D7_0722100 gene; human Pelo homolog). Two sets of gRNAs creating clone 1 and clone 2(red) were used to create independent clones 1 and 2. Recombined sections of PfPelo gene are indicated in purple and gray, respectively. Primers used for creation of recombinant DNA and target sequences of gRNAs are indicated in teal, yellow and red, respectively. **(B)** Western blot analysis of endogenous HA-tagged PfPelo protein from two Cas9 engineered clonal lines (Clone one and Clone 2) of

P. *falciparum* Dd2 cells. Control (con) represents non-engineered *P. falciparum* Dd2 parent line. Biorad Precision Plus Protein molecular weight markers (MWM) are indicated.

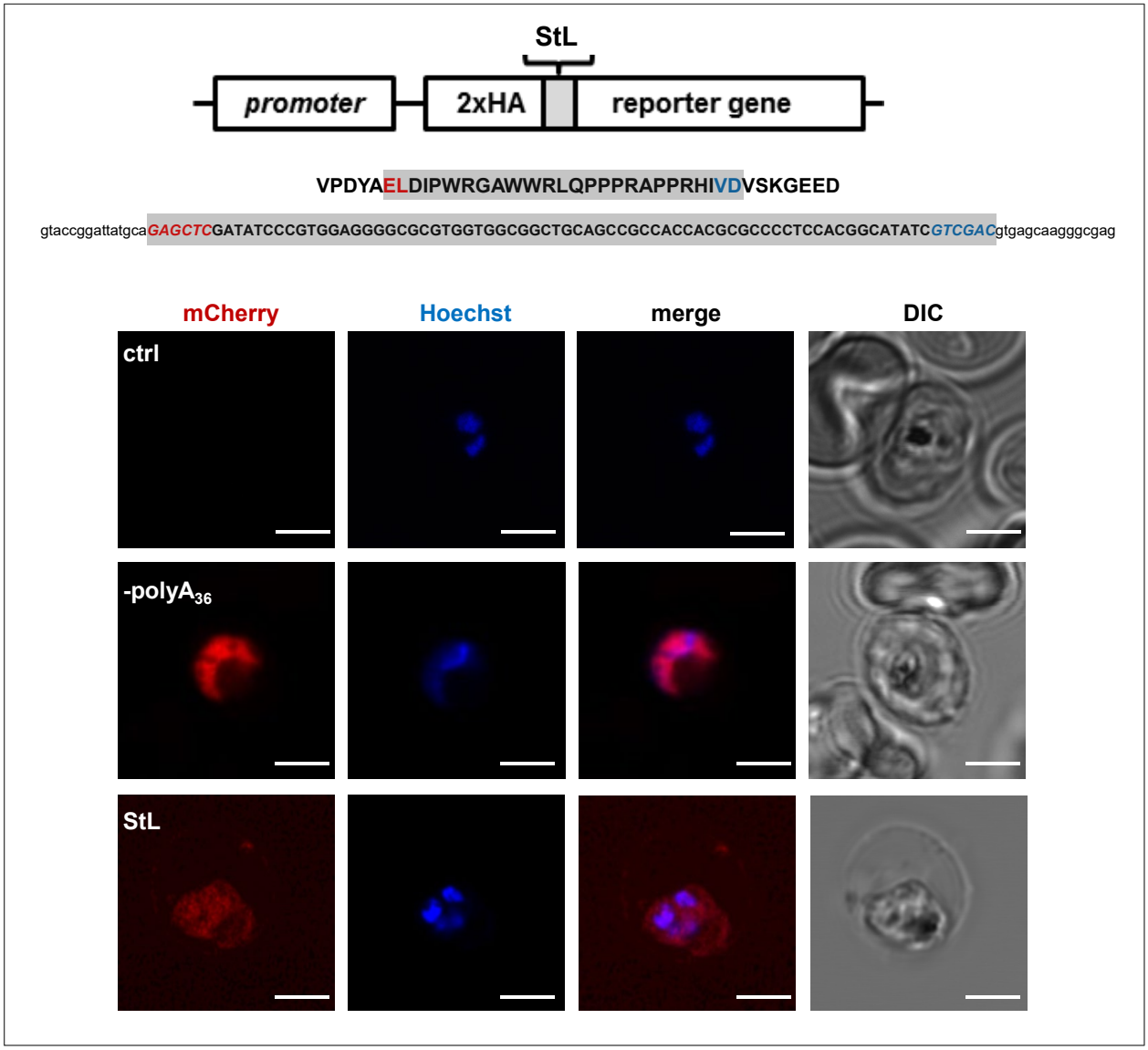

SUPPLEMENTAL FIGURE 2.11 | Schematic of stem-loop reporter construct (StL) used for expression in *P. falciparum*.

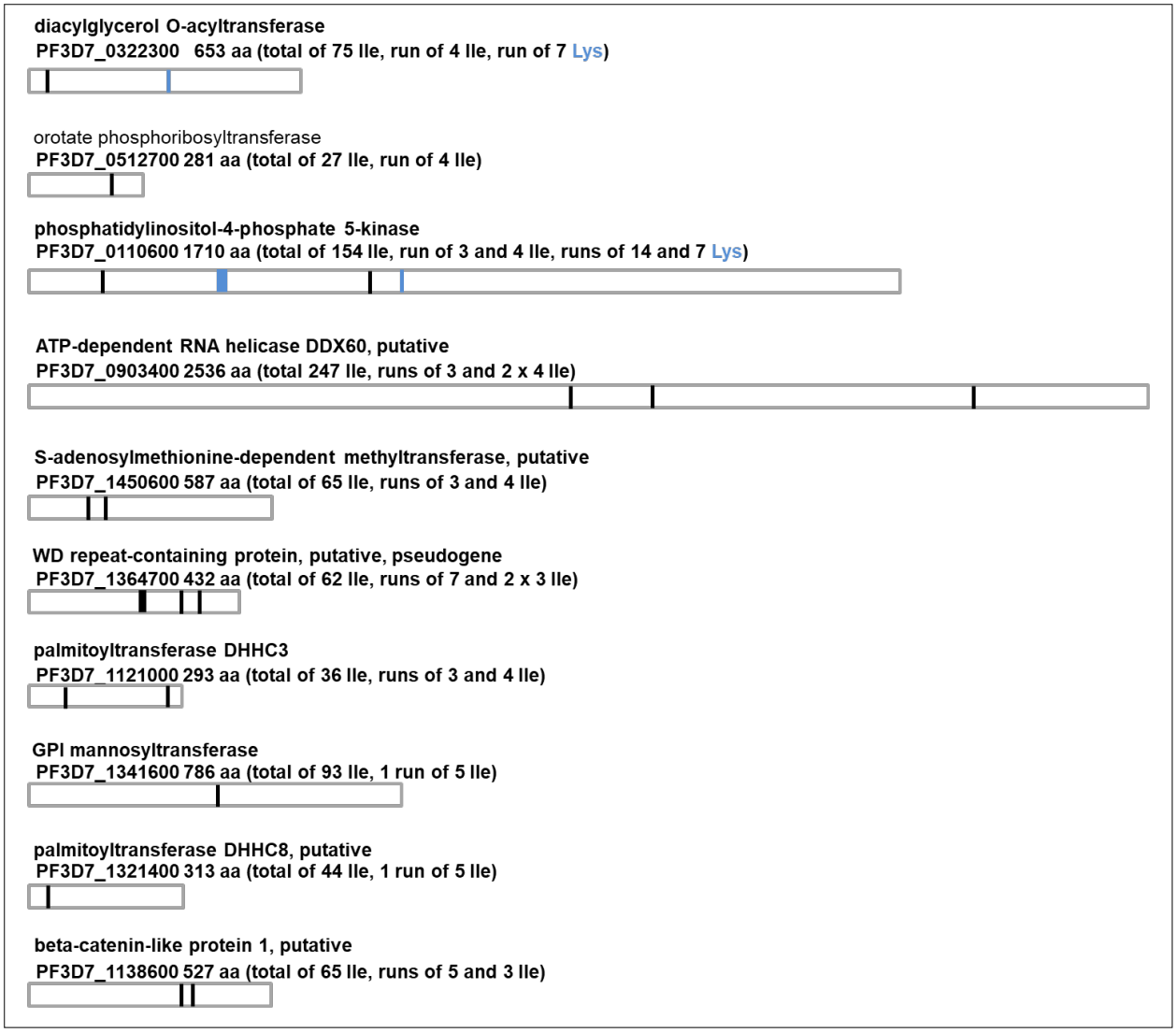

SUPPLEMENTAL FIGURE 2.12 | Schematics of nine *P. falciparum* genes with runs of 3 and more consecutive isoleucine (Ile) residues used in analyses shown in FIGURE 6D.

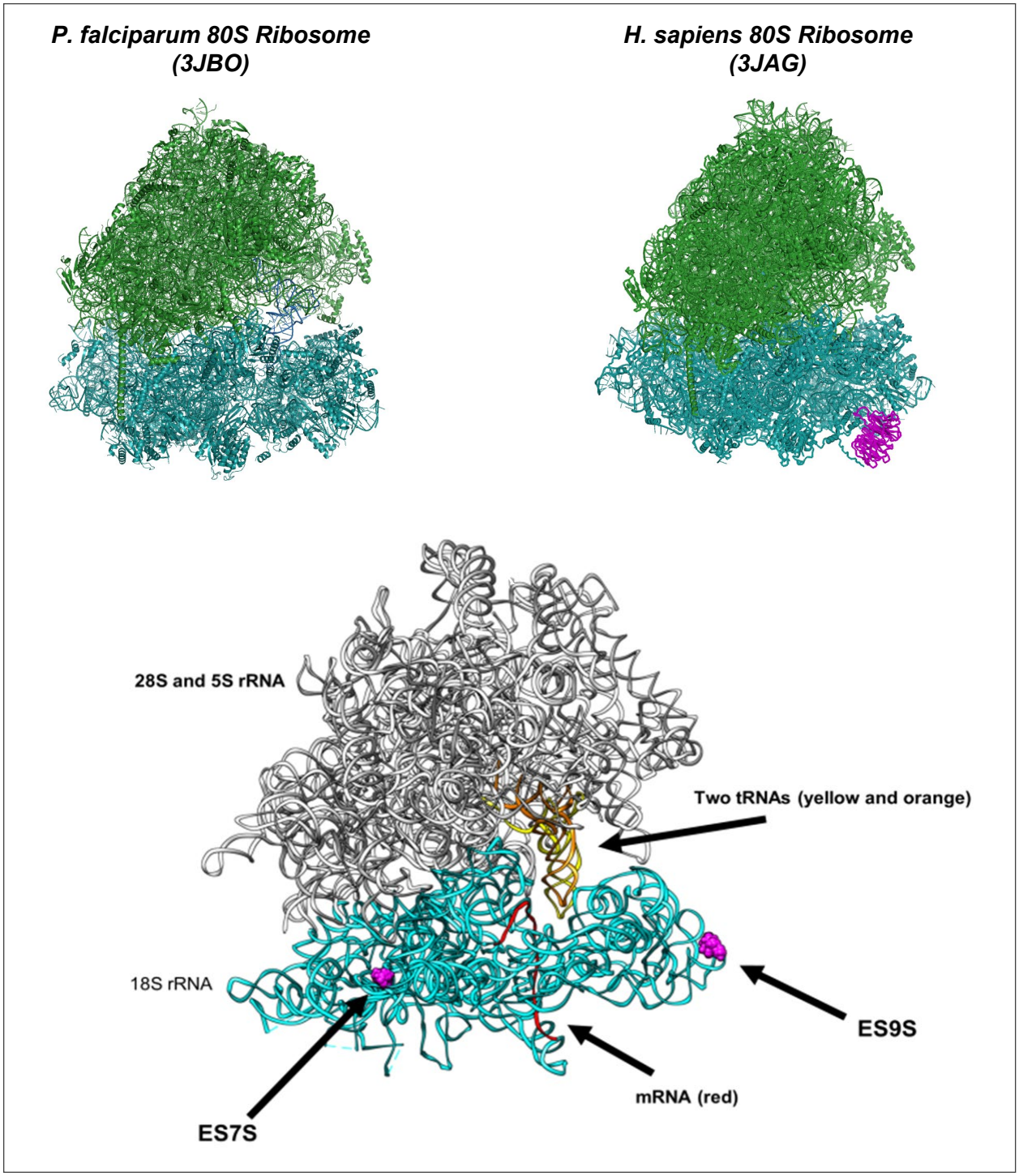

SUPPLEMENTAL FIGURE 2.13 | Structure of *P. falciparum* (PDB code: 3JBO) and H. sapiens (PDB code: 3JAG) ribosomes with receptor for activated kinase C (RACK1) in magenta, previously shown to be absent from *Plasmodium* ribosomes (60S in green, 40S in cyan).

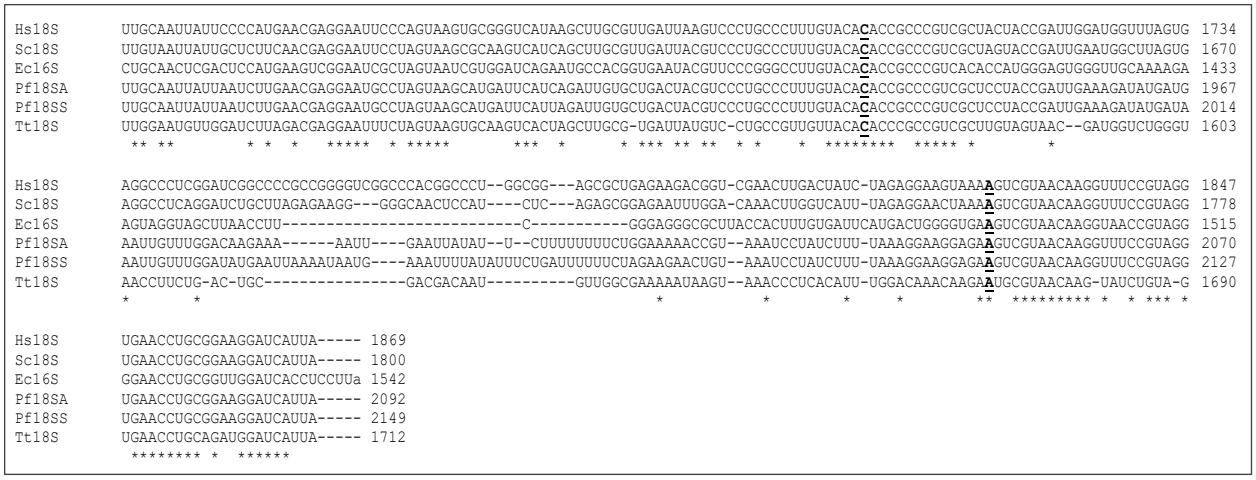

SUPPLEMENTAL FIGURE 2.14 | Segment of sequence alignment of 18S rRNA from P. falciparum (Pf18SA and Pf18SS, A- and S-type of ribosomes), H. sapiens (Hs18S), S. cerevisiae (Sc18S), T. thermophila (Tt18S) and E. coli 16S (Ec16S).

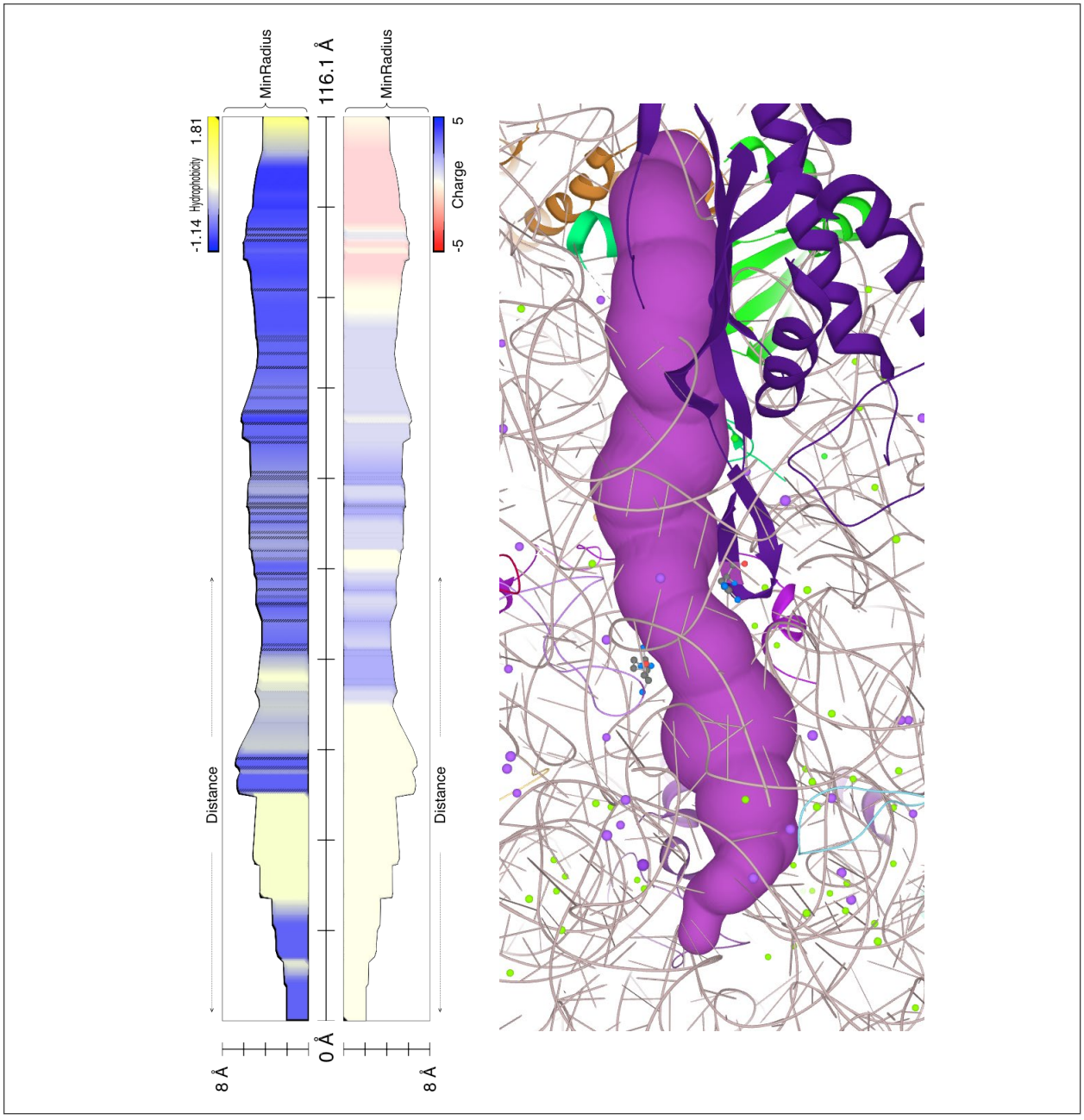

SUPPLEMENTAL FIGURE 2.15 | Polypeptide exit channel from *Haloarcula marismortui* ribosome (PDB: 1jj2) has one long fragment of relatively hydrophobic lining of the tunnel at the entrance (between PTC and constriction site).

SUPPLEMENTAL TABLE 2.1 | GO Term analysis in *P. falciparum*.

ID	Name	Bgd count	Result count	Pct of bgd	Fold enrichment	Odds ratio	P-value	Benjamini	Bonferroni
GO:0016337	single organismal cell-cell adhesion	57	56	98,2	1,56	33,76	8,98E-11	6,69E-08	1,34E-07
GO:0098602	single organism cell adhesion	57	56	98,2	1,56	33,76	8,98E-11	6,69E-08	1,34E-07
GO:0007155	cell adhesion	77	71	92,2	1,47	7,15	2,66E-09	1,32E-06	3,97E-06
GO:0009405	pathogenesis	101	81	80,2	1,28	2,44	0,00010834	0,04035608	0,16142433

SUPPLEMENTAL TABLE 2.2 | Constituents of NGD/NSD, and RQC pathways in *H. sapiens* and *P. falciparum*.

		Homo sapiens	*Plasmodium falciparum*
No-Go Decay/Non- Stop Decay	Pelota	+	+ (PF3D7_0722100)
	HBS1L	+	-
	RACK1	+	+ (PF3D7_0826700)
	XRN1	+	+ (PF3D7_0909400)
	N4BP2 (Cue2, Nonu-1)	+	-
Ribosome Quality Control	CNOT4	+	+ (PF3D7_1235300)
	ABCE1	+	+ (PF3D7_1368200)
	ZNF598	+	+ (PF3D7_1450400)
	ASCC3 (Slh1)	+	+ (PF3D7_1439100)
	NEMF	+	+ (PF3D7_1202600)
	Listerin	+	+ (PF3D7_0615600)
	UBE2D1	+	+ (PF3D7_1203900)

Chapter 3: Immunoprecipitation of RNA Species via Aptamer Tagging in *Plasmodium falciparum*

3.1 Abstract

The AU-rich transcriptome and multiple, distinct ribosomes of *P. falciparum,* as well as other *Plasmodium spp.,* lend the organism to significant study in the realm of protein synthesis. The ability to translate lengthy polyA tracts and the multiple ribosome types are hallmarks of the genus. High-fidelity translation of polyA tracts in *P. falciparum* appears to be driven by multiple factors, however the extent and impact of ribosome modifications, identity and function of aiding RBPs, as well as the functionality and tailoring of RQC machinery are all unknown. While the ribosomes of *Plasmodium spp.* exist as a regulated, heterogeneous pool, the factors that recognize environmental cues and subsequently drive alteration of the ribosome population remain elusive. More fundamentally, does the heterogeneous pool ribosome subunit types lead to heterogeneously derived 80S ribosomes and, if not, how is this maintained?

Current methodologies used in *Plasmodium spp.* are unable to address these questions because of their inability to extract and examine specific parts of the dynamic whole directly. Here, we demonstrate two applications, PP7 mRNA immunoprecipitation (PP7-mRIP) and MS2 rRNA immunoprecipitation (MS2-rRIP), never before implemented in *P. falciparum* using different bacteriophage coat proteins each recognizing their own RNA aptamer. The PP7-mRIP assay is

able to generate differential, substrate-driven mRNA proteome profiles, the constituents of which are identifiable by mass spectrometry. The MS2-rRIP assay demonstrates significant enrichment of tagged versus untagged ribosomes. PP7-mRIP and MS2-rRIP allow for the direct examination of mRNA-bound proteomes and distinct ribosome types, respectively, in *P. falciparum* and therefore could prove instrumental in answering many of the long-lingering questions surrounding post-transcriptional gene regulation and ribosome switching in malaria parasites.

3.2 Introduction

The AU-rich transcriptome[1–6] and multiple, distinct ribosomes[7–13] of *P. falciparum,* as well as other *Plasmodium spp.,* lend the organism to significant study in the realm of protein synthesis. The ability to translate lengthy polyA tracts and the multiple ribosome types are hallmarks of the genus. While some of the "hows" and "whys" surrounding these peculiarities have been discovered[1,2,14,15], many remain unclear. For instance, the high-fidelity translation of polyA tracts in *P. falciparum* appears to be driven by multiple factors: the ribosome, proteins (RBPs, RNA helicases, etc.), and the ribosome-associated quality control machinery[1,2,16,17]. However, the extent and impact of ribosome modifications, identity and function of aiding RBPs, as well as the functionality and tailoring of RQC machinery are all unknown.

Expressing multiple ribosome types, although not a common phenomenon found throughout the kingdoms, is not exclusive to nor unexpected of *Plasmodium spp.* where protein synthesis occurs in multiple hosts with dramatically different system temperatures. Even bacteria have rRNA genes associated with stress response[18]. An analysis of curated 18S sequence data from

the various EuPathDB databases show that other *Apicomplexa* phylum members such as *Cryptosporidium* and *Babesia*, as well as those of the phylum *Microsporidia* (e.g. *Encephalitozoon spp.*), appear to have multiple 18S rRNAs (**FIGURE 3.1**)[19]; all of which can be human infective.

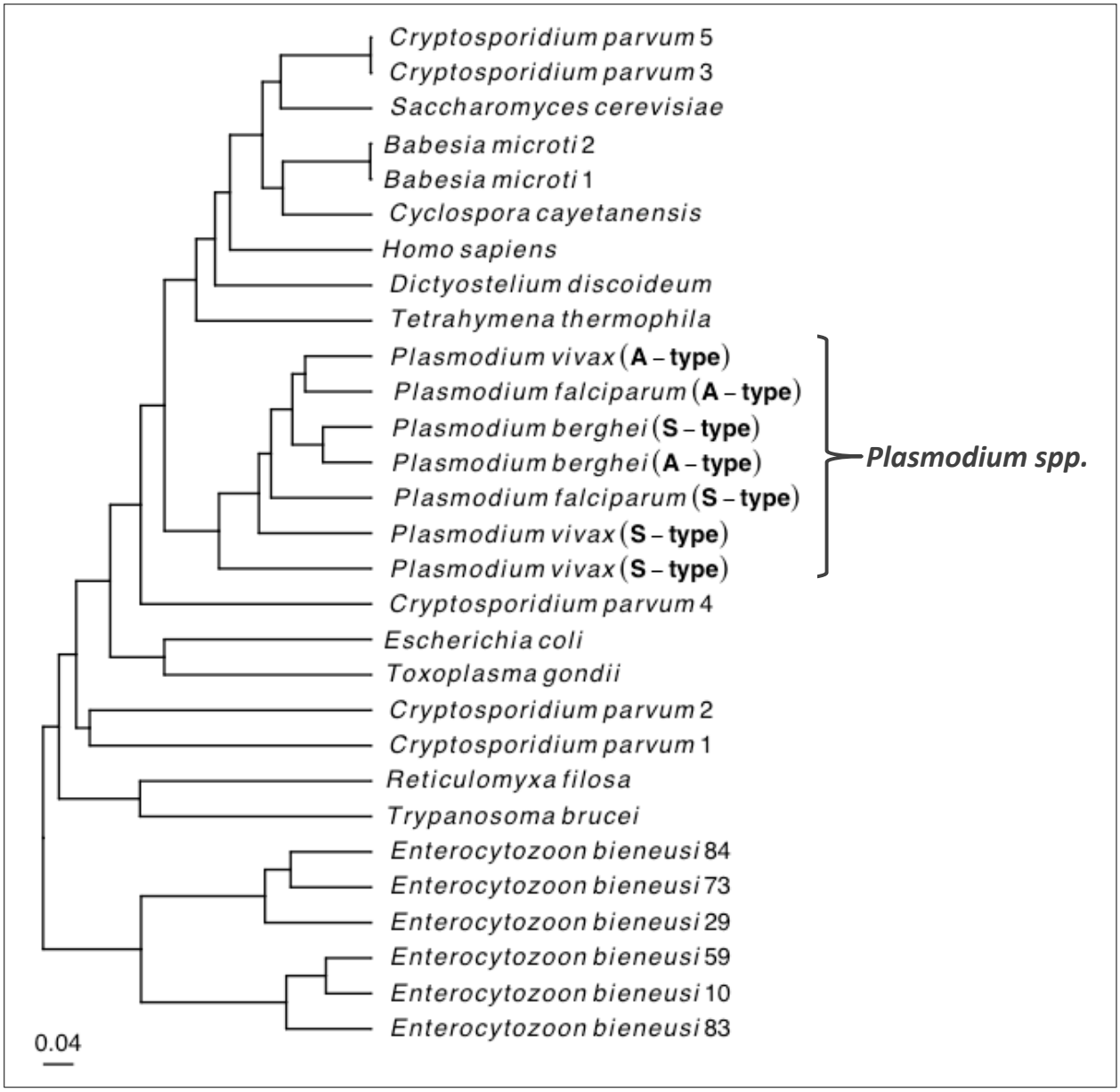

FIGURE 3.1 | Evolutionary tree of 18S/16S rRNAs from selected species. The 18S rRNA sequences collected from EuPathDB[19], *Saccharomyces* Genome Database[20], and EcoCyc *E. coli* Database[21] and a phylogenetic tree generated using RStuio.

The ribosomes of *Plasmodium spp.* exist as a regulated, heterogeneous pool[11], with one type being the dominant member during different points in the parasite life cycle. The regulation of ribosome population dynamics in *P. falciparum* are linked to parasite development[11,13,14,22,23]

and enthalpy changes driven by the parasites' environment[15]. The parasite alters the ribosome population by increased transcription of one ribosome type[24] and active rRNA degradation of the other[14]. However, what is unknown are the factors that recognize environmental cues and subsequently drive alteration of the ribosome population. At an even more root level: while both subunit types exist within the pool, are the 80S ribosome comprised of homogeneous or heterogeneous subunits and, if so, how is this maintained?

Current methodologies used in *Plasmodium spp.* are unable to address these questions because of their inability to extract and examine specific parts of the dynamic whole directly. Here, we demonstrate two applications, PP7 mRNA immunoprecipitation (PP7-mRIP) and MS2 rRNA immunoprecipitation (MS2-rRIP), never before implemented in *P. falciparum* using different bacteriophage coat proteins each recognizing their own RNA aptamer. The PP7-mRIP data show the ability of the assay to identify mRNA substrate-specific RBPs showing the assay's potential in identifying RBPs associated with mRNA translation in the parasite; particularly those involved in polyA translation fidelity. While the MS2-rRIP assay is able to enrich tagged rRNAs over the untagged rRNAs, allowing for further detailed study of the multiple, distinct *Plasmodium* ribosome types, nonfunctional ribosome decay, and more.

3.3 Materials and Methods

3.3.1 Parasite culture and transfection

P. falciparum Dd2 was cultured at 2-5% hematocrit in O^+ erythrocytes in Malaria Culture Medium (MCM): RPMI 1640 supplemented with 5 g/L Albumax II (Gibco), 0.12 mM hypoxanthine (1.2 mL 0.1M hypoxanthine in 1 M NaOH), 10 µg/mL gentamicin[25]. Cultures were grown statically in candle jar atmosphere. As required, cultures were synchronized with 5% (wt/vol) sorbitol.

Asynchronous *P. falciparum* Dd2 parasites were washed twice in 15 mL incomplete Cytomix (25 mM HEPES, 0.15 mM $CaCl_2$, 5 mM $MgCl_2$, 2 mM EGTA, 120 mM KCl, 5 mM K_2HPO_4, 5 mM KH_2PO_4) and resuspended in a total 525 µL with 100 µg of maxi-prep plasmid DNA dissolved in incomplete cytomix (125 µL packed iRBCs and 400 µL DNA/incomplete cytomix), The parasites were transfected in Bio-Rad Gene Pulser cuvette (0.2 cm), 0.31 kV, 950 up, infinity resistance. Selection (10 nM WR99210 or 2 µM DSM-1) was added to parasite 48 h after transfection and used to select resistant parasites[26].

3.3.2 Saponin lysis of infected red blood cells (iRBCs)

The cell iRBCs were resuspended in two volumes of PBS containing 0.15% saponin, and incubated on ice for 10 min, with vigorous mixing every 3 min. Afterward, the samples were centrifuged 7000g, 5 min, 4°C, and the pellets were washed three times more with the same buffer.

3.3.3 Cap Protein Expression and Purification

Briefly, 2.5 mL of overnight culture was inoculated into 500 mL LB-carb and grown to an OD of ~0.6 (about 3 hours). The Rosetta Blue (Millipore Sigma #71059, St. Louis, MO) or BL21 Star (Thermo Fisher Scientific #C601003, Waltham, MA) cells were then induced with a final concentration of either 0.5% arabinose of 1 mM IPTG for 4 hours. The cells were collected by centrifugation and the supernatant aspirated. The cells were resuspended in total of 10 mL TGI+PI buffer (20 mM Tris-HCl pH 7.5, 10% glycerol, 20 mM imidazole with protease inhibitors) and stored overnight in -20℃. The inductions were then thawed and sonicated using a probe sonicator (Amplitude 60, 10 sec on, 45 sec off, 5 mins) on ice. Cellular debris was removed by centrifugation (18,000 x g, 4℃, for 30 min). The supernatant was treated with DNaseI for 20 min on ice. It was then filtered through 0.22 µm syringe filter. The FPLC Ni-NTA column was washed with 5 column volumes (CV) of TGI Buffer with 250 mM NaCl. The clarified lysate was loaded onto the column. The column was washed with 10 CV of TGI Buffer with 250 mM NaCl. The protein was then eluted in three steps with a combination of TGI and TGI with 250 mM salt and 550 mM imidazole (TGI+) buffer: 1) 95% TGI, 5% TGI+, 2) 62% TGI, 38% TGI+, 3) 100% TGI+. Those containing purified protein were pooled. Samples were concentrated using an Amicon Ultra centrifugal concentrator (Millipore Sigma, St. Louis, MO) with a 3 kDa cutoff and applied to a gel filtration column (GE Healthcare HiPrep™ 26/60 Sephacryl™ S-200 HR Cat #1701195-01), previously washed with 0.5 column volumes of distilled water at 1.3 mL /min, then 2 column volumes of TBS at 2.6 mL/min. The column was eluted into 100 fractions. Fractions with a 260 nm peak were analyzed by SDS-PAGE and Coomassie blue staining. Samples with the

purest protein were again pooled, concentrated, and buffer exchanged (TGI with KCl and protease inhibitors) using an Amicon Ultra centrifugal concentrator (Millipore Sigma, St. Louis, MO) with a 3 kDa cutoff.

3.3.4 Design of 3xFlag-PP7 cap protein and PP7 aptamer tagged reporter constructs

The 3xFlag tagged PP7 cap protein (3xFlag-PP7cp) was designed with a 3xFlag tag motif followed by an enterokinase cleavage site with an additional human rhinovirus (hRV) 3C protease cleavage site allowing for optional protease cleavage elution during RNA affinity immunoprecipitation. This was followed by the *Pseudomonas aeroginosa* bacteriophage 7 coat protein (PP7cp)[27] amino acid sequence. The construct was cloned using Rosetta Blue cells into the pBAD arabinose-inducible vector using the NcoI and XhoI sites, which add a 6x histidine tag for purification of the 3xFlag-PP7cp protein, to generate the pBAD-3xFlag-ppSite-PP7cp-6xHis construct. Clones were selected and confirmed by Sanger sequencing (Genewiz, South Plainfield, NJ). The selected clone was then induced with a final concentration of 0.5% arabinose to express the 3xFlag-ppSite-PP7cp-6xHis protein and fractions isolated as above. Fractions were examined by SDS-PAGE and Coomassie blue staining. The sample was then analyzed by western blot.

The mRNA reporter constructs were generated by adapting previously used mCherry-GFP–expressing plasmids[28] to have tandem 3’ UTR PP7 and tobramycin aptamers separated between and on each side by non-structure forming CAA repeats to prevent aptamer collapse. Then,

upon confirmation by Sanger sequencing (Genewiz, South Plainfield, NJ), then twelve lysines encoded by the AAA codon ($K12_{AAA}$) or AAG codon ($K12_{AAG}$) and the previously used stem loop (StL) construct were cloned into the vector between the 2xHA tag and the mCherry protein. Upon confirmation by Sanger sequencing (Genewiz, South Plainfield, NJ), these constructs were then transfected into *P. falciparum* Dd2 parasites and selected for the WR drug resistance marker. Confirmation of plasmid was done by PCR and SDS-PAGE.

3.3.5 Design of MBP-MS2 cap protein and MS2 aptamer tagged ribosomal RNAs

The pMAL-MBP-zz-MS2cp-6xHis protein was generously provided by the Zaher Lab (Washington University, St. Louis, MO). The plasmid was cloned into BL21 cells. The selected clone was grown over night and induced with a final concentration of 1 mM IPTG to express the pMAL-MBP-zz-MS2cp-6xHis protein and fractions isolated as above. Fractions then examined by SDS-PAGE and Coomassie blue staining. The sample was then analyzed by western blot.

The 18S A- and S-type rRNAs were generated by PCR from *P. falciparum* Dd2 cDNA and cloned into the Zero Blunt™ PCR cloning vector with an N-terminal XhoI site and a C-terminal NotI site. The clones were verified by Sanger sequencing (Genewiz, South Plainfield, NJ). A PmeI restriction site was then introduced into the spur region near the 5' end of the gene between two nucleotides (A-type: A_{75}/T_{81}, S-type: G_{75}/T_{76}) by PCR mutagenesis and Sanger sequence verified. The MS2 aptamer was then introduced into the region, using the PmeI site to linearize the vector, flanked by two NheI sites using In-Fusion® recombination cloning (Takara #638910). The constructs were again Sanger sequence verified. These constructs were then cloned into

the EOE vector previously used with the XhoI and NotI sites[28]. The constructs were then introduced into *P. falciparum* Dd2 by transfections as described above and selected with WR.

3.3.6 Pre-RIP Sample Preparation

Parasite cultures may be prepared in a variety of ways depending on the RNA species to be examined as well as the aspect of the parasite life cycle. Here, parasites were grown asynchronously to a 7-10% parasitemia, with stage emphasis on the increased translation that occurs during late stage trophozoites, in at least 1 mL of packed RBCs. The parasites as centrifugated at 500 x g for 5 minutes and the growth media is aspirated from the culture and replaced with MCM containing 200 µM cyclohexamide (CHX), which is optional, and incubated for 10 minutes at 37℃. The parasites are centrifuged as above and the MCM+CHX aspirated. The culture is washed three times with 1X PBS with 200 µM CHX. The parasites are then left on ice until ready for use. At this point, the parasites may be exposed of UV radiation to crosslink proteins and RNA. This is done by resuspending the parasites in 5 mL ice-cold with 1X PBS with 200 µM CHX and placing them in a petri dish. The parasites are then placed in a UV-crosslinking with the lids off and exposed to 400 mJ/cm^2 three times for a total of 1200 mJ/cm^2 with a one-minute rest on ice, lid closed, while shaking to resuspend the culture between each exposure as done previously[16]. However, crosslinking was seen to increase background, potentially increases nonspecific interactions, and was not done for the data shown here. The parasites are then lysed with saponin lysis buffer as above with 200 µM CHX and 15 mM $MgCl_2$ can be added to increase 80S stability. Once the parasite pellet is cleared of hemoglobin, it is ready for parasite lysis. At this point, the parasite pellet may be store at -80℃ or lysed by resuspension

in, here 200 µL, of RIP lysis buffer (50 mM Tris-HCl pH 7.8, 150 mM NaCl, 10% Glycerol, 1% NP40, 15 mM MgOAc, 1X complete protease inhibitors (EDTA-Free), add fresh: 200 µM cyclohexamide, 1 mM DTT, 1 mM AEBSF, 40 U/mL RNAse Inhibitor) and rotated for 10 minutes at 4℃. The lysate may also be flash-frozen in liquid nitrogen and stored at -80℃.

Lastly, prior to loading onto the beads, the total protein was measured using the Bio-Rad DC protein assays. Briefly, a standard curve of biotechnology grade BSA (Amresco #0903-5g) in RIP lysis buffer was made from a 10 mg/mL stock at concentrations 0.0 µg/µL, 0.25 µg/µL, 0.5 µg/µL, 1.0 µg/µL,1.5 µg/µL, 5.0 µg/µL, 10.0 µg/µL. The sample lysate was diluted 1:5 in RIP lysis buffer and 20 µL of the diluted sample lysate or the standard was used with 100 µL of A' reagent (20 µL reagent S for each 1 mL reagent A) and 800 µL reagent B. The sample was vortexed and incubated for 15 minutes. A NanoDrop 2000c (Thermo Fisher Scientific, Waltham, MA) was used with disposable cuvettes (BRAND #759075D) blanked with RIP lysis buffer. The standard curve was read ($R^2 \geq 0.9$). The sample protein concentrations were evaluated. A total of 200 µg was used for each sample. Alternatively, total RNA could be measured and used as a means for equal loading, which requires equipment capable of accurately measuring RNA in a mixed species sample.

3.3.7 Immunoprecipitation of PP7 aptamer tagged reporter constructs - mRIP

Prior to thawing samples, prepare the protein G magnetic beads as follows. As a single batch using 12.5 µL of beads volume per sample, wash the beads with 4X total volume (bead slurry is 50% beads) with 1X PBS + 0.1% Tween 20 by inversion for 1 min, collect beads using magnet and discard supernatant. Resuspend the beads in α-Flag (mAb 1 µg/µL stock) + ice cold 1X PBS +

0.1% Tween 20 using the same volume as above for the was with 5 µg of antibody per 12.5 µL of beads (Life Technologies, #10007D, binding capacity: 8 µg Hs IgG/mg beads). Incubate 30 mins at 4℃ while shaking at 1350 RPM. Use the magnet to remove antibody binding solution. Using the same volume, wash 3x with ice cold of 1X PBS + 0.1% Tween 20, vortexing for 10 s each and discarding the wash supernatant using the magnet. Next, bind the PP7cp to the protein G::α-Flag complexed beads and block. Use 10 µg of PP7cp in in 100 µL RIP Lysis Buffer with DTT/AEBSF but without CHX/RNase Inhibitor per sample. Bind for one hour at 4℃ while shaking at 1350 RPM. Remove supernatant using magnet and wash 3x with 500 µL Low-Salt RIP wash buffer (50 mM Tris-HCl pH 7.8, 150 mM NaCl, 10% Glycerol, 0.1% Tween 20, 15 mM MgOAc, add fresh: 1 mM DTT, 0.1 mM AEBSF, 200 µM cyclohexamide, if desired). Block with 500 µL PP7 blocking buffer (RIP lysis buffer + 0.5 µg/µL of *S. cerevisiae* tRNAs (Invitrogen #AM7119 10 mg/mL stock) + 5% BSA) for one hour at 4℃ while shaking at 1350 RPM. Remove blocking buffer using magnet and wash 3x with 500 µL Low-Salt RIP wash buffer. Store in 100 µL/sample complete RIP Lysis Buffer (w/200 µM cyclohexamide, 1 mM DTT, 1 mM AEBSF, 40 U/mL RNase inhibitor) on ice until ready to be aliquoted into samples. Using 200 µg total protein for each sample in 100 µL RIP lysis buffer, combine with 100 µL blocked protein G::α-Flag::PP7cp complexed beads in RIP lysis buffer. Bind 1 hour at 4℃ while shaking at 1350 RPM. Using magnet, transfer flow-through into a new, labeled microcentrifuge. Wash beads four times with 500 µL of Low Salt RIP wash buffer, vortex 10s, using magnet remove and discard rinses. For increased stringency, wash beads with two to four times with High Salt RIP wash buffer (Low Salt RIP wash buffer with 500 mM NaCl). Elution may be carried out in a number of

ways depending on subsequent applications. To elute by hRV 3C protease (GenScript # Z03092), use 1 µL of hRV 3C protease in 35 µL Low Salt RNA-IP Wash Buffer + 1 mM AEBSF + 40 U/mL RNase inhibitor and incubate overnight at 4℃ shaking at 1350 RPM. Remove and save o/n hRV 3C protease eluate using the magnet. Again, use 1 µL of hRV 3C protease in 35 µL Low Salt RNA-IP Wash Buffer + 1 mM AEBSF + 40 U/mL RNase Inhibitor and incubate 2 hours at 4℃ shaking at 1350 RPM. Remove using the magnet and combine with previous hRV 3C protease eluate. Finally, 35 µL Low Salt RNA-IP Wash Buffer + 1 mM AEBSF + 40 U/mL RNase inhibitor and incubate 30 mins at 4℃ shaking at 1350 RPM. Remove using the magnet and combine with previous hRV 3C protease eluates. This may then be used for downstream processes.

Alternative, the beads may be boiled in sample buffer, but this will increase background. To elute protein for whole eluate sample mass spectrometry, mass spectrometry elution buffer (MSE buffer: 2 M urea, 50 mM Tris-HCl (pH 7.5), 1 mM DTT, 5 µg/mL trypsin) was used. To each sample, 80 µL was added to each tube and incubated for one hour at 25℃ while shaking at 1400 RPM. The beads were washed twice with 60 µL of MSE buffer, using the magnet, and combining with previous eluates (~200 µL final). The samples were then reduced by adding 4 mM DTT and incubating for 30 mins at 25℃ while shaking at 1000 RPM. Samples were subsequently alkylated by adding 10 mM iodoacetamide (500 mM stock) and incubating for 45 mins at 25℃ while shaking at 1000 RPM. Finally, samples were digested by adding 0.5 µg trypsin (0.5 mg/mL stock) and incubating overnight at 25℃ while shaking at 1000 RPM. Samples were store at -80℃ when complete.

3.3.8 Immunoprecipitation of MS2 aptamer tagged reporter constructs - rRIP

Blocking of MS2 is dependent on application. If examining rRNA modifications, tRNA should not be used for blocking as the tRNA modifications will interfere with downstream processing. BSA may also be used, however can obscure downstream protein bands in SYPRO ruby staining. Here, MS2cp and amylose resin were blocked with 5% BSA and 0.5 µg/µL of S. cerevisiae tRNAs for one hour at ambient temperature. To pulldown, use 500 µg of MS2cp in 100 µL RIP buffer per 100 µL amylose resin to be used. Bind at least 100 µg total protein of each sample to MS2cp in total of 200 µL RNAIP blocking buffer overnight at 4℃ while rotating. Wash amylose resin with RIP blocking buffer three times, centrifuge at 2000 x g for 2 mins at 4℃. The samples were then bound to 100 µL packed amylose resin for one hour at 4℃ while rotating. Samples were washed three times in 500 µL RIP wash buffer. Optionally, samples can be divided, treating half with Micrococcal nuclease for one hour at 4℃ while rotating. Again, washed three times in 500 µL RIP lysis buffer. Samples were then eluted for RNA. Samples were eluted using proteinase K and urea, followed by RNA isolation by acid phenol/chloroform isolation[29]. Resin was treated with 200 µL Proteinase K Elution Buffer (160 µL 1.25X Proteinase K Buffer + 5 µL Proteinase K [100 µg, Qiagen stock 20 mg/mL] + 35 µL molecular grade water -> pre-incubate 10 mins at 37℃ to remove RNase. 1.25X Proteinase K Buffer: 125 mM Tris-HCl pH 7.8, 62.5 mM NaCl, 12.5 mM EDTA). Incubate for 20 minutes at 37℃, shaking at 1000 rpm. Then add 200 µL of PK/Urea buffer (100 mM Tris-Cl pH 7.8, 50 mM NaCl, 10 mM EDTA, 7 M Urea). Incubate as above. Alternatively, this can be done by treating sample-bound beads with 500 µL ribozol (VWR N580) and subsequently following the company protocol for RNA isolation. Centrifuge as above and

move supernatant (eluate) to new tube. Add 400 µL acid phenol/chloroform. Vortex and let stand for 5 minutes. Centrifuge at max (16,000 x g) for 15 minutes at 4°C, take aqueous phase. Add one tenth volume 3 M sodium acetate, pH 5.5 and 2.5 volumes 100% ethanol and vortex. If desired, at 10 µL glycogen to help with RNA pellet visualization. Incubate overnight at -80°C. Centrifuge pellet while still frozen at max speed for one hour at 4°C. Remove supernatant. Wash with 70% ethanol. Centrifuge at max speed for 20 minutes at 4°C. Resuspend in nuclease free water.

Note: magnetic beads with α-MBP (Sigma: M6295, 6.5 mg/mL binding capability) may also be used for this protocol, however the amount of MS2cp to be used must be adapted to the binding capability of the antibody.

3.3.9 Immunoblotting

Samples were loaded onto SDS-PAGE gels, running at 15 W, 1h 10 mins. The gels were then transferred to PVDF membrane using semi-dry transfer method running at 25 V for 40 minutes. The PVDF membranes were blocked in 5% milk in PBS + 0.1% Tween 20 (PBST) for 1 hour at room temperature or overnight at 4°C. The membranes were probed with diluted primary antibody (**SUPPLEMENTAL TABLE 3.2**) in PBST with 5% milk. Membranes incubated with HRP-conjugated primaries were incubated similarly, proceeding to imaging instead of secondary. After incubation with the primary antibody, the PVDF membranes were washed three times for 5 min in PBST. Membranes incubated with HRP-conjugated primaries were incubated and washed similarly, washing with PBS, and then proceeding to imaging instead of secondary. The membranes were then incubated with HRP-conjugated secondary antibody diluted 1:2500 in

PBST with 5% milk for 1 hour at room temperature. The membranes were washed as above. Then rinsed with PBS. Prepare Working Solution by mixing equal parts of the Stable Peroxide Solution and the Luminol/Enhancer Solution (34577 Supersignal West Pico Plus and 34096 Supersignal West Femto Maximum Sensitivity Substrate, respectively). We incubate the blot in Working Solution for 5 minutes. Remove the blot from Working Solution and drain excess reagent. Afterward we took images were generated by BioRad Molecular Imager ChemiDoc XRS System with Image Lab software.

3.3.10 Protein analysis by SYPRO ruby staining

Samples from immunoprecipitations were loaded onto SDS-PAGE gels, running at 15 W, 1h 10 mins. Gels were then stained with SYPRO Ruby stain (BioRAD #1703125) over night at ambient temperature while shaking. Gels were then rinsed in SYPRO Ruby destain (7% acetic acid, 10% methanol) twice and destained for one hour. Finally, gels were washed and stored with MilliQ water to remove destain reagent. The gel was then imaged using a BioRad Molecular Imager ChemiDoc XRS System with Image Lab software.

3.3.11 Protein analysis by mass spectrometry

Mass spectrometry analysis of PP7-mRIP samples was performed in a variety of ways, involving both whole eluate sample analysis as well as band or lane analysis subsequent to SYPRO Ruby staining. To analyze entire sample eluates, samples were eluted as above for whole eluate sample analysis. Samples were sent to the Jovanovic Lab at Columbia university for mass spectrometry analysis. Samples that were analyzed after SDS-PAGE separation and SYPRO Ruby

staining were excised from the gel and sent to the Donald Danforth Plant Science Center - Proteomics and Mass Spectrometry core.

3.3.12 Generation of 18S/16S rRNA Evolutionary Dendrograms

The 18S rRNA sequences were collected from EuPathDB[19], *Saccharomyces* Genome Database[20], and EcoCyc *E. coli* Database[21]. Sequences were then read into RStudio, a guided tree generated, and a multiple sequence alignment performed using the Bioconductor Biostrings package[30]. The RNA MSAs were adjusted, staggered, and a distance matrix was calculated using the Bioconductor DECIPHER package[31]. The distance matric was used to generate a hierarchical cluster, which was then used to make a phylogenetic tree. The ggplot2[32] and ggtree[33,34] packages were used to draw the dendrogram.

3.3.13 rRNA enrichment analysis by RT-PCR

RNA isolated from MS2-rRIP was measured and DNase I treated using the TURBO™ DNase kit (Invitrogen #AM2238) and, using the NanoDrop 2000c, 100-250 ng of total RNA was used to generate cDNA using the SuperScript™ IV VILO™ Master Mix kit (item# 11756050 Life Technologies Corporation) for each sample including no reverse transcriptase and no template controls following the manufacturer's protocol. The iQ SYBR Green Supermix (item# 1708886, Bio-Rad) protocol was used for qRT-PCR on the CFX96 Real-Time system with Bio-Rad CFX Manager 3.0 software[35]. To determine the fold enrichment of tagged ribosomes vs untagged ribosomes, the C_t values of the MS2-tagged ribosomes were normalized to untagged A-type ribosomes within the flow-through and elution samples. The fold enrichment was then calculated by normalizing the elution sample C_t values to those of flow-through. The final

enrichment was then calculated by raising two to the inverse of this difference. This results in the following set of calculations:

$$\Delta Ct_{(Flow\ Through)} = Ct_{MS2}^{FT} - Ct_{Awt}^{FT} \qquad \text{Equation 3.0}$$

$$\Delta Ct_{(Elution)} = Ct_{MS2}^{Elu} - Ct_{Awt}^{Elu} \qquad \text{Equation 3.1}$$

$$\Delta\Delta Ct = \Delta Ct_{(Elution)} - \Delta Ct_{(Flow\ Through)} \qquad \text{Equation 3.2}$$

$$Fold\ Enrichment = 2^{-\Delta\Delta Ct} \qquad \text{Equation 3.3}$$

3.4 Results

3.4.1 General description of PP7-mRIP

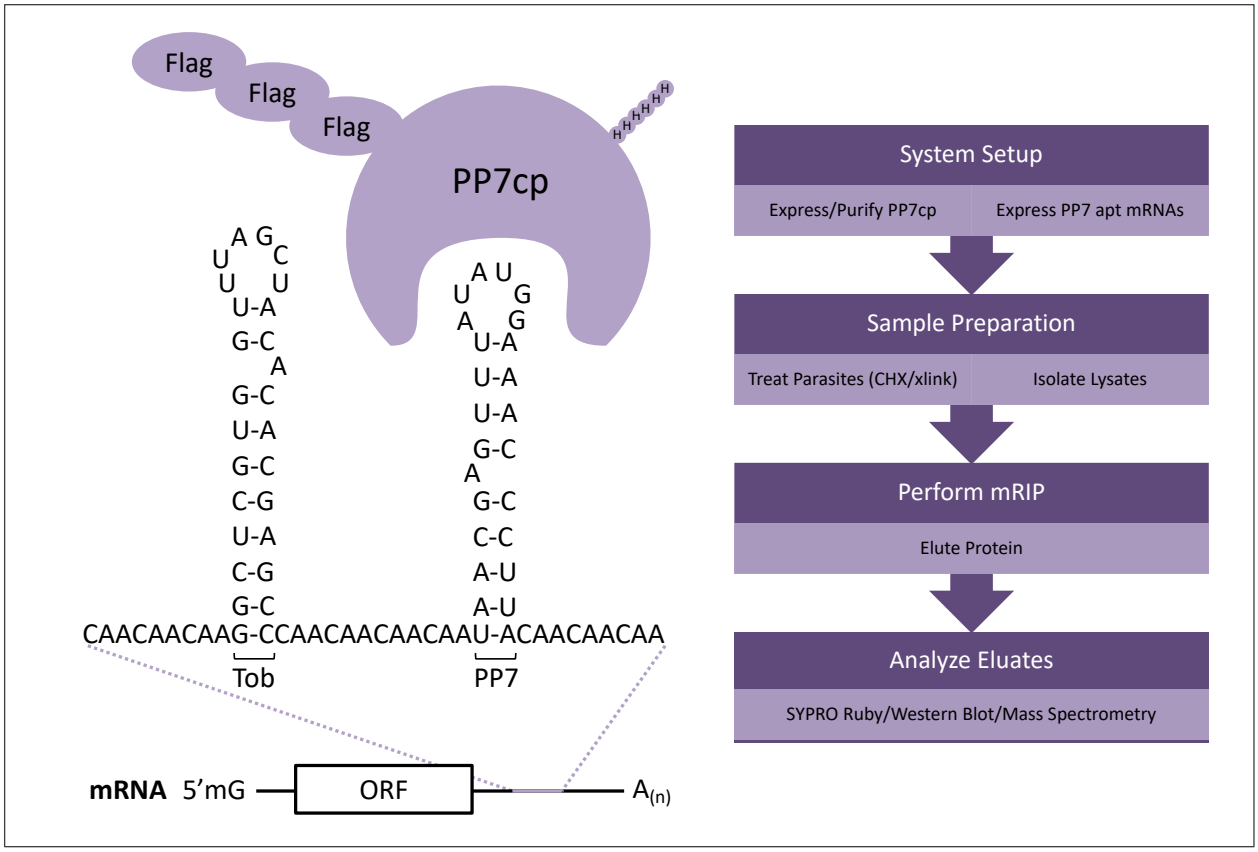

FIGURE 3.2 | Design of PP7-mRIP System and Workflow. The PP7cp is expressed in bacteria and purified while the PP7 aptamer tag is inserted into the mRNA of choice. Parasites can be treated with CHX to halt translation and the proteins cross-linked (xlinked) to the mRNA to if desired. Parasites are freed from RBCs by saponin lysis (SEE MATERIALS AND METHODS). The immunoprecipitation is then performed. Analysis of eluates can be performed by the desired method.

While RNA aptamers have been used to control gene expression[36,37], such an mRIP system has not been used before in *P. falciparum*. The PP7 system components have been previously demonstrated in mammalian cells to pull down on noncoding RNAs (ncRNAs) and mRNAs in search of RBPs[38,39]. Here, the PP7cp has been N-terminally tagged with a 3xFlag tag that is

followed by both an enterokinase and hRV 3C protease cleavage site followed by a C-terminal 6x His tag for purification (**FIGURE 3.2**). The 3xFlag-PP7cp-6xHis protein was expressed and purified as mentioned previously. The 3' UTRs of reporter mRNA constructs were tagged with a single PP7 aptamer surrounded by the non-structure forming CAA repeats to prevent aptamer collapse. Although dependent upon the protein and RNA variant, PP7cp binds the PP7 aptamer with relatively high affinity ($k_d \cong 10^{-9}$ M)[40]. As with previous work, this allows for the use of a single aptamer; while the tobramycin aptamer was included should a subsequent affinity purification step be desired[39].

An mRNA of interest is expressed using the EOE vector with and without the PP7 aptamer in *P. falciparum* (**FIGURE 3.2**). Once selection is complete, a parasite lysate is generated as described above using the desired conditions. A Flag monoclonal antibody (mAb) is bound to protein G magnetic beads (α-Flag magnetic beads may be substituted). The Flag-tagged PP7cp is then bound the α-Flag::Protein G magnetic bead complex and blocked with bovine serum albumin and yeast tRNAs to reduce non-specific protein and RNA interactions. The PP7cp::α-Flag::Protein G magnetic bead complex is then incubated with the parasite lysate. The washed beads can then be eluted in a variety of ways depending on subsequent assays. The hRV 3C protease cleavage site will release the expressed mRNA and its bound proteome from the bead complex and any contaminating proteins or RNAs. The hRV 3C protease is also tagged with a 6x His tag allowing for its removal if desired. Thus, this is the suggested method of elution. The protein can then be analyzed by the desired method (SDS-PAGE with total protein

staining or western blot, mass spectrometry, etc.). RNA may also be analyzed should the circumstances require.

3.4.2 PP7-mRIP produces transcript-selective protein profiles

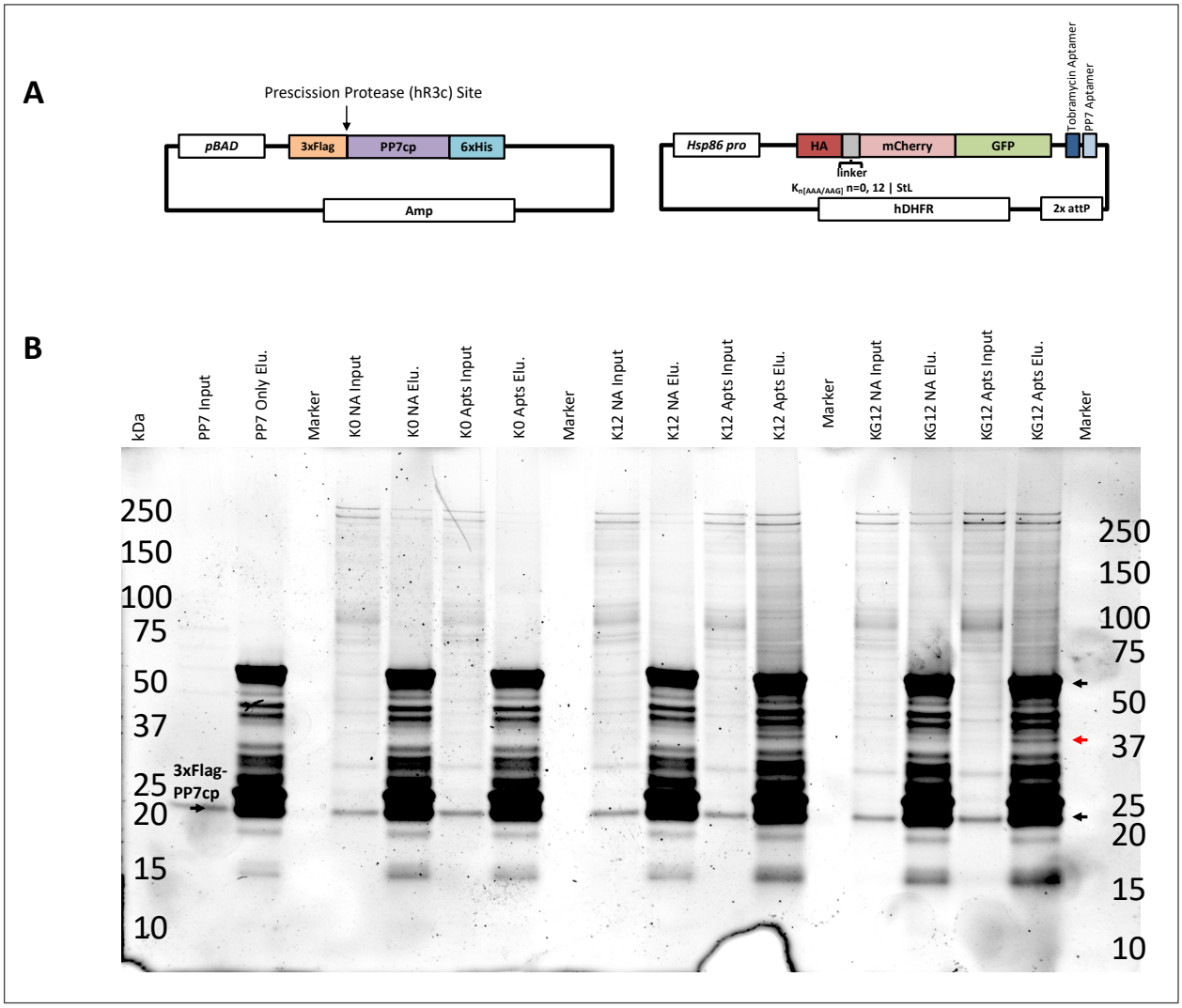

FIGURE 3.3 | PP7-mRIP System Plasmids and SYPRO Ruby Analysis of Eluates. (A) Plasmids used to express PP7cp (left) and the mRNA reporter constructs with PP7 aptamers (right). **(B)** SYPRO Ruby analysis of PP7-mRIP eluates eluted using sample buffer. Red arrow indicates an example of differential banding pattern. Black arrows represent IgG heavy and light chain. PP7cp also indicated by black arrow.

Eluates from the PP7-mRIP assay were analyzed by SDS-PAGE/SYPRO Ruby staining, mass spectrometry, or a combination thereof. Samples were also analyzed by RT-qPCR showing that the tagged mRNAs are more efficiently enriched than untagged mRNAs (**SUPPLEMENTAL FIGURE 3.1**). Visualization of PP7-mRIP pulldowns show transcript-dependent protein profiles (**FIGURE 3.3**). However, the elements used in the PP7-mRIP assay appear to dramatically increase background (*e.g.* magnetic beads), but also have the potential to mask the isolation of proteins that may be in lower abundance (*e.g.* antibody light and heavy chains, PP7cp, etc.), which are seen even with protease elution (**FIGURE 3.4**).

TABLE 3.1 | Mass spectrometry analysis of whole lane PP7-mRIP eluates.

Protein	KG12 Apts - WT Apts	K12 Apts - WT Apts	K12 Apts - KG12 Apts
60S rp L37 (PF3D7_0706400)	-0.29	2.66	2.95
Stevor (PF3D7_0402600)	0.02	2.89	2.86
60S rp L7-3 (PF3D7_1424400)	-0.29	2.24	2.53
60S rp L24 (PF3D7_1309100)	-0.15	2.24	2.40
Hsp110 (PF3D7_1344200)	0.27	2.01	1.74
60S rp L10 (PF3D7_1414300)	-0.58	1.35	1.92
eIF4A (PF3D7_1468700)	0.18	2.10	1.92
Hsp DNAJ homologue Pfj4 (PF3D7_1211400)	0.61	2.52	1.90
PfRACK1 (PF3D7_0826700)	0.17	-0.24	-0.40

To better examine the both specific protein bands as we as the differential complement of proteins between constructs, samples were sent for analysis by mass spectrometry. Initially, a single, prominent band was analyzed in the 37 kDa region (**TABLE 3.1**), which made evident the concerns regarding visible masking of lower abundance proteins those in higher abundance.

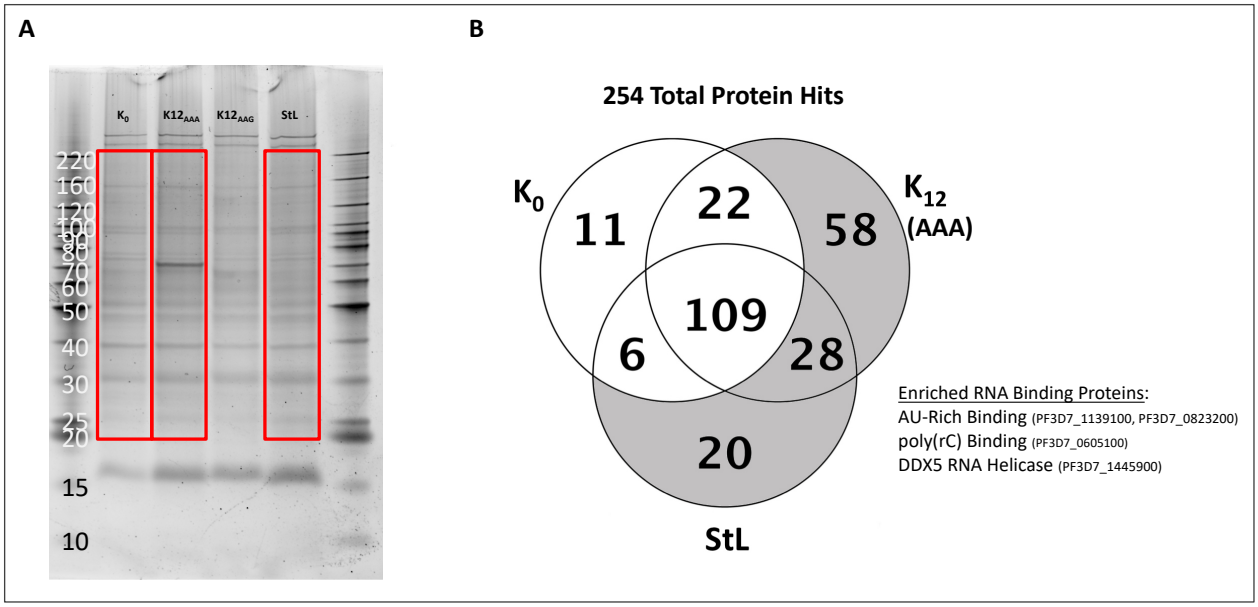

FIGURE 3.4 | Analysis of Whole Lane PP7-mRIP Eluates. (A) Samples were eluted by hRV 3C protease and subsequently ran on tobramycin matrix. Eluates were analyzed by SDS-PAGE followed by SYPRO Ruby staining. While lanes (red boxes) were excised and sent for mass spectrometry. **(B)** Venn diagram of proteins with unique peptides determined by mass spectrometry. A total of 254 hits were found, with a majority found to be shared, as expected, among the samples.

Whole lanes were then sent for analysis, providing a more distinct analysis of the differential mRNA bound proteomes (**FIGURE 3.4**). The proteins shared between the samples were those expected during routine mRNA translation, while those mRNA substrate-specific proteins could be directly linked to their function and known binding motifs (**FIGURE 3.4**). Finally, whole eluates were sent for analysis by mass spectrometry, revealing even more mRNA-specific RBPs (**TABLE 3.2**). Thus, despite high background during analysis by visualization, the PP7-mRIP assay is able to probe the RBP population for mRNA substrate-specific proteins.

TABLE 3.2 | Mass spectrometry analysis showing normalized unique peptide counts of whole PP7-mRIP eluates.

Protein	MW (kDa)	TobPelletWT	TobPelletK12	TobPelletStL
60S ribosomal protein L7, putative (PF3D7_0307200)	31		1	
40S ribosomal protein S11 (PF3D7_0516200)	16	4	5	4

60S ribosomal protein L12, putative (PF3D7_0517000)	18	3	5	4
40S ribosomal protein S9, putative (PF3D7_0520000)	22		2	
40S ribosomal protein S16, putative (PF3D7_0813900)	16		1	
40S ribosomal protein S2 (PF3D7_1026800)	30	5	7	6
40S ribosomal protein S4, putative (PF3D7_1105400)	30	3	2	2
60S ribosomal protein P0 (PF3D7_1130200)	35	11	12	9
60S ribosomal protein L6, putative (PF3D7_1323100)	22	1	1	
60S ribosomal protein L18, putative (PF3D7_1341200)	22	3	2	2
60S ribosomal protein L5, putative (PF3D7_1424100)	34	2	6	2
60S ribosomal protein L7-3, putative (PF3D7_1424400)	33	2	1	1
40S ribosomal protein S5 (PF3D7_1447000)	30		2	1
60S ribosomal protein L27 (PF3D7_1460700)	17	2	2	2
40S ribosomal protein S3 (PF3D7_1465900)	25	10	9	8
40S ribosomal protein S8e, putative (PF3D7_1408600)	25	2	5	
60S ribosomal protein L4 (PF3D7_0507100)	46	2	2	
60S ribosomal protein L14, putative (PF3D7_1431700)	19	2	3	
40S ribosomal protein S19 (PF3D7_0422400)	20	2	5	
40S ribosomal protein S3A, putative (PF3D7_0322900)	30	2		
60S ribosomal protein L24, putative (PF3D7_1309100)	19	1		
ATP-dependent RNA helicase UAP56 (PF3D7_0209800)	52	7	7	4
peptide chain release factor subunit 1, putative (PF3D7_0212300)	48			3
RNA-binding protein, putative (PF3D7_0605100)	86			1
erythrocyte membrane-associated antigen (PF3D7_0703500)	265			1
Obg-like ATPase 1, putative (PF3D7_0722400)	45	2	2	3
ATP-dependent RNA helicase DBP1, putative (PF3D7_0810600)	109	2	3	2
RNA-binding protein, putative (PF3D7_0823200)	32		1	
single-strand telomeric DNA-binding protein GBP2, putative (PF3D7_1006800)	30	5	6	4
PRE-binding protein (PF3D7_1011800)	132	2	7	8
conserved Apicomplexan protein, unknown function (PF3D7_1105800)	31		1	
nucleic acid binding protein, putative (PF3D7_1132300)	32	2	2	1
tudor staphylococcal nuclease (PF3D7_1136300)	129		2	3
RNA-binding protein, putative (PfDd2_110042100)	210		1	
polyadenylate-binding protein 1, putative (PF3D7_1224300)	97	2	5	3
DNA/RNA-binding protein Alba 2 (PF3D7_1346300)	25		3	1
DNA/RNA-binding protein Alba 4 (PF3D7_1347500)	42	5	6	4
rRNA 2'-O-methyltransferase fibrillarin, putative (PF3D7_1407100)	35	3	1	1
CUGBP Elav-like family member 2, putative (PF3D7_1409800)	59	1		

tRNA import protein tRIP (PF3D7_1442300)	46		2	2
ATP-dependent RNA helicase DDX5, putative (PF3D7_1445900)	60		4	4
MA3 domain-containing protein, putative (PF3D7_1457300)	76	1	2	
eukaryotic translation initiation factor 4E (PF3D7_0315100)	27	1	3	
eukaryotic initiation factor 4A-III, putative (PF3D7_0422700)	45		1	
eukaryotic translation initiation factor 3 subunit B, putative (PF3D7_0517700)	84		3	3
eukaryotic translation initiation factor 3 subunit E, putative (PF3D7_0528200)	61		2	4
translation initiation factor IF-2, putative (PF3D7_0607000)	112		1	
eukaryotic translation initiation factor 3 subunit L, putative (PF3D7_0612100)	78		2	
eukaryotic translation initiation factor 3 subunit I, putative (PF3D7_0716800)	37		3	
eukaryotic translation initiation factor 2 subunit alpha (PF3D7_0728000)	38	1		1
elongation factor 1-beta (PF3D7_0913200)	32	7	6	4
eukaryotic translation initiation factor 2 subunit beta (PF3D7_1010600)	25		1	
translation elongation factor EF-1, subunit alpha, putative (PF3D7_1123400)	63			1
eukaryotic translation initiation factor 3 subunit C, putative (PF3D7_1206200)	116	4	5	4
eukaryotic translation initiation factor 3 subunit A, putative (PF3D7_1212700)	166		1	1
elongation factor 1-gamma, putative (PF3D7_1338300)	48	3	5	5
elongation factor 1-alpha (PF3D7_1357000)	49	71	71	70
eukaryotic translation initiation factor 2 subunit gamma, putative (PF3D7_1410600)	51	3	2	1
elongation factor 2 (PF3D7_1451100)	94	13	17	21
eukaryotic initiation factor 4A (PF3D7_1468700)	45	21	24	19

Ribosomal proteins in blue.
RNA binding proteins in grey.
Translation factors in orange.

3.4.3 General description of MS2-rRIP

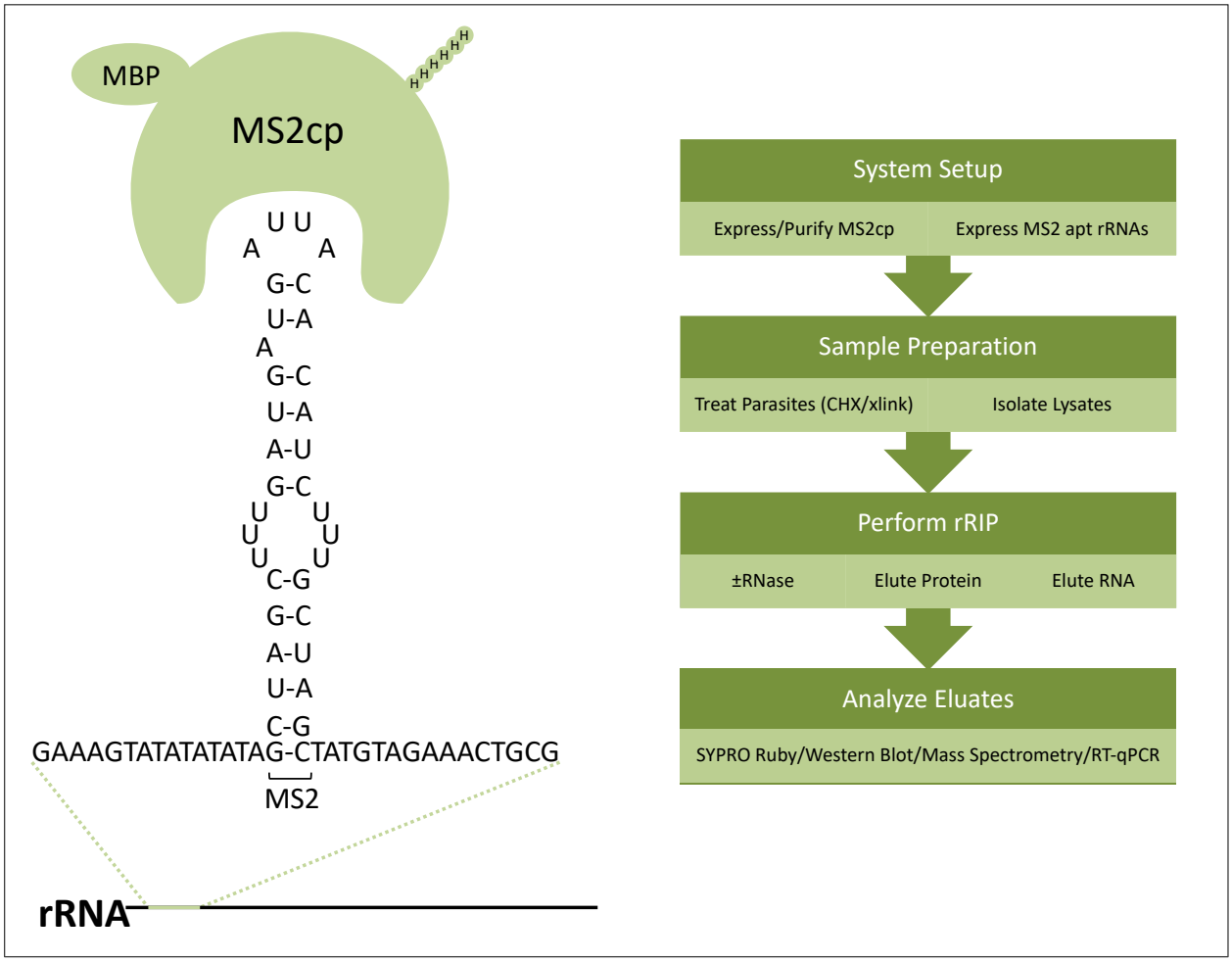

FIGURE 3.5 | Design of MS2-rRIP System and Workflow. The MS2cp is expressed and purified while the MS2 aptamer tag is inserted into the rRNA of choice. Parasites can be treated with CHX to halt translation, the proteins cross-linked (xlinked) to the rRNA, or the polysomes separated into monosomes by RNase treatment to if desired. Parasites are freed from RBCs by saponin lysis (SEE MATERIALS AND METHODS). The immunoprecipitation is then performed. Analysis of eluates can be performed by the desired method.

The MS2 system has been used previously for the affinity purification of ribosomes with a single aptamer placed in a 'spur' of either rRNA subunit[41]. The dissociation constant of the MS2 system can vary depending on the cap protein and aptamer sequence variants that are used.

However, the range of dissociation constant values are generally high with the $K_d \cong 10^{-9}$ M[40]. The use of an RNA aptamer precludes the need for ribosomal proteins[42] that may be heterogeneous in organisms with multiple, distinct ribosomal RNAs such as *P. falciparum*, necessitating the tagging of the core component of the ribosome: its RNA. To compound this issue, whatever the selected complement of ribosomal proteins on the different ribosomes of *P. falciparum*, there is only a single, complete repertoire of ribosomal proteins in the parasite genome[2]. Thus, tagging of a single ribosomal protein will allow for the differential purification of ribosome types from *P. falciparum*.

The maltose binding protein (MBP) N-terminally tagged MS2cp was generously supplied by the Zaher Lab (Washington University, St. Louis, MO) on the IPTG-inducibal pMAL plasmid (NEB) with a 6x His C-terminal tag. The MBP-MS2cp-6xHis protein was expressed and purified as described previously. A single MS2 aptamer sequence was inserted into a spur near the 5' end of the A- and S-type 18S genes. The constructs were then transfected into the parasite and selected with WR (**FIGURE 3.5**). Parasite lysates are then generated using the desired, downstream driven conditions previously described. Lysates are then bound to either a blocked amylose matrix or magnetic beads displaying an α-MBP mAb. The washed beads are then eluted for protein or RNA and utilized in downstream applications (RNA or protein gels, mass spectrometry, qPCR, etc).

3.4.4 MS2-rRIP enriches aptamer tagged rRNAs.

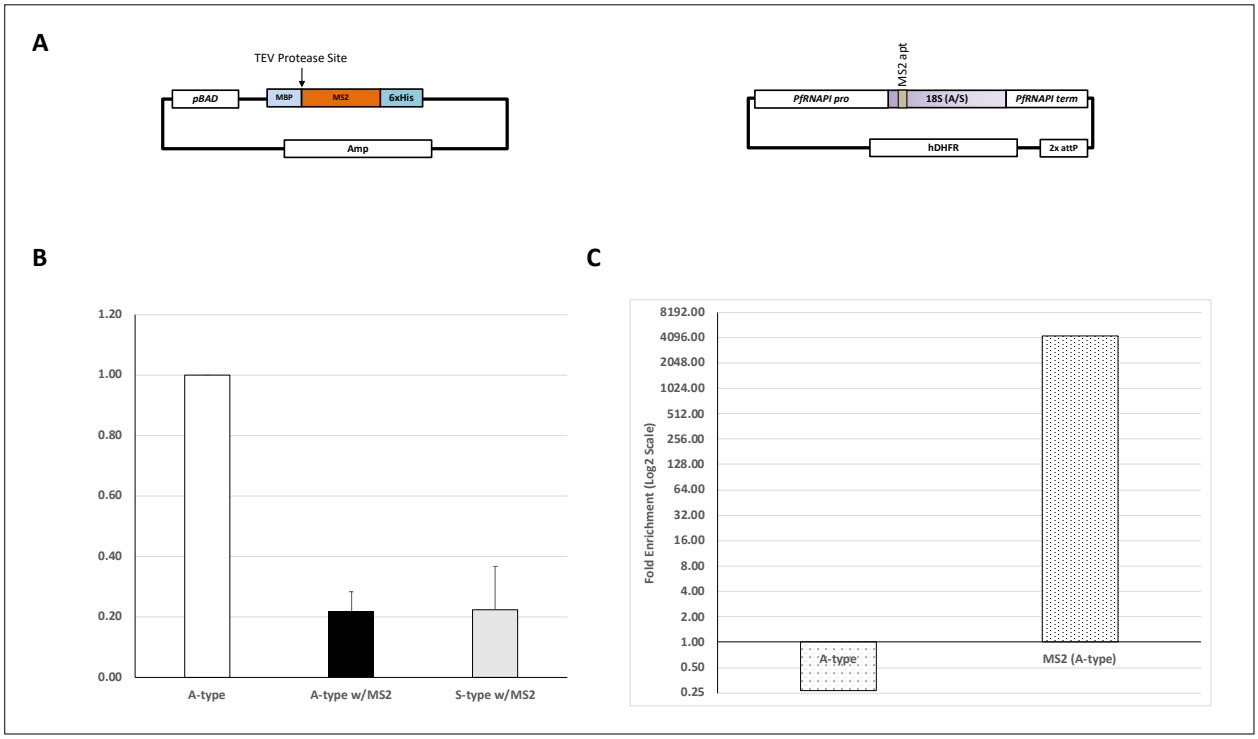

FIGURE 3.6 | MS2-rRIP System Plasmids and RT-qPCR Analysis of Eluates. (A) Plasmids used to express MS2cp in bacteria (left) and the MS2-tagged 18S rRNA expression constructs (right). **(B)** RT-qPCR analysis of plasmid-expressed MS2-tagged A-type and S-type 18S rRNAs vs. untagged endogenous A-type rRNA **(C)** RT-qPCR analysis of MS2-rRIP eluates using MS2-tagged A-type and endogenous A-type specific primers.

Samples from MS2-rRIP were eluted using proteinase K, the RNA isolated, cDNA generated, and qPCR was performed. The MS2-rRIP qPCR data shows an approximate 10 cycle increase in untagged A-type ribosomes, a 2^{10} decrease in RNA, and a 3 cycle decrease in MS2-tagged A-type ribosomes, a 2^{3} increase in RNA, from flow-through to elution. The fold enrichment was calculated as described above, showing >4000-fold increase in MS2-tagged ribosomes (**FIGURE 3.6C**). Additionally, SYPRO Ruby staining was also performed but showed background issues with visualization much like the PP7-mRIP assay (Supplemental **FIGURE 3.2**). Regardless,

ribosome enrichment by the MS2-rRIP assay could therefore provide many insights into ribosome interactions in *P. falciparum*.

3.5 Discussion

Many questions surrounding protein synthesis of the AU-rich transcriptome using multiple, distinct ribosome in *P. falciparum* still remain. However, the means to address these questions have not been previously available. Here, using two aptamer-based systems, also capable of being used in combination[43], were ported into *P. falciparum*. The PP7-mRIP assay is able to generate differential mRNA proteome profiles, which are substrate driven, and the constituents of each profile identifiable by mass spectrometry (**FIGURES 3.3–3.4 AND TABLES 3.1–3.2**). The PP7-mRIP assay provides a means of examining mRNA specific RBPs, RQC machinery recruitment and gene discovery, and many other post-transcriptional elements of gene expression in *P. falciparum*. The significant enrichment tagged versus untagged ribosomes demonstrated by the MS2-rRIP assay (**FIGURE 3.6C**) allows the study of ribosome type switching, 80S subunit composition, ribosomal protein repertoire selection, preferential mRNA translation, NRD pathway characterization, and more.

While these systems enable the study of several post-transcriptional gene expression and regulation questions previously out of reach, they are not without their limitations. However, there are many modifications that would help to overcome or reduce them. A main issue is the background and non-specific binding even with blocking generated by the system components (*e.g.* magnetic beads, antibodies, etc.). To overcome this, pre-incubation of lysates with beads, beads alone, or beads and mABs would help to deplete non-specific interacting proteins and/or

RNAs. Co-expression of the aptamer binding proteins in the parasite could also improve specificity, although using inducible methods would be recommended as *in vivo* binding may affect the function and stability of the RNA substrate. The use of higher-affinity aptamer sequences, such as those generated using the SELEX system[44], could also reduce background and improve efficiency. The use of tandem RIP tags (*e.g.* tobramycin aptamer) and protocol can also improve specificity but may also result in loss of some RBPs given the change in experimental conditions. Lastly, rRNAs are highly expressed and long-lived. Even with few genes, *P. falciparum* show a high abundance rRNAs, the means of which is also of experimental import. This can affect the enrichment of tagged ribosomes and result in contamination of samples with untagged ribosomes. Although previous work has shown that rRNA sequence drives its localization to the nucleolar region in *P. falciparum*[45], expression may be increased by modifying plasmids to have the RNAPI promoter and terminator. However, these are unknown in the parasite and lengthy promoter regions may be necessary short regions (≤1000 bp) did not improve expression over the RNAPII promoter.

The development and adaptation of PP7-mRIP and MS2-rRIP allow for the direct examination of mRNA-bound proteomes and distinct ribosome types, respectively, in *P. falciparum*. These systems could also be used in the mosquito vector, as well as ported into other *Plasmodium* species. Thus, PP7-mRIP and MS2-rRIP could prove instrumental in answering many of the long-lingering questions surrounding post-transcriptional gene regulation and ribosome switching in malaria parasites.

3.6 References

1. Pavlovic Djuranovic, S., Erath, J., Andrews, R. J., Bayguinov, P. O. & Joyce, J. Plasmodium falciparum translational machinery condones polyadenosine repeats. *Elife* **9**, e57799 (2020).
2. Erath, J., Djuranovic, S. & Djuranovic, S. P. Adaptation of Translational Machinery in Malaria Parasites to Accommodate Translation of Poly-Adenosine Stretches Throughout Its Life Cycle. *Front. Microbiol.* **10**, 2823 (2019).
3. Szafranski, K., Lehmann, R., Parra, G., Guigo, R. & Glockner, G. Gene Organization Features in A/T-Rich Organisms. *J. Mol. Evol.* **60**, 90–98 (2005).
4. Glockner, G. Large Scale Sequencing and Analysis of AT Rich Eukaryote Genomes. *Curr. Genomics* **1**, 289–299 (2000).
5. Vembar, S. S. *et al.* Complete telomere-to-telomere de novo assembly of the Plasmodium falciparum genome through long-read (>11 kb), single molecule, real-time sequencing. *DNA Res.* **23**, 339–351 (2016).
6. Gardner, M. J. *et al.* Genome sequence of the human malaria parasite Plasmodium falciparum. *NatureNature* **419**, (2002).
7. Rogers, M. J. *et al.* Structural features of the large subunit rRNA expressed in Plasmodium falciparum sporozoites that distinguish it from the asexually expressed subunit rRNA. *RNA* **2**, 134–45 (1996).
8. McCutchan, T. F. *et al.* Primary sequences of two small subunit ribosomal RNA genes

from Plasmodium falciparum. *Mol. Biochem. Parasitol.* **28**, 63–68 (1988).

9. McCutchan, T. F., Li, J., McConkey, G. A., Rogers, M. J. & Waters, A. P. The cytoplasmic ribosomal RNAs of Plasmodium spp. *Parasitol. Today* **11**, 134–138 (1995).

10. Nishimoto, Y. *et al.* Evolution and phylogeny of the heterogeneous cytosolic SSU rRNA genes in the genus Plasmodium☆. *Mol. Phylogenet. Evol.* **47**, 45–53 (2008).

11. Thompson, J. *et al.* Heterogeneous ribosome populations are present in Plasmodium berghei during development in its vector. *Mol. Microbiol.* **31**, 253–260 (1999).

12. Gunderson, J. *et al.* Structurally distinct, stage-specific ribosomes occur in Plasmodium. *Science (80-.).* **238**, 933–937 (1987).

13. Li, J. *et al.* Regulation and trafficking of three distinct 18 S ribosomal RNAs during development of the malaria parasite. *J. Mol. Biol.* **269**, 203–213 (1997).

14. Waters, A. P., Syin, C. & McCutchan, T. F. Developmental regulation of stage-specific ribosome populations in Plasmodium. *Nature* **342**, 438–440 (1989).

15. Fang, J. & McCutchan, T. F. Thermoregulation in a parasite's life cycle. *Nature* **418**, 742–742 (2002).

16. Bunnik, E. M. *et al.* The mRNA-bound proteome of the human malaria parasite Plasmodium falciparum. *Genome Biol.* **17**, 1–18 (2016).

17. Wong, W. *et al.* Cryo-EM structure of the Plasmodium falciparum 80S ribosome bound to the anti-protozoan drug emetine. *Elife* **3**, (2014).

18. Leppek, K. & Barna, M. An rRNA variant to deal with stress. *Nat. Microbiol.* **4**, 382–383 (2019).

19. Aurrecoechea, C. *et al.* EuPathDB: the eukaryotic pathogen genomics database resource. *Nucleic Acids Res.* **45**, D581–D591 (2017).

20. Cherry, J. M. *et al.* Saccharomyces Genome Database: the genomics resource of budding yeast. *Nucleic Acids Res.* **40**, D700–D705 (2012).

21. Keseler, I. M. *et al.* The EcoCyc database: reflecting new knowledge about Escherichia coli K-12. *Nucleic Acids Res.* **45**, D543–D550 (2017).

22. Li, J., Wirtz, R. A., McConkey, G. A., Sattabongkot, J. & McCutchan, T. F. Transition of Plasmodium vivax ribosome types corresponds to sporozoite differentiation in the mosquito. *Mol. Biochem. Parasitol.* **65**, 283–289 (1994).

23. Zhu, J. D. *et al.* Stage-specific ribosomal RNA expression switches during sporozoite invasion of hepatocytes. *J. Biol. Chem.* **265**, 12740–4 (1990).

24. Waters, A. P. *Advances in Parasitology, Volume 34*. (Academic Press, 1994).

25. Trager, W. & Jensen, J. B. Human malaria parasites in continuous culture. 1976. *J. Parasitol.* **91**, 484–6 (2005).

26. Fidock, D. A. & Wellems, T. E. Transformation with human dihydrofolate reductase renders malaria parasites insensitive to WR99210 but does not affect the intrinsic activity of proguanil. *Proc. Natl. Acad. Sci.* **94**, 10931–10936 (1997).

27. Lim, F., Downey, T. P. & Peabody, D. S. Translational Repression and Specific RNA Binding by the Coat Protein of the Pseudomonas Phage PP7. *J. Biol. Chem.* **276**, 22507–22513 (2001).

28. Russo, I., Oksman, A. & Goldberg, D. E. Fatty acid acylation regulates trafficking of the

unusual Plasmodium falciparum calpain to the nucleolus. *Mol. Microbiol.* **72**, 229–245 (2009).

29. Cottrell, K. A. & Djuranovic, S. Urb-RIP – An Adaptable and Efficient Approach for Immunoprecipitation of RNAs and Associated RNAs/Proteins. *PLoS One* **11**, e0167877 (2016).

30. Pagès, H., Aboyoun, P., Gentleman, R. & DebRoy, S. Biostrings: Efficient manipulation of biological strings. (2019).

31. Wright, E. S. Using DECIPHER v2.0 to Analyze Big Biological Sequence Data in R. *R J.* **8**, 352–359 (2016).

32. Wickham, H. *ggplot2: Elegant Graphics for Data Analysis*. (Springer-Verlag New York, 2016).

33. Yu, G., Smith, D., Zhu, H., Guan, Y. & Lam, T. T.-Y. ggtree: an R package for visualization and annotation of phylogenetic trees with their covariates and other associated data. *Methods Ecol. Evol.* **8**, 28–36 (2017).

34. Yu, G., Lam, T. T.-Y., Zhu, H. & Guan, Y. Two methods for mapping and visualizing associated data on phylogeny using ggtree. *Mol. Biol. Evol.* **35**, 3041–3043 (2018).

35. Arthur, L. L. *et al.* Translational control by lysine-encoding A-rich sequences. *Sci. Adv.* **1**, e1500154 (2015).

36. Ganesan, S. M., Falla, A., Goldfless, S. J., Nasamu, A. S. & Niles, J. C. Synthetic RNA–protein modules integrated with native translation mechanisms to control gene expression in malaria parasites. *Nat. Commun.* **7**, 10727 (2016).

37. Goldfless, S. J., Wagner, J. C. & Niles, J. C. Versatile control of Plasmodium falciparum gene expression with an inducible protein–RNA interaction. *Nat. Commun.* **5**, 5329 (2014).

38. Hogg, J. R. & Collins, K. Human Y5 RNA specializes a Ro ribonucleoprotein for 5S ribosomal RNA quality control. *Genes Dev.* **21**, 3067–3072 (2007).

39. Hogg, J. R. & Collins, K. RNA-based affinity purification reveals 7SK RNPs with distinct composition and regulation. *Rna* **13**, 868–880 (2007).

40. *RNA Processing: Disease and Genome-Wide Probing*. **907**, (Springer International Publishing, 2016).

41. Youngman, E. M. & Green, R. Affinity purification of in vivo-assembled ribosomes for in vitro biochemical analysis. *Methods* **36**, 305–312 (2005).

42. Halbeisen, R. E., Scherrer, T. & Gerber, A. P. Affinity purification of ribosomes to access the translatome. *Methods* **48**, 306–310 (2009).

43. Gesnel, M.-C., Del Gatto-Konczak, F. & Breathnach, R. Combined Use of MS2 and PP7 Coat Fusions Shows that TIA-1 Dominates hnRNP A1 for K-SAM Exon Splicing Control. *J. Biomed. Biotechnol.* **2009**, 1–6 (2009).

44. Lim, F. RNA recognition site of PP7 coat protein. *Nucleic Acids Res.* **30**, 4138–4144 (2002).

45. Mancio-Silva, L., Zhang, Q., Scheidig-Benatar, C. & Scherf, A. Clustering of dispersed ribosomal DNA and its role in gene regulation and chromosome-end associations in malaria parasites. *Proc Natl Acad Sci U S A* **107**, 15117–15122 (2010).

3.7 Supplemental Material

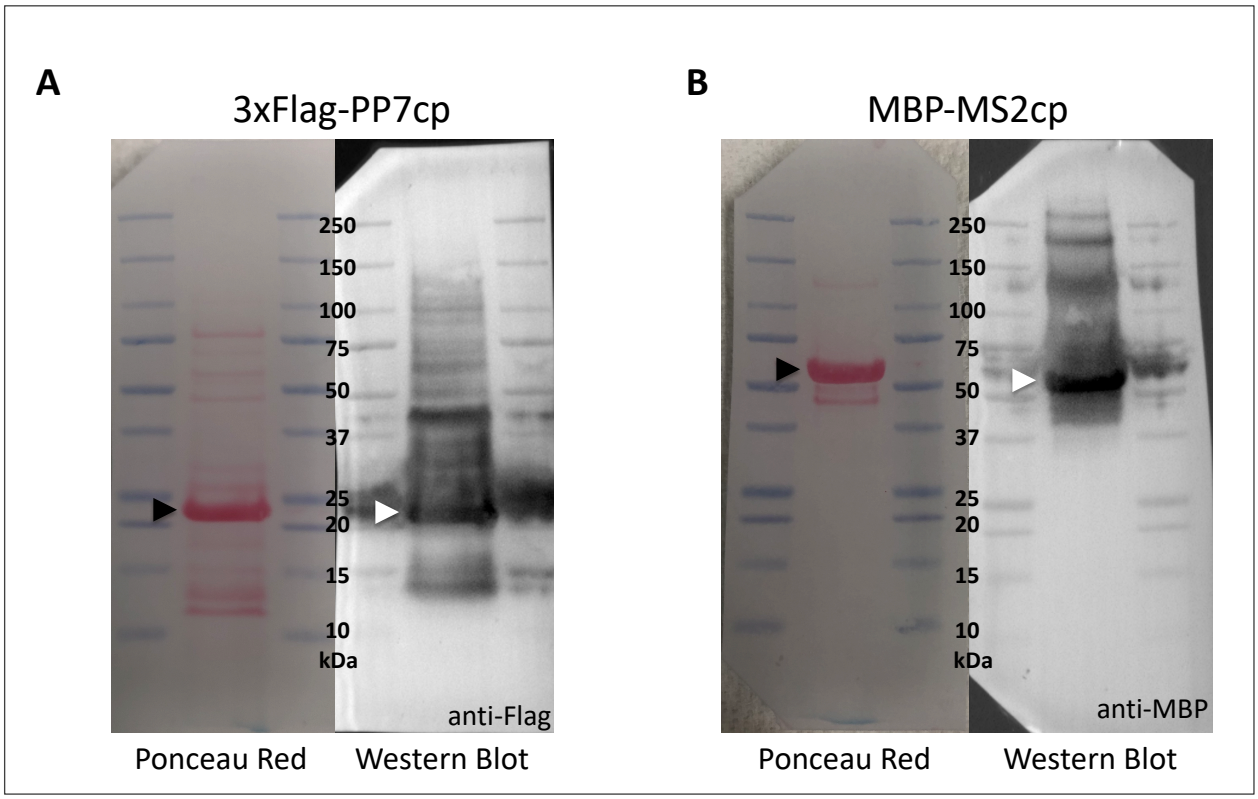

SUPPLEMENTAL FIGURE 3.1 | Ponceau Red and Western Blotting of Purified Recombinant 3xFlag-PP7cp and MBP-MS2cp Proteins. (**A**) Ponceau red staining (left) and western blotting using anti-Flag mAb (right) of purified 3xFlag-PP7cp protein product. (**B**) Ponceau red staining (left) and western blotting using anti-MBP mAb (right) of purified MBP-MS2cp protein product. *Note: Arrows indicate expected product band.*

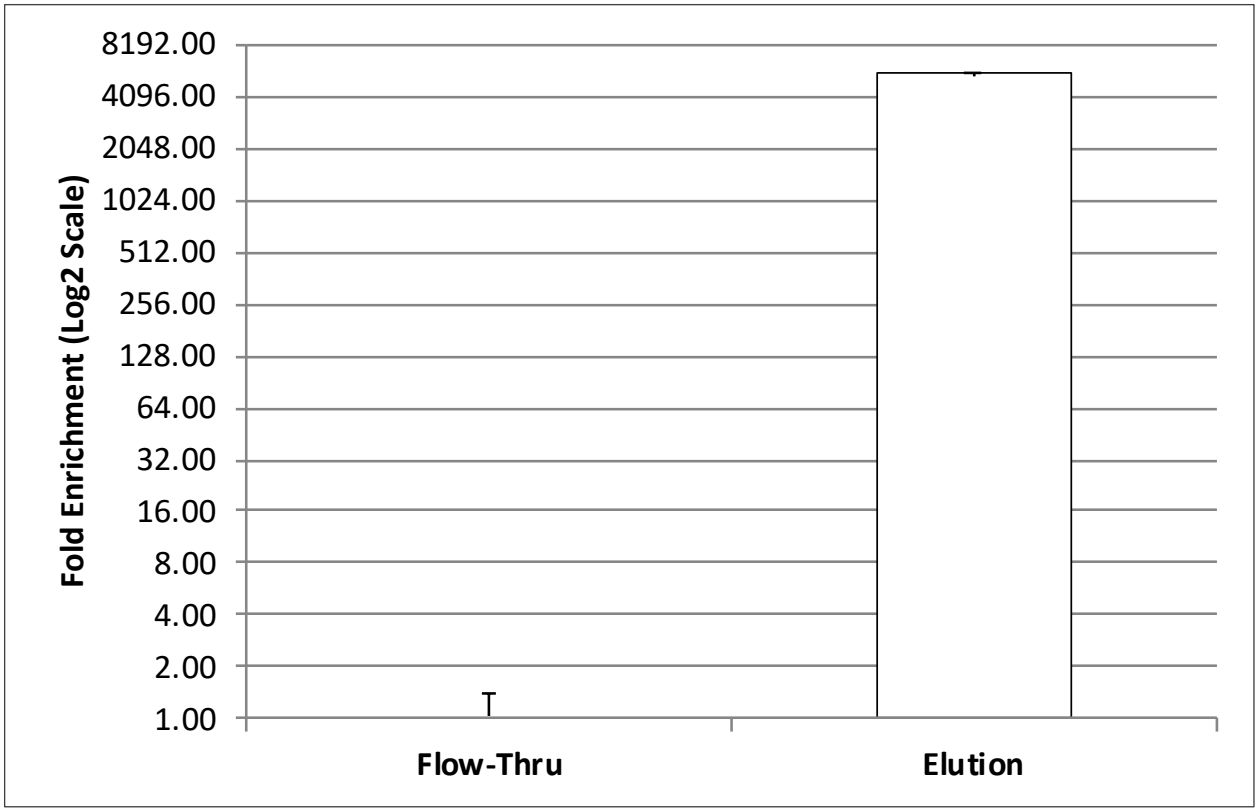

SUPPLEMENTAL FIGURE 3.2 | RT-qPCR Analysis of PP7-mRIP. Eluates from PP7-mRIP were analyzed by qPCR to determine fold enrichment.

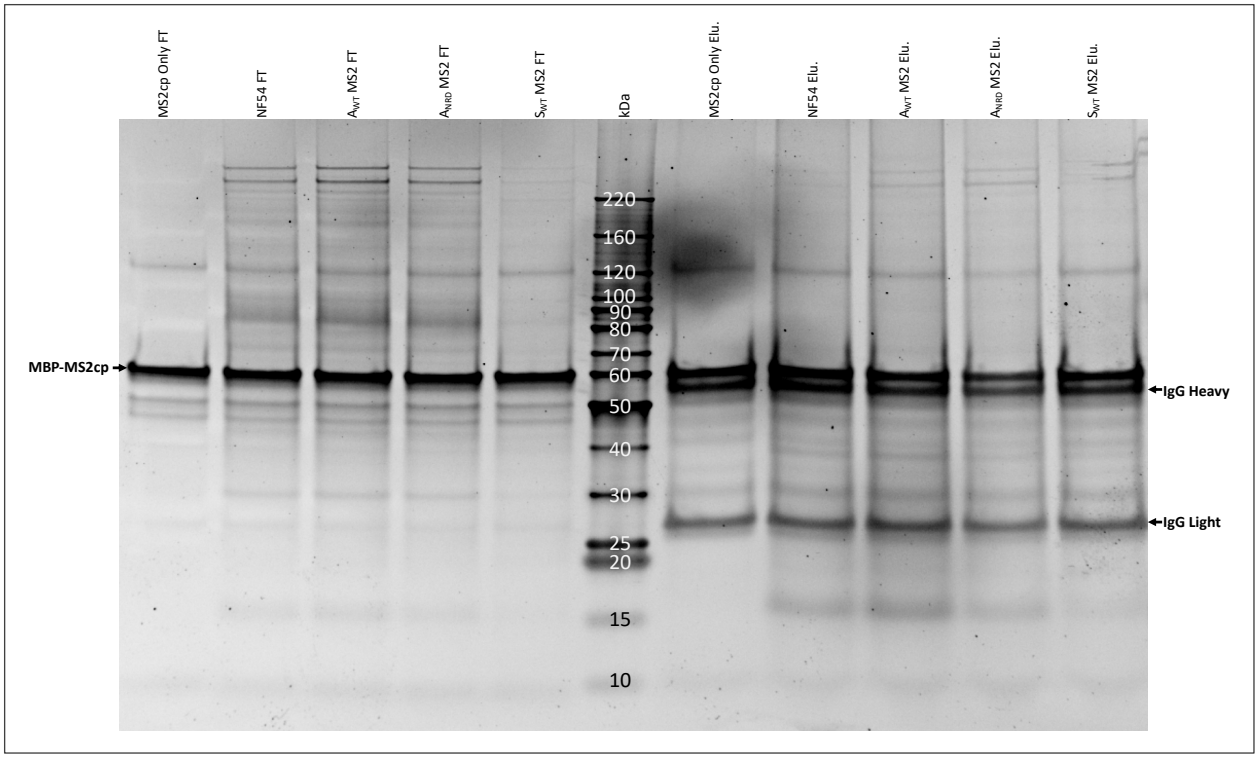

SUPPLEMENTAL FIGURE 3.3 | SDS-PAGE, SYPRO Ruby Analysis of MS2-rRIP. Eluates from MS2-rRIP were separated by SDS-PAGE and subsequently stained with SYPRO Ruby gel stain.

SUPPLEMENTARY TABLE 3.1 | Cloning Primers and oligonucleotides.

Primer/Oligo Name	Sequence [5'→3']
PP7ppsiteF1	CTTGAAGTCCTTTTCCAGGGTCCGTCCAAAACCATCGTTC
3xFlagppSiteNcoIF1	gagaccatggACTACAAAGACCATGACGGTGATTATAAAGATCATGACATCGATTACAAGGAT GACGATGACAAGCTTGAAGTCCTTTTC
PP76xHisXmaIR1	gagaCCCGGGCTAGTGGTGGTGGTGGTGCTCGAGGGAACGGCCCAGCGGCACAAGG
Hsp863utrPP7AptClaIF	CAACAATAAGGAGTTTATATGGAAACCCTTACAACAACAA atcgatgtcgagttatataatatatttatg
GFPTobAptNotIR	TTGTTGGGCACGAGTGTAGCTAAACCTCGTGCCTTGTTGTTG gcggccgcTTATTTGTACAGTTC
GFPAptF	Gagacaattggcgatggcc
GFPAptR	CTCCTTATTGTTGTTGTTGGGCACGAG
UTRAptF	CTCGTGCCCAACAACAACAATAAGGAG
UTRAptSwaIRev	gcgcATTTAAATATTACTTTTTTCGgatctttattatttaaatattacttttttcg
GFPKpnI_R1	gagaGGTACCTTATTTGTACAGTTCATCCATGC
SP6ProTobPP7F1	ATTTAGGTGACACTATAGCCCTTGTTAATAGAATCGAG
SP6TobPP7R1	GTAGACCCCATTGTGAGTAC
Pf18S_atyp_MS2LpInstr_F1	TAGTAGTAGTTTTGATCATATGTAGAAACTGCGAAC
Pf18S_atyp_MS2LpInstr_R1	ATGTGTAGAAATGATCATATATATATATACTTTCAC
Pf18S_styp_MS2LpInstr_F1	TAGTAGTAGTTT TGATCA TAATATATTGAAACTGCG
Pf18S_styp_MS2LpInstr_R1	ATGTGTAGAAA TGATCA CTTACATATGTACTTTCAC
Pf18S:G584U_F1	TTAATTCCAGCTCCAATAGC
Pf18S:G584U_R1	CGCGGCTGCTGGCACCAGAC
Pf18S:G584U_F2	TCCATTCCAGCTCCAATAGC
Pf18S:A2047C_F1	CAGTCGTAACAAGGTTTCCG
Pf18S:A2047C_R1	CTCCTTCCTTTAAAAGATAG
Pf18S:A2047C_F2	CCTTCGTAACAAGGTTTCCG
PfS18S5UTR_F	GATAGTGTGTTTAATCGTTATAATATAC
PfS58_R	TTATATTTTAAAAATATTAATACATTTCTTTTCTTTC
Pf18SAtypRNAPILSpromF	gagaccgcggTAATTCTGTGTCTAAAGATAATAACATTAATAAAAC
Pf18SAtypRNAPIMpromF	gagaccgcggAATATAATTATATATAAACAGTAAAATAAATTTAAGC
Pf18SAtypRNAPIpromR	gagactcgagACTATATATATTATTTCTTATTCATAAAAAAATTTAG
PfRNAPI_termF00	CGATCTGTTGAGGCTTATCCCTAGTGGTAAAGTG
PfRNAPI_termR00	CACATTTTAAAAAGAAATAATAAAATGCAAGGG
dEOESacIISeqF	CTCGACTCCTCCCCGCGG
Pf18SBegAntiparallelSeq	GCATATGACTACTGGCAAGATCAACCAGGTT

Pf18SEndAntiparallelSeq	GGTTTCCGTAGGTGAACCTGCGGAAGGATCATTA
dEOEMCSSeqR	CATATTTATTAAATCTAGAATTCGAGCTC
PfRNAPIp_atypF00	CGCAAATGAGCGTCAGGGCGCTGCTCG
PfRNAPIp_atypF	gagaccgcggTTAATAGACCATTTTATTAAAATTTTTGCTTCATATGAGG

SUPPLEMENTARY TABLE 3.2 | RT-qPCR Primers.

Primer/Oligo Name	Sequence [5'→3']
Pf18SAtypqPCR_F2 (WT A-type)	GTATATATATATTTTATATGTAGAAACTGCG
Pf18SAtypqPCR_R1b (WT A-type)	CAAATACTTATCCAAAGATAAAAATC
NheIMS2TagqPCRF1 (MS2 A-type and S-type)	GCTAGCTTTTGATGAGGATTACCCATCTTTG
Pf18SAtypqPCR_R3 (MS2 A-type)	CGATTGATACACACTAAATAAAATAAATTTATTACG
Pf18SStypqPCR_F1a (WT S-type)	GTACATATGTAAGTAATATATTGAAACTGCG
Pf18SStypqPCR_R2a (WT S-type)	CGATTGATAATACACATATTTTATG
Pf18SStypqPCR_R3 (MS2 S-type)	GAATTATTCCATGAATGCCT
Pf28S_AqPCRF1 (WT A-type)	CGTAATAAATTTATTTTATTTAGTGTGTATCAATCG
Pf28S_qPCRR1 (WT A-type)	CTATTTAATTGCTCATTCCTGAGTAC
gfpPP7aptTestqPCRF1	ATACTCCAATTGGCGATGGC
gfpPP7aptTestqPCRR1	TCGAAAGGGCAGATTGTGTG
gfpPP7aptTestqPCRF2	GTTTGTAACAGCTGCTGG
gfpPP7aptTestqPCRR2	GACCCCATTGTGAGTACAT
dEOEAptqPCRF1	GAAGATGGAAGCGTTCAAC
dEOEwAptqPCR1	CCTTATTGTTGTTGTTGGGC
dEOEwoAptqPCR1	TTATATAACTCGACGCGGC
dEOEAptqPCR1	GTAGACCCCATTGTGAGTACATA

SUPPLEMENTARY TABLE 3.3 | Antibodies.

Designation	Identifier	Dilution
anti-Flag (mouse)	Sigma Cat # F1804-1MG	1:1000
anti-MBP (mouse)	Sigma Cat # M6295	1:1000
anti-mouse-HRP	Cell Signaling Cat # 7076S	1:2500

Chapter 4: Ribosomal Binding of RACK1 in *Plasmodium falciparum*

4.1 Abstract

The receptor for activated C-kinase 1 (RACK1), a highly conserved eukaryotic protein, is known to have many, varying biological roles and functions. Previous work has established that RACK1 binds ribosomes; exploring regions of importance in ribosome binding in human and yeast cells. RACK1 has also been shown to be integral for multiple aspects of mRNA translation from efficient, cap-dependent mRNA translation initiation to recruitment of factors necessary for multiple mRNA/ribosome-associated quality control pathways. As such, most recent data has established the primary role of RACK1 as a ribosomal protein in human and yeast cells. In *Plasmodium falciparum*, RACK1 has been shown to be required for parasite growth. However, conflicting evidence has been presented about the role of RACK1 in mRNA translation and ribosome binding. Given the aforementioned importance of RACK1 as a regulatory component of mRNA translation, the case could be made in parasites for either of the binary options: bound or unbound to the ribosome. Here we explore the binding properties of the PfRACK1 to the human and *P. falciparum* ribosome. Based on bioinformatic and structural analysis, as well as previously explore modifications, mutant and chimeric RACK1 proteins were generated. The mutant and chimeric proteins were then express in human and parasite cells. The ribosomal binding of RACK1 variants in human and parasite cells shown here suggests that although

RACK1 proteins have highly conserved sequences and structure across the species, variation exists in the factors that drive ribosomal binding.

4.2 Introduction

The WD domain, which folds into a β-propeller structure, is typically characterized by the repetition of glycine (G)–histidine (H) and tryptophan (W)-aspartic acid (D) dipeptide repeats[1]. It also happens to be incredibly abundant throughout the eukaryotic tree of life[2]. This domain is primarily associated with signalosome assembly[3], providing the means for signal transduction, and there are as yet no WD domain proteins with intrinsic enzymatic capabilities[1]. A typical structure for WD domains is the seven-bladed WD β-propeller, with the N-terminus and C-terminus completing the final 7th blade to close the structure[4]. Besides signal transduction, WD domains are involved in processes ranging from those involved in organism proliferation to virulence in lower eukaryotes[5] or immune response in higher eukaryotes[1,6,7]. One of the most intensely studied WD domain containing proteins is the receptor for activated C-kinase 1 (RACK1).

RACK1 is a highly conserved, eukaryotic, seven-bladed WD β-propeller repeat scaffolding protein[7]. RACK1 was initially associated with protein kinase C signaling, the reason for its namesake[8]. However, RACK1 is now known to have many, varying biological roles and functions. Recently, the primary role of RACK1 has been shown to be as a ribosomal protein[9–11]. In this capacity, RACK1 has been shown to necessary for efficient, cap-dependent mRNA translation initiation[9,10,12–15] as well as activation of many ribosome quality control (RQC)-

associated pathways[16–20]. In *P. falciparum*, RACK1 is required for parasite growth during IDC stages, with knockdown during ring stage result in growth arrest in the trophozoite stage[21]. What remains unclear are the functions of RACK1 in the parasite, given the lack of a PKC IIβ homolog[15], particularly its role in protein synthesis.

Ostensibly conflicting evidence has been provide regarding RACK1 ribosomal binding if *P. falciparum*. Structural data show that RACK1 does not copurify with schizont 80S ribosomes[22,23], while mass spectrometry of polysome profiling data paints a contradictory picture[24]. Here, we demonstrate that RACK1 expression in *P. falciparum* follows that of other ribosomal proteins, binds to the parasite ribosome, and is present during active translation. The data also suggests that the RACK1::40S binding dynamics are quite different between mammalian and parasites, with emphasis on binding being distributed throughout the protein or even on the C-terminal region; potentially the loop motif. Finally, PfRACK1 is also localized to the parasite cytoplasm during the schizont stage although previously thought to be distributed to the RBC cytoplasm.

4.3 Results

4.3.1 PfRACK1 expression follows other ribosomal proteins.

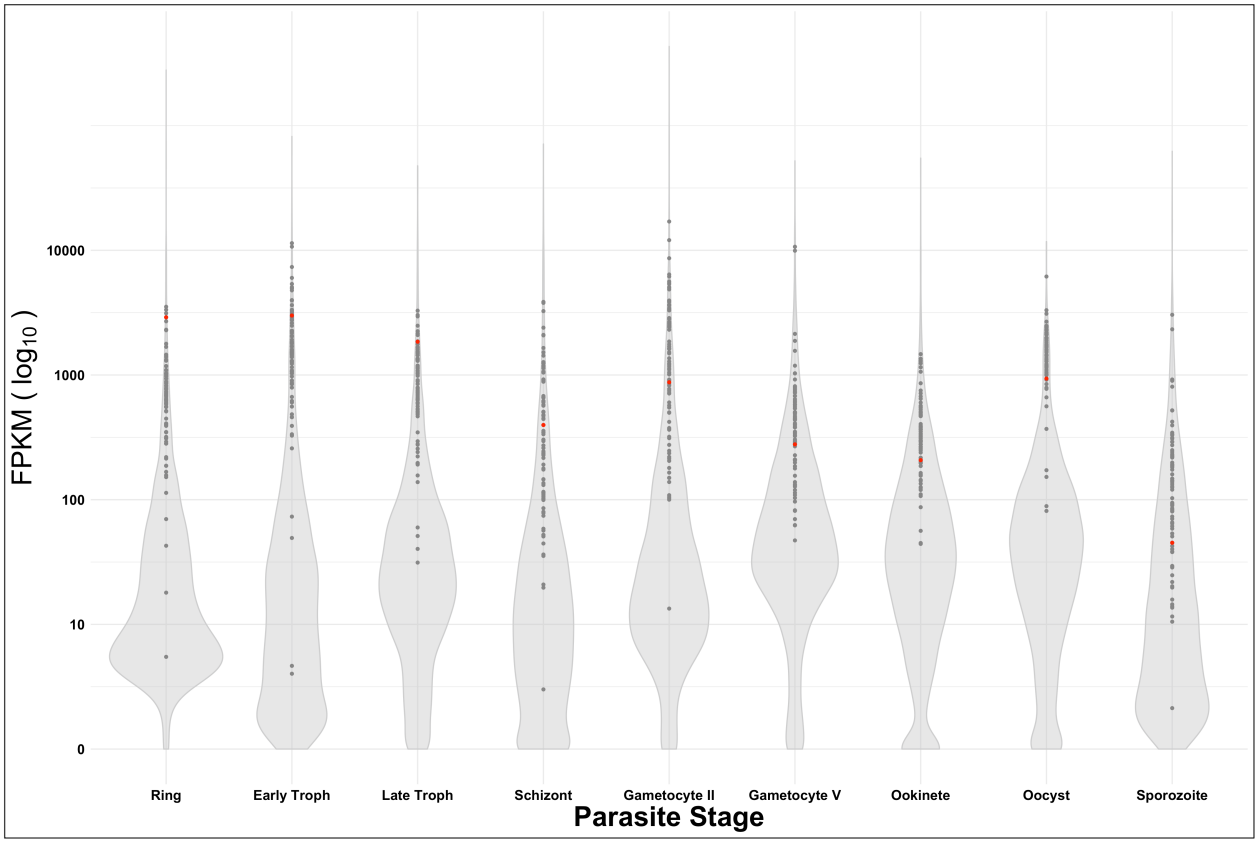

FIGURE 4.1 | Transcriptional analysis of PfRACK1 in comparison with other parasite proteins throughout the *P. falciparum* life cycle. RNASeq data from PlasmoDB showing all proteins (violin plot), ribosomal protein (dot plot), and PfRACK1 (red dot) transcript expression in *P. falciparum* 3D7 throughout the parasite life cycle. The x-axis indicates the parasite stage and the y-axis (log_{10} scale) represents transcript fragments per kilobase of exon model per million reads mapped.

Transcriptional analysis of PfRACK1 was performed to compare its expression with other ribosomal proteins. The analysis shows that the PfRACK1 gene, like other ribosomal proteins, is highly expressed in comparison to the average total protein transcript expression at each stage and in a pattern similar to other ribosomal proteins (**FIGURE 4.1**). Interestingly, PfRACK1

expression drops by approximately one $\log_{10}$ from the early trophozoite stage where translation is high to when the parasites transition into the schizont stage. Thus, the data suggests that PfRACK expression follows that of other ribosomal proteins and significant changes in expression are seen during stages where protein synthesis dramatically increases of decreases.

4.3.2 A *de novo* structure PfRACK1: the sequence and structure of PfRACK1 are highly conserved

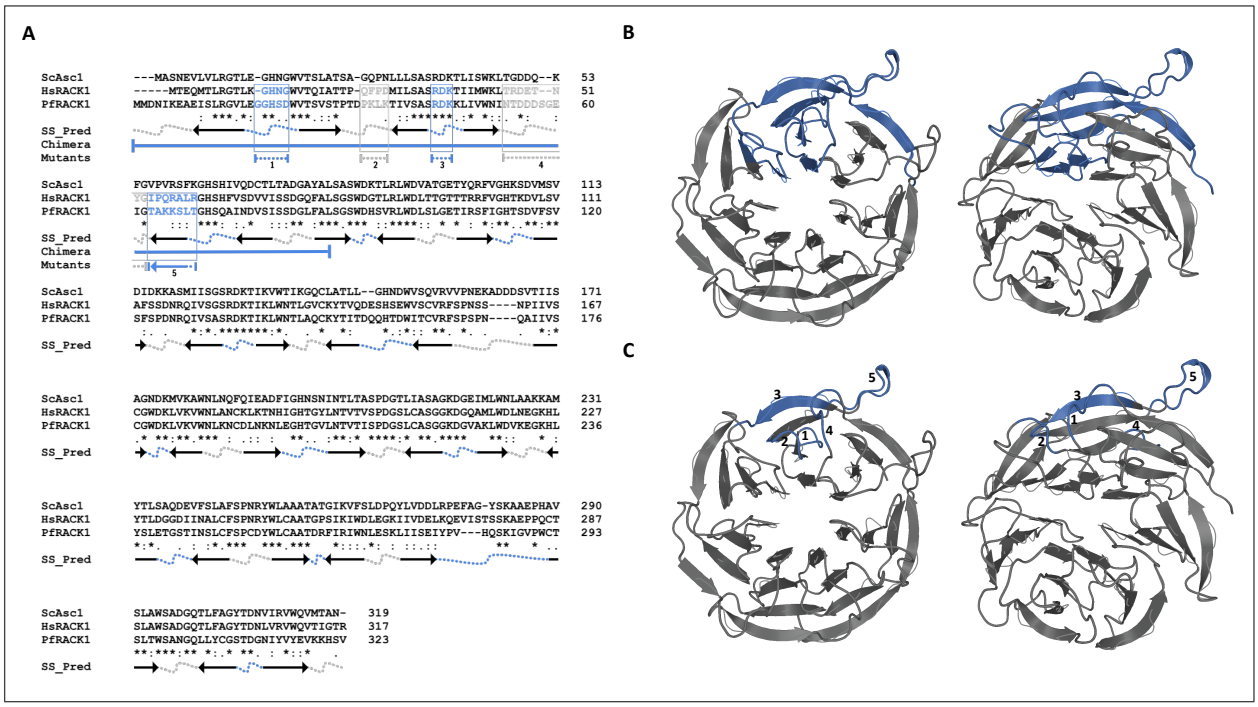

FIGURE 4.2 | Comparative bioinformatic analysis of RACK1 homologs in *S. cerevisiae* (ScAsc1), *H. sapiens* (HsRACK1), and *P. falciparum* (PfRACK1) homologs. (A) Sequence alignment of yeast Asc1, human RACK1, and *P. falciparum* RACK1 amino acid sequences generated by Clustal Omega. The SS_Pred is the secondary structure prediction using MPI Bioinformatics toolkit Quick2D tool. Arrows: beta strands. Arrows represent beta strands, with heads pointing from the N-terminal to C-terminal direction showing the orientation of the beta strand in the β-propeller. Dotted lines represent loops found between beta strands where grey notates solvent-facing loops and blue indicates ribosome-facing loops. Chimera (χ): proteins generated by region exchanged between human and parasite RACK1 proteins shown in solid blue lines. Mutants: short RACK1 regions mutated from HsRACK1 sequence to PfRACK1 sequence, or vice versa, and expressed in HAP1 (1-5) or parasite (3, 5) lines. Clustal Omega consensus symbols: Asterisks (*) indicates fully conserved resdue. Colon (:) indicates conservation between residues of strongly similar properties (approximation of > 0.5 in the Gonnet PAM 250 matrix). Period (.) indicates conservation between residues of weakly similar properties (approximation of =< 0.5 and > 0 in the Gonnet PAM 250 matrix). **(B-C)** A SWISS-MODEL generated de novo model of PfRACK1 displaying **(B)** chimeric region and **(C)** mutated regions in blue. Left: Ribosome facing surface. Right: 25-degree rotation.

Bioinformatic analysis was performed on the human, yeast, and *P. falciparum* RACK1/Acs1 proteins. The HsRACK1 and ScAsc1 proteins share a 53.82% sequence identity, while HsRACK1 and PfRACK1 have 59.55% sequence identity. The PfRACK1 and ScAsc1 proteins share less sequence identity at 42.99%. A multiple sequence alignment combined with secondary structure analysis of these RACK1 proteins was performed to further determine what features, if any, would affect the binding of PfRACK1 to the 40S ribosome subunit. The analysis demonstrates a conservation of the β-sheet blades and loop features and positioning (**FIGURE 4.2A**). Combining this data with the *de novo* structure of PfRACK1 modeled onto the parasite 80S ribosome, a majority of the ribosome facing loop residues appear conserved in nature (**FIGURE 4.2B–C**).

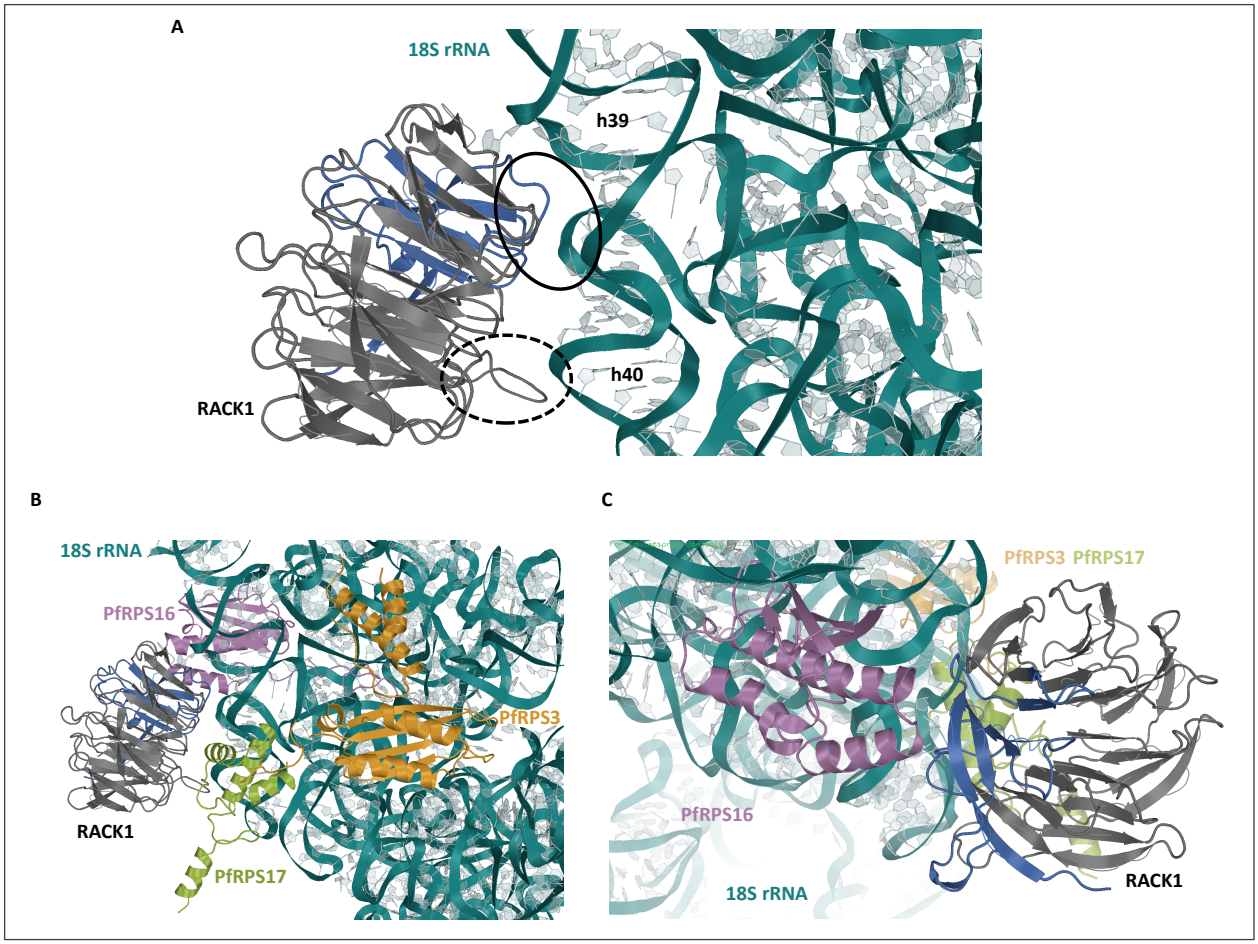

FIGURE 4.3 | Structural analysis of the PfRACK1 protein binding to *P. falciparum* 40S Ribosome subunit. All structures displayed are P falciparum proteins/RNA. **(A)** The structure of the *P. falciparum* 80S ribosome (RCSB PDB ID: 3jbo) was structurally aligned with the human 80S ribosome (RCSB PDB ID: 3jag). The de novo model of PfRACK1 generated by SWISS-MODEL was structurally aligned with that of the human 80S bound RACK1. The view shown is that which been previously published arguing for the importance of the regions noted in RACK1 binding to the ribosome. Solid circle: region vital for HsRACK1:Hs80S binding. Dotted circle: Loop region that varies highly species to species, and while not required, may influence binding. **(B)** The same view as above, however ribosomal binding proteins with potential interactions are shown. **(C)** A 180-degree flipped view to show additional RPS16 (uS9) and RACK1 interactions. Note: Region in blue is that when exchanged between human and P. falciparum enabled binding of parasite RACK1 to the human 40S ribosome.

HsRACK1 has been previously shown to bind to the human 40S ribosome, with emphasis placed on helices 39 and 40 of the 18s rRNA and the N-terminal region of RACK1. This was modeled for *P. falciparum* and displayed as previously published for HsRACK1 interaction with the human 80S ribosome[25] (**FIGURE 4.3A**). The helices 39 and 40 of the parasite 18S rRNA reveal the potential for highly similar interactions between the PfRACK1 protein and the *P. falciparum* 18S rRNA. Previous work also examined ribosomal proteins in this region: RPS16 (uS9), RPS17 (eS17), and RPS3 (uS3) (**FIGURE 4.3B–C**), which are also in close proximity. Therefore, residues that may interact with these proteins must also be taken into consideration. Those residues on PfRPS16 and PfRPS17 within 3-5 Å range are also highly conserved (**SUPPLEMENTAL FIGURE 4.1**), and therefore are not expected to hinder binding. The residues of PfRPS3 are also highly conserved, however it appears that there may be a C-terminal truncation of 18 residues when compared with HsRPS3 that may impact interaction of the disordered region of the protein (**SUPPLEMENTAL FIGURE 4.1**).

Overall, the data shows high sequence and structural conservation of the PfRACK1 protein compared with HsRACK1. This is particularly true of ribosomes facing residues. Additionally, the potential rRNA interactions also appear to be conserved in the parasite, as do those of RPS16 (uS9), RPS17 (eS17), and RPS3 (uS3) with the exception of a potential alteration to the RPS3 C-terminal disordered region. Taken together, this data suggests that PfRACK1 should be able to bind to the parasite 40S ribosomal subunit.

4.3.3 Binding of RACK1 to the ribosome

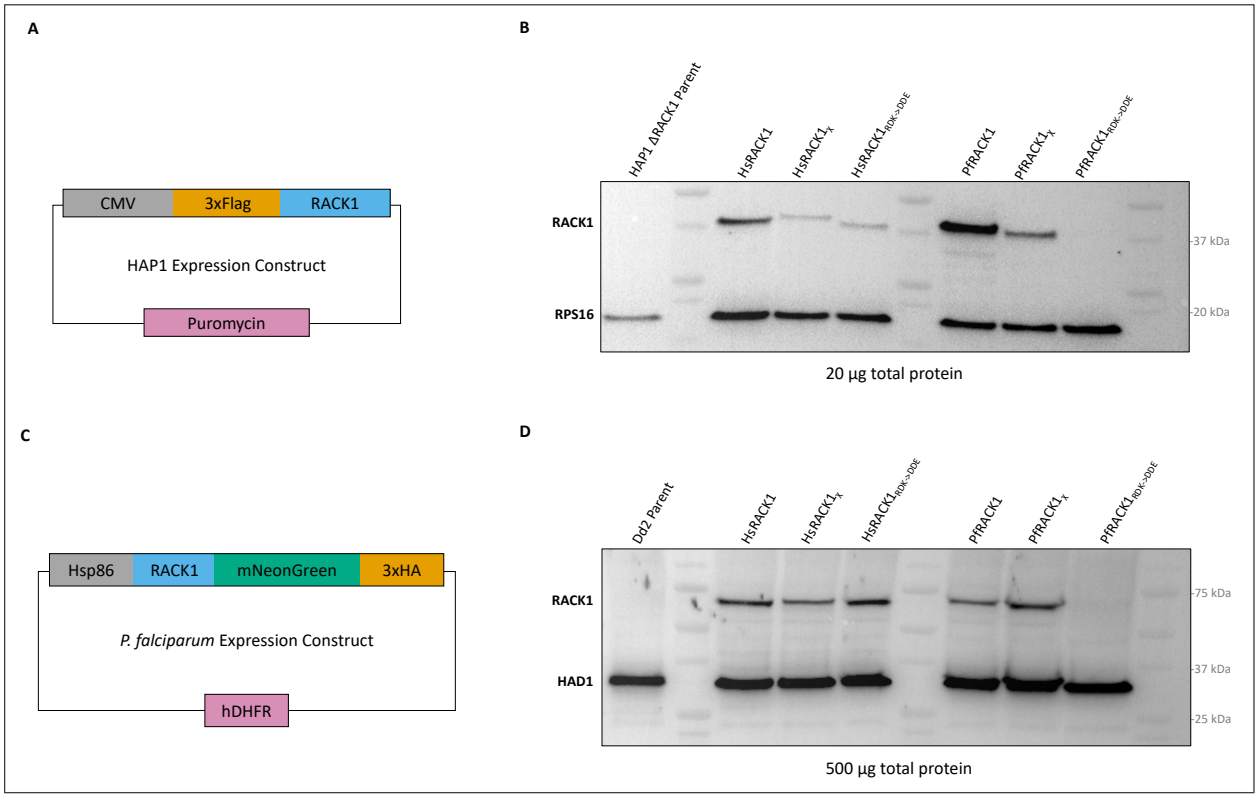

FIGURE 4.4 | Expression of RACK1 variants in mammalian HAP1 ΔRACK1 cells and *P. falciparum* parasites. (A) Schematic of plasmid constructs for RACK1 variant expression in mammalian HAP1 cells (left) and *P. falciparum* parasites (right). **(B)** Western blot using anti-Flag antibody of HAP1 ΔRACK1 cell expressing RACK1 variants. 40S ribosomal protein 16 (uS9) blotted as control. **(C)** Western blot using anti-HA antibody of *P. falciparum* parasites expressing RACK1 variants. Haloacid dehalogenase-like hydrolase (HAD) blotted as control.

To examine binding of PfRACK1, mutants were generated based on bioinformatic analysis (**FIGURE 4.2A**), as well as previous work[7,9,10], and expressed in HAP1 ΔRACK1 cells and *P. falciparum* parasites (**FIGURE 4.4**). While most of the ribosome facing loop residues appear conserved, previous work has shown that small single or double amino acid changes in key regions are able to significantly change binding, thus the RDK->DDE mutation in the was

included as a control to help demonstrate a loss or lack of binding (**FIGURE 4.2A, MUTANT 3**)[7]. Previous work emphasized the importance of the N-terminal region in RACK1 binding to the human 40S ribosomal subunit[7]. To address this, chimeric RACK1 variants were generated by exchanging the N-terminal regions of the HsRACK1 (residues 1-79) and PfRACK1 (residues 1-88).

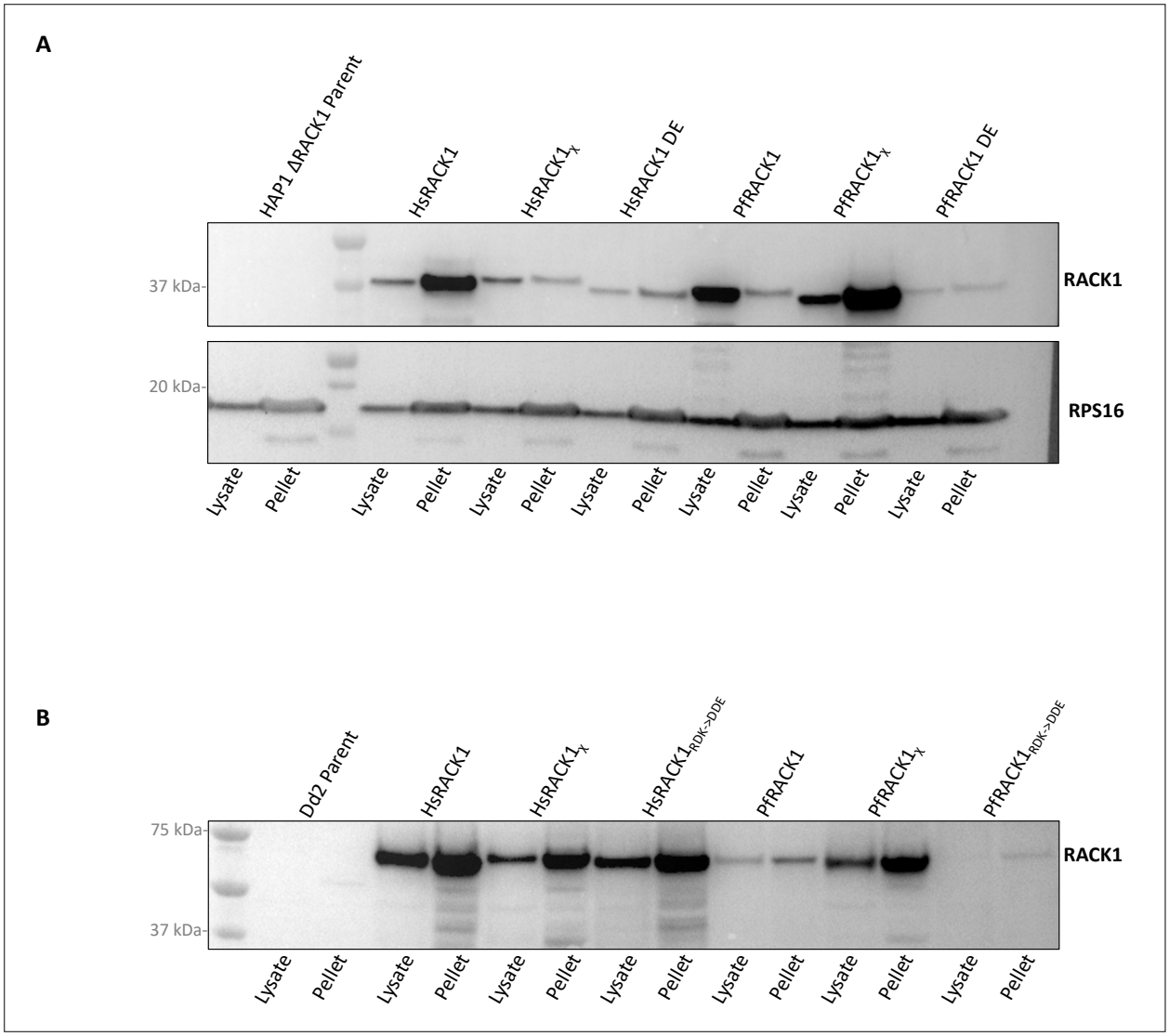

FIGURE 4.5 | Ribosomal binding of RACK1 variants in mammalian HAP1 ΔRACK1 cells and *P. falciparum* parasites. (A) Western blot of lysates and post-sucrose cushion centrifugation pellets of HAP1 ΔRACK1 cells expressing N-terminally 3xFlag tagged RACK1 variants. 40S ribosomal protein 16 (uS9) blotted as control. **(B)** Western blot of lysates and post-sucrose cushion centrifugation pellets from *P. falciparum* parasites expressing C-terminally 3xHA-tagged RACK1 variants.

Binding to the 40S subunit was then assessed by isolation of crude ribosomes through a sucrose cushion. The RACK1 variants expressing in HAP1 cells harboring the human RACK1 N-terminal region were able to bind, while those that had the parasite RACK1 N-terminal region did not

show significant binding; similar to the loss of binding of the RDK->DDE mutation (**FIGURE 4.5A**). Interestingly, all variants appeared to bind in *P. falciparum* parasite, potentially even the RDK->DDE mutants, suggesting a different in RACK1::40S subunit binding dynamics in the parasite (**FIGURE 4.5B**). This difference in binding dynamics was also seen in an RT-qPCR analysis of rRNAs from total RNA isolated after HA-immunoprecipitation of RACK1 of crude ribosome pellets (**SUPPLEMENTAL FIGURE 4.3**). The data suggests that while PfRACK1 does indeed bind, HsRACK1 and PfRACK1$_{\chi}$ bind with significantly greater affinity (**SUPPLEMENTAL FIGURE 4.3B**).

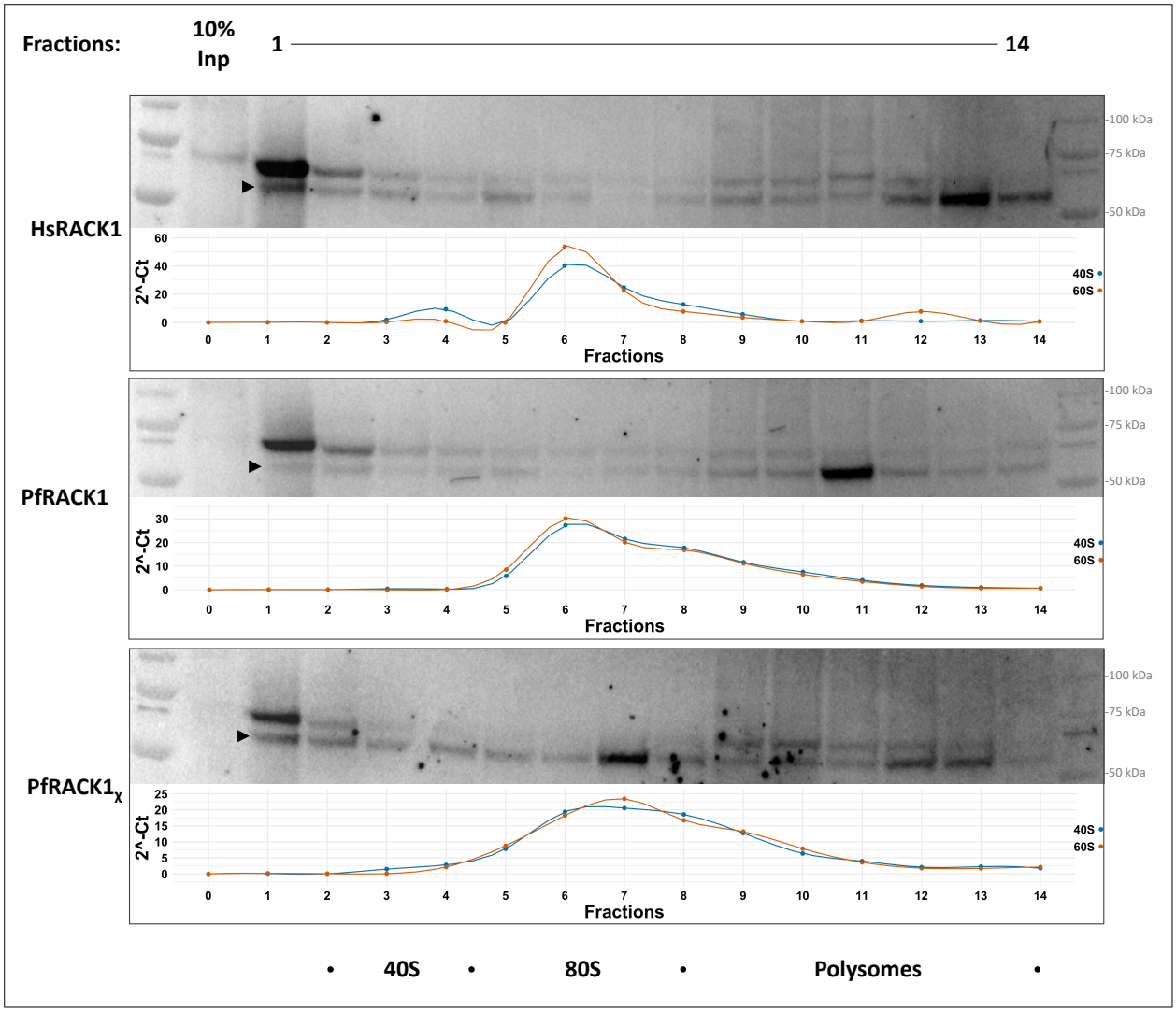

FIGURE 4.6 | Polysome profiling of HsRACK1, PfRACK1, and PfRACK1$_\chi$ variants in *P. falciparum* Dd2 parasites. Polysome profiling fractions generated from *P. falciparum* parasites expressing HsRACK1, PfRACK1, and PfRACK1$_\chi$ variants were analyzed. Western blot shows RACK1 variant polysome fraction localization. RT-qPCR analysis shows localization of 18S and 28S rRNAs associated with the 40S and 80S subunits, respectively. Arrowhead indicates non-specific band found in parent line not correlating to RACK1 variants.

Polysome profiling was performed to determine if the variants are involved in active translation and therefore truly bound to the 40S subunit. Western blot analysis of polysome profiling show that PfRACK1 is indeed bound to the ribosome during translation (**FIGURE 4.6, SUPPLEMENTAL**

FIGURE 4.3). While the 40S fractions show similar RACK1 variant binding between HsRACK1, PfRACK1, and PfRACK1$_\chi$, the polysome fractions show exhibit a different binding pattern with a reduction of PfRACK1 and an increase in the HsRACK1 and PfRACK1$_\chi$ variants. Summarily, these data suggest that while yeast RACK1 has been shown previously to bind to the human 40S ribosome subunit, the *P. falciparum* PfRACK1 protein does not, even with an almost 60% sequence similarity. However, all the RACK1 variants appear to bind in the parasite, suggesting a difference in the factors that drive RACK1 binding in *Plasmodium spp*. Finally, PfRACK1 was found in the 80S monosome and polysome fractions supporting its function as a ribosomal protein in *P. falciparum* despite not being found in the schizont-generated parasite 80S ribosome structure[22,23].

4.3.4 PfRACK1 localizes to the parasite cytoplasm

Previous work has stated that in *P. falciparum*, RACK1 is dispersed from the parasite cytoplasm into the red blood cell during the schizont stage, the stage from which all previous ribosome structural data is based. To reevaluate this phenomenon, live imaging microscopy was performed on *P. falciparum* Dd2 lines expressing C-terminally tagged mNeonGreen RACK1 variants. Images were taken of the Dd2 parent line (**FIGURE 4.7A**), Dd2 expressing PfRACK1 (**FIGURE 4.7B**), and Dd2 expressing PfRACK1$_\chi$ (**FIGURE 4.7C**).

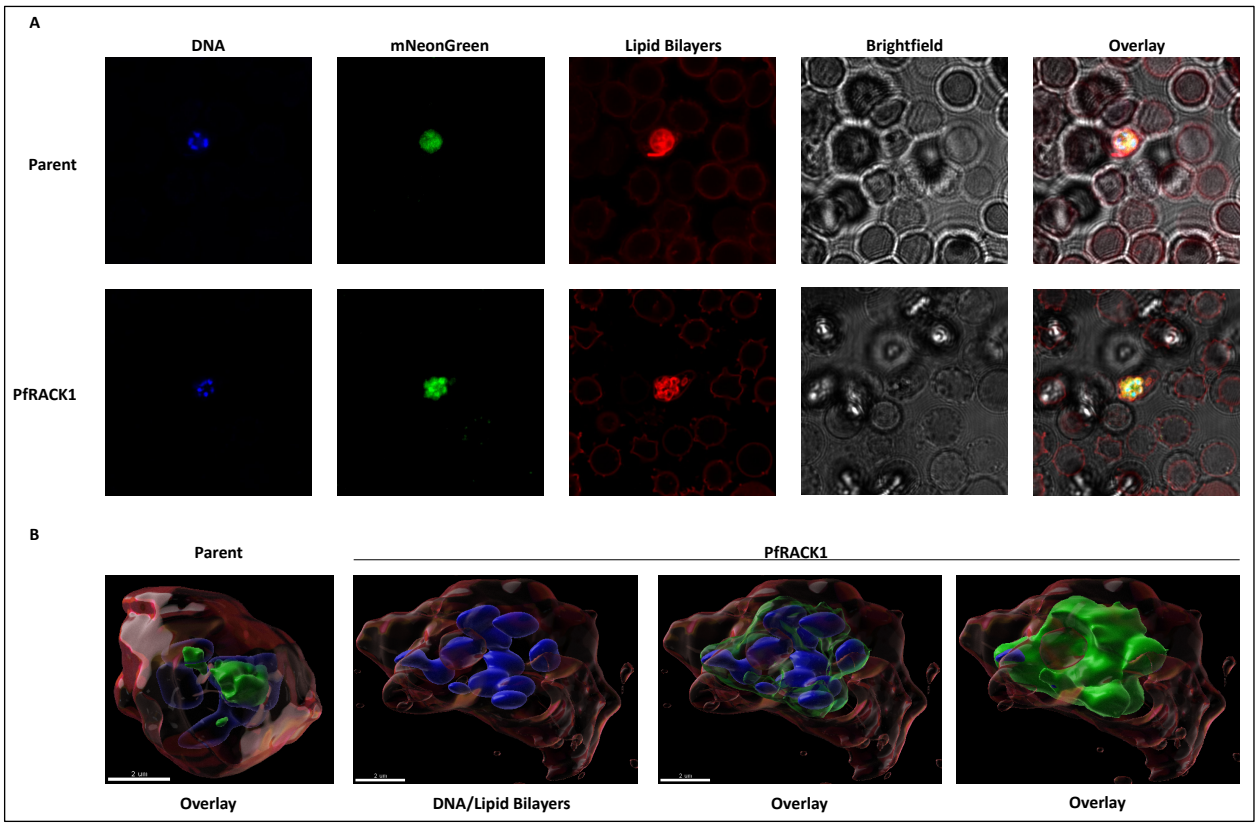

FIGURE 4.7 | Airyscan confocal fluorescence imaging microscopy of mNeonGreen-tagged PfRACK1 expressed in *P. falciparum*. **(A)** Hoechst Stain (DNA), mNeonGreen (RACK1), BODIPY TR ceramide (lipid bilayers). Top) Dd2 parent line. Bottom) Dd2 parent line expressing mNeonGreen-tagged PfRACK1. **(B)** Two-dimensional overlay using Imaris software analysis of Airyscan images. Left) Dd2 parent line. Right) Dd2 parent line expressing mNeonGreen-tagged PfRACK1.

Imaging of schizonts did not show dispersal of RACK1 into the red blood cell cytoplasm, but rather the proteins remain in the parasite cytoplasm surrounding the daughter cells. Parasites may not have been at a late enough stage to see this phenomenon or this is an artifact due to perforation of the parasitophorous vacuole prior to daughter cell release[26].

4.4 Discussion

Transcriptional analysis of PfRACK1, one of the most abundant parasite proteins[21,27], demonstrates that the protein follows expression of other ribosomal proteins (**FIGURE 4.1**). Bioinformatic and structural analysis reveal that PfRACK1 maintains all the hallmark characteristics of homologs where ribosomal binding is seen (**FIGURES 2–3**). To examine PfRACK1 binding of the 40S ribosome subunit, RACK1 variants were generated based on bioinformatic and structural analysis and subsequently expressed in HAP1 ΔRACK1 mammalian cells and *P. falciparum* parasites (**FIGURE 4.4**). Previous work has demonstrated that the yeast RACK1 homologue Asc1 is able to bind the human 40S ribosome subunit[9]. Here the data show that although PfRACK1 shares a higher identity with HsRACK1 than ScAsc1 (59.55 % vs. 53.82%), however PfRACK1 was unable to bind the human ribosome (**FIGURE 4.5A**). Analysis of binding in the parasite show that not only does PfRACK1 bind the ribosome (**FIGURE 4.5B**, **FIGURE 4.6, SUPPLEMENTAL FIGURE 4.3B**), but that also the binding dynamics differ from that of human ribosomes (**FIGURE 4.5B**, **FIGURE 4.6, SUPPLEMENTAL FIGURE 4.3B**), with less emphasis on the N-terminus for binding in the parasite. Polysome profiling data also show that PfRACK1 is indeed found in the 80S and polysome fractions (**FIGURE 4.6, SUPPLEMENTAL FIGURE 4.4**), but that there is a reduction in the presence of PfRACK1 in this faction compared to the HsRACK1 and PfRACK1$_{\chi}$ variants again suggesting an alteration in PfRACK1 binding of the 40S subunit. However, the residues or post-translational modification that drive these differences remain unknown.

Lastly, previous work has suggested that PfRACK1 is exported during the schizont stage into the RBC cytoplasm[21]. To explore RACK1 localization, mNeonGreen tagged RACK1 variants were

expressed in the parasite. The E64-treated parasites were examined by confocal microscopy with airyscan and the RACK1 locale determined in relation to parasite DNA and lipid bilayers. This data shows that RACK1 variant remain within the parasite cytoplasm (**FIGURE 4.7**). While this data suggests that RACK1 is found within the parasite during the schizont stage, it is possible that the parasites were not incubated long enough to see release of the protein into the RBC cytoplasm. However, this phenomenon is most likely due to the perforation of the parasitophorous vacuole that occurs at this stage[26].

RACK1 does not copurify with schizont 80S ribosomes[22,23]. The presences of RACK1 on the ribosome seen in crude ribosomes and polysome profiling data here and from others[28], while indicating that PfRACK1 does indeed bind the ribosome, does not exclude the possibility for a change in PfRACK1::40S ribosome binding dynamics in the schizont stage. Interestingly, there is an almost $\log_{10}$ reduction in PfRACK1 transcript expression in the schizont stage (**FIGURE 4.1**). One could speculate that drastic reduction of PfRACK1 expression and binding, which has previously been shown to globally downregulate mRNA translation[10], perhaps via a post-translational modification event at key residues during the schizont stage would be energetically favorable as the parasite prepares to release short-live merozoites; and may also hold true for sporozoites.

4.5 Materials and Methods

4.5.1 Mammalian cell culture, lentiviral production, and transduction

Human embryonic kidney (HEK) 293T cells were cultured in Dulbecco's modified Eagle's medium (DMEM) (Gibco) and supplemented with 10% fetal bovine serum, 5% penicillin and streptomycin (Gibco), and L-glutamine (Gibco). HAP1 cells were cultured in Iscove's Modified Dulbecco's Medium (IMDM) (Gibco) and supplemented with 10% Fetalgro® Bovine Growth Serum (RMBIO), 5% penicillin and streptomycin (Gibco), and L-glutamine (Gibco). Cells were grown at 37 °C with 5% CO_2.

Tools for lentiviral production were generously provided by the You Lab (Washington University, St. Louis, MO). The RACK1 variants to be expressed were cloned into the pCDH vector using the XbaI and NotI restriction sites and confirmed by Sanger sequencing. Plasmid DNA from pCDH-RACK1, pCMV-VSVG vector (addgene 8454), and psPAX2 vector (addgene 12260) was isolated from bacterial midipreps (Invitrogen). Before transfection (20-24 hours), 1.5 million HEK 293T cells in a 6 cm dish. The packaging vectors, pCMV-VSVG and psPAX2, were combined in a ratio of 1:9. For transfection, 3 µg of expression vector and 3 µg of combined packaging vectors were also combined in 400 µL of OPTI-MEM (Gibco). To this, 18 µL (1:3 ratio of DNA to transfection reagent) of X-tremeGENE™ 9 DNA transfection reagent (MilliPore Sigma). The mixture was incubated for 30 mins at room temperature. The medium of HEK 293T cells was replaced with pre-warmed regular growth medium. The transfection mixture was added, and cell put back in the incubator at 37 °C with 5% CO_2. On the next day, 1 mL of fetal

bovine serum (FBS) was added. The medium containing virus was collected at 48 hours and 72 hours after transfection. The supernatant containing the virus was centrifugated at 15,000 x g and then filtered using 0.45 μm filter to remove any 293T cells or debris. The virus was stored at 4 °C for up to 1 week or kept at -80 °C for long term storage, and freeze-thawing avoided.

For lentiviral transduction, HAP1 cells were seed such that they will be about 60-70% confluent at the time of transduction. To assess viral titer, cells were plated in 12-well plates. However, a 1:4 dilution was found to be sufficient enough for an almost 100% transduction. At 20-24 hours after plating, polybrene was added to a final concentration of 8μg/mL to cells and the desired amount of lentivirus was added. At 48 hours after transduction, cells were re-plated and selected with 3 μg/mL puromycin for 24 hours, two to three times.

4.5.2 Parasite cell culture and transfection

P. falciparum Dd2 was cultured at 2-5% hematocrit in O^+ erythrocytes in Malaria Culture Medium (MCM): RPMI 1640 supplemented with 5 g/L Albumax II (Gibco), 0.12 mM hypoxanthine (1.2 mL 0.1M hypoxanthine in 1 M NaOH), 10 μg/mL gentamicin[29]. Cultures were grown statically in candle jar atmosphere. As required, cultures were synchronized with 5% (wt/vol) sorbitol.

Asynchronous *P. falciparum* Dd2 parasites were washed twice in 15 mL incomplete Cytomix (25 mM HEPES, 0.15 mM $CaCl_2$, 5 mM $MgCl_2$, 2 mM EGTA, 120 mM KCl, 5 mM K_2HPO_4, 5 mM KH_2PO_4) and resuspended in a total 525 μL with 100 μg of maxi-prep plasmid DNA dissolved in incomplete cytomix (125 μL packed iRBCs and 400 μL DNA/incomplete cytomix), The parasites

were transfected in Bio-Rad Gene Pulser cuvette (0.2 cm), 0.31 kV, 950 up, infinity resistance. Selection (10 nM WR99210 or 2 µM DSM-1) was added to parasite 48 h after transfection and used to select resistant parasites[30].

4.5.3 Saponin lysis of infected red blood cells (iRBCs)

The cell iRBCs were resuspended in two volumes of PBS containing 0.15% saponin, and incubated on ice for 10 min, with vigorous mixing every 3 min. Afterward, the samples were centrifuged 7000g, 5 min, 4°C, and the pellets were washed three times more with the same buffer.

4.5.4 Parasite staining and confocal microscopy with airyscan

To examine localization of RACK1 variants in the parasite, confocal microscopy using the Zeiss LSM 880 Confocal with Airyscan was performed. Primarily late trophozoite, early schizont stage parasites were treated for 6 hours with E64 to inhibit parasite release. Parasites were then washed twice using parasite imaging medium (RPMI without phenol red and with hypoxanthine) containing E64. Parasites were incubated for 30 min with Hoechst stain to label DNA and BODIPY™ TR ceramide to label lipids. Parasites were again washed 3 times with imaging medium containing E64. Cultures were dotted onto slides and sealed beneath coverslips. Brightfield images and z-stacks were collected using a Zeiss LSM 880 Confocal with Airyscan confocal microscope using a 40X oil objective. DNA was visualized by Hoechst stain (diode: 405 nm, ex: 350 nm, em: 461 nm), RACK by mNeonGreen (laser: 488 nm, ex: 506, em:

517), and lipid bilayers by BODIPY™ TR ceramide (laser: 561 nm, ex:589/em:617) Image analysis and generation was done using Imaris (Oxford Instruments) and Fiji ImageJ software.

4.5.5 Transcriptional analysis of PfRACK1

Ribosomal proteins were queried from PlasmoDB[31], excluding apicoplast and mitochondrial genes. Ribosomal proteins during the human stage were defined as those with RNAseq expression data in the minimum of the 80th percentile during ring, early trophozoite, late trophozoite, schizont, gametocyte II, or gametocyte V[32] or during sporozoite stage[33]. Ribosomal proteins expressed during the mosquito stage were defined as those with RNAseq expression data in the minimum of the 80th percentile during ookinete[32], oocyte, or sporozoite stage[33].

4.5.6 *De novo* RACK1 modeling

The RACK1 variants were modeled using SWISS-MODEL[34–38]. Briefly, the RACK1 variant amino acid sequences were entered into the SWISS-MODEL server. The SWISS-MODEL software generates a list of potential structural templates based on the input. The software then aligns and models the input RACK1 variants on the selected templates and subsequently evaluates the quality of the model. Templates are then selected initially based on the GMQE score, coverage, and resolution. A final template is then selected based on the QMEAN score. Here, all RACK1 variants aligned and modeled well with the 4aow.1.A template, an X-ray crystallography generated structure of human RACK1[39].

4.5.7 Bioinformatic and structural analysis

Sequence analysis of RACK1 and ribosomal protein amino acid sequences was done by alignment using the Clustal Omega multiple sequence alignment tool[39]. The NCBI blastp suit was used to perform pair-wise sequence identity analysis on RACK1 amino acid sequences[40,41]. The secondary structure prediction was performed using the Quick2D tool in the MPI Bioinformatics Toolkit[42–48]. All structural alignments were performed using PyMOL (Schrodinger LLC.). The resulting *de novo* PfRACK1 model was added to the previously generated *P. falciparum* 80S structure (3JBO)[23]. First, the *de novo* PfRACK1 model was structurally aligned to the human RACK1 protein found in the previously generated *H. sapiens* 80S structure (3JAG)[49]. The *P. falciparum* 80S structure was then structurally to the *H. sapiens* 80S structure. Interacting residues between the 80S ribosome and RACK1 protein were those found to be within a 3-5 Å range.

4.5.8 RACK1 variant construction

The PfRACK1 gene was codon optimized for expression in human cells. The HsRACK1 gene was cloned from cDNA. None of the expressed RACK1 variants have the typical intron that appears to be conserved in the gene. Based on bioinformatic and structural analysis, RACK1 variants were designed. The swapping of the N-terminal regions, and other mutants were generated by mutagenesis PCR, whereby the 5’ and 3’ PCR products were produced overlapping in the mutated regions. These products were combined by stitching PCR and cloned into the desired

expression vectors. Clones of vectors with RACK1 variants were confirmed by Sanger sequencing.

4.5.9 Crude ribosome preparation and polysome profiling

Crude ribosome pellets and polysome profiling in *P. falciparum* cells was done based on previous work[24]. Parasites were grown to 7-10% parasitemia in 1.5 to 2.0 mL of packed iRBCs. Parasites were treated with culture medium containing 200 µM cyclohexamide (CHX) for 10 minutes at 37℃. They were then washed three times with 1X PBS + 200 µM CHX. Samples were then flash-frozen in liquid nitrogen and stored at -80℃ overnight. To the frozen samples, 2 volumes of lysis buffer (25 mM potassium HEPES pH 7.2, 400 mM potassium acetate, 15 mM magnesium acetate, 1% IGEPAL® CA-360, 200 µM CHX, 1 mM DTT, 1 mM AEBSF, 40 U/mL RNase inhibitor) and 0.5 mg of acid washed glass beads (Sigma #G8772) were added. Samples were rotated end-over-end at 4℃ for 10 minutes. Samples were centrifugated for 5 minutes at 1000xg. Supernatants were transferred to a new tube and centrifugated at 14000 x g for 10 minutes. The supernatant was layered over 1 M sucrose cushion (1 M sucrose, 25 mM potassium HEPES pH 7.2, 400 mM potassium acetate, 15 mM magnesium acetate, 200 µM CHX, 1 mM DTT, 1 mM AEBSF, 40 U/mL RNase inhibitor) in a ratio of 2 mL lysate to 1 mL sucrose cushion. The balanced tubes were then placed in a TLA 100.3 rotor and centrifuged for 30 minutes at 335,000 x g at 4℃ using an Optima™ Max-XP Beckman Coulter ultracentrifuge. The supernatants were removed. The crude ribosome pellets were washed with 500 µL wash buffer (25 mM potassium HEPES pH 7.2, 400 mM potassium acetate, 15 mM magnesium acetate, 200

µM CHX, 1 mM DTT, 0.1 mM AEBSF, 10 U/mL RNase inhibitor) three times. After washing, the crude ribosome pellets were then resuspended in 200 µL of lysis buffer. The resuspensions were again layered over 1 mL of 1 M sucrose cushion and the pelleting repeated as above. Washing was repeated as previous. The crude ribosome pellets used in polysome profiling were then resuspended in 200 µL of ribosome resuspension buffer and, if not immediately used, flash frozen in liquid nitrogen and store at -80℃ for later use. Crude ribosome pellets used for immunoblotting were resuspended in sample buffer at 37℃ for 20 minutes, boiled at 95℃ for 5 minutes, and chilled on ice. Sucrose gradients were generated using polysome profiling buffer (25 mM potassium HEPES pH 7.2, 400 mM potassium acetate, 15 mM magnesium acetate, 200 µM CHX, 1 mM DTT, 1 mM AEBSF) with 10%, 20%, 30%, 40%, and 50% sucrose layers in 14 mm x 89 mm polyallomer centrifuge tubes (Beckman #331372). Total RNA of resuspended crude ribosomes was measured to ensure a minimum of 300 µg total was loaded onto the gradient. Samples were layered over the gradient and balanced using polysome profiling buffer. The gradients were centrifuged at 35,000 RPM (acceleration 3, deceleration 4) for 2 hours and 40 minutes at 4℃ using an Optima™ L-100 XP Beckman Coulter ultracentrifuge in a SW41 swing bucket rotor. Centrifuged gradients were then fractionated using a density gradient fractionation system (BRANDEL #BR188176). Samples were collected into 1.7 mL microcentrifuge tubes with an equal volume of Ribozol™ (VWR #VWRVN580) with 1% SDS for RNA or 3 volumes of 20% TCA in MilliQ water for protein. Samples were mixed by vortexing. RNA was stored at -80℃ if not isolated immediately. RNA was isolated following manufacturer protocol and used in RNA gel electrophoresis. Protein samples were stored or incubated at 4℃

overnight to precipitate protein. Samples were then centrifuge at 20,000 x g, 4℃ for 30 minutes. Supernatant was removed. The pellets were washed with 100% acetone twice. Pellets were then solubilized in sample buffer for western blot analysis.

Crude ribosome pellets and polysome profiling in mammalian cells was done based on previous work[50]. HAP1 cells were grown to 80-90% confluency in a 10 cm dish. Cells were washed three times with 5 mL of ice-cold PBS + 200 µM CHX. A 400 µL volume of lysis buffer (20 mM Tris-HCl pH 7.4, 150 mM NaCl, 5 mM $MgCl_2$, 1% v/v Triton X-100, 200 µM CHX, 1 mM DTT, 1 mM AEBSF, 40 U/mL RNase inhibitor) was then added dropwise to the place and cells were scraped off and collected into a 1.7 mL microcentrifuge tube. The lysate was pipetted several times and incubated on ice for 10 minutes. The samples were then centrifugated at 20,000 x g for 10 minutes at 4℃ to remove cell debris. The lysate was transferred into a new tube. If not used immediately, lysates were flash frozen in liquid nitrogen and stored at -80℃. Crude ribosome pellets were generated by layering 200 µL of lysate over 0.9 mL of 1M sucrose cushion (1 M sucrose, 20 mM Tris-HCl pH 7.4, 150 mM NaCl, 5 mM $MgCl_2$, 200 µM CHX, 1 mM DTT, 1 mM AEBSF, 40 U/mL RNase inhibitor). The balanced tubes were then placed in a TLA 100.3 rotor and centrifuged for 1 hour at 100,000 x g at 4℃ using an Optima™ Max-XP Beckman Coulter ultracentrifuge. The supernatants were removed. The crude ribosome pellets were washed with 500 µL wash buffer (20 mM Tris-HCl pH 7.4, 150 mM NaCl, 5 mM $MgCl_2$, 0.1% v/v Tween 20, 200 µM CHX, 1 mM DTT, 0.1 mM AEBSF, 10 U/mL RNase inhibitor) three times. Crude ribosome pellets used for immunoblotting were resuspended in sample buffer at 37℃ for 20 minutes, boiled at 95℃ for 5 minutes, and chilled on ice. Polysome profiling was performed by

layering clarified HAP1 cell lysates over sucrose gradient generated with polysome profiling buffer (20 mM Tris-HCl pH 7.4, 150 mM NaCl, 5 mM $MgCl_2$, 200 µM CHX, 1 mM DTT, 1 mM AEBSF, 40 U/mL RNase inhibitor) and centrifugation performed as above. Samples were collected and isolated at above for RNA gel electrophoresis and western blot analysis.

4.5.10 Immunoblotting

Samples were loaded onto SDS-PAGE gels, running at 15 W, 1h 10 mins. The gels were then transferred to PVDF membrane using semi-dry transfer method running at 25 V for 40 minutes. The PVDF membranes were blocked in 5% milk in PBS + 0.1% Tween 20 (PBST) for 1 hour at room temperature or overnight at 4℃. The membranes were probed with diluted primary antibody (see **SUPPLEMENTARY TABLE 4.3** for antibodies) in PBST with 5% milk. After incubation with the primary antibody, the PVDF membranes were washed three times for 5 min in PBST. Membranes incubated with HRP-conjugated primaries were incubated and washed similarly, washing with PBST, and then proceeding to imaging instead of secondary. The membranes were then incubated with HRP-conjugated secondary antibody diluted 1:2500 in PBST with 5% milk for 1 hour at room temperature. The membranes were washed as above. Then rinsed with PBS. Prepare Working Solution by mixing equal parts of the Stable Peroxide Solution and the Luminol/Enhancer Solution (34577 SUPERSIGNAL WEST PICO PLUS, 34096 SUPERSIGNAL WEST FEMTO MAXIMUM SENSITIVITY SUBSTRATE respectively). We incubate the blot in Working Solution for 5 minutes. Remove the blot from Working Solution and drain excess reagent. Afterward we took images were generated by BioRad Molecular Imager CHemiDoc XRS System with Image Lab software.

4.5.11 Polysome rRNA analysis by RT-qPCR

RNA isolated from polysome profiling fractions were qPCR. Using the NanoDrop 2000c, 50 ng of total RNA was used to generate cDNA via the iScript Advance cDNA Kit for RT-qPCR (BioRAD #1725037), for each sample including no reverse transcriptase and no template controls following the manufacturer's protocol. The iTaq Universal SYBR Green Supermix (BioRAD #1725121) protocol was used for qRT-PCR on the CFX96 Real-Time system with Bio-Rad CFX Manager 3.0 software[51]. The 2^{-Ct} value were calculated and plotted for each fraction.

4.5.12 HA-tag immunoprecipitation of *P. falciparum* Dd2 expressed RACK1 variants

Mixed *Plasmodium falciparum* Dd2 parasites were harvested at 7-10% parasitemia. For examination of RACK1 variant expression, parasites were released from RBCs by saponin lysis as previously described. Parasites were then lysed using passive lysis buffer (Promega #E1910) and the total protein concentration was calculated by RC/DC kit (BioRad #5000122). For each reaction, 25 µL of magnetic HA beads was washed twice in 1X PBS with 0.1% Tween 20 and then twice in binding buffer (50 mM Tris pH7.5, 150 mM NaCl, 1% IGEPAL CA-630, 5% glycerol, and protease inhibitors (Thermo Fisher #A32955): apoptin, leupeptin, bestatin, E-64, AEBSF, pepstatin A). A total of 500 µg of protein was loaded onto the HA beads and bound overnight at 4℃. The beads were then washed three times with 1 mL of wash buffer (50 mM Tris pH7.5, 150 mM NaCl, 1% IGEPAL CA-630, 5% glycerol). Beads were then eluted in 50 µL of sample buffer and examined by western blot analysis.

4.5.13 Analysis of RACK1 variant rRNA binding by HA immunoprecipitation in *P. falciparum* parasites

Mixed *Plasmodium falciparum* Dd2 parasites were harvested at 7-10% parasitemia. Parasites were released lysed and crude ribosome pellets were generated as previously described. The total protein concentration in each crude ribosome pellet was calculated by RC/DC kit (BioRad #5000122). For each HA immunoprecipitation, 50 µL of magnetic HA beads was washed three times with 1X PBS + 0.1% Tween 20 followed by three washes with polysome parasite lysis buffer. The beads were then blocked with polysome parasite lysis buffer containing 4% BSA and 0.5 µg/mL *S. cerevisiae* tRNAs for one hour at 4℃ while rotating. A total of 680 µg of protein was loaded onto the HA beads and bound for one hour at 4℃ while rotating. The beads were then washed three times with 1 mL of polysome wash buffer. Beads were split in half. For protein, beads were then eluted in 35 µL of sample buffer and examined by western blot analysis as previously described. For RNA, beads were eluted with 400 µL Trizol + 1% SDS at 36℃ while shaking. RNA was isolated by per the manufacturer's protocol. Using the NanoDrop 2000c, 50 ng of total RNA was used to generate cDNA via the iScript Advance cDNA Kit for RT-qPCR (BioRAD #1725037), for each sample including no reverse transcriptase and no template controls following the manufacturer's protocol. The iTaq Universal SYBR Green Supermix (BioRAD #1725121) protocol was used for qRT-PCR on the CFX96 Real-Time system with Bio-Rad CFX Manager 3.0 software[51]. The ΔCt was calculated by subtracting the Dd2 parent line values from each sample. The ΔΔCt value was then calculated by normalization to the wild-type PfRACK1 variant. Plots were then generated using the calculated $2^{-\Delta\Delta Ct}$ values for each variant.

4.6 References

1. Jain, B. P. & Pandey, S. WD40 Repeat Proteins: Signalling Scaffold with Diverse Functions. *Protein J.* **37**, 391–406 (2018).

2. Li, D. & Roberts, R. Human Genome and Diseases: WD-repeat proteins: structure characteristics, biological function, and their involvement in human diseases. *Cell. Mol. Life Sci.* **58**, 2085–2097 (2001).

3. Ron, D. *et al.* Cloning of an intracellular receptor for protein kinase C: a homolog of the beta subunit of G proteins. *Proc. Natl. Acad. Sci.* **91**, 839–843 (1994).

4. Smith, T. F., Gaitatzes, C., Saxena, K. & Neer, E. J. The WD repeat: a common architecture for diverse functions. *Trends Biochem. Sci.* **24**, 181–185 (1999).

5. Yuan, L. *et al.* A RACK1-like protein regulates hyphal morphogenesis, root entry and in vivo virulence in Verticillium dahliae. *Fungal Genet. Biol.* **99**, 52–61 (2017).

6. Bradford, W. *et al.* Eukaryotic G Protein Signaling Evolved to Require G Protein-Coupled Receptors for Activation. *Sci. Signal.* **6**, ra37–ra37 (2013).

7. Adams, D. R., Ron, D. & Kiely, P. A. RACK1, A multifaceted scaffolding protein: Structure and function. *Cell Commun. Signal.* **9**, 22 (2011).

8. Smith, B. L. & Mochly-Rosen, D. Inhibition of protein kinase C function by injection of intracellular receptors for the enzyme. *Biochem. Biophys. Res. Commun.* **188**, 1235–1240

(1992).

9. Johnson, A. G. *et al.* RACK1 on and off the ribosome. *RNA* **25**, 881–895 (2019).

10. Gallo, S. *et al.* RACK1 Specifically Regulates Translation through Its Binding to Ribosomes. *Mol. Cell. Biol.* **38**, 1–16 (2018).

11. Sengupta, J. *et al.* Identification of the versatile scaffold protein RACK1 on the eukaryotic ribosome by cryo-EM. *Nat. Struct. Mol. Biol.* **11**, 957–962 (2004).

12. Thompson, M. K., Rojas-Duran, M. F., Gangaramani, P. & Gilbert, W. V. The ribosomal protein Asc1/RACK1 is required for efficient translation of short mRNAs. *Elife* **5**, 1–20 (2016).

13. Nilsson, J., Sengupta, J., Frank, J. & Nissen, P. Regulation of eukaryotic translation by the RACK1 protein: a platform for signalling molecules on the ribosome. *EMBO Rep.* **5**, 1137–1141 (2004).

14. Kouba, T., Rutkai, E., Karásková, M. & Valášek, L. S. The eIF3c/NIP1 PCI domain interacts with RNA and RACK1/ASC1 and promotes assembly of translation preinitiation complexes. *Nucleic Acids Res.* **40**, 2683–2699 (2012).

15. Ceci, M. *et al.* Release of eIF6 (p27BBP) from the 60S subunit allows 80S ribosome assembly. *Nature* **426**, 579–584 (2003).

16. Sugiyama, T. *et al.* Sequential Ubiquitination of Ribosomal Protein uS3 Triggers the

Degradation of Non-functional 18S rRNA. *Cell Rep.* **26**, 3400-3415.e7 (2019).

17. Joazeiro, C. A. P. Ribosomal Stalling During Translation: Providing Substrates for Ribosome-Associated Protein Quality Control. *Annu. Rev. Cell Dev. Biol.* **33**, 343–368 (2017).

18. Kuroha, K. *et al.* Receptor for activated C kinase 1 stimulates nascent polypeptide-dependent translation arrest. *EMBO Rep.* **11**, 956–961 (2010).

19. Ikeuchi, K., Yazaki, E., Kudo, K. & Inada, T. Conserved functions of human Pelota in mRNA quality control of nonstop mRNA. *FEBS Lett.* **590**, 3254–3263 (2016).

20. Sundaramoorthy, E. *et al.* ZNF598 and RACK1 Regulate Mammalian Ribosome-Associated Quality Control Function by Mediating Regulatory 40S Ribosomal Ubiquitylation. *Mol. Cell* **65**, 751-760.e4 (2017).

21. Blomqvist, K., DiPetrillo, C., Streva, V. A., Pine, S. & Dvorin, J. D. Receptor for Activated C-Kinase 1 (PfRACK1) is required for Plasmodium falciparum intra-erythrocytic proliferation. *Mol. Biochem. Parasitol.* **211**, 62–66 (2017).

22. Wong, W. *et al.* Cryo-EM structure of the Plasmodium falciparum 80S ribosome bound to the anti-protozoan drug emetine. *Elife* **3**, (2014).

23. Sun, M. *et al.* Dynamical features of the Plasmodium falciparum ribosome during translation. *Nucleic Acids Res.* **43**, gkv991 (2015).

24. Bunnik, E. M. *et al.* The mRNA-bound proteome of the human malaria parasite Plasmodium falciparum. *Genome Biol.* **17**, 1–18 (2016).

25. Nielsen, M. H., Flygaard, R. K. & Jenner, L. B. Structural analysis of ribosomal RACK1 and its role in translational control. *Cell. Signal.* **35**, 272–281 (2017).

26. Hale, V. L. *et al.* Parasitophorous vacuole poration precedes its rupture and rapid host erythrocyte cytoskeleton collapse in Plasmodium falciparum egress. *Proc. Natl. Acad. Sci.* **114**, 3439–3444 (2017).

27. von Bohl, A. *et al.* A WD40-repeat protein unique to malaria parasites associates with adhesion protein complexes and is crucial for blood stage progeny. *Malar. J.* **14**, 435 (2015).

28. Caro, F., Ahyong, V., Betegon, M. & DeRisi, J. L. Genome-wide regulatory dynamics of translation in the Plasmodium falciparum asexual blood stages. *Elife* **3**, 1–24 (2014).

29. Trager, W. & Jensen, J. B. Human malaria parasites in continuous culture. 1976. *J. Parasitol.* **91**, 484–6 (2005).

30. Fidock, D. A. & Wellems, T. E. Transformation with human dihydrofolate reductase renders malaria parasites insensitive to WR99210 but does not affect the intrinsic activity of proguanil. *Proc. Natl. Acad. Sci.* **94**, 10931–10936 (1997).

31. Aurrecoechea, C. *et al.* PlasmoDB: a functional genomic database for malaria parasites. *Nucleic Acids Res.* **37**, D539–D543 (2009).

32. López-Barragán, M. J. *et al.* Directional gene expression and antisense transcripts in sexual and asexual stages of Plasmodium falciparum. *BMC Genomics* **12**, 587 (2011).

33. Zanghì, G. *et al.* A Specific PfEMP1 Is Expressed in P. falciparum Sporozoites and Plays a Role in Hepatocyte Infection. *Cell Rep.* **22**, 2951–2963 (2018).

34. Waterhouse, A. *et al.* SWISS-MODEL: homology modelling of protein structures and complexes. *Nucleic Acids Res.* **46**, W296–W303 (2018).

35. Bienert, S. *et al.* The SWISS-MODEL Repository—new features and functionality. *Nucleic Acids Res.* **45**, D313–D319 (2017).

36. Guex, N., Peitsch, M. C. & Schwede, T. Automated comparative protein structure modeling with SWISS-MODEL and Swiss-PdbViewer: A historical perspective. *Electrophoresis* **30**, S162–S173 (2009).

37. Studer, G. *et al.* QMEANDisCo—distance constraints applied on model quality estimation. *Bioinformatics* **36**, 1765–1771 (2020).

38. Bertoni, M., Kiefer, F., Biasini, M., Bordoli, L. & Schwede, T. Modeling protein quaternary structure of homo- and hetero-oligomers beyond binary interactions by homology. *Sci. Rep.* **7**, 10480 (2017).

39. Ruiz Carrillo, D. *et al.* Structure of human Rack1 protein at a resolution of 2.45 Å. *Acta Crystallogr. Sect. F Struct. Biol. Cryst. Commun.* **68**, 867–872 (2012).

40. Altschul, S. F. *et al.* Protein database searches using compositionally adjusted substitution matrices. *FEBS J.* **272**, 5101–5109 (2005).

41. Altschul, S. Gapped BLAST and PSI-BLAST: a new generation of protein database search programs. *Nucleic Acids Res.* **25**, 3389–3402 (1997).

42. Zimmermann, L. *et al.* A Completely Reimplemented MPI Bioinformatics Toolkit with a New HHpred Server at its Core. *J. Mol. Biol.* **430**, 2237–2243 (2018).

43. Klausen, M. S. *et al.* NetSurfP-2.0: Improved prediction of protein structural features by integrated deep learning. *Proteins Struct. Funct. Bioinforma.* **87**, 520–527 (2019).

44. Hanson, J., Yang, Y., Paliwal, K. & Zhou, Y. Improving protein disorder prediction by deep bidirectional long short-term memory recurrent neural networks. *Bioinformatics* btw678 (2016). doi:10.1093/bioinformatics/btw678

45. Jones, D. T. & Cozzetto, D. DISOPRED3: precise disordered region predictions with annotated protein-binding activity. *Bioinformatics* **31**, 857–863 (2015).

46. Yan, R., Xu, D., Yang, J., Walker, S. & Zhang, Y. A comparative assessment and analysis of 20 representative sequence alignment methods for protein structure prediction. *Sci. Rep.* **3**, 2619 (2013).

47. Heffernan, R., Yang, Y., Paliwal, K. & Zhou, Y. Capturing non-local interactions by long short-term memory bidirectional recurrent neural networks for improving prediction of protein secondary structure, backbone angles, contact numbers and solvent accessibility.

Bioinformatics **33**, 2842–2849 (2017).

48. Jones, D. T. Protein secondary structure prediction based on position-specific scoring matrices 1 1Edited by G. Von Heijne. *J. Mol. Biol.* **292**, 195–202 (1999).

49. Brown, A., Shao, S., Murray, J., Hegde, R. S. & Ramakrishnan, V. Structural basis for stop codon recognition in eukaryotes. *Nature* **524**, 493–496 (2015).

50. McGlincy, N. J. & Ingolia, N. T. Transcriptome-wide measurement of translation by ribosome profiling. *Methods* **126**, 112–129 (2017).

51. Arthur, L. L. *et al.* Translational control by lysine-encoding A-rich sequences. *Sci. Adv.* **1**, e1500154 (2015).

52. The UniProt Consortium. UniProt: a worldwide hub of protein knowledge. *Nucleic Acids Res.* **47**, D506–D515 (2019).

53. Sievers, F. *et al.* Fast, scalable generation of high-quality protein multiple sequence alignments using Clustal Omega. *Mol. Syst. Biol.* **7**, 539 (2011).

4.7 Supplemental Material

SUPPLEMENTAL FIGURE 4.1 | Multiple sequence alignment of *H. sapiens* and *P. falciparum* RPS3 (uS3), RPS16 (uS9), RPS17 (eS17) proteins. The *H. sapiens* and *P. falciparum* sequences were collected from the UniProt database[52] and PlasmoDB[31], respectively, and aligned using the Clustal Ω MSA tool[53]. Residues in the 3-5 Å range were determined using PyMol.

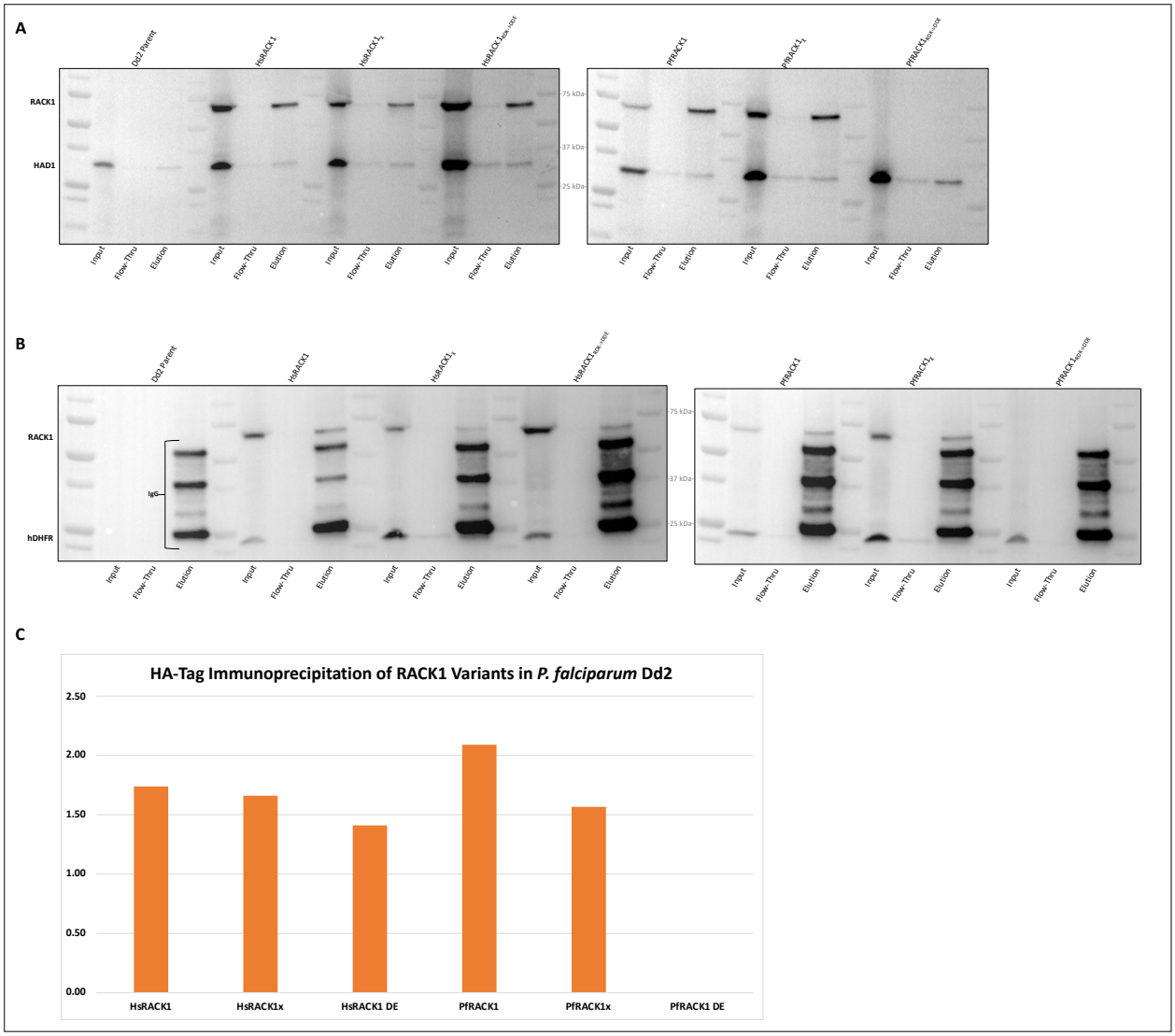

SUPPLEMENTAL FIGURE 4.2 | HA-immunoprecipitation of RACK1 variants expressed in *P. falciparum* Dd2. (A) Samples were blotted with mouse anti-HA-HRP antibody and rabbit anti-PfHAD1/anti-rabbit-HRP. **(B)** Samples were blotted with mouse anti-HA and mouse anti-hDHFR antibodies and subsequently blotted with anti-mouse-HRP antibody. **(C)** Quantification of HA-immunoprecipitation using HAD1 to normalize lanes and calculation of the subsequent ratio of elution to input.

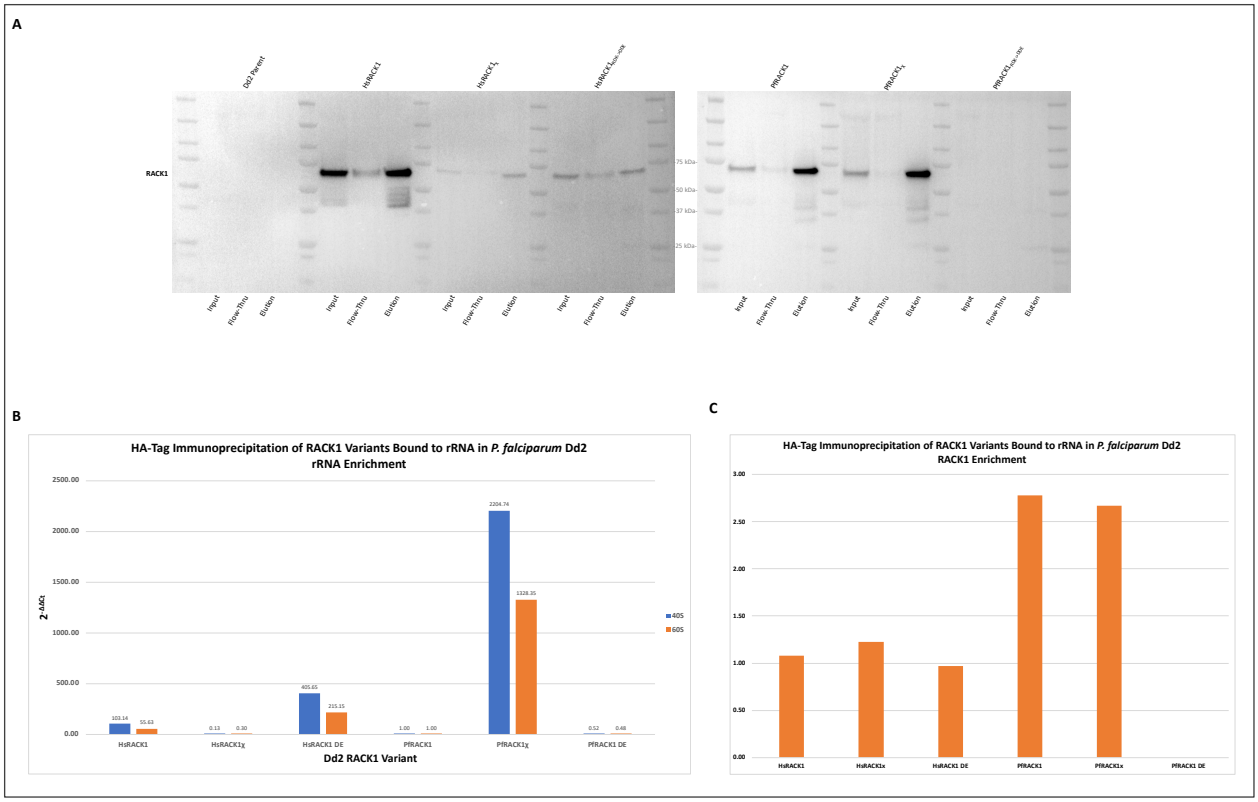

SUPPLEMENTAL FIGURE 4.3 | HA-immunoprecipitation of RACK1 variants bound to rRNA expressed in *P. falciparum* Dd2. (A) Samples were blotted with mouse anti-HA-HRP antibody to show enrichment of HA-tagged RACK1 variants. **(B)** RT-qPCR was performed on RNA isolated from HA-immunoprecipitations. Samples were normalized to Dd2 parent line and then to the PfRACK1 wild type variant. The $2^{-\Delta\Delta Ct}$ was calculated and plotted for each RACK1 variant. **(C)** Quantification of HA-immunoprecipitation calculating ratio of elution to input for each RACK1 variant.

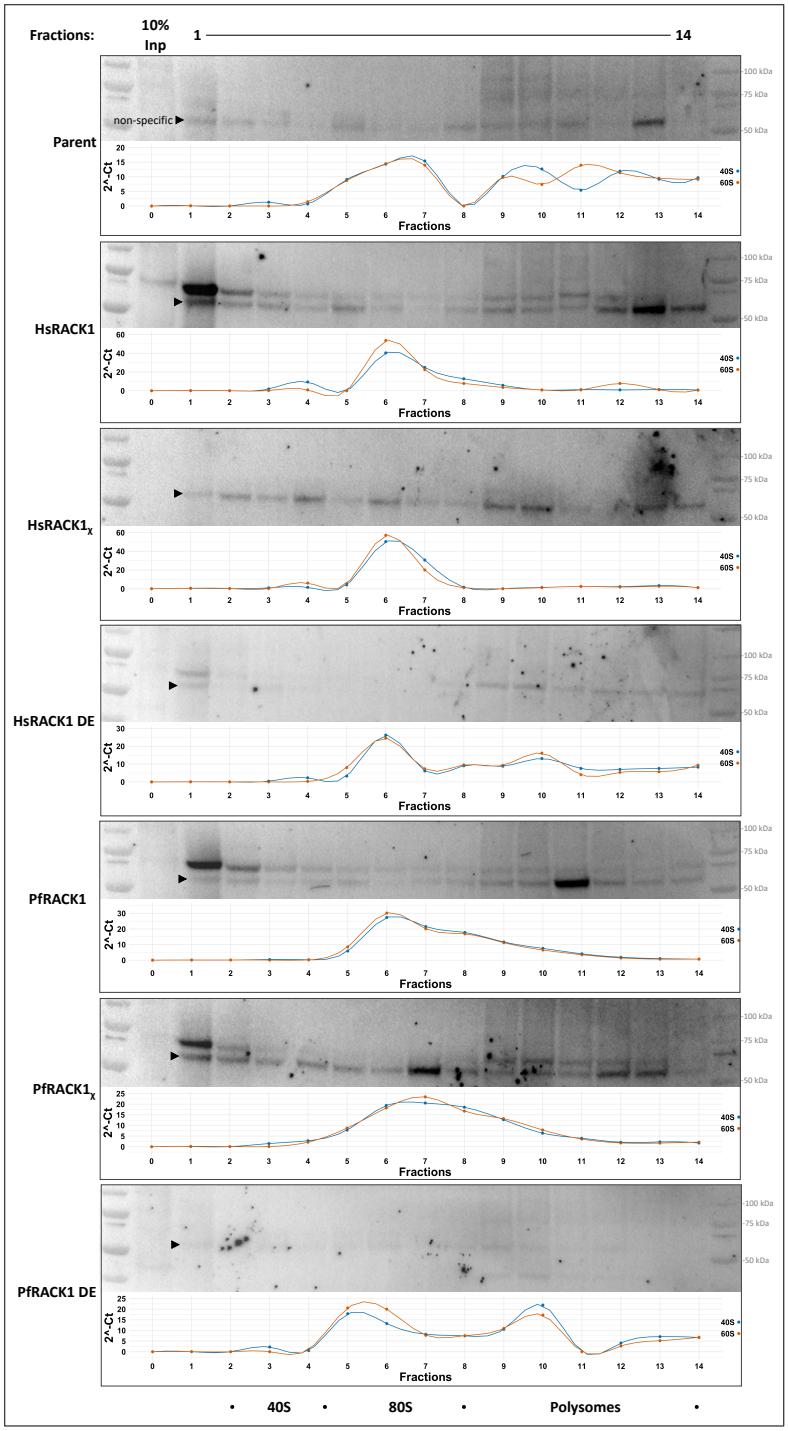

SUPPLEMENTAL FIGURE 4.4 | Polysome profiling of RACK1 variants in *P. falciparum* parasites. Polysome profiling fractions generated from *P. falciparum* parasites expressing RACK1 variants were analyzed. Western blot shows RACK1 variant polysome fraction localization. RT-qPCR analysis shows localization of 18S and 28S rRNAs associated with the 40S and 80S subunits, respectively. Arrowhead indicates non-specific band found in parent line not correlating to RACK1 variants.

SUPPLEMENTARY TABLE 4.1 | Cloning Primers and oligonucleotides.

Primer/Oligo Name	Sequence [5'→3']
PfRACK1R1	AACTGAGTGTTTTTTAACTTCATATAC
PfRACK1XhoIF1	cgcgCTCGAGATGgTaGATAATATAAAAGAAGCTG
HsRACK1FlagF1	GACTACAAAGACCATGACGGTGATTATAAAGATCATGACATCGATTACAAGGAT GACGATGACAAGATGACTGAGCAGATGACCC
HsRACK1Not1R1	gcgGCGGCCGCCTAGCGTGTGCCAATGGTC
rcPfRACK1FlagF1	GACTACAAAGACCATGACGGTGATTATAAAGATCATGACATCGATTACAAGGAT GACGATGACAAGATGATGGACAACATCAAAGAGG
rcPfRACK1Not1R1	gcgGCGGCCGCTCAGACGCTGTGCTTCTTC
FlagXbaIF1	gcgTCTAGAATGGACTACAAAGACCATGACGG
NtermHsrcPFRACK1F1	cctcagatggccagtttgccctc agcggctcttgggatcac
NtermHsrcPfRACK1R1	gtgatcccaagagccgct gagggcaaactggccatctg
NtermrcPfHsRACK1F1	gcgacggcctgtttgccctg tcaggctcctgggatggaacc
NtermrcPfHsRACK1R1	ggttccatcccaggagcctga cagggcaaacaggccgtcgc
mNeonGreenHsRACK1F1	GGTGACCATTGGCACACGC gctagc GGAAGTGGAGGAGTGAGCAAG
mNeonGreenrcPfRACK1F1	CGAAGTGAAGAAGCACAGCGTC gctagc GGAAGTGGAGGAGTGAGCAAG
HAStpNotIR1	gcg gcggccgc TCAGGCATAATCTGGAACATCGTAAGG
mNeonGreenStpNotIR1	gcg gcggccgc TCACTTGTACAGCTCGTCCATGCC
HsRACK1SalIF1	gcgc gtcgac ATGACTGAGCAGATGACCCTTCG
HsRACK1mNeonGreenR1	CTTGCTCACTCCTCCACTTCC gctagc GCGTGTGCCAATGGTCACC
rcPfRACK1SalIF1	gcgc gtcgac ATGATGGACAACATCAAAGAGGCC
rcPfRACK1mNeonGreenR1	CTTGCTCACTCCTCCACTTCC gctagc GACGCTGTGCTTCTTCACTTCG
FlagAvrIIF1	gcg cctagg GACTACAAAGACCATGACGG
FlagStpNotIR1	gcg gcggccgc TCACTTGTCATCGTCATCCTTGT
HsRACK1DEMutF1	CATGATCCTCTCCGCCTCT GACGATGAG ACCATCATCATGTGGAAACTGAC

HsRACK1DEMutR1	GTCAGTTTCCACATGATGATGGT CTCATCGTC AGAGGCGGAGAGGATCATG
rcPfRACK1DEMutF1	CCATCGTGTCCGCCAGC GACGACGAG AAACTGATCGTGTGGAACATCAAC
rcPfRACK1DEMutR1	GTTGATGTTCCACACGATCAGTTT CTCGTCGTC GCTGGCGGACACGATGG
HsRACk1mutF1 (IPQRALR -> TAKKSLT)	CCAGGGATGAGACCAACTATGGA acagccaagaagtctctgaca GGTCACTCCCACTTTGTTAGTGATG
HsRACk1mutR1 (IPQRALR -> TAKKSLT)	CATCACTAACAAAGTGGGAGTGACC tgtcagagacttcttggctgt TCCATAGTTGGTCTCATCCCTGG
rcPfRACK1mutF1 (TAKKSLT -> IPQRALR)	GACAGCGGCGAGATCGGC attccacagcgtgctctgcgg GGCCACAGCCAGGCC
rcPfRACK1mutR1 (TAKKSLT -> IPQRALR)	GGCCTGGCTGTGGCC ccgcagagcacgctgtggaat GCCGATCTCGCCGCTGTC
HsRACK1ybbREag1R1	gcg CGGCCG CTA GGCCAGCTTGCTGGCGATGAACTCCAGGCTGTC GCGTGTGCCAATGG
rcPfRACK1ybbREag1R1	gcg CGGCCG TCA GGCCAGCTTGCTGGCGATGAACTCCAGGCTGTC GACGCTGTGCTTCT
HsRACK1mutF2 (QFPD -> PKLK)	CCCAGATCGCTACTACCCCG cccaagctgaaa ATGATCCTCTCCGCCTCTCG
HsRACK1mutR2 (QFPD -> PKLK)	CGAGAGGCGGAGAGGATCAT tttcagcttggg CGGGGTAGTAGCGATCTGGG
rcPfRACK1mutF2 (PKLK -> QFPD)	GCGTGTCCACACCTACAGAC cagttcccggac ACCATCGTGTCCGCCAGCCG
rcPfRACK1mutR2 (PKLK -> QFPD)	CGGCTGGCGGACACGATGGT gtccgggaactg GTCTGTAGGTGTGGACACGC
HsRACK1mutF3 (TRDETNYG -> NTDDDSGE	aacaccgacgacgacagcggcgag ATTCCACAGCGTGCTCTGCG
HsRACK1mutR3 (TRDETNYG -> NTDDDSGE	ctcgccgctgtcgtcgtcggtgtt CAGTTTCCACATGATGATGGTCTTATCTCG
rcPfRACK1mutF3 (NTDDDSGE -> TRDETNYG)	accagggatgagaccaactatgga ATCGGCACAGCCAAGAAGTCTC
rcPfRACK1mutR3 (NTDDDSGE -> TRDETNYG)	tccatagttggtctcatccctggt GATGTTCCACACGATCAGTTTCTTGTCC
HsRACK1mutF4 (GHNG -> GGHSD)	CTTCGTGGCACCCTCAAG ggcggacactctgat TGGGTAACCCAGATCGCTACTAC
HsRACK1mutR4 (GHNG -> GGHSD)	GTAGTAGCGATCTGGGTTACCCA atcagagtgtccgcc CTTGAGGGTGCCACGAAG

rcPfRACK1mutF4 (GGHSD -> GHNG)	TGCGGGGAGTTCTGGAA ggccacaacggc TGGGTCACCAGCGTGTC
rcPfRACK1mutR4 (GGHSD -> GHNG)	GACACGCTGGTGACCCA gccgttgtggcc TTCCAGAACTCCCCGCA

SUPPLEMENTARY TABLE 4.2 | RT-qPCR Primers.

Primer/Oligo Name	Sequence [5'→3']
Pf18SAtypqPCR_F2 (WT A-type)	GTATATATATATTTTATATGTAGAAACTGCG
Pf18SAtypqPCR_R1b (WT A-type)	CAAATACTTATCCAAAGATAAAAATC
Pf28S_AqPCRF1 (WT A-type)	CGTAATAAATTTATTTTATTTAGTGTGTATCAATCG
Pf28S_qPCRR1 (WT A-type)	CTATTTAATTGCTCATTCCTGAGTAC

SUPPLEMENTARY TABLE 4.3 | Antibodies.

Designation	Identifier	Dilution
anti-Flag (mouse)	Sigma Cat # F1804-1MG	1:1000
anti-HA (mouse)	Santa Cruz # sc-7392 (F-7)	1:1000
anti-HA-HRP (mouse)	Santa Cruz #sc-7392 (F-7)	1:1000
anti-RPS16 (rabbit)	Sigma # SAB1100505	1:1000
anti-hDHFR (mouse)	Santa Cruz # sc-377091 (A-9)	1:1000
anti-mouse-HRP	Cell Signaling Cat # 7076S	1:2500
anti-rabbit-HRP	Cell Signaling Cat # 7076S	1:2500

Chapter 5: Future Directions

5.1 Translation fidelity, frame maintenance, and quality control in *P. falciparum*

To date, only the NMD pathway has been indirectly characterized in *P. falciparum*[1,2]. Like any other organism, *P. falciparum* must contend with all the issues surrounding the translation of mRNA into protein[3–12]. This suggests that these pathways might be necessary to ensure proper protein synthesis and subsequently parasite survival. However, with the exception of recent publish work[13], this area remains largely unexplored.

It has been demonstrated that polyA tracts are translated in *P. falciparum* with high fidelity, no apparently frameshifting, and do not elicit activation of quality control pathways[13]. While the lack of PfRACK1 on schizont-derived 80S ribosome structures[14,15] could be proposed as an adaptation of polyA tract translation, it conflicts with the data presented here in Chapter 4 and that of others[16]. It also poses a host of new problems when considering the protein's importance in translation initiation[17–22] and translation quality control mechanisms[5,6,9,12,23–27]. An absence of RACK1 would also not explain the lack of frameshifting on polyA tracts in the parasite[13,27]. Nor would it prevent the formation of the stall-inducing α-helical structure caused by consecutive adenosine π-stacking[6,7] within the conserved mRNA channel and decoding

center of the parasite[14,15]. The question remains: How does *P. falciparum* efficiently translation polyA tracts with high fidelity, while maintaining reading frame, and without eliciting translation-associated quality control mechanisms?

The parasite proteins discovered in Chapter 3 found to be differentially bound to mRNAs in a substrate-dependent manner may be responsible for the high-fidelity translation of polyA and structure-containing messages. The AU-rich RNA binding proteins, mRNA structure-binding proteins, and RNA helicases found to be bound to the mRNAs may be contributing to this fidelity and warrant further study. Proteins found on all mRNAs, particularly those unique to the parasite, perhaps with RNA helicase activity, and an association with the ribosome should not be overlooked. Previous work has demonstrated a precedence for parasite-specific helicases such as the kDDX60 RNA helicase found to be associated with the head of the 40S subunit in *Trypanosoma brucei brucei*, as well as other kinetoplastids, and thought to be associated with aiding 40S scanning of the highly methylated mRNA splice leader sequences in the organism[28]. Thus, *Plasmodium spp.* may also have evolved a genus specific protein to aid in polyA translation, but this protein may always be found on the ribosome or mRNA, unseen in structures so far due to purification techniques[29], and therefore remains elusive.

The answer may also be found in the recent work that has shown multi-protein bridging factor 1 (Mbf1), Rps3 (uS3), and yeast RACK1 homolog Asc1 are all involved in reading frame maintenance[27]. Wang et al., 2018 proposed that Asc1 acts to trigger abortive translation while

MBF1 and Rps3 work cooperatively to prevent stalled ribosomes from frameshifting[27]. An MBF1 homolog is present[30] in *P. falciparum*, is potentially essential[31], but has yet to be characterized. The *P. falciparum* MBF1 shows only a 37.96% shared identity with the yeast homology and 43.52% identity with the human homolog, but residues that result in frameshifting upon mutation are conserved in nature, if not entirely, with the yeast and human homologs[27]. Work in Chapter 4 describes the potential for PfRACK1 involvement given its conservation; as well as the conserved but altered nature of the PfRPS3 protein whereby it shares a relatively high identity with human (and yeast) homologs, but a truncation of the disordered C-terminal tail thought to be important for RQC-mediated quality control. Nevertheless, all residues implicated in frame maintenance are conserved in the parasite. Future study utilizing the methods developed in Chapter 3 combined with mutations in parasite proteins RACK1, MBF1, and RPS3 examining the effects and interactions of these proteins in *P. falciparum* are required, potentially providing insight into its hallmark, paradigm-breaking polyA translation ability.

5.2 Mechanism of ribosome switching in *P. falciparum*

The multiple, distinct ribosomes of *Plasmodium spp.* have been well documented[32,33,42,43,34–41]. Interestingly, whether 80S ribosome 60S and 40S subunit composition is homogeneously or heterogeneously has not been explored. It is known that the parasite actively regulates the dynamics of its heterogeneous ribosome population through increased transcription and ribosome degradation, which are associated with progression through the parasite life cycle and host temperature changes[35–37,42,44,45]. However, the factors involved in these processes remain unclear. Simplistically, how does the parasite know which rRNA gene expression to

increase and which rRNAs to degrade? Ribosome biogenesis is an energetically costly affair, and thus efficient ribosome maintenance would be a necessity for parasite survival[46–48].

While changes in temperature may explain increases and decreases in rRNA transcript production[45], how the parasite goes about actively selecting and degrading the most abundant RNA in the cell is ostensibly less clear. The notion of combing through thousands of ribosomes would be costly in and of itself. A self-reporting mechanism would be more efficient. The Non-functional Ribosome Decay (NRD) pathway is one such mechanism that would provide an eloquent means of selectively altering the parasite ribosome population by utilizing the inefficiency of a given ribosome type at a given temperature[4,10–12,49–53].

This pathway has yet to be discerned in *Plasmodium*, although evidence of its constituents can be found in PlasmoDB[30]. Given the conservation of the parasite ribosome decoding region[14,15], experiments could be performed using the methodologies developed in Chapter 3 combined with ribosomes harboring NRD-inducing mutations[4] to capture those factors involved. Future experimentation would then rely on inhibition of NRD factors, perhaps by knockdown, to examine changes in rRNA population dynamics at different temperatures.

5.3 Origin and evolution of homopolymeric tracts in *P. falciparum*

While polyadenosine (polyA) and polylysine (polyK) tracts in *Plasmodium spp.* are clearly linked, the factors driving their presence within the parasite genome may not be. *Plasmodium spp.* have gone to great lengths to enable the translation of polyA stretches in order to generate

polyK tract-containing proteins. While previous work has shown the presence[40,54,55] of these tracts and the ability to translate them without issue[13], why they exist is less understood.

Plasmodium spp. show not only an increase in intergenic AT-richness, but also that of the coding region, including the ribosomal RNA, which has not affected genome organization[13,40,56,57]. The factors driving polyA track retention in the parasite have been widely explored from lowered metabolic cost of A+T nucleotides, environmental factors like oxidative stress, nutrient availability, and an AT-driven positive feedback loop causing increased indels and amplicon breakpoints[40,55,58–64]. A specific mechanism for polyA retention remains unknown. However, it is likely driven by the combination of these factors with an additional factor being the production of proteins that contain polyK stretches, with the previous driving them to be encoded by polyA tracts.

While previous studies have attempted to the determine role of homopolymeric amino acids found in the parasite genome[40,65,66], such details remain elusive. Although polyK-containing proteins are found in all stages of the parasite, we did find that *Plasmodium* also has polyK enrichment in those proteins found in the cellular and pathological cell adhesion ontology group[13]. Thus, we have hypothesized that polyK may help with initial red blood cell (RBC) attachment and human immune system evasion. As the *Plasmodium* merozoite is non-motile, it relies on chance interaction with a new RBC driven by flow through the circulatory system. Therefore, having patches of charged protein could help to improve that initial cell-to-cell

adhesion, facilitating invasion. Homopolymeric lysine residues have been shown to make poor antigens[67], which may aid the parasite in host immune evasion for a majority of its proteins.

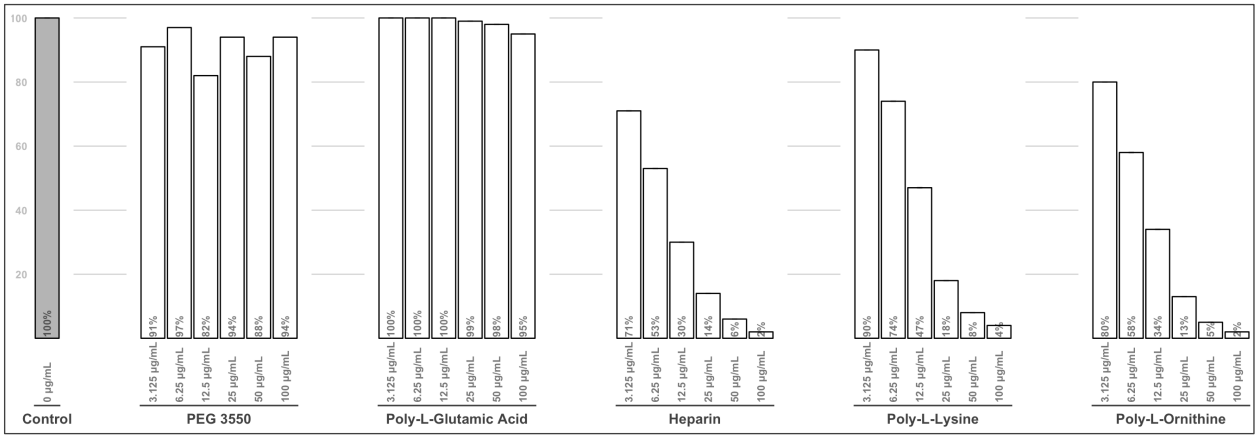

FIGURE 5.1 | Treatment of *P. falciparum* parasites with polyamino acids, heparin, and PEG 3550. Plasmodium falciparum parasites were treated with varying concentrations of PEG 3550, poly-L-glutamic acid, heparin, poly-L-lysine, and poly-L-ornithine for 96 hours in triplicate. Parasitemia for each concentration was calculated as a percentage of the untreated control.

Polylysine compounds has been previously employed as antimicrobials[68–71]. Interestingly, initial investigation of poly-L-lysine as an antimalarial showed that treatment of parasites with poly-L-lysine, and poly-L-ornithine, resulted in a significant reduction in parasitemia while the negatively charged poly-L-glutamic acid had no effect (**FIGURE 5.1**). These data suggest the potential for poly-L-lysine, poly-L-ornithine, as well as analogues or combination molecules, as antimalarials with great efficacy. The mechanism by which poly-L-lysine impacts parasitemia – be it through parasite invasion, development, or egress – requires further study. Elucidation of this mechanism, particularly *in vivo*, may provide insights into the long sought after function(s) of polyK tracts in *Plasmodium spp.* proteins.

5.4 References

1. Yeoh, L. M. *et al.* Alternative splicing is required for stage differentiation in malaria parasites. *Genome Biol.* **20**, 151 (2019).

2. Sorber, K., Dimon, M. T. & DeRisi, J. L. RNA-Seq analysis of splicing in Plasmodium falciparum uncovers new splice junctions, alternative splicing and splicing of antisense transcripts. *Nucleic Acids Res.* **39**, 3820–3835 (2011).

3. Cole, S. E., LaRiviere, F. J., Merrikh, C. N. & Moore, M. J. A Convergence of rRNA and mRNA Quality Control Pathways Revealed by Mechanistic Analysis of Nonfunctional rRNA Decay. *Mol. Cell* **34**, 440–450 (2009).

4. LaRiviere, F. J., Cole, S. E., Ferullo, D. J. & Moore, M. J. A Late-Acting Quality Control Process for Mature Eukaryotic rRNAs. *Mol. Cell* **24**, 619–626 (2006).

5. Karamyshev, A. L. & Karamysheva, Z. N. Lost in Translation: Ribosome-Associated mRNA and Protein Quality Controls. *Front. Genet.* **9**, 1–13 (2018).

6. Chandrasekaran, V. *et al.* Mechanism of ribosome stalling during translation of a poly(A) tail. *Nat. Struct. Mol. Biol.* **26**, 1132–1140 (2019).

7. Tesina, P. *et al.* Molecular mechanism of translational stalling by inhibitory codon combinations and poly(A) tracts. *EMBO J.* **39**, e103365 (2020).

8. Jackson, K. E. *et al.* Protein translation in Plasmodium parasites. *Trends Parasitol.* **27**, 467–476 (2011).

9. Joazeiro, C. A. P. Ribosomal Stalling During Translation: Providing Substrates for Ribosome-Associated Protein Quality Control. *Annu. Rev. Cell Dev. Biol.* **33**, 343–368 (2017).

10. Doma, M. K. & Parker, R. RNA Quality Control in Eukaryotes. *Cell* **131**, 660–668 (2007).

11. Houseley, J. & Tollervey, D. The Many Pathways of RNA Degradation. *Cell* **136**, 763–776 (2009).

12. Shoemaker, C. J. & Green, R. Translation drives mRNA quality control. *Nat. Struct. Mol. Biol.* **19**, 594–601 (2012).

13. Pavlovic Djuranovic, S., Erath, J., Andrews, R. J., Bayguinov, P. O. & Joyce, J. Plasmodium falciparum translational machinery condones polyadenosine repeats. *Elife* **9**, e57799 (2020).

14. Sun, M. *et al.* Dynamical features of the Plasmodium falciparum ribosome during

translation. *Nucleic Acids Res.* **43**, gkv991 (2015).

15. Wong, W. *et al.* Cryo-EM structure of the Plasmodium falciparum 80S ribosome bound to the anti-protozoan drug emetine. *Elife* **3**, (2014).

16. Bunnik, E. M. *et al.* The mRNA-bound proteome of the human malaria parasite Plasmodium falciparum. *Genome Biol.* **17**, 1–18 (2016).

17. Gallo, S. *et al.* RACK1 Specifically Regulates Translation through Its Binding to Ribosomes. *Mol. Cell. Biol.* **38**, 1–16 (2018).

18. Thompson, M. K., Rojas-Duran, M. F., Gangaramani, P. & Gilbert, W. V. The ribosomal protein Asc1/RACK1 is required for efficient translation of short mRNAs. *Elife* **5**, 1–20 (2016).

19. Kouba, T., Rutkai, E., Karásková, M. & Valášek, L. S. The eIF3c/NIP1 PCI domain interacts with RNA and RACK1/ASC1 and promotes assembly of translation preinitiation complexes. *Nucleic Acids Res.* **40**, 2683–2699 (2012).

20. Sengupta, J. *et al.* Identification of the versatile scaffold protein RACK1 on the eukaryotic ribosome by cryo-EM. *Nat. Struct. Mol. Biol.* **11**, 957–962 (2004).

21. Nilsson, J., Sengupta, J., Frank, J. & Nissen, P. Regulation of eukaryotic translation by the RACK1 protein: a platform for signalling molecules on the ribosome. *EMBO Rep.* **5**, 1137–1141 (2004).

22. Ceci, M. *et al.* Release of eIF6 (p27BBP) from the 60S subunit allows 80S ribosome assembly. *Nature* **426**, 579–584 (2003).

23. Sundaramoorthy, E. *et al.* ZNF598 and RACK1 Regulate Mammalian Ribosome-Associated Quality Control Function by Mediating Regulatory 40S Ribosomal Ubiquitylation. *Mol. Cell* **65**, 751-760.e4 (2017).

24. Ikeuchi, K. & Inada, T. Ribosome-associated Asc1/RACK1 is required for endonucleolytic cleavage induced by stalled ribosome at the 3’ end of nonstop mRNA. *Sci. Rep.* **6**, 28234 (2016).

25. Kuroha, K. *et al.* Receptor for activated C kinase 1 stimulates nascent polypeptide-dependent translation arrest. *EMBO Rep.* **11**, 956–961 (2010).

26. Ikeuchi, K., Izawa, T. & Inada, T. Recent Progress on the Molecular Mechanism of Quality Controls Induced by Ribosome Stalling. *Front. Genet.* **9**, 1–7 (2019).

27. Wang, J., Zhou, J., Yang, Q. & Grayhack, E. J. Multi-protein bridging factor 1(Mbf1), Rps3 and Asc1 prevent stalled ribosomes from frameshifting. *Elife* **7**, 1–26 (2018).

28. Bochler, A. *et al.* Unique features of mRNA translation initiation in trypanosomatids. *bioRxiv* **5**, (2019).

29. Regmi, S., Rothberg, K. G., Hubbard, J. G. & Ruben, L. The RACK1 signal anchor protein from Trypanosoma brucei associates with eukaryotic elongation factor 1A: A role for translational control in cytokinesis. *Mol. Microbiol.* **70**, 724–745 (2008).

30. Aurrecoechea, C. *et al.* PlasmoDB: a functional genomic database for malaria parasites. *Nucleic Acids Res.* **37**, D539–D543 (2009).

31. Zhang, M. *et al.* Uncovering the essential genes of the human malaria parasite Plasmodium falciparum by saturation mutagenesis. *Science (80-.).* **360**, eaap7847 (2018).

32. Gunderson, J. *et al.* Structurally distinct, stage-specific ribosomes occur in Plasmodium. *Science (80-.).* **238**, 933–937 (1987).

33. van Spaendonk, R. M. L. *et al.* Functional Equivalence of Structurally Distinct Ribosomes in the Malaria Parasite, Plasmodium berghei. *J. Biol. Chem.* **276**, 22638–22647 (2001).

34. VELICHUTINA, I. V., ROGERS, M. J., McCUTCHAN, T. F. & LIEBMAN, S. W. Chimeric rRNAs containing the GTPase centers of the developmentally regulated ribosomal rRNAs of Plasmodium falciparum are functionally distinct. *RNA* **4**, S1355838298980049 (1998).

35. Thompson, J. *et al.* Heterogeneous ribosome populations are present in Plasmodium berghei during development in its vector. *Mol. Microbiol.* **31**, 253–260 (1999).

36. Waters, A. P., Syin, C. & McCutchan, T. F. Developmental regulation of stage-specific ribosome populations in Plasmodium. *Nature* **342**, 438–440 (1989).

37. Li, J., Wirtz, R. A., McConkey, G. A., Sattabongkot, J. & McCutchan, T. F. Transition of Plasmodium vivax ribosome types corresponds to sporozoite differentiation in the mosquito. *Mol. Biochem. Parasitol.* **65**, 283–289 (1994).

38. Rogers, M. J. *et al.* Structural features of the large subunit rRNA expressed in Plasmodium falciparum sporozoites that distinguish it from the asexually expressed subunit rRNA. *RNA* **2**, 134–45 (1996).

39. McCutchan, T. F., Li, J., McConkey, G. A., Rogers, M. J. & Waters, A. P. The cytoplasmic ribosomal RNAs of Plasmodium spp. *Parasitol. Today* **11**, 134–138 (1995).

40. Erath, J., Djuranovic, S. & Djuranovic, S. P. Adaptation of Translational Machinery in Malaria Parasites to Accommodate Translation of Poly-Adenosine Stretches Throughout Its Life Cycle. *Front. Microbiol.* **10**, 2823 (2019).

41. Nishimoto, Y. *et al.* Evolution and phylogeny of the heterogeneous cytosolic SSU rRNA genes in the genus Plasmodium☆. *Mol. Phylogenet. Evol.* **47**, 45–53 (2008).

42. Zhu, J. D. *et al.* Stage-specific ribosomal RNA expression switches during sporozoite invasion of hepatocytes. *J. Biol. Chem.* **265**, 12740–4 (1990).

43. McCutchan, T. F. *et al.* Primary sequences of two small subunit ribosomal RNA genes from Plasmodium falciparum. *Mol. Biochem. Parasitol.* **28**, 63–68 (1988).

44. Li, J. *et al.* Regulation and trafficking of three distinct 18 S ribosomal RNAs during development of the malaria parasite. *J. Mol. Biol.* **269**, 203–213 (1997).

45. Fang, J. & McCutchan, T. F. Thermoregulation in a parasite's life cycle. *Nature* **418**, 742–742 (2002).

46. Trinkle-Mulcahy, L. Nucleolus. in *Nuclear Architecture and Dynamics* 257–282 (Elsevier, 2018). doi:10.1016/B978-0-12-803480-4.00011-9

47. Davis, J. H. & Williamson, J. R. Structure and dynamics of bacterial ribosome biogenesis. *Philos. Trans. R. Soc. B Biol. Sci.* **372**, 20160181 (2017).

48. Granneman, S. & Tollervey, D. Building Ribosomes: Even More Expensive Than Expected? *Curr. Biol.* **17**, R415–R417 (2007).

49. Doma, M. K. & Parker, R. Revenge of the NRD: Preferential Degradation of Nonfunctional Eukaryotic rRNA. *Dev. Cell* **11**, 757–758 (2006).

50. Limoncelli, K. A., Merrikh, C. N. & Moore, M. J. ASC1 and RPS3 : new actors in 18S nonfunctional rRNA decay. *RNA* **23**, 1946–1960 (2017).

51. Fujii, K., Kitabatake, M., Sakata, T., Miyata, A. & Ohno, M. A role for ubiquitin in the clearance of nonfunctional rRNAs. *Genes Dev.* **23**, 963–974 (2009).

52. Sugiyama, T. *et al.* Sequential Ubiquitination of Ribosomal Protein uS3 Triggers the Degradation of Non-functional 18S rRNA. *Cell Rep.* **26**, 3400-3415.e7 (2019).

53. Hashimoto, S., Sugiyama, T., Yamazaki, R., Nobuta, R. & Inada, T. Identification of a novel trigger complex that facilitates ribosome-associated quality control in mammalian cells. *Sci. Rep.* **10**, 3422 (2020).

54. Gardner, M. J. *et al.* Genome sequence of the human malaria parasite Plasmodium falciparum. *NatureNature* **419**, (2002).

55. Hamilton, W. L. *et al.* Extreme mutation bias and high AT content in Plasmodium falciparum. *Nucleic Acids Res.* **45**, gkw1259 (2017).

56. Glockner, G. Large Scale Sequencing and Analysis of AT Rich Eukaryote Genomes. *Curr. Genomics* **1**, 289–299 (2000).

57. Szafranski, K., Lehmann, R., Parra, G., Guigo, R. & Glockner, G. Gene Organization Features in A/T-Rich Organisms. *J. Mol. Evol.* **60**, 90–98 (2005).

58. Guler, J. L. *et al.* Asexual Populations of the Human Malaria Parasite, Plasmodium falciparum, Use a Two-Step Genomic Strategy to Acquire Accurate, Beneficial DNA Amplifications. *PLoS Pathog.* **9**, e1003375 (2013).

59. Huckaby, A. C. *et al.* Complex DNA structures trigger copy number variation across the Plasmodium falciparum genome. *Nucleic Acids Res.* **47**, 1615–1627 (2019).

60. Dietel, A.-K., Merker, H., Kaltenpoth, M. & Kost, C. Selective advantages favour high genomic AT-contents in intracellular elements. *PLOS Genet.* **15**, e1007778 (2019).

61. Seward, E. A. & Kelly, S. Dietary nitrogen alters codon bias and genome composition in parasitic microorganisms. *Genome Biol.* **17**, 226 (2016).

62. Leirião, P., Rodrigues, C. D., Albuquerque, S. S. & Mota, M. M. Survival of protozoan intracellular parasites in host cells. *EMBO Rep.* **5**, 1142–1147 (2004).

63. Babbitt, S. E. *et al.* Plasmodium falciparum responds to amino acid starvation by entering into a hibernatory state. *Proc. Natl. Acad. Sci.* **109**, E3278–E3287 (2012).

64. Liu, J., Istvan, E. S., Gluzman, I. Y., Gross, J. & Goldberg, D. E. Plasmodium falciparum ensures its amino acid supply with multiple acquisition pathways and redundant proteolytic enzyme systems. *Proc. Natl. Acad. Sci.* **103**, 8840–8845 (2006).

65. Muralidharan, V., Oksman, A., Iwamoto, M., Wandless, T. J. & Goldberg, D. E. Asparagine repeat function in a Plasmodium falciparum protein assessed via a regulatable fluorescent affinity tag. *Proc. Natl. Acad. Sci.* **108**, 4411–4416 (2011).

66. Muralidharan, V. & Goldberg, D. E. Asparagine Repeats in Plasmodium falciparum Proteins: Good for Nothing? *PLoS Pathog.* **9**, e1003488 (2013).

67. Asai, D. J. *Antibodies in Cell Biology*.

68. Alkekhia, D. & Shukla, A. Influence of poly-l-lysine molecular weight on antibacterial efficacy in polymer multilayer films. *J. Biomed. Mater. Res. - Part A* **107**, 1324–1339 (2019).

69. Ahn, M. *et al.* Poly-lysine peptidomimetics having potent antimicrobial activity without hemolytic activity. *Amino Acids* **46**, 2259–2269 (2014).

70. Vidal, L. *et al.* Lauryl-poly-L-lysine: A New Antimicrobial Agent? *J. Amino Acids* **2014**, 1–10 (2014).

71. Tan, Z. *et al.* The antimicrobial effects and mechanism of ε-poly-lysine against

Staphylococcus aureus. *Bioresour. Bioprocess.* **6**, 11 (2019).

1. Yeoh, L. M. *et al.* Alternative splicing is required for stage differentiation in malaria parasites. *Genome Biol.* **20**, 151 (2019).
2. Sorber, K., Dimon, M. T. & DeRisi, J. L. RNA-Seq analysis of splicing in Plasmodium falciparum uncovers new splice junctions, alternative splicing and splicing of antisense transcripts. *Nucleic Acids Res.* **39**, 3820–3835 (2011).
3. Cole, S. E., LaRiviere, F. J., Merrikh, C. N. & Moore, M. J. A Convergence of rRNA and mRNA Quality Control Pathways Revealed by Mechanistic Analysis of Nonfunctional rRNA Decay. *Mol. Cell* **34**, 440–450 (2009).
4. LaRiviere, F. J., Cole, S. E., Ferullo, D. J. & Moore, M. J. A Late-Acting Quality Control Process for Mature Eukaryotic rRNAs. *Mol. Cell* **24**, 619–626 (2006).
5. Karamyshev, A. L. & Karamysheva, Z. N. Lost in Translation: Ribosome-Associated mRNA and Protein Quality Controls. *Front. Genet.* **9**, 1–13 (2018).
6. Chandrasekaran, V. *et al.* Mechanism of ribosome stalling during translation of a poly(A) tail. *Nat. Struct. Mol. Biol.* **26**, 1132–1140 (2019).
7. Tesina, P. *et al.* Molecular mechanism of translational stalling by inhibitory codon combinations and poly(A) tracts. *EMBO J.* **39**, e103365 (2020).
8. Jackson, K. E. *et al.* Protein translation in Plasmodium parasites. *Trends Parasitol.* **27**, 467–476 (2011).
9. Joazeiro, C. A. P. Ribosomal Stalling During Translation: Providing Substrates for

Ribosome-Associated Protein Quality Control. *Annu. Rev. Cell Dev. Biol.* **33**, 343–368 (2017).

10. Doma, M. K. & Parker, R. RNA Quality Control in Eukaryotes. *Cell* **131**, 660–668 (2007).
11. Houseley, J. & Tollervey, D. The Many Pathways of RNA Degradation. *Cell* **136**, 763–776 (2009).
12. Shoemaker, C. J. & Green, R. Translation drives mRNA quality control. *Nat. Struct. Mol. Biol.* **19**, 594–601 (2012).
13. Pavlovic Djuranovic, S., Erath, J., Andrews, R. J., Bayguinov, P. O. & Joyce, J. Plasmodium falciparum translational machinery condones polyadenosine repeats. *Elife* **9**, e57799 (2020).
14. Sun, M. *et al.* Dynamical features of the Plasmodium falciparum ribosome during translation. *Nucleic Acids Res.* **43**, gkv991 (2015).
15. Wong, W. *et al.* Cryo-EM structure of the Plasmodium falciparum 80S ribosome bound to the anti-protozoan drug emetine. *Elife* **3**, (2014).
16. Bunnik, E. M. *et al.* The mRNA-bound proteome of the human malaria parasite Plasmodium falciparum. *Genome Biol.* **17**, 1–18 (2016).
17. Gallo, S. *et al.* RACK1 Specifically Regulates Translation through Its Binding to Ribosomes. *Mol. Cell. Biol.* **38**, 1–16 (2018).
18. Thompson, M. K., Rojas-Duran, M. F., Gangaramani, P. & Gilbert, W. V. The ribosomal protein Asc1/RACK1 is required for efficient translation of short mRNAs. *Elife* **5**, 1–20 (2016).

19. Kouba, T., Rutkai, E., Karásková, M. & Valášek, L. S. The eIF3c/NIP1 PCI domain interacts with RNA and RACK1/ASC1 and promotes assembly of translation preinitiation complexes. *Nucleic Acids Res.* **40**, 2683–2699 (2012).

20. Sengupta, J. *et al.* Identification of the versatile scaffold protein RACK1 on the eukaryotic ribosome by cryo-EM. *Nat. Struct. Mol. Biol.* **11**, 957–962 (2004).

21. Nilsson, J., Sengupta, J., Frank, J. & Nissen, P. Regulation of eukaryotic translation by the RACK1 protein: a platform for signalling molecules on the ribosome. *EMBO Rep.* **5**, 1137–1141 (2004).

22. Ceci, M. *et al.* Release of eIF6 (p27BBP) from the 60S subunit allows 80S ribosome assembly. *Nature* **426**, 579–584 (2003).

23. Sundaramoorthy, E. *et al.* ZNF598 and RACK1 Regulate Mammalian Ribosome-Associated Quality Control Function by Mediating Regulatory 40S Ribosomal Ubiquitylation. *Mol. Cell* **65**, 751-760.e4 (2017).

24. Ikeuchi, K. & Inada, T. Ribosome-associated Asc1/RACK1 is required for endonucleolytic cleavage induced by stalled ribosome at the 3’ end of nonstop mRNA. *Sci. Rep.* **6**, 28234 (2016).

25. Kuroha, K. *et al.* Receptor for activated C kinase 1 stimulates nascent polypeptide-dependent translation arrest. *EMBO Rep.* **11**, 956–961 (2010).

26. Ikeuchi, K., Izawa, T. & Inada, T. Recent Progress on the Molecular Mechanism of Quality Controls Induced by Ribosome Stalling. *Front. Genet.* **9**, 1–7 (2019).

27. Wang, J., Zhou, J., Yang, Q. & Grayhack, E. J. Multi-protein bridging factor 1(Mbf1), Rps3

and Asc1 prevent stalled ribosomes from frameshifting. *Elife* **7**, 1–26 (2018).

28. Aurrecoechea, C. *et al.* PlasmoDB: a functional genomic database for malaria parasites. *Nucleic Acids Res.* **37**, D539–D543 (2009).

29. Zhang, M. *et al.* Uncovering the essential genes of the human malaria parasite Plasmodium falciparum by saturation mutagenesis. *Science (80-.).* **360**, eaap7847 (2018).

30. Gunderson, J. *et al.* Structurally distinct, stage-specific ribosomes occur in Plasmodium. *Science (80-.).* **238**, 933–937 (1987).

31. van Spaendonk, R. M. L. *et al.* Functional Equivalence of Structurally Distinct Ribosomes in the Malaria Parasite, Plasmodium berghei. *J. Biol. Chem.* **276**, 22638–22647 (2001).

32. Zhu, J. D. *et al.* Stage-specific ribosomal RNA expression switches during sporozoite invasion of hepatocytes. *J. Biol. Chem.* **265**, 12740–4 (1990).

33. McCutchan, T. F. *et al.* Primary sequences of two small subunit ribosomal RNA genes from Plasmodium falciparum. *Mol. Biochem. Parasitol.* **28**, 63–68 (1988).

34. VELICHUTINA, I. V., ROGERS, M. J., McCUTCHAN, T. F. & LIEBMAN, S. W. Chimeric rRNAs containing the GTPase centers of the developmentally regulated ribosomal rRNAs of Plasmodium falciparum are functionally distinct. *RNA* **4**, S1355838298980049 (1998).

35. Thompson, J. *et al.* Heterogeneous ribosome populations are present in Plasmodium berghei during development in its vector. *Mol. Microbiol.* **31**, 253–260 (1999).

36. Waters, A. P., Syin, C. & McCutchan, T. F. Developmental regulation of stage-specific ribosome populations in Plasmodium. *Nature* **342**, 438–440 (1989).

37. Li, J., Wirtz, R. A., McConkey, G. A., Sattabongkot, J. & McCutchan, T. F. Transition of

Plasmodium vivax ribosome types corresponds to sporozoite differentiation in the mosquito. *Mol. Biochem. Parasitol.* **65**, 283–289 (1994).

38. Rogers, M. J. *et al.* Structural features of the large subunit rRNA expressed in Plasmodium falciparum sporozoites that distinguish it from the asexually expressed subunit rRNA. *RNA* **2**, 134–45 (1996).

39. McCutchan, T. F., Li, J., McConkey, G. A., Rogers, M. J. & Waters, A. P. The cytoplasmic ribosomal RNAs of Plasmodium spp. *Parasitol. Today* **11**, 134–138 (1995).

40. Erath, J., Djuranovic, S. & Djuranovic, S. P. Adaptation of Translational Machinery in Malaria Parasites to Accommodate Translation of Poly-Adenosine Stretches Throughout Its Life Cycle. *Front. Microbiol.* **10**, 2823 (2019).

41. Nishimoto, Y. *et al.* Evolution and phylogeny of the heterogeneous cytosolic SSU rRNA genes in the genus Plasmodium☆. *Mol. Phylogenet. Evol.* **47**, 45–53 (2008).

42. Li, J. *et al.* Regulation and trafficking of three distinct 18 S ribosomal RNAs during development of the malaria parasite. *J. Mol. Biol.* **269**, 203–213 (1997).

43. Fang, J. & McCutchan, T. F. Thermoregulation in a parasite's life cycle. *Nature* **418**, 742–742 (2002).

44. Trinkle-Mulcahy, L. Nucleolus. in *Nuclear Architecture and Dynamics* 257–282 (Elsevier, 2018). doi:10.1016/B978-0-12-803480-4.00011-9

45. Davis, J. H. & Williamson, J. R. Structure and dynamics of bacterial ribosome biogenesis. *Philos. Trans. R. Soc. B Biol. Sci.* **372**, 20160181 (2017).

46. Granneman, S. & Tollervey, D. Building Ribosomes: Even More Expensive Than Expected?

Curr. Biol. **17**, R415–R417 (2007).

47. Doma, M. K. & Parker, R. Revenge of the NRD: Preferential Degradation of Nonfunctional Eukaryotic rRNA. *Dev. Cell* **11**, 757–758 (2006).

48. Limoncelli, K. A., Merrikh, C. N. & Moore, M. J. ASC1 and RPS3 : new actors in 18S nonfunctional rRNA decay. *RNA* **23**, 1946–1960 (2017).

49. Fujii, K., Kitabatake, M., Sakata, T., Miyata, A. & Ohno, M. A role for ubiquitin in the clearance of nonfunctional rRNAs. *Genes Dev.* **23**, 963–974 (2009).

50. Sugiyama, T. *et al.* Sequential Ubiquitination of Ribosomal Protein uS3 Triggers the Degradation of Non-functional 18S rRNA. *Cell Rep.* **26**, 3400-3415.e7 (2019).

51. Hashimoto, S., Sugiyama, T., Yamazaki, R., Nobuta, R. & Inada, T. Identification of a novel trigger complex that facilitates ribosome-associated quality control in mammalian cells. *Sci. Rep.* **10**, 3422 (2020).